Technische Universität München
TUM School of Engineering and Design

Satellite altimetry-derived ocean tide model development and applications

Michael Geofrey Hart-Davis

Complete reprint of the dissertation approved by the TUM School of Engineering and Design of the Technical University of Munich for the award of the

Doktor der Ingenieurwissenschaften (Dr.-Ing.)

Chair:
Prof. Dr. Niklas Boers

Examiners:
1. Prof. Dr. -Ing. Florian Seitz
2. Prof. Ole Baltazar Andersen
3. Assistant Prof. Dr.ir. Cornelis Slobbe

The dissertation was submitted to the Technical University of Munich on 02.11.2023 and accepted by the TUM School of Engineering and Design on 19.02.2024.

Abstract

The surface fluctuation caused by ocean tides remains one of the most crucial components of sea level variability. For several applications, accurate knowledge of ocean tides is crucial, either for removing the contribution from the total sea level or for inclusion to accurately describe oceanic processes. Significant efforts have been made for decades in the development of global ocean tide models. The era of satellite altimetry has resulted in significant advances in the accuracy of tide models, largely thanks to TOPEX/Poseidon and its respective successors. The consistent orbiting of satellite altimetry has provided regular retrieval of sea level measurements at the same positions over the last few decades. Extensive time series of measurements are vital for advancing our estimations of ocean tides. Recent accuracy assessments have concluded that tides in the open ocean are well documented; however, challenges remain in the coastal and polar regions. The complexity of estimating tides in the coastal region stems from several factors. Despite the role altimetry has played in the open oceans, the impact of land on the radar returns means that sea level estimations are not routinely available closer to the coast.

Furthermore, tides are much more complex in the coastal regions due to the complex coastline structures and bathymetry changes. In recent years, considerable efforts have been made to improve and increase the retrievals of sea level data closer to the coast based on advanced processing techniques or by using geophysical corrections optimised for the near coastal region. Advances in coastal altimetry have positively impacted tidal estimations and, subsequently, modelling efforts in this region.

In this thesis, a new global ocean tide model is developed and presented, which utilises these advances in altimetry to improve the estimations of ocean tides in the coastal region. The developed model is presented in the application as an ocean tidal correction for satellite altimetry, where additional methods are explored to better estimate the minor tidal constituents for these corrections. For the first time, a regional version of the model is used to force an operational ocean model of the Northwest European Continental Shelf at its boundaries to improve the representation of tides within the model.

Despite the model development itself, several additional tools and datasets were produced to help in the evaluation and validation of the model. This included the extension of a tidal constituent database, TICON, to include almost three times the number of tide gauges, which are used in the validation of the different versions of the model. Additionally, a tidal prediction software, termed TIPTOE, was produced, which takes the tidal constituents provided by global models and derives a tidal height estimation at any time and position. This can be used for various applications, but in particular in the derivation of tidal corrections for satellite altimetry. An additional tool was produced to derive sea level variances based on different tidal corrections for respective altimetry missions, which is used to validate the model developments by assessing the impact different tide models have on the sea level variances.

The global EOT20 model produced within this thesis utilises multi-mission satellite altimetry produced at DGFI-TUM to conduct residual tidal analysis based on twenty-six years' worth of data. The model is evaluated against state-of-the-art tide models compared to two independent datasets based on tide gauges and ocean bottom pressure sensors in the open ocean, shelf seas and coastal regions. From this validation, it was concluded that EOT20 significantly improved the accuracy of tidal estimations, particularly in the coastal region, with respect to the previous iteration of the global model, EOT11a. Compared to the other global tide models, EOT20 showed the lowest error margin for the eight major tidal constituents in the coastal region and remained consistent with the best-performing models in the open ocean and shelf seas. Additional validation was done by deriving the satellite altimetry correction for three separate altimetry missions and contrasting the resultant sea level variances from respective models. As in the tide gauge analysis, EOT20 showed improvements compared to EOT11a and FES2014b, with particular reductions in variances seen in the coastal regions. It is concluded that the developed EOT20 model achieves a significant improvement in tidal estimation in the coastal region and is suitable for a variety of applications.

An investigation into improving the altimetry tidal correction by improving the inclusion of minor tidal constituents is presented. Despite their contribution being significantly less overall than major tides, minor tides are still vital in providing accurate tidal corrections and reducing the overall error of tidal estimations. When minor tides cannot be estimated by altimetry-derived models based on signal-to-noise or aliasing issues, admittance approaches are used to infer these tides from the major tides. In this thesis, these approaches are evaluated against deriving eight minor constituents from the altimetry-derived models as well as from numerical models which are not constrained by the previously mentioned. The results demonstrated that the accuracy of the tidal correction is improved when directly estimating four of the constituents and inferring the remaining constituents. A novel approach of combining empirical and numerical models in deriving the tidal is also presented and demonstrates comparable results to the admittance approaches. These results suggest that future corrections could benefit from the combination of constituents from both empirical and numerical models to reduce the overall error of tidal estimations.

Finally, a regional version of the EOT model, EOT-NECS, is applied to an operational ocean model to improve the overall water level estimations along the Northwest European Continental Shelf. This was done by forcing the ocean model, DCSM-FM, at its boundaries with tidal constituents provided by EOT-NECS and conducting a series of experiments on the resultant accuracy of the predicted total water levels. The EOT-NECS model incorporated five additional altimetry missions and extended the time series of missions already used. This resulted in the derivation of further tidal constituents previously not included, as well as an increased spatial resolution of the model, which, when compared to TICON-3, showed improvements within this region compared to the global model. When applying the model to DCSM-FM, the results demonstrated a clear improvement in model accuracy in terms of tidal height and total water level predictions.

This thesis presents clear advancements in the global estimation of ocean tides and highlights its importance in geophysical applications. It is also clear that despite the progress made, there are still many areas where tide models can be developed and improved, particularly in complex coastal regions and in the higher latitudes. It is, therefore, recommended that special attention be placed on tides in complex regions, such as fjords, estuaries and inlets, as well as in the polar oceans to help increase the reliability and subsequent usability of global tide models in these regions.

Preface

As a child, I was always fascinated by the ocean motion, particularly puzzled by these two questions: Why was the beach bigger when I arrived than when I left, and why do we keep moving our towels further up the beach? A particular memory is a beach called Blouberg in Cape Town, South Africa, which contains a small rocky outcrop that my family and I loved to walk to. The problem was, sometimes we could walk to this outcrop, and sometimes we could not. As I grew older, my Mother and I would always look at these "High and Lows" charts on the beaches or in the newspapers, and I started to learn when was the best time to go to the beach, to visit this rocky outcrop and when was the best time for my longboard.

The answer to these never-ending questions in my little head was, of course, ocean tides.

In some way or another, tides have contributed a significant amount to my life. In recognition of this, the chapter pages within this thesis show the tidal heights estimated over the days of my birth derived from a tide gauge in East London, South Africa, where I was born. Each line represents the tidal height calculated from each of the major tidal constituents.

Entering my PhD having studied physical oceanography, I had thought that the problem of understanding ocean tides was well understood. After quickly being humbled by the complexity, importance and wonder that is ocean tides, I realised that this challenge was going to be bigger than I expected. Diving into the literature by the pioneers of ocean tide theory, such as George Darwin, Arthur Doodson, Walter Munk, David Cartwright, Phil Woodworth, Ole Andersen and Richard Ray, to mention only the tip of the iceberg, I was engulfed in the variety of complex dynamical features described and influenced by ocean tides. I was ready for this challenge.

Then came the world of satellite altimetry and geodesy. Entering the field of geodesy as an ocean person (coined by Mathis Bloßfeld) was another intimidating component of my PhD. The millions of acronyms, the countless geophysical corrections and the vast number of orbiting scientific satellites were a big surprise. However, I was welcomed and guided through the community by my colleagues at DGFI-TUM as well as within the NEROGRAV research group, largely benefited by the countless visits to the offices of Denise Dettmering and Christian Schwatke and the privilege of sharing an office with Marcello Passaro, all of whom were always happy to answer my basic questions and allow me to feed off their vast amounts of knowledge.

Looking back on my thesis, a lot of it stems from the greatest gift I was given throughout my PhD: freedom. Freedom to think, experiment, collaborate and discuss. As a scientist, I think it is fundamental to try and fail as well as to think independently about how to solve certain objectives. Throughout my PhD, I tried things that failed, I tried things that had already been done, or I tried things that were simply illogical. I also communicated to try to describe my ideas and try to absorb the opinions and knowledge of others. In particular, there were debates with Julius Oelsmann and slightly one-sided discussions with Ole Andersen, Richard Ray, Roman Sulzbach, Michael Schindelegger and Björn Backeberg. I also had the pleasure of collaborating with a vast network of scientists from around the world, ranging from South Africa to Europe to the United States.

These collaborations resulted in the gain of insights from different perspectives and the broadening of my own understanding.

The ideas that stem from these collaborations, experiments and discussions all eventually ended up in my black book of ideas, which I maintained throughout my PhD. Although the success rate of these ideas is probably one out of ten, if I am being very generous, some ideas resulted in the greatest progressions of my work and shaped my PhD into the thesis it has become. In this book, I still have the original ideas of each manuscript that I wrote in my thesis, the comments from colleagues on these ideas, as well as the eventual structure of the manuscripts I wanted to write about these ideas.

All my scientific publications and research strongly benefited from public discussion either during the review process or from international conferences and research visits. The discussions within the broader community helped fine-tune the research and open the door for further opportunities to be explored. One major benefactor was the discussions resulting from the first paper of this thesis, which resulted in extensive communication and collaborative discussions leading to the publication of the final paper of this thesis.

Contents

Abstract ii

Preface iv

1 Introduction 2
- 1.1 Background and Motivation . . . 2
- 1.2 Objectives and Outline of this Thesis . . . 4

2 Ocean Tides and Tidal Analysis 7
- 2.1 The theory of ocean tides . . . 7
- 2.2 Methods of tidal analysis . . . 11
- 2.3 Measuring ocean tides . . . 13
- 2.4 Tides from and for satellite altimetry . . . 13
  - 2.4.1 Geophysical corrections . . . 17

3 Validation tools and datasets for global ocean tide models 23
- 3.1 In-situ databases . . . 23
  - 3.1.1 TICON-td: third-degree tidal constituent dataset . . . 23
  - 3.1.2 TICON-3: global tidal constituent dataset . . . 24
  - 3.1.3 ArcTiCA: Arctic tidal constituent atlas . . . 24
- 3.2 TIPTOE: tidal prediction in the ocean . . . 26
- 3.3 SLAVA: sea level anomaly variance analysis . . . 28

4 Tide model developments 31
- 4.1 Introduction . . . 31
- 4.2 The EOT model . . . 32
- 4.3 Elastic tide decoupling . . . 37
- 4.4 Capsize optimisation . . . 39
- 4.5 Land-sea mask . . . 41
- 4.6 Model coastal flagging . . . 42
- 4.7 P-1: EOT20: a global ocean tide model from multi-mission satellite altimetry . . . 43
- 4.8 P-2: Regional Evaluation of Minor Tidal Constituents for Improved Estimation of Ocean Tides 46
- 4.9 Additional altimetry data for high-resolution regional tide modelling . . . 47

5 Application of tidal developments 50
- 5.1 Third degree tides . . . 50
- 5.2 Polar ocean tides . . . 52

5.3 P-3: Altimetry-derived tide model for improved tide and water level forecasting along the European Continental Shelf 54

6 Conclusion and Outlook **58**

6.1 Conclusions on objectives 58

6.2 Recommendations and future work 60

Bibliography **65**

List of Figures **73**

List of Tables **75**

A Appendix **77**

A.1 Publications 77

A.1.1 P-1 EOT20: a global ocean tide model from multi-mission satellite altimetry 77

A.1.2 P-2 Regional Evaluation of Minor Tidal Constituents for Improved Estimation of Ocean Tides 94

A.1.3 P-3 Altimetry-derived tide model for improved tide and water level forecasting along the European Continental Shelf 110

A.2 Additional publications 128

A.3 Associated Datasets 128

Acknowledgements **130**

CHAPTER 1

INTRODUCTION

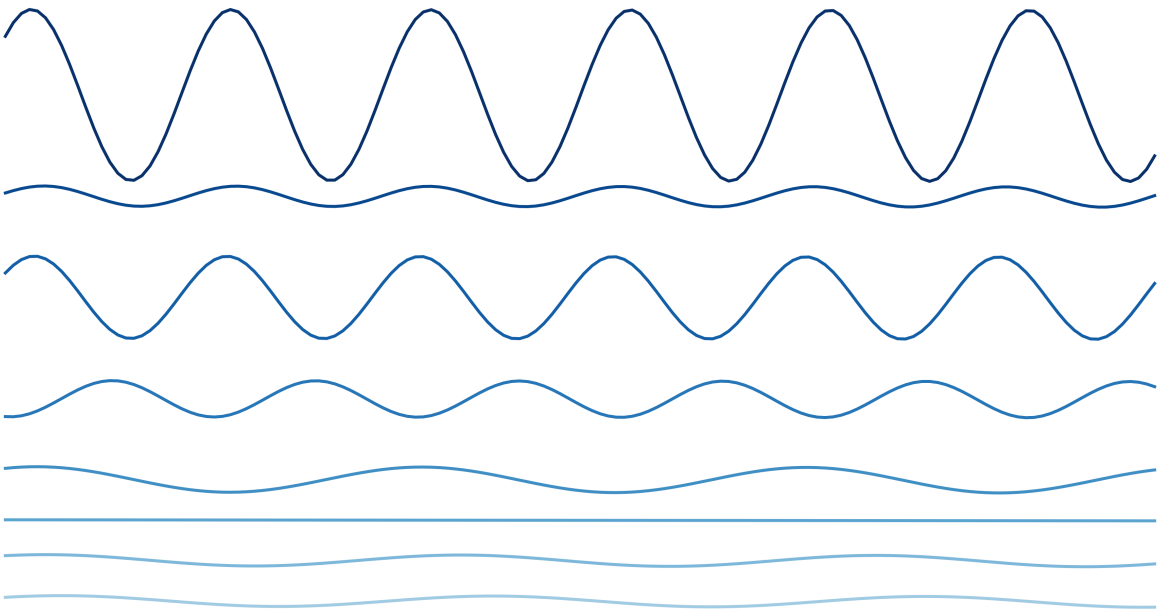

What you do makes a difference, and you have to decide what kind of difference you want to make.
- Jane Goodall

1 Introduction

1.1 Background and Motivation

The ocean covers more than 70% of the Earth's surface. The complex small and large-scale processes driving ocean circulation are crucial for various reasons, mainly the driving and regulation of global climate processes. One such oceanographic process that continues to puzzle scientists is ocean tides.

Ocean tides, like several other physical oceanographic processes, have been challenging mariners and fishermen for thousands of years. So, naturally, theories on the physical mechanisms responsible for ocean tides have been discussed for centuries. Studies have found references to tides as early as the ancient Greek civilisations (Cartwright, 2001) and evidence of understandings dating back to periods 2,500 - 1,500 BC, based on fossils found by Indian archaeologists (Panikkar and Srinivasan, 1971; Cartwright, 2001). The connection between the ocean height and the Moon has long been theorised, with relatively satisfactory rule-of-thumb tide predictions being made and published and methods used to produce tide tables often being kept secret (Munk and Cartwright, 1966).

Although ocean tides have been studied for a long time, advances in our understanding of tides continue to take place. These advances are being motivated by tides' importance, particularly in providing accurate current and future sea level predictions. The rise and fall of the ocean tides can cause changes in the sea level that often exceed one meter, with tides in regions such as the Bay of Fundy known to exceed fifteen meters. Therefore, to account for these fluctuations and allow for accurate monitoring of changes in the sea level, the ocean tides need to be removed from sea-level measurements. As we have been studying ocean tides for centuries, the process of doing so has become relatively well-known.

The harmonic method, which decomposes the full tidal signal into several harmonic constants (or constant frequencies) that can be individually derived and assessed, was a tremendous breakthrough in tidal expertise (Darwin, 1891). Since then, the harmonic method has continued to be developed mainly by Doodson (1921), who proposed what would eventually become known as the Doodson numbers, which proposed the description of each harmonic constant, or tidal constituent, by a set of six signed integers derived from the planetary motions within the Earth, lunar and solar system. Although hundreds of tidal constituents exist, studies have shown the majority of the overall tidal signal is expressed as the sum of fourteen constituents (Egbert and Ray, 2017), commonly referred to as the 'major' tides. These constituents are the largest and can easily be distinguished within in-situ measurements and are usually the subject of the most focus on tidal developments. Figure 1.1 shows a spectral analysis of two tide gauges taken from GESLA-3 (Haigh et al., 2022). It is clear that specific frequencies peak in both datasets, which coincide with well-known and defined tidal frequencies such as the M_2, S_2 and S_1, as highlighted here. However, the remaining constituents, commonly termed 'minor' tides, cannot always be wholly neglected as the variance they are responsible for can result in root-mean-square (RMS) errors of greater than 7 cm in some regions (Egbert and Ray, 2017).

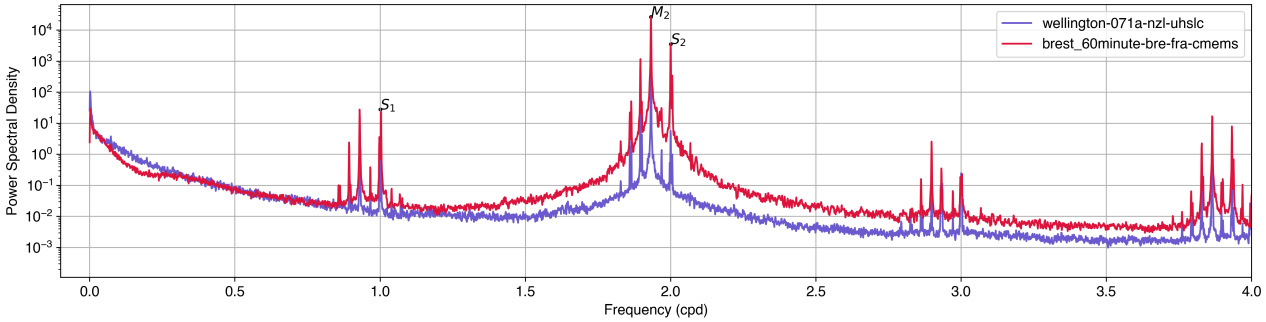

Figure 1.1 Spectral analysis of two different tide gauge time-series taken from GESLA-3 (Haigh et al., 2022), showing the power spectral density at respective frequencies in cycles per day (cpd). The tide gauges presented here are from Wellington, New Zealand and Brest, France.

For in-situ measurements with long enough time-series lengths, such as tide gauges, these major and minor tides can be determined and accounted for without additional information. However, for measurements with relatively infrequent temporal sampling, such as those from satellite altimetry and gravimetry, tide models are required to accurately account for their influence. This is due to the repeat orbit of altimetry measurements, meaning that tidal aliasing influences the altimetry's ability to be used, particularly for the minor constituents.

Several types of ocean tide models exist and continue to be developed. The major types of models are empirical, assimilative and numerical. Each model type has its own set of benefits and weaknesses. Empirical, data-constrained models rely purely on observations, mainly from satellite altimetry. They can make accurate determinations of the major constituents but are restricted by tidal aliasing when it comes to minor constituents. The continued extension of the currently flying altimeter missions has meant that the minor constituents are becoming easier to determine and study (Ray, 2020b). The estimation of minor constituents is usually inferred using admittance approaches (Munk and Cartwright, 1966; Petit and Luzum, 2010; Rieser et al., 2012) from the major constituents, but with the increased time-series of altimetry data, certain minor constituents can be directly estimated from these models. Numerical, data-unconstrained models, which are derived following varying approaches mainly driven by the shallow water equations, do not have a limitation on which constituents can estimate reliably. However, in terms of the accuracy of estimations, they fall behind models that include observations. Despite this, one benefit of data-unconstrained models is the ability to more easily provide a wider range of tidal constituents than is possible from data-constrained models (Sulzbach et al., 2021). Data assimilative models, such as FES2014b (Lyard et al., 2021), are hydrodynamic models that assimilate data from satellite altimetry and/or in-situ measurements. The combination of numerically refined models with measurements of ocean tides results in high accuracy commonly seen from these model types.

A recent accuracy assessment of state-of-the-art tide models was done by Stammer et al. (2014), which concluded that tides in the open ocean were relatively well predicted. At the same time, the shelf and coastal regions showed the highest model errors. The complex nature of tides near the coast, coupled with the difficulty of obtaining reliable satellite observations near the coast due to land contamination (Fok, 2012), result in relatively high errors from satellite-derived tide models. In recent years, advances have been made in coastal altimetry processing from the optimisation of geophysical corrections for coastal regions (Scharroo and Smith, 2010; Fernandes and Lázaro, 2016; Carrere et al., 2016) as well as the significant increase in the amount of retrieved, reliable data closer to the coast (Passaro et al., 2018b).

These advancements in coastal altimetry have resulted in significant improvements in tidal estimations made by regional versions of the Empirical Ocean Tide (EOT) model with respect to the previous global model, EOT11a (Savcenko and Bosch, 2012), which were presented in the PhD thesis of Piccioni (2021). The regional results of model developments based on applying improved coastal altimetry processing presented in Piccioni (2021), serve as a robust framework and launchpad for further research to be done as well as the eventual extension of these results into a global tide model.

1.2 Objectives and Outline of this Thesis

Ocean tides influence a variety of geophysical processes studied and estimated from a variety of techniques, for example, satellite altimetry, satellite gravimetry and ocean models. Therefore, substantial importance lies in accurately accounting for ocean tides to improve the accuracy of these studied geophysical processes and their downstream applications. The main aim of this thesis is to reduce the error of tidal estimations in a global ocean tide model, with emphasis on the coastal region, and to evaluate the developed model in various applications. Within this thesis, applications such as an ocean tidal correction for satellite altimetry and a boundary forcing for an operational ocean model are presented. However, several other applications exist and are introduced later in this thesis.

Three scientific objectives form the basis of this thesis:

- **O-1**: Reduce the error with respect to tide gauges of an updated global ocean tide model while remaining in line with global models in the open ocean and shelf regions.
- **O-2**: Increasing the accuracy of the tidal correction for satellite altimetry by optimising the methods of accounting for minor tidal constituents.
- **O-3**: Improve the prediction of ocean tides within an operational ocean model of the Northwest European Continental Shelf by improving the ocean tide forcing at the open boundaries.

These scientific objectives are discussed in three published chapters of this thesis, which are as follows:

- **P-1**: Hart-Davis, M.G., Piccioni, G., Dettmering, D., Schwatke, C., Passaro, M. and Seitz, F., 2021. EOT20: A global ocean tide model from multi-mission satellite altimetry. *Earth System Science Data*, 13(8), pp.3869-3884. 10.5194/essd-13-3869-2021.
- **P-2**: Hart-Davis, M.G., Dettmering, D., Sulzbach, R., Thomas, M., Schwatke, C. and Seitz, F., 2021. Regional evaluation of minor tidal constituents for improved estimation of ocean tides. *Remote Sensing*, 13(16), p.3310. 10.3390/rs13163310.
- **P-3**: Hart-Davis, M.G., Laan, S., Schwatke, C., Backeberg, B., Dettmering, D., Zijl, F., Verlaan, M., Passaro, M. and Seitz, F., 2023. Altimetry-derived tide model for improved tide and water level forecasting along the European continental shelf. *Ocean Dynamics*, 73(8), pp.475-491. https://doi.org/10.1007/s10236-023-01560-0

To achieve the main aim and the objectives of this thesis, particular effort is required on the validation metrics used to evaluate the model performances. This means that a large section of this thesis is dedicated to producing validation metrics for the model developments, which included updating existing in-situ measurement databases,

developing tidal prediction software to derive the tidal correction for satellite altimetry, and developing variance analysis software to derive the variances for altimetry missions based on chosen geophysical corrections.
These developments were targeted for use within this thesis, but also with an eye on additional studies and future research. This resulted in the publication of four additional manuscripts, which do not serve the main objectives of this thesis but were benefited by the developments of this thesis. These associated publications are listed below:

- **AP-1**: Sulzbach, R., Wziontek, H., Hart-Davis, M.G., Dobslaw, H., Scherneck, H.G., Van Camp, M., Omang, O.C.D., Antokoletz, E.D., Voigt, C., Dettmering, D. and Thomas, M., 2022. Modeling gravimetric signatures of third-degree ocean tides and their detection in superconducting gravimeter records. *Journal of Geodesy*, 96(5), pp.1-22, https://doi.org/10.1007/s00190-022-01609-w.
- **AP-2**: Hart-Davis M.G., Howard S., Ray R., Andersen O., Padman L., Nilsen F., Dettmering D. ArcTiCA: Arctic Tidal Constituents Atlas. *Nature Scientific Data* [in review]. Preprint: https://doi.org/10.21203/rs.3.rs-3277941/v1
- **AP-3**: Andersen, O.B., Rose, S.K. and Hart-Davis, M.G., 2023. Polar Ocean Tides—Revisited Using Cryosat-2. Remote Sensing, 15(18), p.4479. https://doi.org/10.3390/rs15184479
- **AP-4**: Passaro M., Rautiainen L., Dettmering D., Restano M., Hart-Davis M.G., Schlembach F., Särkkä J., Müller F. L., Schwatke C., Benveniste J., 2022. Validation of an Empirical Subwaveform Retracking Strategy for SAR Altimetry. *Remote Sensing*, 14(16), 4122, https://doi.org/10.3390/rs14164122
- **AP-5**: Hauk M., Wilms J., Sulzbach R., Panafidina N., Hart-Davis M., Dahle C., Müller V., Murböck M. and Flechtner F., 2023. Satellite gravity field recovery using variance covariance information from ocean tide models. AGU Earth and Space, https://doi.org/10.1029/2023EA003098

The thesis is outlined as follows: Chapter 2 discusses the theory of ocean tides and tides in satellite altimetry. Chapter 3 provides improved validation metrics and datasets, which are crucial for the later chapters to help achieve the scientific objectives of this thesis. Chapter 4 discusses the tide model developments done within this thesis, which contributed to each of the publications. Chapter 5 puts the developments done in Chapters 3 and 4 into context by providing applications of these developments. An overall summary with conclusions and recommendations for future research is given in Chapter 6. The three scientific articles are presented in their journal format in the Appendix.

CHAPTER 2

OCEAN TIDES AND TIDAL ANALYSIS

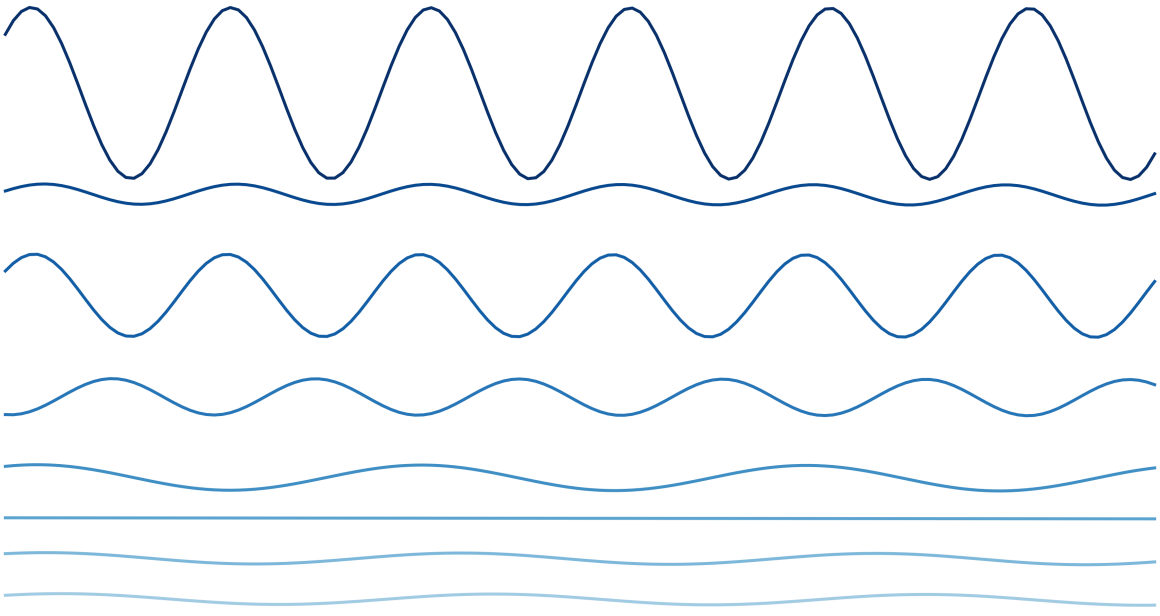

From the dawn of scientific enquiry, basic questions about the mechanisms of how the Moon and Sun drive tides have inspired distinguished philosophers and Earth scientists

- David Cartwright

2 Ocean Tides and Tidal Analysis

2.1 The theory of ocean tides

A significant milestone in the history of ocean tide theory came from the famous *Philosophae Naturalis Principia Mathematica* books of Isaac Newton (Newton, 1833) where he describes observed phenomena, including discussions on ocean tides, by his theory of universal gravitational attraction (Cartwright, 1999). Subsequent discussions on the topic, particularly essays published by Euler, Maclaurin and Bernoulli, refined the detail of the theory as well as its real-life application (Cartwright, 1999) and eventually resulted in the establishment of the Equilibrium tide theory.

The Equilibrium tide theory that originates from the work of Newton and the subsequent refinements describes two tidal bulges: one towards the tide-generating force (TGF) and one opposite these forces, which is illustrated in the schematic in Figure 2.1. The distance between L and P_1 is smaller than that of L and O, meaning that P_1 experiences a greater force of attraction than that of O. This difference results in a greater attraction towards the Moon, which causes a bulge in the water mass towards the Moon. As this difference varies throughout the Earth's surface, the TGF can be estimated at any point. The displacement of the water caused by the tide-generating bodies results from the tangential component of the TGF and not the radial component (Pugh and Woodworth, 2014). This may seem slightly unintuitive but is explained when considering Earth's own gravitational attraction. Illustrated in the triangular schematic in the bottom right of Figure 2.1, the force expressed by the TGF can be decomposed into a tangential (a_h) and radial component (a_r). The radial component of the force is opposed by Earth's own gravity, which is considerably larger, while the tangential component is unopposed in the natural world, resulting in a variation in the water body in the tangential direction.

The TGF at any point of the Earth can be estimated, using P_4 in Figure 2.1 as an example:

$$\mathrm{TGF}_{P_4} = -\frac{Gm_1}{R}[1 - 2\frac{\rho}{R}\cos\phi + \frac{\rho^2}{R^2}]^{-\frac{1}{2}}, \tag{2.1}$$

where R is the distance between the two centres of mass of the Earth and Moon in this example, ρ the radius of the Earth, ϕ the angle between the Earth-Moon line and the radius to P_4, m_l the mass of the Moon and G is the universal gravitational constant.

The Equilibrium theory states that the free surface, $\bar{\zeta}$, is assumed to be a level surface which is influenced by the combination of Earth's gravity as well as the tide generating force (Pugh and Woodworth, 2014). Equilibrium tide theory ignores the realistic dynamic nature of ocean tides by assuming the Earth is entirely and uniformly covered by water. Despite showing no spatial resemblance to real observed ocean tides, the Equilibrium Tide is an essential reference system for tidal analysis (Pugh and Woodworth, 2014). As defined in Pugh and Woodworth (2014) the Equilibrium Tide can be determined for latitude θ_p as follows:

$$\bar{\zeta} = \rho\frac{m_c}{m_e}\left[C_0(t)\left(\frac{3}{2}\sin^2\phi_p - \frac{1}{2}\right) + C_1(t)\sin 2\phi_p \; + C_2(t)\cos^2\phi_p\right], \tag{2.2}$$

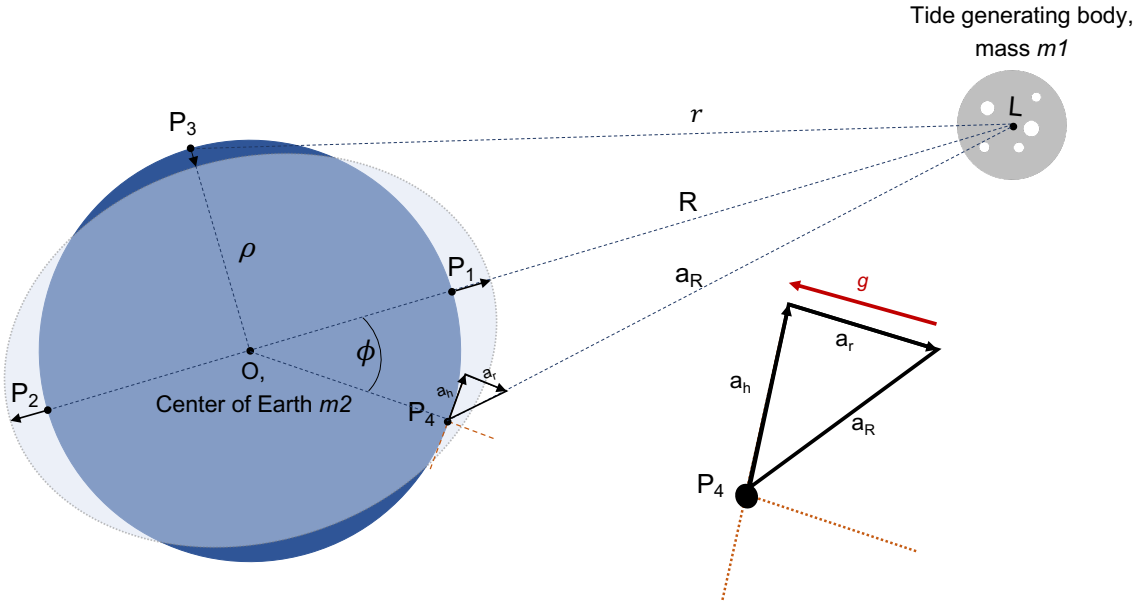

Figure 2.1 A schematic demonstrating the tide generating forces of the Earth-Moon system. Schematic inspired by Pugh and Woodworth (2014).

where m_c is the mass of the celestial object (which in most examples are the Moon, m_l, or the Sun, m_s) and m_e is Earth's mass.

The three time-dependent coefficients characterise the three main species of tides: long-period species $C_0(t)$, diurnal species $C_1(t)$ at one cycle per day ($cosC_p$), and semi-diurnal species $C_2(t)$ at two cycles per day ($cos2C_p$) which can all be expressed as (following Pugh and Woodworth (2014)):

$$\begin{aligned} C_0(t) &= \left(\frac{a}{R_l}\right)^3 \left(\frac{3}{2}\sin^2 d_l - \frac{1}{2}\right) \\ C_1(t) &= \left(\frac{a}{R_l}\right)^3 \left(\frac{3}{4}\sin 2d_l \cos C_p\right) \\ C_2(t) &= \left(\frac{a}{R_l}\right)^3 \left(\frac{3}{4}\cos^2 d_l \cos 2C_p\right). \end{aligned} \tag{2.3}$$

Here, R_l is the mean distance between the centre of Earth and the centre of the celestial object, d_l is the celestial body declination, and C_p is the hour angle of position P. Using this formulation, we can derive the $\bar{\zeta}$ decomposed by the contributions of each of these components. In Figure 2.2, the above equations for the derivation of the $\bar{\zeta}$ are done at the lunar declination zero. The long-period tides reach maximum amplitudes in the higher latitudes, with zero amplitudes being estimated at 35.27° north and south. For the diurnal tidal components, the amplitudes, and therefore the $\bar{\zeta}$, are zero at the equator and on the poles, while they reach maximums at 45° latitude. For the semi-diurnal tides, maximum amplitudes are seen around the equator and decrease towards zero at the poles. The combination of these components would cause the bulge towards the tide-generating object that would move from east to west around the Earth's surface.

In reality, this is clearly not the case as the water body is not unopposed by land masses, the bottom topography is not uniformly distributed, and the Earth's rotation influences the water bodies. This results in the observed ocean tides differing from the predicted Equilibrium Tides based on the dynamic response of the ocean to these forces. However, the Equilibrium Tide, although considerably smaller than the observed tides, remains crucial

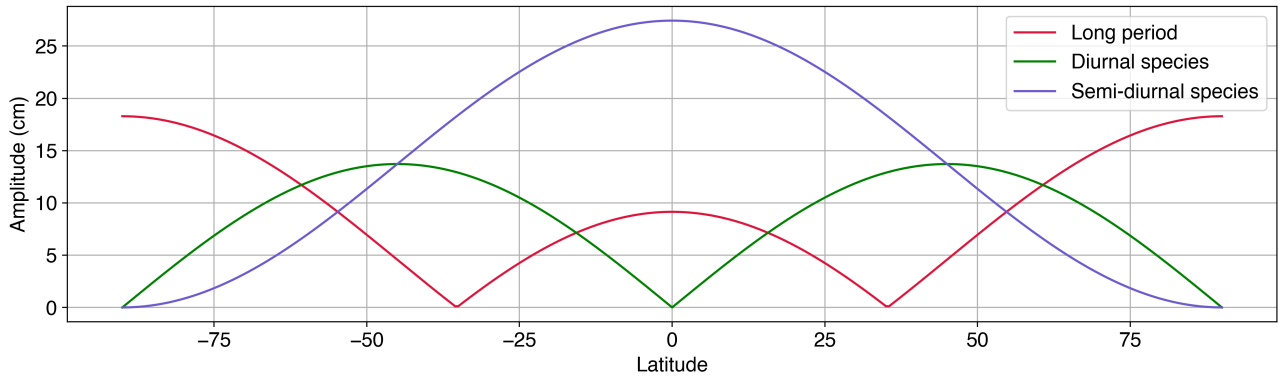

Figure 2.2 An example of the latitudinal differences of the Equilibrium Tide amplitudes as derived from Equation 2.2 for the long-period, diurnal and semi-diurnal tidal species'.

as a reference against which observed amplitudes and phases of tides can be related (Pugh and Woodworth, 2014), more on this later.

To describe how the different contributions make up the realistic tide, a schematic in Figure 2.3 is presented. In Equilibrium tide theory, the two high tide bulges rotate around the ocean surface aligned with the rotation of the Moon around the Earth or the Earth around the Sun. When applying simple land boundaries to a basin, as shown in Figure 2.3A, the high and low tide waves propagate horizontally across the basin and build at the respective boundaries until the tide-generating body causes the high tide wave to move across the basin. The additional factor of the rotation of the Earth causes the deflection through Coriolis forces of the water masses to the right and left in the northern and southern hemispheres, respectively. So when taking this into account, the tidal wave propagates around the basin as simply described in Figure 2.3B and C, which rotates approximately every 12 hours as shown in Figure 2.3D. The rotation of the tidal wave occurs around a fixed point, known as the amphidromic point, which itself experiences no variations in tidal height. The tidal heights in this idolised system increase with distance further away from the amphidromic points. Additional factors influencing the variations in the tides include the bottom topography, which can either amplify or reduce tides, the coastline structure, which influences the rotation of the tidal wave across a given basin (Pugh and Woodworth, 2014) as well as sea ice, which can dampen the amplitude of the tide.

The combination of all these contributions gives rise to the physical characteristics of the tidal components, and what makes this system even more complex is that these characteristics vary based on the tidal species as well as within the tidal species. To explain this further requires a bit more insight into the decomposition of ocean tides into individual tidal constituents. Recall Figure 1.1 where tide gauges were analysed based on the spectral density, and certain frequencies clearly stand out in both datasets. Although the dynamics experienced at individual tide gauges vary, these periodic oscillations induced by ocean tides are noted at all locations (Pugh and Woodworth, 2014). When assessing a time series of data, these individual frequencies of the ocean tide, termed tidal constituents, can be analysed separately. Several methods to do so exist, with two being discussed below: the harmonic method and the response method.

The harmonic method was first developed by Darwin (1891) and later refined by several, particularly by Doodson (1921). The principle is that the tidal signal can be decomposed into a finite number of tidal constituents of known constant frequencies. Therefore, the tidal signal at time t can be determined as the sum of these finite tidal constituents by using the following:

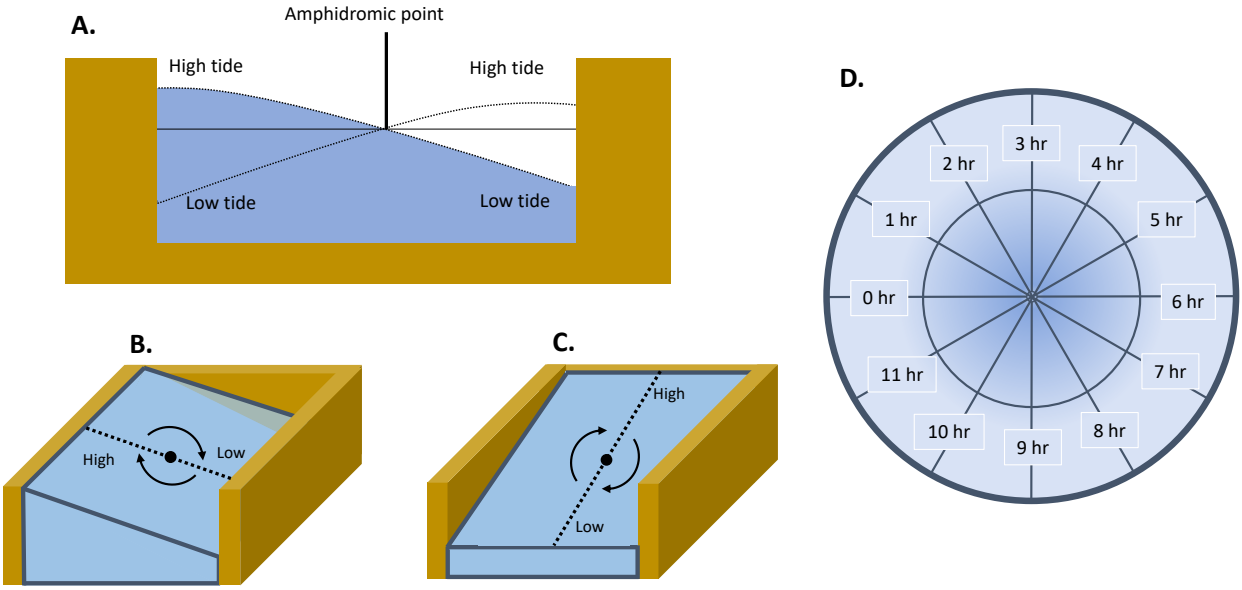

Figure 2.3 Schematic describing the dynamic nature of the ocean tides.

$$\zeta(t) = \sum H_n cos(\theta_n t - g_n), \tag{2.4}$$

where H_n and g_n are the amplitude and phase of the constituents n on the Equilibrium Tide, respectively, and θ_n is the tidal argument based on the angular speed in radians (Egbert and Ray, 2017). The tidal argument was re-expressed by Doodson (1921) in terms of six well-known variables which are unique to each constituent:

$$\theta_n(t) = k_1\tau(t) + k_2 s(t) + k_3 h(t) + k_4 p(t) + k_5 N'(t) + k_6 p_1(t) \tag{2.5}$$

with the terms described in Table 2.1. These known variables (k_1, k_2...) are referred to as Doodson numbers, and examples of several of the largest constituents are presented in Table 2.2. Modern studies often include a seventh argument, $k_7\pi/2$, not included in Doodson's work, which ensures that the cosine functions of each constituent have positive amplitudes (Egbert and Ray, 2017). The Doodson numbers in Table 2.2 differ from those originally described by Doodson by the addition of five for the second to the sixth numbers, to avoid any negative numbers in the notation, which makes it easier to use in applications.

Additionally, terms are added to Equation 2.4 to account for the nodal modulation of these tidal constituents. The nodal tide is a harmonic signal that is caused by the precession of the lunar ascending node, which varies over an 18.6-year period (Pugh, 1987; Parker, 2018; Hagen et al., 2021). Accounting for the nodal modulation for each constituent is done by incorporating amplitude f_n and phase modulation u_n terms into Equation 2.4 as follows:

$$\zeta(t) = \sum f_n(t) H_n cos(\theta_n t + u_n(t) - g_n). \tag{2.6}$$

The f_n and u_n terms can be derived simply based on the descriptions of Doodson and Warburg (1941) with an example of each presented for the M_2 tide here:

$$\begin{aligned} f &= 1 - 0.00041\cos\ell' + 0.00114\cos 2h \\ u &= 0.372^\circ \sin\ell' + 0.065^\circ \sin 2h, \end{aligned} \tag{2.7}$$

where $\ell' = h - p$ (Ray, 2022).

Table 2.1 Astronomical arguments taken from Egbert and Ray (2017)

Symbol	Definition	Period
τ	Mean lunar time	Lunar day
s	Mean longitude of Moon	Tropical month
h	Mean longitude of Sun	Tropical year
p	Mean longitude of lunar perigee	8.85 years
N'	Negative mean longitude of lunar node	18.6 years
p_1	Mean longitude of solar perigee	20,942 years

Table 2.2 The characteristics of the major tidal constituents within each tidal species, with the Equilibrium Tide amplitudes taken from Apel (1987).

Tidal Species	**Name**	**Doodson Numbers**	**Equilibrium Amplitude (m)**	**Period (hr)**
Semi-diurnal	n_1=2	$k_1k_2k_3k_4k_5k_6$		
Principal lunar	M_2	255.555	0.242334	12.4206
Principal solar	S_2	273.555	0.112841	12.0000
Lunar elliptic	N_2	245.455	0.046398	12.6584
Lunisolar	K_2	275.555	0.030704	11.9673
Diurnal	n_1=1			
Lunisolar	K_1	165.555	0.141565	23.9344
Principal lunar	O_1	145.555	0.100514	25.8194
Principal solar	P_1	163.555	0.046843	24.0659
Elliptic lumar	Q_1	135.455	0.019256	26.8684
Long Period	n_1=0			
Fortnightly	M_f	075.555	0.041742	327.85
Monthly	M_m	065.455	0.022026	661.31
Semiannual	S_{sa}	056.554	0.019446	4383.05

In application, accounting for these modulations has a large impact on estimations, with an example demonstrated in Figure 2.4. Here, the yearly M_2 tide is estimated through harmonic analysis of the Newlyn tide gauge obtained from GESLA-3 (Haigh et al., 2022). A clear 18.6-year cycle can be seen in the amplitude and phase estimations without applying the nodal correction, with some periods showing above 5-centimetre differences in amplitude estimations. Studies have also shown that the nodal modulation can change water levels by up to 30 centimetres, which can have serious implications on coastal processes (Peng et al., 2019).

2.2 Methods of tidal analysis

The harmonic method forms the basis for tidal analysis, ranging from satellite altimetry to tide gauges to modelling efforts. Within this thesis, the harmonic method is exclusively used either in deriving tidal constituents from sea level observations from satellite altimetry or in-situ observations or in producing tidal height predictions

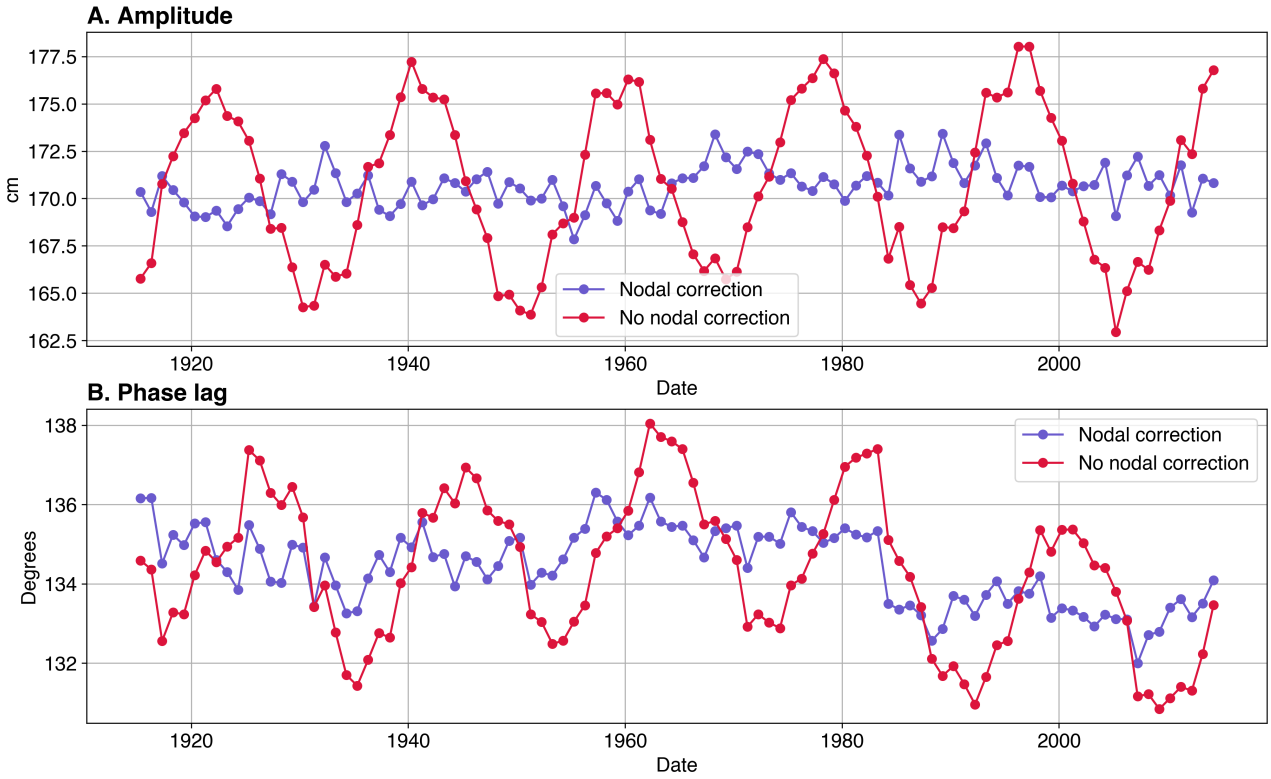

Figure 2.4 The yearly estimated (A) amplitude and (B) phase of the M_2 tide with and without applying the nodal modulation terms estimated from the Newlyn tide gauge in Cornwall, Great Britain, obtained from GESLA-3 (Haigh et al., 2022).

based on already known tidal constituents. However, another approach, the response method, is also commonly used and is briefly discussed below.

The response method for tidal analysis was first introduced in Munk and Cartwright (1966) and is based on electrical engineering techniques which describe that the output of a system is dependent on the input into the system as well as the response of that system (Pugh and Woodworth, 2014).

As described in Pugh and Woodworth (2014), in tidal analysis, the Equilibrium Tide is described as the input and the observed tidal oscillations as the output, with the response of the ocean to these gravitational forces being what is analysed in this method.

The basis of this method is the 'credo of smoothness' assumption (Munk and Cartwright, 1966), which assumes that the ratio of the output (observed tide) to input (Equilibrium Tide) of the system, also known as Admittance, does not vary dramatically in terms of frequency within one frequency band (e.g., in the diurnal or semi-diurnal band) (Pugh and Woodworth, 2014). This method has successfully been applied in tide modelling efforts from satellite altimetry for decades, particularly by the DTU series of ocean tide models (Andersen, 1995). Smith et al. (1997) compared both the harmonic and response methods and found millimetre differences in the estimated tides. Therefore, the selection between the two methods may be based on one's preferences, but one such reason for favouring the response method is that it does not succumb to the aliasing-related issues experienced by the harmonic method for the solar tides (Ray, 2007) (more on this later).

2.3 Measuring ocean tides

Regardless of the method used, tidal analysis relies heavily on sea level measurements to produce estimations. As the name suggests, tide gauges have been critical sources of data for advancing tidal understanding as well as for making predictions for centuries (Cartwright, 1999). Before the emergence of satellite altimetry, these gauges were the sole source to help develop and validate global tide models. In-situ measurements of tides, which can also be derived from ocean bottom pressure sensors (Ray, 2013) and GNSS Reflectometry (GNSS-R) (Tabibi et al., 2020), are deployed and maintained by governments and agencies, with several efforts being made to collect and harmonise all the available measurements (Holgate et al., 2013; Haigh et al., 2022).

These records have allowed for the continued study of the spatial and temporal characteristics of ocean tides as well as the evaluation of human influence, such as by land reclamation and flood defences (Haigh et al., 2020), on changes in tidal characteristics. Thanks to these data, early empirical tide models, models that are data-driven, were able to reach astonishing levels of accuracy. This is demonstrated by a global model developed in Schwiderski (1980) presented in Figure 2.5. The spatial characteristics of the M_2 presented in this model, including the positions of known amphidromic points and the direction of the waves, agree remarkably well with modern tide models. These early models, based on considerably less data than what is available currently, give great confidence to the theoretical understanding of ocean tides, which has continued to grow.

Despite the clear benefit of these in-situ measurements on our understanding of ocean tides, as well as other sea-level processes, these measurements do not provide full coverage of the ocean. There are several reasons for this. Firstly, the financial costs associated with either deploying or maintaining the instruments often result in poorer countries having considerably fewer deployments of tide gauges. On top of this, several political factors result in local governments not prioritising these types of long-term investigations. This can be seen in most maps of observations coverage, such as that of the Permanent Service for Mean Sea Level (PSMSL) (Holgate et al., 2013) as well as tide-specific databases such as TICON (Piccioni et al., 2019a) clearly demonstrating heavy weighting of observations to the northern hemisphere.

Tide gauges are usually fixed to the coast and, therefore, do not provide coverage across the shelf and open ocean regions. Here, studies have utilised ocean bottom pressure data to fill in data in these regions (Ray, 2013). However, the deployment and maintenance of the moorings to house the required sensors are extremely expensive, resulting in reduced spatial coverage of these observations. Furthermore, for both these measurement types, the polar regions are very poorly covered due to harsh weather and due to the sensitivity of data in these regions resulting from geopolitical reasons (Cancet et al., 2019).

In the mid-80s, a technique to measure the ocean's surface would be launched that would revolutionise our understanding of ocean tides and change ocean tide models forever: satellite altimetry.

2.4 Tides from and for satellite altimetry

The basic principle of satellite altimetry is that a pulse of microwave radiation with a known power is transmitted towards the Earth's surface, interacts with the surface, and part of the pulse returns back to the altimeter (Chelton et al., 2001; Andersen and Scharroo, 2011). The total travel time of each pulse is accurately recorded. The distance between the Earth's surface and the altimeter, also known as the range (R), is calculated based on the total travel time of the pulse. When using the orbital height of the satellite, H, which is usually referenced to

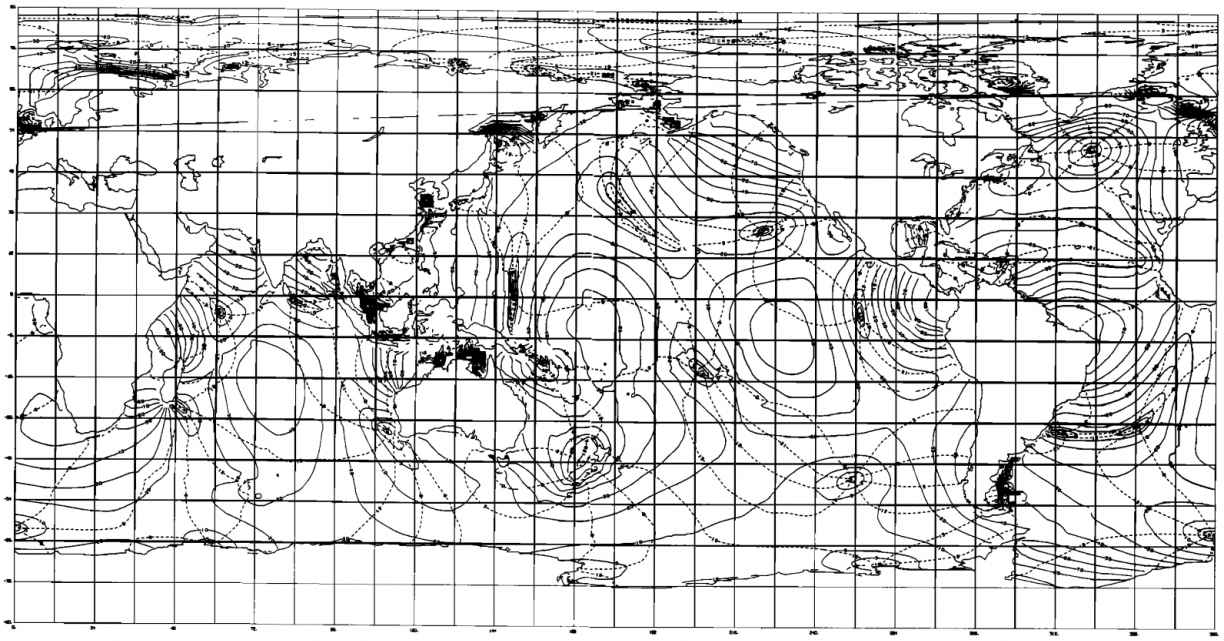

Figure 2.5 Global atlas of the amplitude (solid lines) and phase (dashed lines) of the M_2 tide, as derived by the Schwiderski model and taken from Schwiderski (1980).

an ellipsoid, the sea surface height (SSH) can be obtained following the formulation described in Andersen and Scharroo (2011):

$$SSH = H - (R + h_{geo}), \tag{2.8}$$

and the sea level anomaly (SLA) can be obtained by additionally subtracting the mean sea surface, mss, as:

$$SLA = H - (R + h_{geo}) - mss, \tag{2.9}$$

with h_{geo} being the range and geophysical corrections which are applied to account for processes which influence the pulse return. The recorded echo of the transmitted radar pulse, termed the waveform, also contains information about the roughness of the sea surface, such as the significant wave heights (Benveniste, 2011). The footprint of the pulse varies between 2 to 7 km over the ocean based on the significant wave height of the surface (Gommenginger et al., 2011). To obtain the highest possible accuracy of range measurements, particularly in the coastal regions, large efforts have been placed on waveform retracking (Gommenginger et al., 2011). Various approaches exist to retrack the waveforms, with recent advances showing significant improvements in both the accuracy of estimations and the number of retrievals in the coastal regions (Passaro et al., 2014) and in sea ice leads (Passaro et al., 2018b). The pulse repetition frequency of each satellite usually varies between 20 and 40 Hz, but the measurements are regularly averaged over 1 Hz along the satellite track, approximately every 7 km (Benveniste, 2011). In certain applications, such as in sea ice and coastal regions, the along-track averaging can occur at higher frequencies, with Pujol et al. (2022), for example, averaging the measurements into 5 Hz products ($\tilde{1}$.2 km). The repeat orbit and the cross-track sampling distance vary between the respective altimetry missions.

The launch of the Geosat altimeter, as well as the ERS altimeters, resulted in a great new perspective of the ocean surface, which was used in a variety of studies, including that of ocean tides (Cartwright and Ray, 1991; Andersen, 1995). However, the launch of the TOPEX/Poseidon on a tide-favourable, non-sun-synchronous orbit

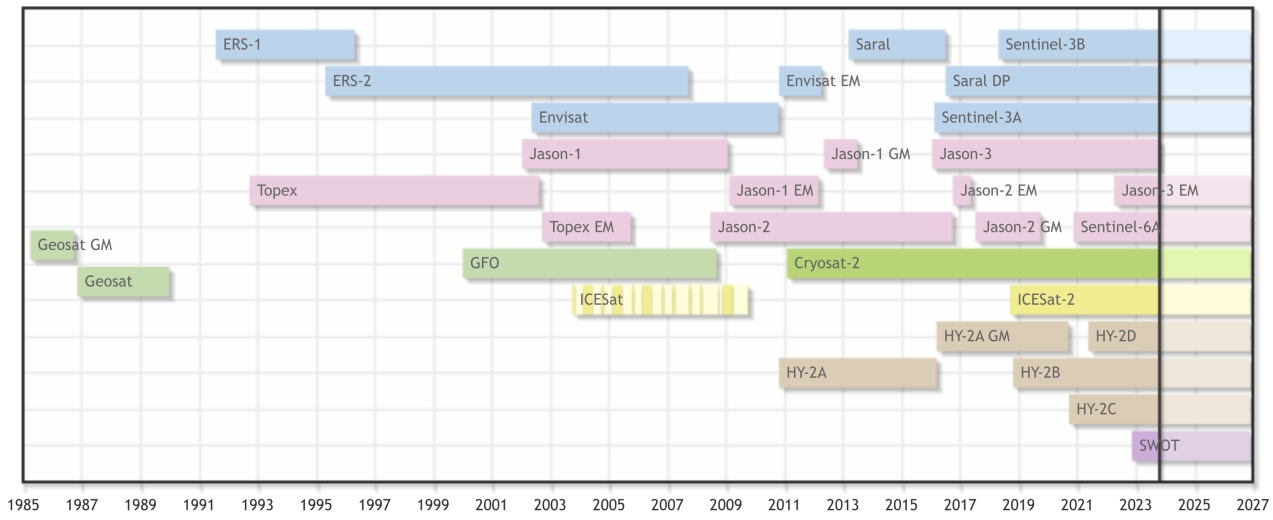

Figure 2.6 The available past and currently orbiting satellite altimetry datasets taken from the OpenADB website of DGFI-TUM (Schwatke et al., 2014).

in the early 1990s resulted in an even greater advancement in our global understanding of ocean tides. A few years after its launch, assessments of tide models showed significant advances in accuracy (Shum et al., 1997), and the field had taken a great leap forward in terms of our understanding of ocean tides.

Currently, several different satellite altimeters have flown and continue to fly, which can all contribute to the understanding of the ocean surface, with an overview of altimetry missions presented in Figure 2.6. As of 2023, over thirty years of continuous measurements have been made available from these satellites, with several efforts existing to continue the orbits of previous missions. This is particularly the case with the European Remote-Sensing Satellite (ERS), Envisat and Saral/ALtiKa (ERS/EN/SA) altimeters as well as the TOPEX/Poseidon, Jason and Sentinel-6a (TP/JA/S6) altimeters, which both provide near continuous measurements along a consistent orbit.

Satellite altimetry continues to allow for advances in our understanding of the physics of ocean tides (Ray, 2020b), resulting in continued improvements in the accuracy of tidal predictions. This is vital as ocean tides are a necessary geophysical correction to allow for the study of a variety of oceanographic processes from satellite altimetry, as in Equation 2.9. This is due to the tidal signal creating large variability within the retrieved estimations, so short and long-term time series analysis would be overwhelmed by these short-frequency signals, which can be seen in Figure 2.7A. Doing so, and doing so accurately, allowed for the further investigation of other sea surface processes, such as SLA and surface currents.

This resulted in significant efforts in ocean tide modelling to provide so-called tidal corrections for the respective satellite altimetry missions. These models can either be empirical, data assimilative or numerical models. Historically, models that rely on satellite altimetry observations perform the best in terms of providing accurate estimations of the tides (Stammer et al., 2014). This is largely thanks to the TP/JA/S6 series of altimeters, which have been orbiting on a tide-favourable orbit for over thirty years.

For these empirical models, SLA data is taken from altimetry missions, which have already been corrected for the ocean tides using a prior correction provided by a tide model, and residual tidal analysis is conducted to estimate the residual ocean tides. The tides estimated from satellite altimetry are of the residual geocentric tide, which requires an additional step to retrieve the ocean or load tide contributions. This is described in Chapter

4.3. These tides are usually reapplied to the original tidal correction to produce a new 'semi-empirical' tide model. This approach has successfully been used in several models (Savcenko and Bosch, 2012; Ray, 2013; Cheng and Andersen, 2017). Data-constrained or data assimilating numerical models, for example, FES2014b (Lyard et al., 2021), can provide high-resolution estimations of tidal constituents, which is extremely valuable in coastal regions. Furthermore, these models can provide estimations of a larger number of constituents as they are less restricted by aliasing-related issues.

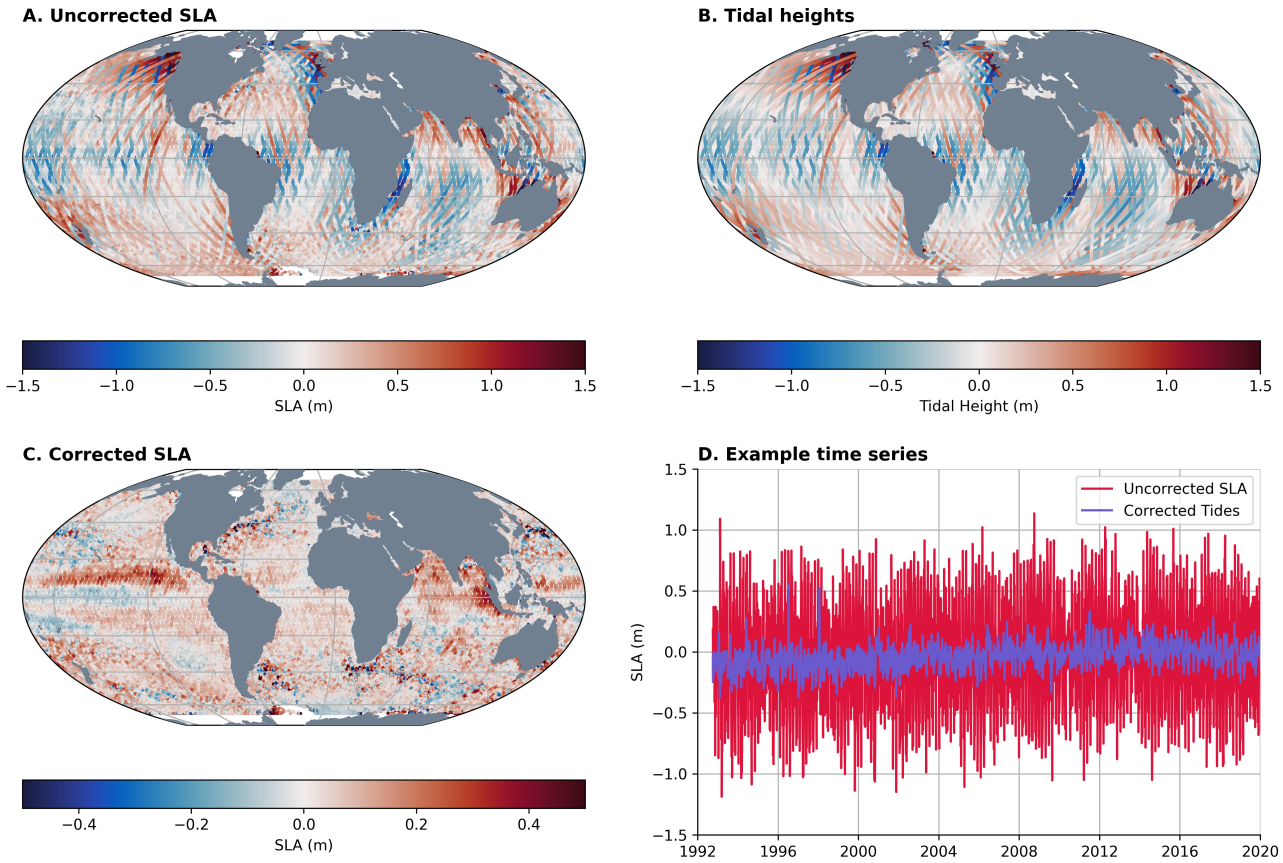

Figure 2.7 (A) Sea level estimation from a Jason-3 cycle which is not corrected for ocean tides. (B) The tidal height estimated from FES2014b (Lyard et al., 2021). (C) The sea level estimation corrected for the tides from B. (D) is a time series of a single along-track position either corrected or uncorrected for ocean tides.

As numerical models are never perfect with respect to reality, these semi-empirical models can serve as an adjustment to these numerical models, often resulting in improved model estimates (Savcenko and Bosch, 2012; Cheng and Andersen, 2017). Typically, the resultant tide models provide gridded maps of tidal constituents, which can be converted into tidal heights following the approaches mentioned in Equation 2.6 and Chapter 3.2, which are then applied to the satellite altimetry.

An example of a single cycle of Jason-3 is presented in Figure 2.7. When contrasting Figure 2.7A and B, the variations in SLA caused by ocean tides are clearly visible within both subplots, with it being difficult to interpret any other oceanographic feature in A. When the tides are removed (Figure 2.7C), more physical processes can be seen, such as the variability in SLA in western boundary regions such as the Agulhas Current and the Gulf Stream. Furthermore, the time series of a single position (Figure 2.7D) contains much less noise and experiments on local changes in sea level, and long-term changes can be better interpreted.

2.4.1 Geophysical corrections

Although tidal estimations from satellite altimetry are reaching high levels of accuracy, limitations remain. In the coastal regions, the retrieval of altimetry data is impacted by land contamination of the radar returns (Passaro et al., 2018b). This is particularly crucial as tides in near-shore regions are extremely variable (Egbert et al., 2010). Further, most observations used to validate model developments are susceptible to these tidal dynamics, which the altimetry simply cannot see, making validating the models difficult. The issue of radar retrieval in the polar regions is similar, as sea ice restricts accurate retrieval of SLA data, particularly in the winter months, biasing the tide estimations to summer months (Bij de Vaate et al., 2021). On top of the altimetry retrievals themselves, the choice of geophysical corrections used to determine the SLA also influences the tidal estimations.

Several corrections are usually applied to obtain the SLA, particularly in the context of residual tidal research, which is as follows: the dry troposphere, wet troposphere, ionosphere, dynamic atmosphere, load tide, ocean tide, solid Earth tide, pole tide, and mean sea surface (Andersen and Scharroo, 2011). Additional corrections can also be included, such as the mesoscale (Zaron and Ray, 2018; Ray and Byrne, 2010) and internal tide corrections (Zaron, 2017). However, research is still being conducted on whether these corrections should be applied globally in the context of ocean tidal research. Much like the tidal correction, these corrections are modelled by numerical or empirical models, which are themselves not perfect in their accuracy. Besides the general accuracy issues, errors at tidal frequencies are especially critical, particularly for solar tides driven by the daily solar cycle. These geophysical corrections also have regional strengths and weaknesses. The selection, therefore, of these geophysical corrections can have a significant impact on the tides and deciding the set of corrections is not always a trivial task.

To demonstrate the presence of tidal frequencies within geophysical corrections, harmonic analysis is done on two different ionospheric corrections based on thirty years of TP/JA/S6 data (Figure 2.8) inspired by Ray (2020a) who described differences in tidal frequencies within ionospheric corrections, which can particularly be seen in the amplitude differences of the two presented constituents. The selection of the orbit solutions based on the different reference frame realisations also affects the tidal estimation, particularly when multiple altimeters are used using different orbit solutions (Ray et al., 2023).

Radiational, tides generated by the atmospheric and solar forcings (Williams et al., 2018), and gravitational tidal components cannot be well separated from measurements due to the generation of tides at the same frequencies within both components, meaning ocean tide models include both of these components within (Carrere et al., 2016). The danger here lies in the potential double-counting of these tides within the model, which has been discussed in several studies (Ray and Ponte, 2003; Williams et al., 2018).

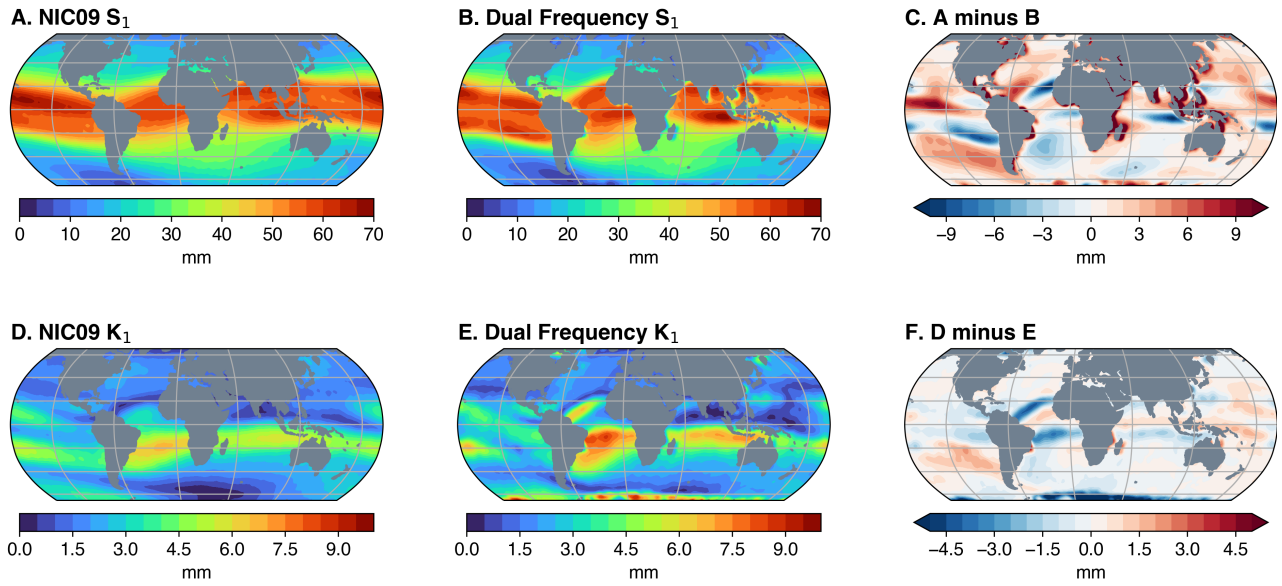

Figure 2.8 The S_1 [A and B] and K_1 [D and E] amplitudes determined from two different ionospheric corrections and their respective differences [C and F]. Inspired by Ray (2020a).

The Dynamic Atmosphere Correction (DAC) is applied in altimetry applications to account for the atmospheric contribution to the radar return. Radiational tides majorly influence the DAC, but additional processing is done to this correction to remove the contributions of these tides from the correction (Carrere et al., 2016), allowing for altimetry-derived models to appropriately estimate these tides. This particular processing of the DAC has resulted in advances in tidal estimations as well as sea level estimations (Carrere et al., 2016). However, as this correction is model-based, tidal frequencies remain within this correction (Ray et al., 2023), which could result in an overestimation of the respective constituents.

Tidal aliasing

Several altimetry missions can be used in the estimation of ocean tides, which all have different orbit characteristics in terms of latitudinal extent and repeat sampling (Table 2.3). The most commonly used series of altimeters for tidal estimations is the TP/JA/S6 series. The orbit of TP/JA/S6 is specifically designed to be tide favourable (Provost et al., 1995), with the repeat sampling frequency designed to reduce tidal aliasing. Tidal aliasing, i.e. the misrepresentation of tides, is caused by the temporal sampling of the altimeter missions, meaning extended time-series lengths are required to appropriately resolve specific tidal frequencies. As the altimeters do not revisit the exact locations at periods sufficient for that of tidal frequencies, these tidal frequencies are under-sampled according to the Nyquist theorem and, therefore, aliased to longer periods (Parke et al., 1987).

These aliased periods vary from constituent to constituent and from satellite to satellite depending on the orbit of the respective missions (Andersen, 1995). For the major tidal constituents, these aliasing periods do not hinder the determination of tidal constituents as the altimeters being used often have followed the same repeat orbits for years, if not decades. To simply illustrate how the aliasing effect comes about, Figure 2.9 presents an example for three constituents of different frequencies. In this example, the constituents are sampled every one day (blue line), which results in the M_2 and N_2 constituents being aliased onto sinusoids of much longer periods. With a sufficient time-series length, these constituents are still resolvable, requiring 14.77 and 9.61 days worth of data, respectively. However, for the S_2 constituent, the one-day sample measures the same position or phase

on the S_2 sinusoid and, therefore, does not allow for the capturing of the tide. This illustration is the same in sun-synchronous satellites, which also do not capture the full characteristics of the tide and have infinite aliasing periods for these constituents.

These aliasing period, f_a for a satellite with a repeat orbit of P days can be determined using several approaches (Parke et al., 1987; Wang, 2004), with the formulation by Wang (2004) given as:

$$f_a = MOD(\frac{f_k + f_s}{2}, f_s) - \frac{f_s}{2}, \tag{2.10}$$

for a constituent with a frequency f_k and a satellite with a frequency f_s. Figure 2.10A provides the respective aliasing periods of several constituents based on the TP/JA/S6 and the ERS/EN/SA series of altimeters.

Table 2.3 The orbit details of several altimetry missions used within this thesis.

Altimeters	Repeat Cycle (days)	Latitudinal range
TP/JA/S6	9.9156	±66°
ERS/EN/SA	35	±81.45°
Sentinel3a/b	27	±81.5°

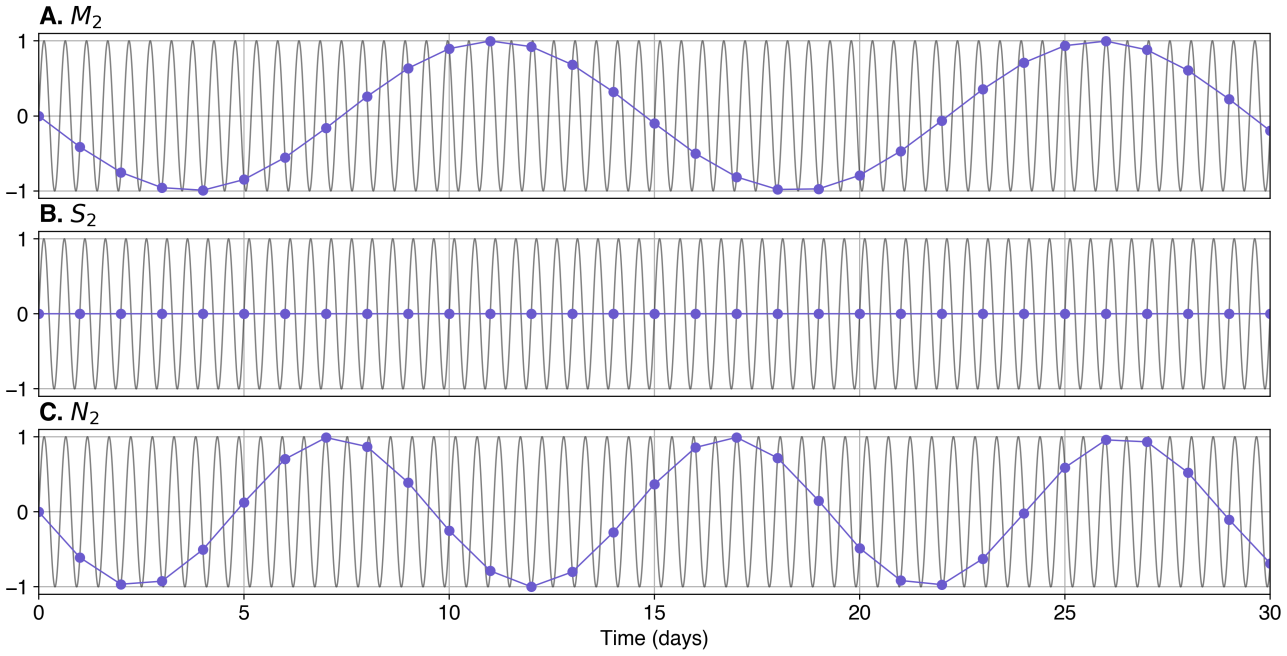

Figure 2.9 Schematic of three tidal constituents sampled at exactly one day, with the black line representing the tidal amplitude over time while the blue line represents the sampled tidal amplitude every one day.

It can be seen that for these daily and twice daily tides, several weeks of data from these repeat orbits are required to appropriately resolve these tides. Furthermore, due to the sun-synchronous orbit of the ERS/EN/SA series, it is not possible to resolve the S_1 and S_2 tides as their aliasing periods are infinite. Several other tidal constituents are aliased to annual or semi-annual periods, which is problematic as this corresponds with frequencies of substantial non-tidal ocean variability (Ray, 2007).

An additional consideration when determining tidal constituents from altimetry that needs to be taken into account is the separation of constituents with comparable frequencies. This is determined through the Rayleigh

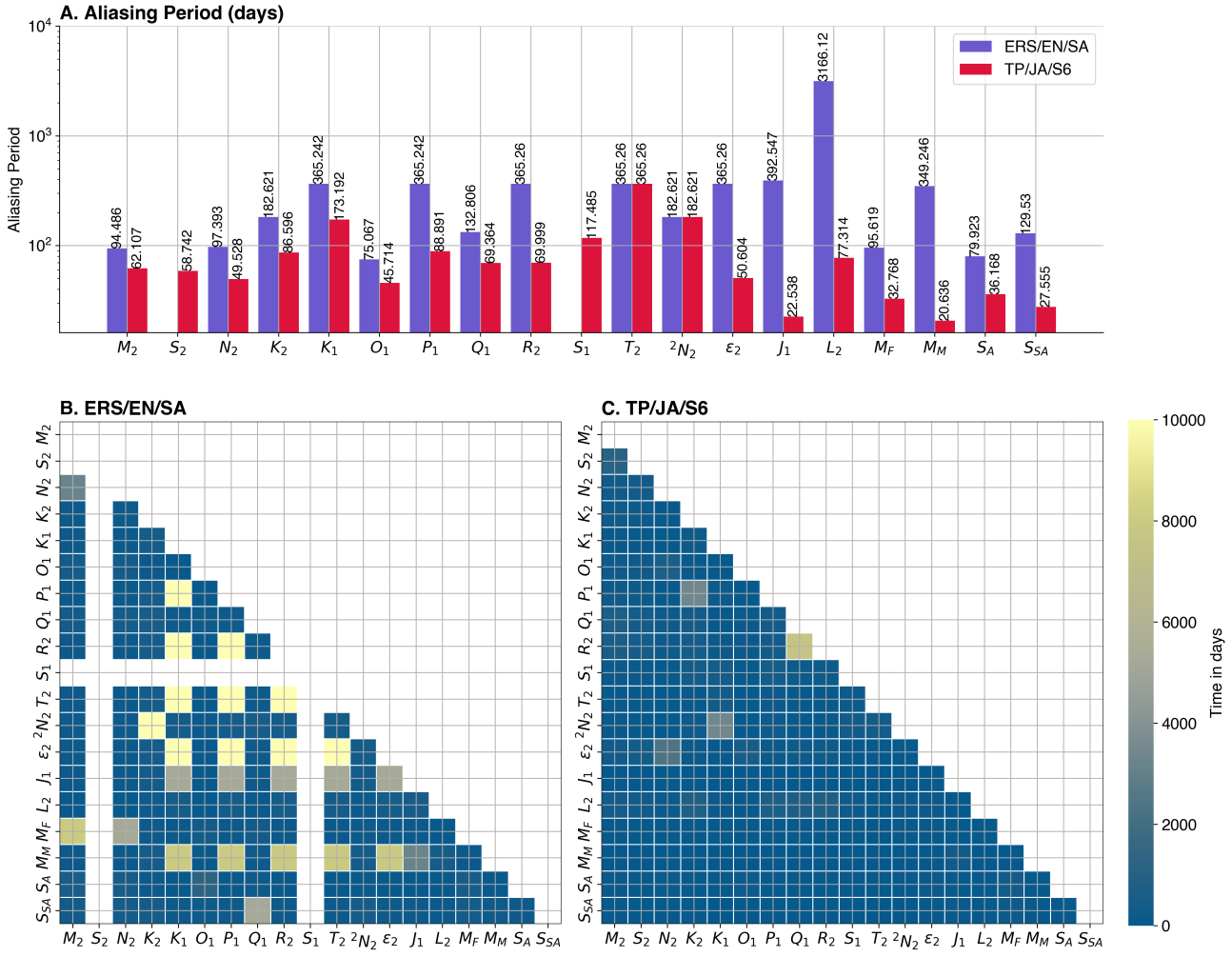

Figure 2.10 [A] The aliasing period in days of the ERS/EN/SA and TP/JA/S6 satellites as well as the Rayleigh criteria calculated for these satellites, respectively [B and C].

criteria, which calculates the length of time series required to separate tidal constituents from one another based on the sampling frequency (Tierney et al., 1998; Savcenko and Bosch, 2007). Although these constituents are determinable, errors creep in when insufficient time-series lengths are used. Like the aliasing period, these criteria vary between constituents and altimeters. An example is given in Figure 2.10B and C, where the Rayleigh criteria in days are determined for ERS/EN/SA and TP/JA/S6 satellites. This demonstrates the difficulty of separating several constituents in ERS/EN/SA, not only for the main solar tides S_2 and S_1, which are aliased to infinity but also other solar constituents such as K_1 and P_1, which require a long time-series to separate. This further highlights the benefit of the TP/JA/S6 tide favourable orbit. Although most altimetry-based tide estimates are based on the larger tidal constituents, several studies are being done to derive more and more constituents of relatively small signals (Ray, 2020b).

The derivation of these constituents directly is essential to correctly resolve the full tidal signal (Ray, 2017) but, without using any admittance approaches (Munk and Cartwright, 1966; Petit and Luzum, 2010), is challenging due to how small these components can be with respect to altimetry-based noise. The amount of noise in the SLA data may come from altimetry processing-related errors (Zaron and de Carvalho, 2016), particularly in the coastal regions, or noise generated from non-tidal oceanic variability (Zaron and Ray, 2018). These effects vary

between regions and can cause substantial errors in tidal estimations with, for example, Ray and Byrne (2010) demonstrating significant improvements in along-track estimation of tides when using a mesoscale correction to remove non-tidal variability from the SLA. These effects all mean that the selection of tidal constituents to be derived from satellite altimetry requires care to provide the most suitable tidal estimation without introducing significant errors.

CHAPTER 3

VALIDATION TOOLS AND DATASETS FOR GLOBAL OCEAN TIDE MODELS

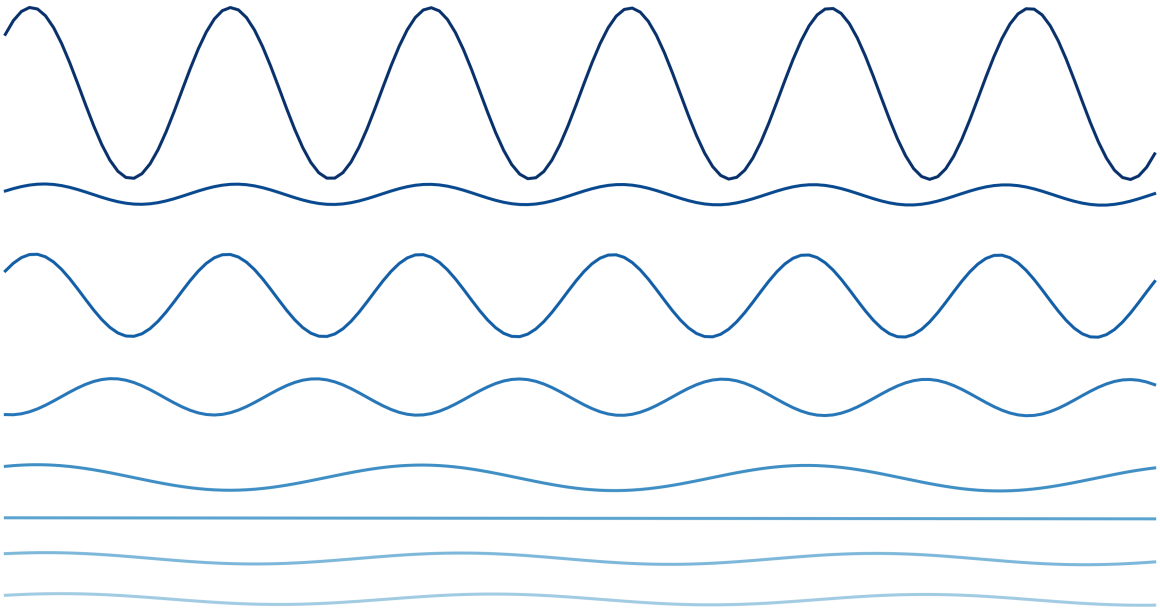

Topex/Poseidon was the most successful ocean experiment of all time

- Walter Munk

3 Validation tools and datasets for global ocean tide models

3.1 In-situ databases

In-situ databases are crucial sources of information for not only understanding tidal processes but also in the validation of ocean tide model developments. Regarding model validation, tide gauges and ocean bottom pressure sensors have been used in several studies (Stammer et al., 2014). TICON (Tidal Constants) is a DGFI-TUM developed database of tidal constituents derived from the GESLA-2 dataset (Woodworth et al., 2016) with the primary objective being to serve as an independent validation dataset for model developments (Piccioni et al., 2019a). In this thesis, two separate updates of this dataset were produced for applications within and outside of this thesis: TICON-td and TICON-3. An additional dataset created for the Arctic Ocean region, ArcTiCA, is presented and discussed. These three datasets are independent of one another and contain different processing steps based on the objectives of each dataset. These are described in the following subsections.

3.1.1 TICON-td: third-degree tidal constituent dataset

Studies of third-degree tides have become increasingly common in recent years, largely driven by the more than thirty years of continuous altimetry observations (Ray, 2020b; Woodworth, 2019). Although these tides are considered relatively small, especially compared to the amplitudes of the semi-diurnal and diurnal tides, in some regions, their amplitudes can reach the centimetre scale, making them important for accurate derivation of the full tidal heights. In this thesis, a special update to TICON, termed TICON-td (third-degree), was produced, with the objective being to utilise this dataset in the validation of four third-degree tides estimated from a numerical tide model. These four tides were: ${}^3M_1$, ${}^3M_3$, ${}^3N_2$ and ${}^3L_2$. Evaluating these tides both from in-situ measurements and numerical models is crucial in examining the importance of these constituents, in particular on the full tidal correction estimation, as well as in providing insight on what the best method is to derive these third-degree constituents. The major change, in comparison with the full TICON database, was the restriction of the tide gauge time series to lengths that exceed ten years. To be consistent with previous studies of these tides, the nodal corrections were also applied to these constituents and were taken from (Ray, 2020b). This was done in an attempt to improve the reliability of the estimations of these constituents due to these tidal frequencies being similar to frequencies of degree-two tides and, therefore, requiring a long time-series of observations to properly separate (Ray, 2020b; Sulzbach et al., 2022). Additionally, a mean surrounding depth, within a two-degree radius, of the tide gauge was estimated to allow for the removal of all gauges that have a mean depth of less than 500 meters in order to only select gauges that are further from coastal regions. This step was done based on the requirements of the experiment of comparing these results with a numerical ocean tide model, TiME (Sulzbach et al., 2021), which was not optimised for the coastal regions.

Finally, based on the experiment requirements, gauges that are within two degrees of one another are removed so that the mean statistics are not influenced by duplicates of the same processes, which may either benefit or harm the overall evaluation of the model. The resultant dataset, TICON-td, is provided in **AD-4** and was used to validate a global tide model in **AP-1** (Sulzbach et al., 2022).

3.1.2 TICON-3: global tidal constituent dataset

In late 2021, an update was made to the GESLA database (GESLA-3, Haigh et al. (2022)), which increased the number of high-frequency tide gauge measurements globally almost three-fold. Not only were the number of tide gauges significantly increased, but already available tide gauges time series were also extended. This update meant that an update to TICON was necessary to incorporate all these new datasets, termed TICON-3.

For the most part, the fundamentals and eventual results of TICON-3 match that of the original TICON database, including the inclusion of the same forty tidal constituents. The main differences in the processing are as follows: 1) a stricter time-series length constraint of at least one year of data and 2) an additional description of the position of the gauges. The first point was made to reduce the usage of tide gauges that have less than one year's worth of data, either due to the availability of data only being a few months or due to having large gaps within the data. The reasoning behind this was to reduce the potential error in resultant tidal estimations that occur from having too few observational points. This is particularly relevant to tides with small amplitudes or have long periods as they require a relatively long time series to safely determine from sea-level measurements.

The second point, relating to providing the geographical location of the in-situ tide gauge, was made possible by the inclusion of this information within the GESLA-3 database. This information may be necessary for users of the TICON-3 database to determine the usability of the tide gauge in their respective applications. Three labels are provided within the database: "Coastal", "Lake", or "River".

The resultant developed TICON-3 database was published on Pangaea (**AD-3**). This new dataset included 3,471 tide gauges globally (Figure 3.1), which was an increase of 2,326 tide gauges with respect to TICON. The new dataset also contains more extended time series, crucial for the reliability of tidal estimations. The overall changes in the mean amplitude and phase of all forty constituents further highlight the value of the increased time-series lengths (shown in the User Manual of **AD-3**), with some gauges having changes in mean amplitudes that exceed a few millimetres. Although small, these changes in amplitude and phase estimations are useful in the application of this dataset for the validation of tide models. This dataset was used in the validation of tide modelling efforts produced in **P-3**.

3.1.3 ArcTiCA: Arctic tidal constituent atlas

Tides in the Arctic Ocean play a crucial role in the distribution of sea ice as well as in the mixing of deep Arctic waters (Kowalik and Proshutinsky, 1994). Historically, empirical tide models do not provide estimates of tides in the higher latitudes due to the lack of coverage of tide-favourable altimetry missions above and below 66°N and 66°S, respectively. Although altimetry missions have flown above these latitudes for decades, their sun-synchronous orbits have meant they were unfavourable for reliable tidal estimations in the regions. In recent years, the Cryosat-2 mission has provided unprecedented coverage in these regions, reaching latitudes of 88° and having a repeat orbit of $\tilde{3}69$ days. This repeat orbit itself is also impractical for tidal estimations, but what makes Cryosat-2 useful for tidal estimations is the sub-cycles of the mission.

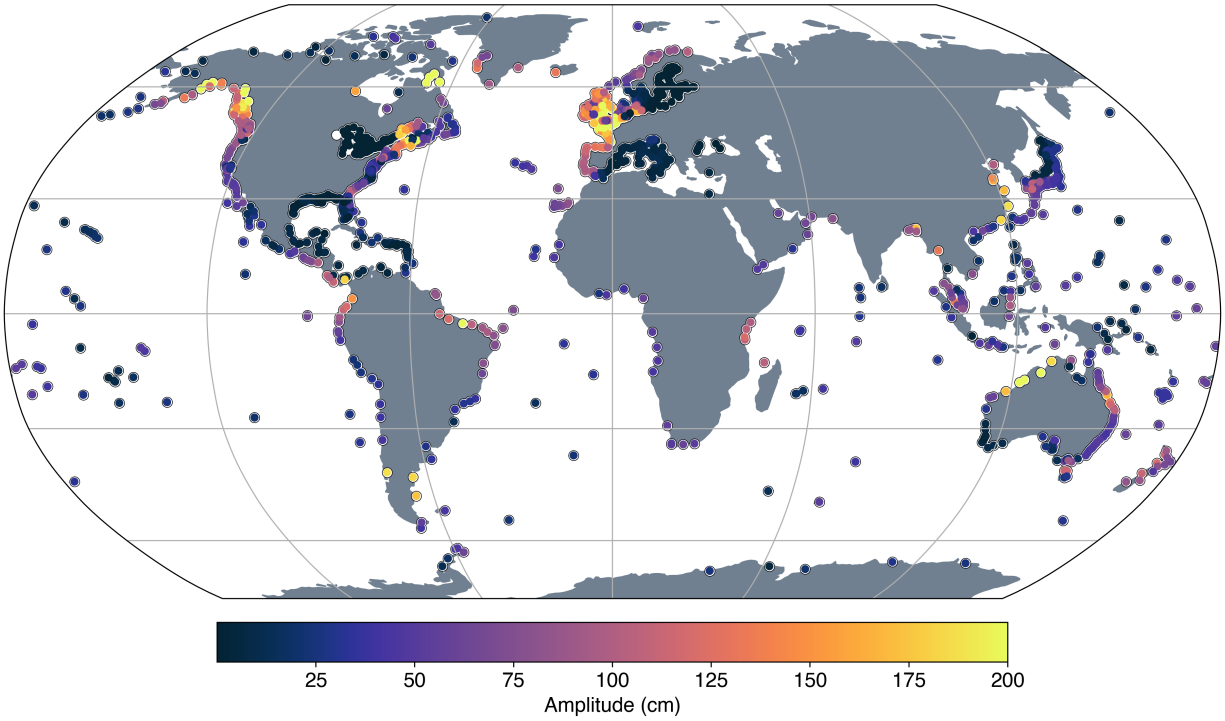

Figure 3.1 Global distribution of the TICON-3 database, showing the estimated amplitude of the M2 tidal constituent.

These near-repeat sub-cycles occur as the spacing of the satellite tracks begins to reduce towards the higher latitudes. Zaron (2018) demonstrated how these sub-cycles can be used to make reliable estimations in the Antarctic region, with this methodology applicable to the Arctic Ocean as well. These results have demonstrated the ability of future empirical models to make tidal estimations into these regions.

With future development work in mind, in-situ databases for these regions become increasingly crucial to allow for the validation of model developments. Global databases of tidal constituents, such as TICON-3, contain very limited observations in both the Arctic and Antarctic regions based on the sea-level databases used containing limited datasets in these regions. An effort to increase the amount of tidal constituent data in the Antarctic has been made and was published in Howard et al. (2020). For the Arctic Ocean, no such database exists. In the TICON-3 dataset, only twenty-one gauges are available above 70°N, with the distribution being focused around North America and the northern European coasts.

In an attempt to resolve this lack of in-situ data, a concerted effort was made to produce an Arctic Ocean database of tidal constituents based on a variety of different data sources. This effort resulted in the creation of the Arctic Tidal Constituent Atlas (ArcTiCA), with the dataset itself published (**AD-6**) and the associate manuscript available (**AP-2**). Within this dataset, over 1,900 tidal constituent measurements are provided, with 399 of these being found above 70°N (Figure 3.2). A total of 29 different data sources are used to provide data, which is time-series data from tide gauges, ocean bottom pressure sensors and GNSS-R, as well as tidal constituents derived from available datasets and previously published scientific literature. As far as possible, all available metadata is provided for every entry within this dataset to help users determine its usability for respective applications. Additionally, two different flags were created and provided within this dataset, which are aimed at aiding users with making judgements on the reliability of the estimations. The usability of this data is demonstrated in Chapter 5.2.

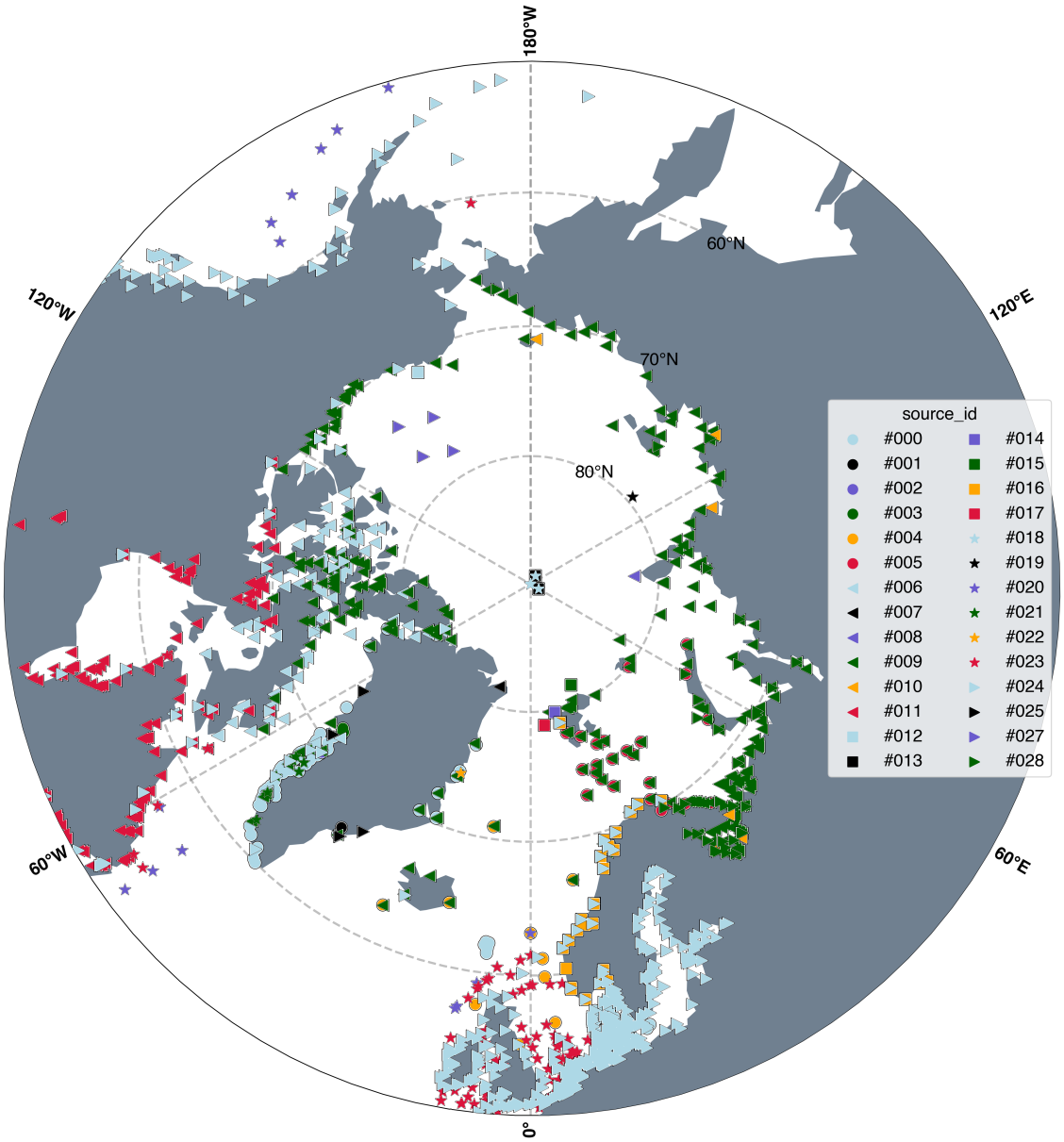

Figure 3.2 The distribution of the sources of data used to create the ArcTiCA dataset.

3.2 TIPTOE: tidal prediction in the ocean

Tidal constituents from tide models or from in-situ measurements have long been used to provide predictions of tidal height. Over the years, the approaches to do so have evolved, and currently, several software programs exist to make such tidal predictions (Pawlowicz et al., 2002; Codiga, 2011, e.g.). For this thesis, where requirements for prediction software were not met by publicly available software, a new software program termed TIdal Prediction in The OcEan (TIPTOE) was developed. This development allowed for the prediction of ocean tides from in-situ-based measurements as well as tide models, which is common in most software programs, but also allowed for the easy experimentation on minor tide inference techniques as well as the merging of two (or more) different ocean tide models.

Going from tidal constituents to a tidal height prediction is well documented and is described in Chapter 2.1 and in greater detail within Schureman (1958) and Pugh and Woodworth (2014). Most tide models contain varying numbers of tidal constituents, but in most applications, linear admittance approaches (Munk and Cartwright, 1966; Petit and Luzum, 2010) are used to infer constituents when they are not provided. Although in an ideal world, direct estimations of all tidal constituents are preferable, this is not always possible due to a variety of factors. For altimetry-based estimations, a major limitation on the estimation of constituents is the signal-to-noise ratio of the altimetry data used when trying to estimate the smaller tidal signals. Additionally, aliasing issues (Chapter 2.4) means insufficient data is available to safely estimate certain tidal constituents. Hence, for altimetry-based estimations of certain tidal constituents, linear admittance can make a more accurate estimation.

An example demonstrating the multiple capabilities of the TIPTOE software is presented in Figure 3.3 where the tidal height is estimated in multiple scenarios at a point in the German Bight (54°N, 8.5°E) over 24 hours. The examples are 1) using only the M_2 tide from EOT20; 2) using the major eight tides from EOT20; 3) adding linear admittance estimations of eighteen constituents onto the major eight tides from EOT20; and 4) combining the eight major tides from EOT20 with twenty-six constituents from FES2014b. The combination of tide models to form one tidal correction is unique, at least currently, in the TIPTOE software and allows for the optimisation of the tidal height estimation based on using constituents from different tide models.

The software is used to make the tidal correction for along-track altimetry but can also be used to make gridded estimations of the tidal heights. A Jason-3 cycle is presented for the Atlantic Ocean, where the ocean tide height is estimated from the EOT20 model (Figure 3.4A). This cycle of Jason-3 orbits for about ten days, which means that the tides themselves are extremely variable between passes, as expected. This tidal correction is then used to estimate the SLA from the along-track data, which can then be used in a wide variety of applications. Additionally, the tidal heights can be used on grids to derive tidal heights over wide regions, which better describes the variability of the tides over time. An example of six-hourly time steps of a one-day period for the Atlantic Ocean is given in Figure 3.4B-E, which shows how significantly the tides vary over six-hour periods across the Atlantic Ocean and demonstrates a capability of TIPTOE to predict tides at any point across the ocean from any ocean tide model. TIPTOE was used in both **P-1** and **P-2** to derive ocean tidal corrections from the respective models, which were eventually used to evaluate the accuracy of the tide models.

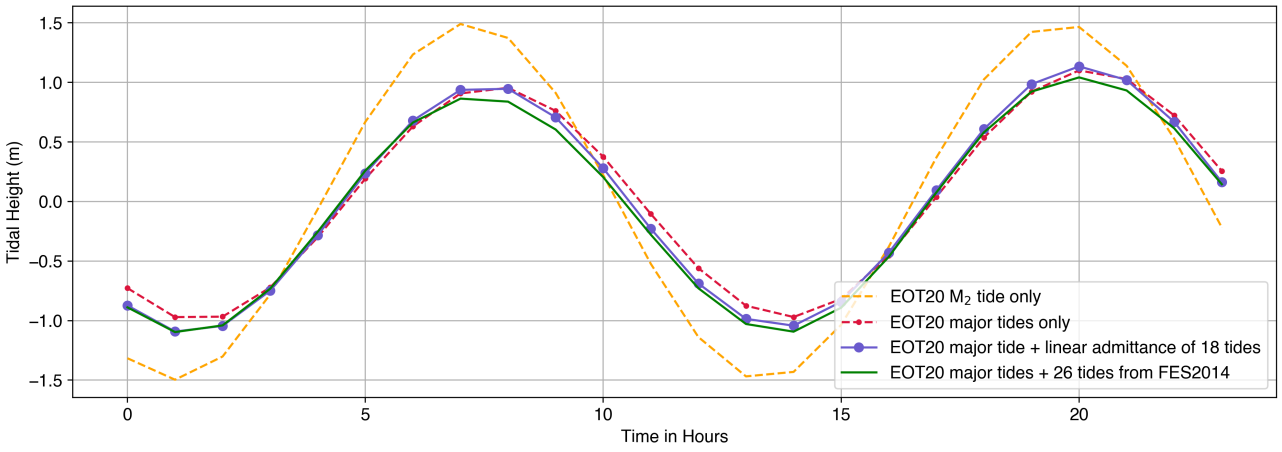

Figure 3.3 Demonstration of the capabilities of the TIPTOE software to predict the tidal height over time in multiple scenarios.

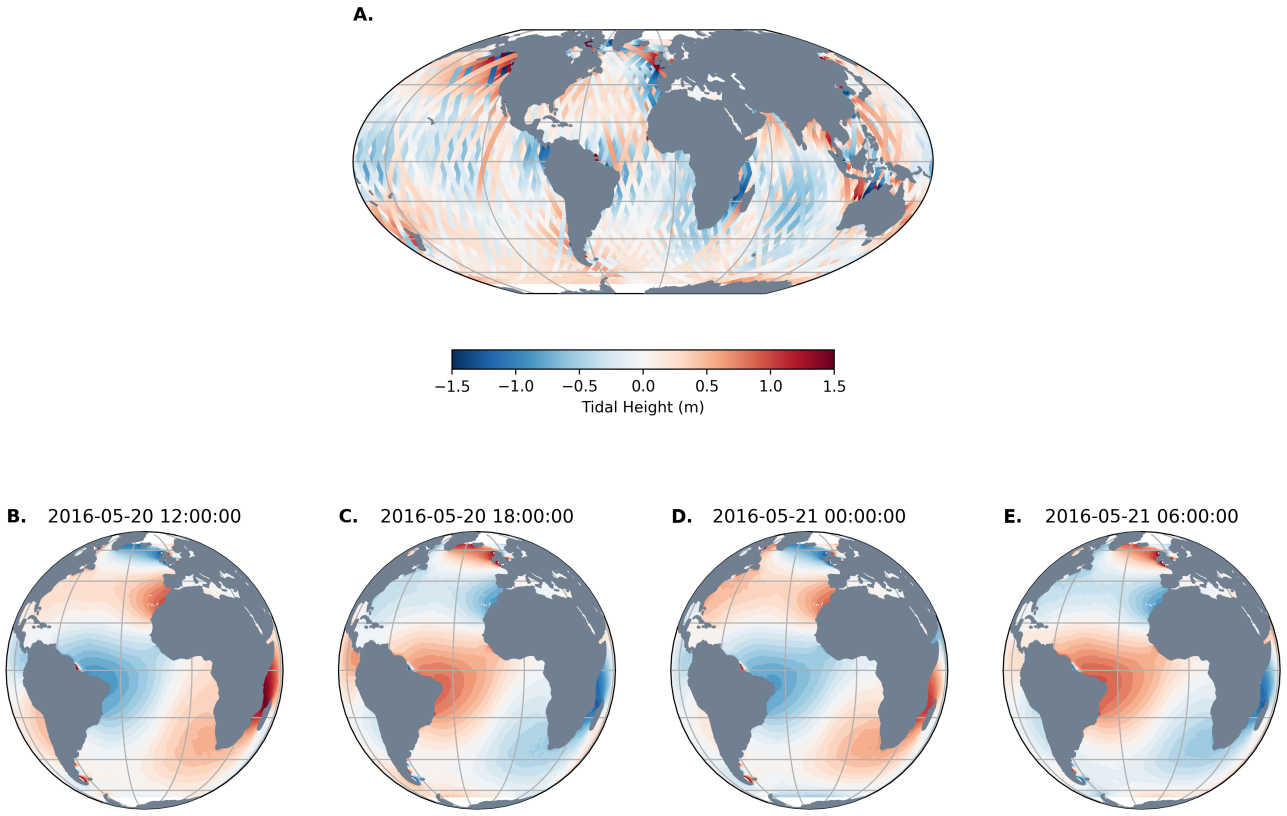

Figure 3.4 The tidal height estimated from EOT20 constituents for cycle 10 of Jason-3 (A) and across the entire Atlantic Ocean for 24 hours (B to E).

3.3 SLAVA: sea level anomaly variance analysis

Once the ocean tide correction has been created, this can be applied as a geophysical correction to derive the SLA from the along-track satellite altimetry described in 2.1. This presents the opportunity to evaluate the accuracy of ocean tide models by assessing the impact the different tidal corrections have on the variances of the SLA. The idea behind this is that when the ocean tides are more accurately removed in the creation of the SLA, there would be a reduction in SLA variances. Therefore, the best-performing correction should reduce the variances of the SLA the most. When complemented with tide gauge assessments of tidal models, this technique can be crucial for assessing model developments, particularly in the open ocean, where in-situ measurements are limited. This approach has been used in several studies to evaluate corrections, including for ocean tide models in the validation of the FES2014b model in Carrere et al. (2021).

With that in mind, the gridded SLA Variance Analysis (SLAVA) approach was developed and used in this thesis. The approach used is as follows:

1. Estimate the SLA using the desired set of geophysical corrections.
2. Grid the SLA into four-by-four-degree grids for each cycle of the selected mission to allow for comparison between missions on different orbits.
3. Once completed for the entire mission, the overall mission variance for each grid cell is estimated.
4. Switch out a single geophysical correction, e.g. the ocean tide correction, and repeat steps 1 - 3.

5. Contrast the two different estimated SLA variances.

The results of the above procedure will provide an overall mean-variance difference between the corrections used but also express this on the global map to provide regional differences.

An example of the results of SLAVA is presented in Figure 3.5, where the same set of geophysical corrections were used to determine the SLA for the Sentinel-3A altimetry mission, with the ocean tide correction being changed to be either EOT20 (**P-1**) or GTSM (Wang et al., 2022a). In this example, where an empirical tide model is compared to a numerical tide model, both products demonstrate known causes of variances of altimetry data within western boundary currents. The variance of the SLA generated using GTSM was subtracted from the SLA variances generated using EOT20 (Figure 3.5C) with negative values, shown in blue, indicating a higher variance from GTSM and positive values, shown in red, indicating a higher variance from EOT20. This example shows an overall reduction in variance when using EOT20 as the tidal correction, which is somewhat expected based on EOT20 being designed for altimetry applications. Of equal significance are the regional variations in the variance differences, which is helpful for the development of both models in identifying where additional effort is required to understand the degradation of tidal estimations.

SLAVA was used in both **P-1** and **P-2** of this thesis as a tool to evaluate ocean tide model developments as well as to evaluate the inclusion of minor tidal constituents from different approaches. Additionally, SLAVA was used in a study to evaluate the use of two different altimetry retrackers for the Sentinel-3A mission in **AP-4** Passaro et al. (2022).

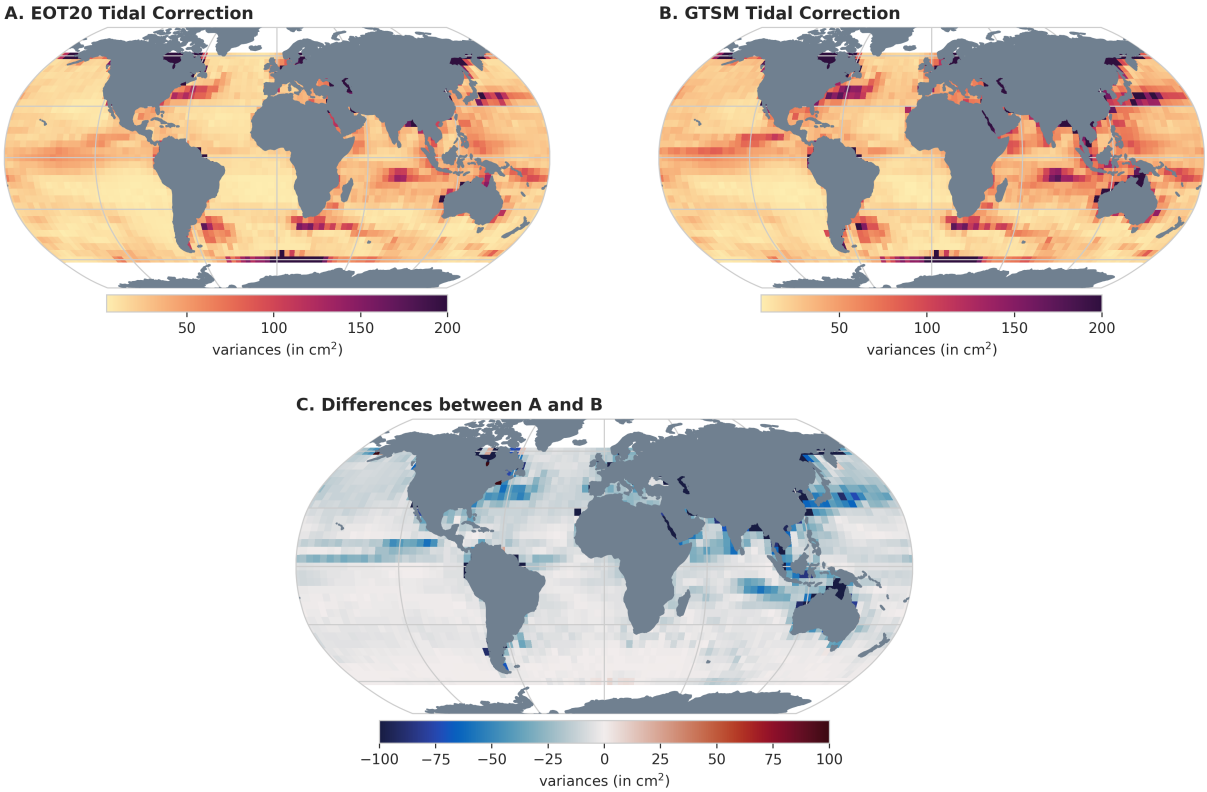

Figure 3.5 The gridded SLAVA estimated for the Sentinel-3A mission using EOT20 (A) and GTSM (B) ocean tide corrections. (C) presents the variance differences between using GTSM and EOT20, with negative differences (blue) indicating a higher variance when using GTSM and positive differences (red) when EOT20 has a higher variance.

CHAPTER 4

TIDE MODEL DEVELOPMENTS

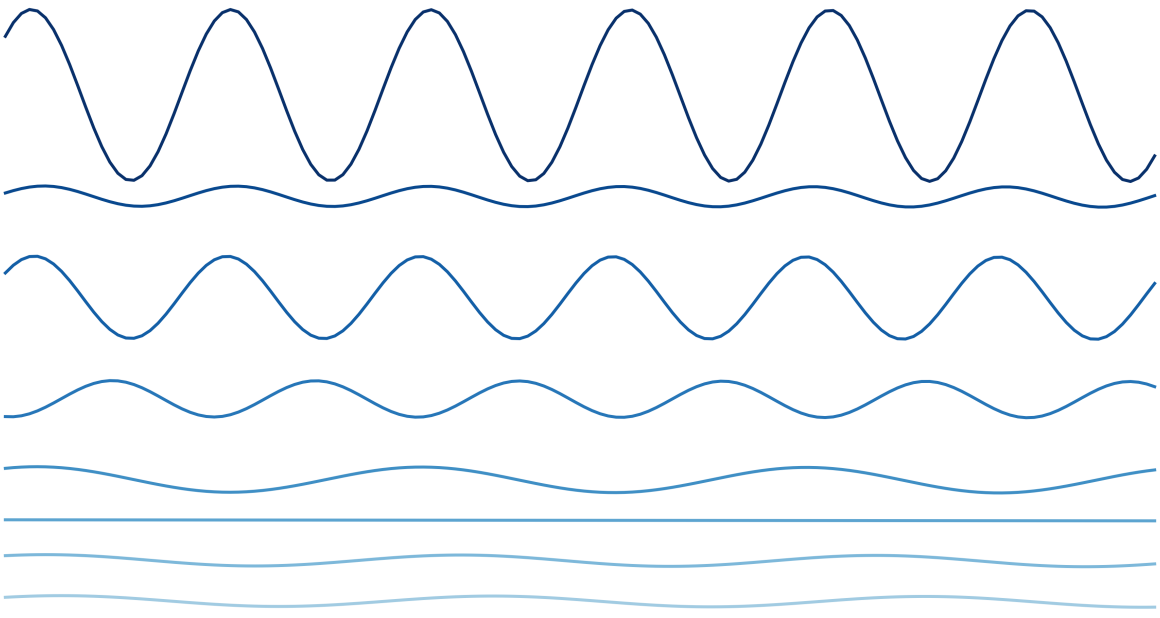

To raise new questions, new possibilities, to regard old problems from a new angle, requires creative imagination and marks real advance in science.

- Albert Einstein

4 Tide model developments

4.1 Introduction

The most recent evaluation of global ocean tide models concluded that difficulties remain both in the coastal regions and higher latitudes (Stammer et al., 2014). Therefore, the development of current and future iterations should focus on these regions in order to have the most valuable impact on our understanding of ocean tides. As mentioned earlier in this thesis, based on these presented difficulties, one of the main aims of this thesis is to present improved estimations of ocean tides in the coastal region within a global tide model. With the next global tide model iteration in mind, regional experiments are crucial for determining the feasibility of model developments in a global configuration. This is particularly important as the model itself is data intensive and requires large datasets to make estimations and, therefore, requires large computational effort and time when doing model simulations.

In order to determine the optimal regions for regional experiments, the standard deviation of global models and the availability of in-situ measurements was assessed. Five global models, namely DTU16 (Cheng and Andersen, 2017), EOT11a (Savcenko and Bosch, 2012), FES2014b (Lyard et al., 2021), GOT4.10 (Ray, 2013) and TPX09 (Egbert and Erofeeva, 2002) were used to derive the standard deviation of tidal estimations. As the models have variable spatial resolutions, all models were re-gridded onto a 0.5-degree spatial grid, which was the coarsest resolution of the models tested. The results of the global standard deviation assessment for the M_2 tide are presented in Figure 4.1. Besides expected deviations in the higher latitudes, deviations are seen in complex tidal regimes such as the North Sea, Patagonian Shelf, Northern Australia and around New Zealand.

Coupled with the model standard deviations, publicly available global in-situ measurement datasets were also analysed. This was obtained from TICON (Piccioni et al., 2019a), termed TICON-1 in this thesis, and from an ocean bottom pressure dataset curated by Richard Ray (Ray, 2013), termed the RR dataset in this thesis. The global distribution of these datasets is presented in Figure 4.2. The distribution of the measurements is strongly weighted to the Northern Hemisphere, with numerous measurements available along the European and North American coastlines. What is particularly evident is the lack of in-situ observations in the open ocean, however, the RR dataset of curated bottom pressure measurements does an essential job of filling in the open ocean gaps.

Combining these two assessments resulted in thirteen different regional models being developed, visualised in Figure 4.3. These models were aimed at being the focus areas for model developments before the global model was run but also to aid in refining the validation procedures, with several key points being the subject of investigation. Instead of describing each regional model, the model developments, which were confirmed throughout these regions, are presented in the following section.

Beyond this thesis, the re-gridded models and their differences were used by (Hauk et al., 2023) (AP-5) to derive variance-covariance matrices to reduce the temporal aliasing relating to tides in gravity field solutions

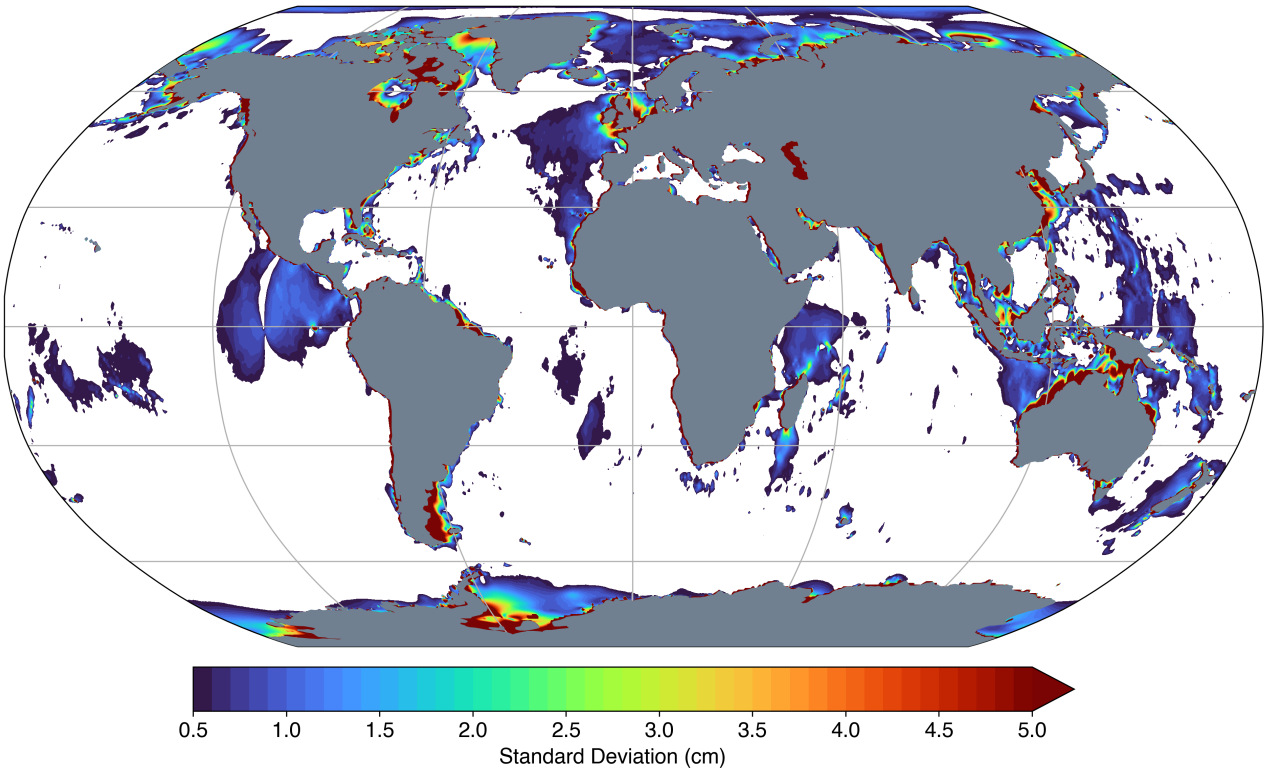

Figure 4.1 Standard deviation of the M_2 tidal amplitude from the five major global ocean tide models. Deviations below 0.5 cm are masked out with white to emphasise regions of high deviations.

from the Gravity Recovery and Climate Experiment (GRACE) and the GRACE Follow-On (GRACE-FO) mission. The variance-covariance matrices are available in AD-2 (Sulzbach et al., 2023).

4.2 The EOT model

The EOT model has been produced for decades at DGFI-TUM. Although over the years this model has evolved significantly, the general principle of deriving tidal constituents from along-track satellite altimetry has remained the same.

EOT uses the TP/JA/S6 series of satellite altimeters as the backbone of the model, largely thanks to its continuous, tide-favourable orbit (Provost et al., 1995) for over thirty years. As of 2023, this orbit has been flown by five different altimeters, namely TOPEX/Poseidon, Jason-1, Jason-2, Jason-3 and the currently flying Sentinel-6a. Within EOT, these satellites, as well as their respective extended missions, are combined with the satellites from the ERS/EN/SA orbit. This includes data from ERS-1c, ERS-1g, ERS-2, Envisat and Saral, which provide data across the same orbit from 1992 to the present day but with significant gaps within the data between satellite operations periods. This orbit is a great complement to the orbit of TP/JA/S6 as it improves the spatial coverage of retrieved SLA data, but they cannot be used on their own for tidal analysis due to its sun-synchronous orbit causing aliasing related issues for several tidal constituents (Figure 2.10). Similarly, Sentinel-3a and Sentinel-3b are also useful for tidal analysis as they provide a unique orbit and greater spatial coverage but are also not able to provide full tidal estimations as a result of their sun-synchronous orbits.

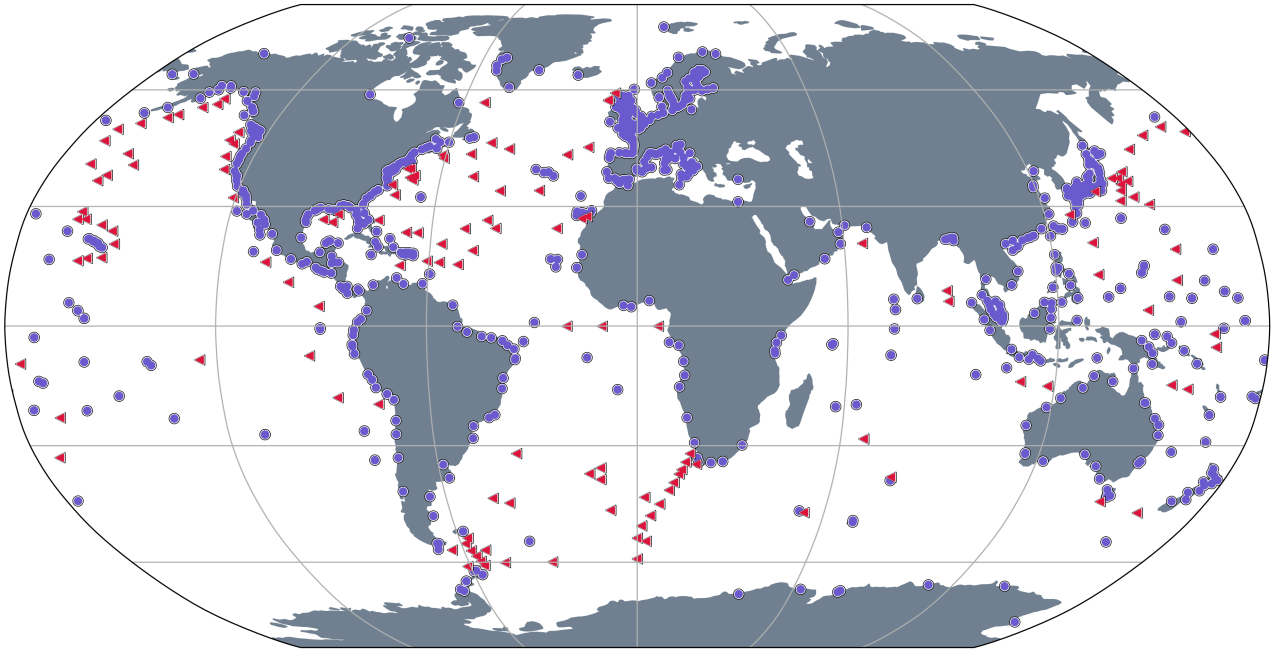

Figure 4.2 Distribution of in-situ measurements from the TICON-1 database (o) (Piccioni et al., 2019a) and the RR dataset (◃) (Ray, 2013).

Due to the availability of these respective altimetry datasets, either due to processing times or the satellites not yet orbiting, not all of the above-mentioned satellites are used in each study of this thesis. In the respective publications of this thesis, the exact satellites used are described. For the experiments described in the subsequent chapters, the following eleven altimetry datasets are used throughout with those in ***italics*** including their extended missions: ***TOPEX/Poseidon***, ***Jason-1***, ***Jason-2***, Jason-3, ERS-1c, ERS-1g, ERS-2 and Envisat.

For each of these altimetry datasets, the 1-Hz SLA is derived and obtained from the Open Altimetry Database (OpenADB; `https://openadb.dgfi.tum.de/`), with the SLA being derived following Equation 2.9. Throughout this thesis, h_{geo}, H and mss are kept consistent with each iteration of the model. A summary of where the h_{geo}, R and mss are obtained from is presented in Table 4.1. Where possible, the ALES retracker (Passaro et al., 2014) is used, which, alongside the geophysical corrections, has been chosen to optimise the retrieval of SLA data in regions closer to the coast to allow for better tidal estimations.

A final step is done to determine the radial error of the respective missions. This is done by multi-mission crossover analysis (MMXO), which allows for the harmonised combination of the different altimetry data and the appropriate use of the multiple different datasets in applications of these data, particularly in tidal analysis (Bosch et al., 2014). Figure 4.4 shows the impact the radial error correction has on the resultant SLA time series when combining multiple different datasets, with this having significant impacts on the amplitude and phase estimations of tidal constituents.

Once the SLA has been created from all the missions, the first step is to bin the data into grid nodes to create a time series of SLA data from which tidal analysis can be done. The selection of the distribution of these nodes as well as the radius of data to be used within each node (see Chapter 4.4), is important in optimising the estimations in coastal regions. EOT uses a triangular grid structure based on the geodesic polyhedron (Fuchs, 2016), which is preferred over a regular grid in terms of computational efficiency but also allows for consistent distance between nodes from mid to high latitudes (Piccioni et al., 2019b).

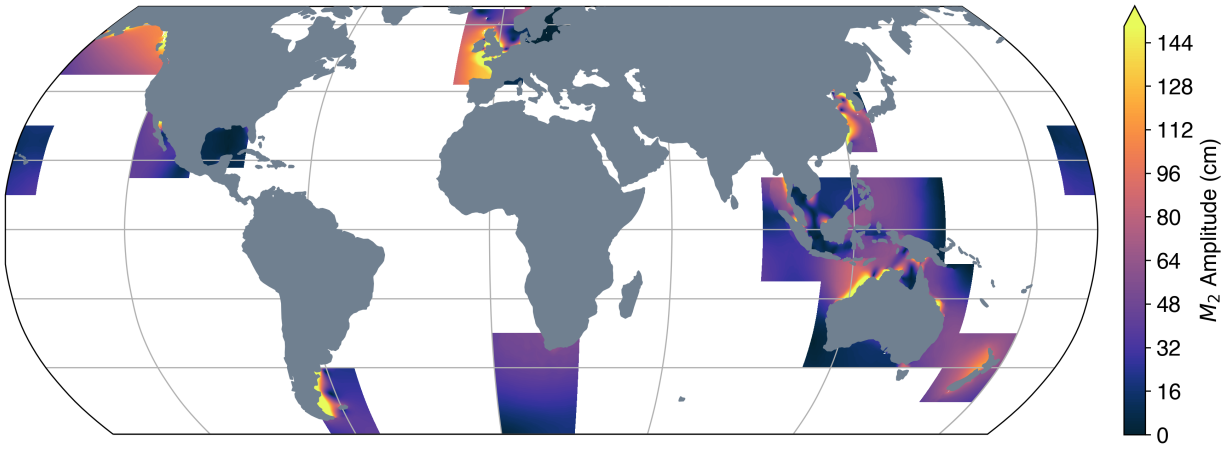

Figure 4.3 The distribution of the regional experiments done within this thesis.

Table 4.1 List of corrections and parameters used to compute SLA.

Parameter	Model	Reference
ALES sea state bias	ALES	Passaro et al. (2018b)
ERS sea state bias	REAPER	Brockley et al. (2017)
TOPEX sea state bias	TOPEX	Chambers et al. (2003)
Atmospheric loading before 2017	DAC-ERA	Carrere et al. (2016)
Atmospheric loading from 2017	DAC	Carrère et al. (2011)
Wet troposphere	GPD+	Fernandes and Lázaro (2016)
Dry troposphere	VMF3	Landskron and Böhm (2018)
Ionosphere	NIC09	Scharroo and Smith (2010)
Ocean and load tide	FES2014	Lyard et al. (2021)
Solid Earth and pole tide	IERS 2010	Petit and Luzum (2010)
Mean sea surface (MSS)	DTU18MSS	Andersen et al. (2016)
Radial error	MMXO17	Bosch et al. (2014)

As altimeters do not pass through the centre of each node, the SLA data is weighted using a Gaussian weighting function described in Savcenko and Bosch (2012). Within each node, all observations collected within the radius of each node, ψ, are weighted (w_{dist}) as follows:

$$w_{dist} = e^{-\beta\psi^2} \tag{4.1}$$

where,

$$\beta = \frac{ln(2)}{\tau^2}. \tag{4.2}$$

Here, $\tau = 0.5\psi$ is the half-weight width and determines the steepness of the Gaussian function (Piccioni et al., 2018). For each individual pass of the respective altimeters, this Gaussian function provides a weighting to each SLA estimation, allowing for a time series to be created at each node.

Following the appropriate weighting of the SLA, the next step is to do a Variance Component Estimation (VCE) of the respective altimetry missions. The VCE is a crucial step in combining the respective altimetry missions and is designed to improve the accuracy of the model by appropriately weighting each mission based

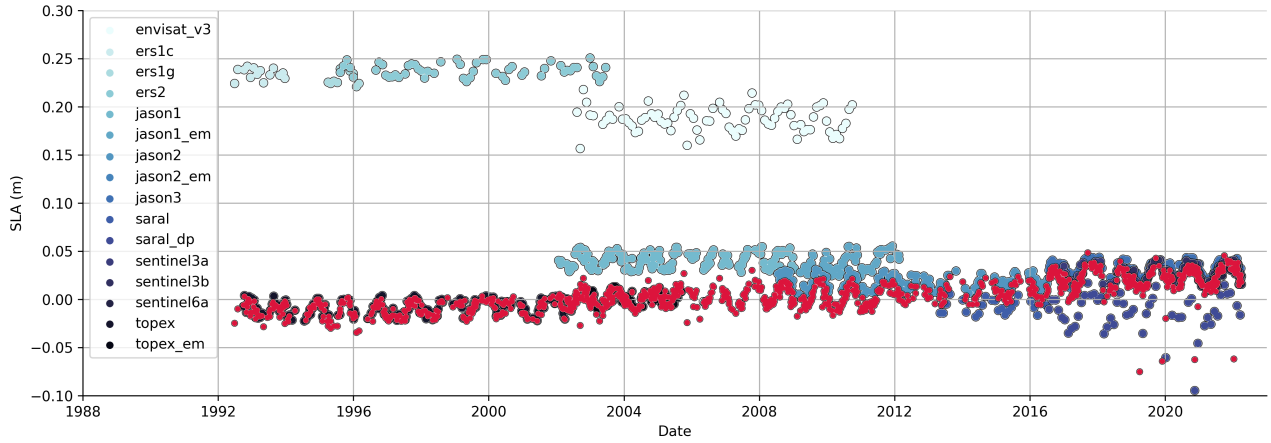

Figure 4.4 SLA within a grid point obtained from seventeen altimetry datasets before the radial error is applied (blue colours) and after the radial error correction is applied (red).

on the variances determined within each node. VCE is used in a variety of geodetic applications (e.g. Teunissen and Amiri-Simkooei, 2007; Dettmering et al., 2011; Erdogan et al., 2020), with several different methods used to determine the VCE (Teunissen and Amiri-Simkooei, 2007).

For altimetry-based tide modelling, Savcenko and Bosch (2012) implemented a VCE method into EOT11a that appropriately weights the respective altimetry missions which follow the methods described in Teunissen and Amiri-Simkooei (2007) and Eicker (2008). This methodology is continued within the EOT developments of this thesis and is briefly described below.

The formulation is as follows:

$$N_x X = N_y, \tag{4.3}$$

with Nx and Ny equal to the weighted sum:

$$N_x = \sum_{m=1}^{k} \frac{1}{\sigma_m^2} N_{x,m} \tag{4.4}$$

$$N_y = \sum_{m=1}^{k} \frac{1}{\sigma_m^2} N_{y,m} \tag{4.5}$$

The variances, σ, is determined for each altimetry mission, m, through iterating:

$$\sigma_m^2 = \frac{\Omega_m}{r_m}, \tag{4.6}$$

with $\Omega_m = \hat{v}' P_{bb} \hat{v}$, where $\hat{v}$ is the vector of the residuals and P_{bb} the dispersion matrix of the measurements. r_m is the partial redundancy, which can be determined using the number of measurements of the respective mission, n_m, from the following:

$$r_m = n_m - \frac{1}{\sigma_i^2} tr(N_m N^{-1}). \tag{4.7}$$

These calculations are produced for each altimetry dataset at each node, with the datasets each being weighted in percentages, totalling up to 100% regardless of the number of datasets used within the model. The VCEs provide a great spatial pattern of the variances of the different missions, which can provide insights into several factors, particularly on the benefits of the retracker used in the coastal regions, as well as gaps in the data. An example is provided in Figure 4.5 where four different missions are presented in the North-East Atlantic, and it can be seen that there are completely different spatial patterns in the respective weighting resulting from individual mission variances. It can also be seen that although the TP/JA/S6 orbit missions are critical for tidal estimation, the addition of different satellite orbits serves the model well in helping to provide increased spatial coverage for more reliable estimations to be made.

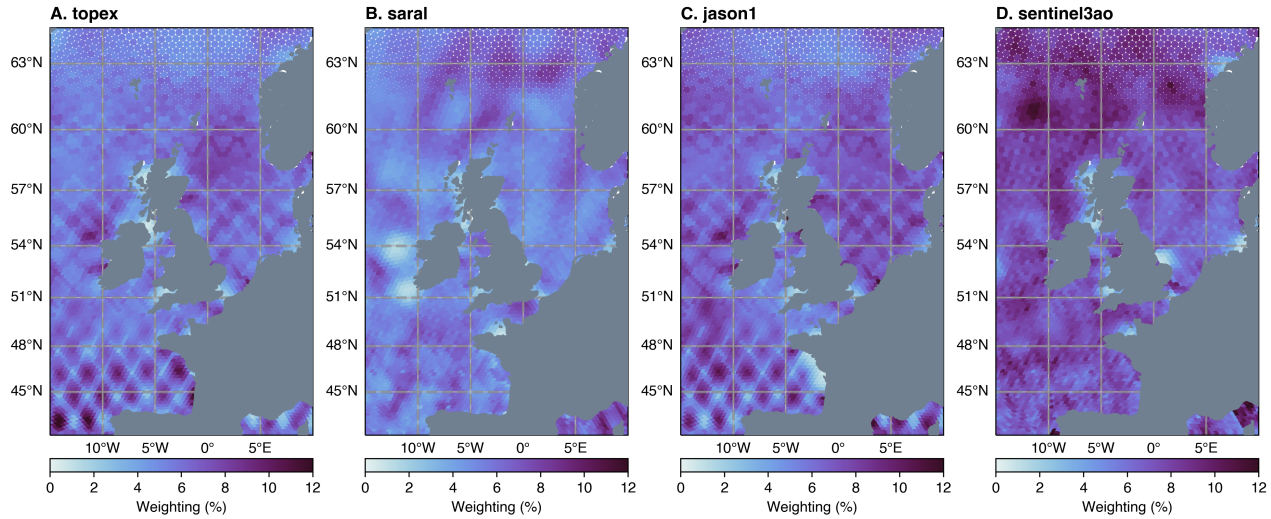

Figure 4.5 An example of the spatial variability of the weighting (in %) of four of the eleven altimetry datasets used, obtained for each grid node of the model after the VCE estimation has been done.

The VCE also provides a total variance of the altimetry data used in the tidal estimation, which is great in identifying certain regions for improvement within the model for future work. Although this metric itself may not be a perfect way to evaluate model developments or the inclusion of additional altimetry missions, when coupled with in-situ validations, the assessment of the total variance changes within the model can provide some valuable insight into developments. This will be discussed later in this thesis.

Once completed, a time series of observations is obtained similar to the example in Figure 4.4 for each node of the model. On these time series, harmonic analysis is conducted to produce estimates of a set list of tidal constituents, which varies within this thesis based on the objectives of each manuscript. Additionally, EOT makes estimations of the mission offsets and SLA trends for each grid node. The estimated mission offset is added to each mission to reduce the standard deviations of the SLA data that is estimated and to allow for more reliable estimations (Savcenko and Bosch, 2012).

These residual ocean and load tides are finally recombined with the reference tide model, FES2014 (Lyard et al., 2021), to provide a full ocean and load tide estimation for the respective experiments. In **P-3**, a different model is experimented with, where the SLA data is uncorrected for FES2014 ocean and load tides and a full estimation is made directly from the observations. In this model version, there are no differences in the model processing itself.

4.3 Elastic tide decoupling

Estimates of tides from satellite altimetry are termed the geocentric tides, which are a combination of solid Earth, ocean, loading and pole tides. As stated by Savcenko and Bosch (2012), the solid Earth tides are well-modelled, and the pole tides do not coincide with the tidal frequencies of the ocean and load tides. Therefore, when conducting a residual tidal analysis from satellite altimetry, the estimations are a combination of the ocean and load tides termed the elastic tide. In order to evaluate and utilise the ocean and load tide components individually, they need to be decoupled from one another.

Several techniques exist to decompose the elastic tides into the ocean and load tide components, with the method described in Cartwright and Ray (1991) being used within this thesis. This approach, as further

described in the context of EOT in Savcenko and Bosch (2012), uses spherical harmonic decomposition to decompose the elastic tides using the following formula:

$$Z_e(\phi, \lambda) = \sum_{n,m} a_{n,m} Y_{nm}(\phi, \lambda), \tag{4.8}$$

where the spherical harmonic admittances of the ocean tides can be described by:

$$Z_o(\phi, \lambda) = \sum_{n,m} a^o_{n,m} Y_{nm}(\phi, \lambda), \tag{4.9}$$

while the load tide admittance is described by:

$$Z_l(\phi, \lambda) = \sum_{n,m} \alpha_n a^o_{n,m} Y_{nm}(\phi, \lambda). \tag{4.10}$$

Where $\alpha_n = \frac{3}{2n+1} \frac{\rho_w}{\rho_e} h'_n$, with the Love numbers, h'_n, taken from Farrell (1972) and ρ_w being the water density and ρ_e the solid Earth density (Savcenko and Bosch, 2012). After the estimations of the load tide admittance, Z_l, the ocean tide admittance can be obtained by subtracting Z_l from Z_e.

An example of the decomposition of the elastic tide into the ocean and load tides is presented in Figure 4.6 from EOT11a. The mean difference between the ocean and load tide components is estimated to be 6.1% in terms of the M_2 amplitude, meaning separating the two is necessary, at least from the full tidal estimations, as amplitudes can reach well above 1 cm. In terms of residual tidal analysis, which is the main technique used in the EOT model, the importance of this separation significantly declines. This is due to residual amplitudes being considerably less than full amplitudes and being only in the range of low centimetres, meaning the load tide contributions would be nearly negligible in some regions. However, considering regions with larger tidal signals, these contributions are still necessary and, therefore, should be handled appropriately to accurately determine ocean tides.

Regional experiments were conducted to validate the ocean tide estimations produced following the above-mentioned decomposition. An example is given for the North West European continental shelf (Table 4.2), where empirical estimations were derived, and the elastic and ocean tides were compared to in-situ measurements to highlight the value of this decomposition. RMS differences show improvements for individual constituents that exceed millimetres, whereas, for the M_2, which has the largest tidal signal in this region, the improvement is 0.5 cm. The results of the regional experiments demonstrate the importance of conducting the decomposition to derive the ocean tides from the elastic tides. Therefore, for the remainder of this thesis, as well as in all scientific publications produced in this thesis using the EOT model, this approach was utilised to extract the ocean tides.

Although not a focus of this thesis, load tides, which are simply the response of the solid Earth to the mass redistribution caused by ocean tides (Farrell, 1972; You and Yuan, 2021), are useful themselves. They influence a variety of geodetic observation techniques, including Very-Long-Baseline Interferometry (VLBI) and GNSS (Männel et al., 2019), and, therefore, need to be critically modelled to reduce error in these measurements. In these applications, load tides are taken from global ocean tide models with differences between models ranging between 1-2 mm (Andersson, 2020). Based on regional experiments, providing the regional load tides is not useful as regional studies using the aforementioned measurements still rely on a global model. Therefore, load tides are only made public and provided by the global model in publication **P-1**.

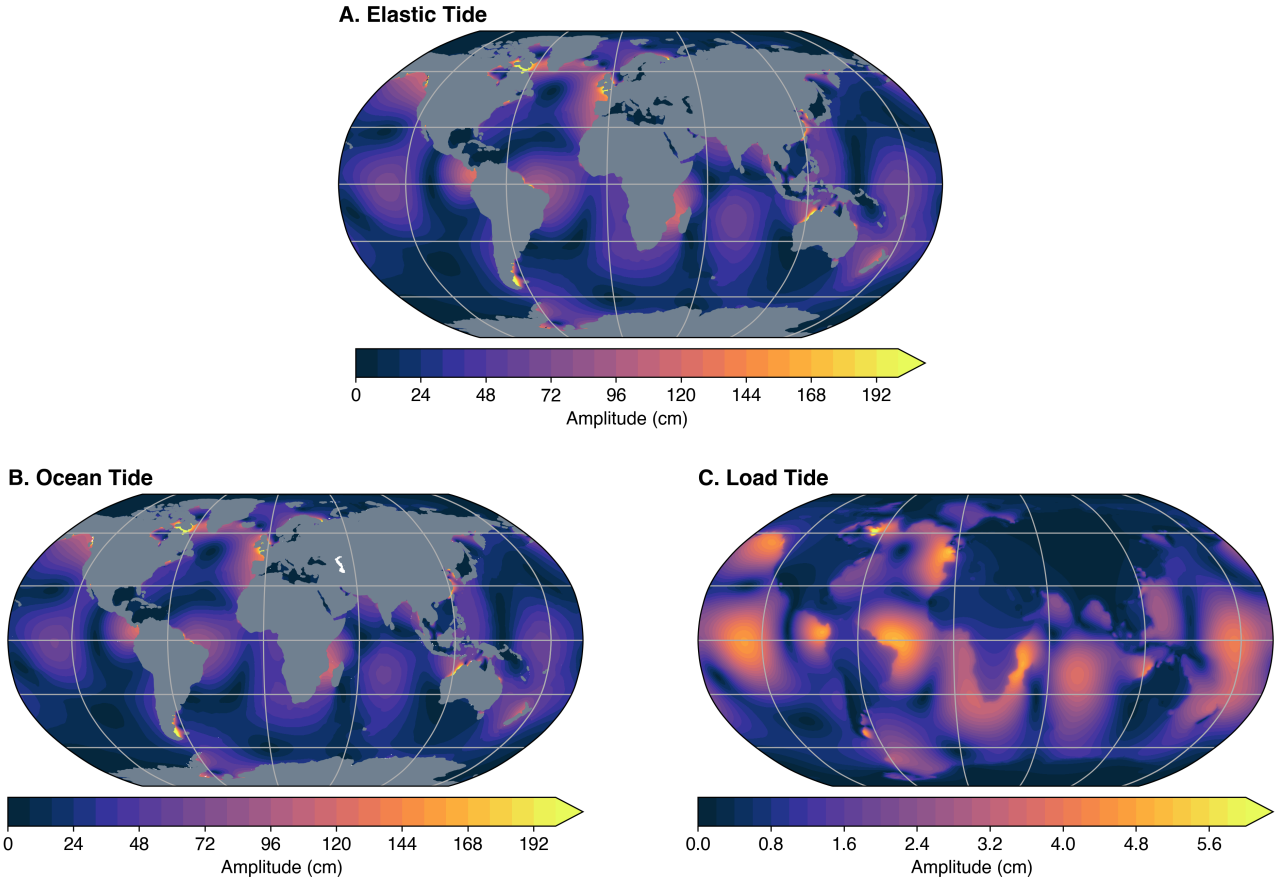

Figure 4.6 The amplitude of the (A) elastic tide, (B) ocean tide and (C) load tide of the M_2 tidal constituent from EOT11a.

Table 4.2 The RMS with respect to TICON-3 of the eight major tidal constituents of the modelled elastic and ocean tides in the North West European continental shelf. To contextualise these errors, the mean tidal signal is also derived.

Constituent	Elastic Tide (RMS in cm)	Ocean Tide (RMS in cm)	Tidal Signal (in cm)
M_2	5.147	4.632	85.672
S_2	6.985	6.721	27.099
N_2	6.443	6.264	15.625
K_2	4.437	4.297	7.850
K_1	2.080	2.043	4.922
O_1	2.173	2.133	5.215
P_1	1.072	1.076	1.853
Q_1	0.943	0.963	1.610

4.4 Capsize optimisation

Capsizes are crucial when considering altimetry-based estimations of ocean tides. A capsize is the area around each grid node from which altimetry data is used to make a tidal estimation for the respective node. The definition of this is crucial in terms of allowing reliable estimations of ocean tides and capturing the spatial variability of the ocean tides as best as possible.

The first consideration when defining the capsize is the orbits of the respective altimetry missions. In general, and also within this thesis, empirical tide models rely heavily on TP/JA/S6 series of altimeters because of the suitability of this orbit for tidal estimations, particularly of solar tides. Therefore, it is logical to base the capsize radius on the spatial distance between different passes of this orbit. At the equator, passes of TP/JA/S6 have a maximum separation of 330 km, while at 66°N/S, the latitudinal maximum of this mission, the maximum separation decreases to 200 km. Other satellite missions used in this thesis have different orbits and, therefore, have different cross-track separations than those of the TP/JA/S6 orbit. As the orbits of these missions are not optimised to tidal estimations based on their sun-synchronous orbits, no considerations of the orbit separations will be made on the determination of the capsize radius as the TP/JA/S6 orbit will be prioritised.

As one of the main objectives (**P-1**) is to obtain improved coastal estimations of tidal constituents, varying the capsize radius based on the maximum separation of the orbit to attempt to capture the spatial variability of the tides is an important consideration. A simple approach to determine the capsize radius, cap, based on the maximum separation of the TP/JA/S6 orbit at the respective latitudes, ϕ in degrees, can be given as follows:

$$cap = 330 - 3 * (\phi). \tag{4.11}$$

Another approach towards optimising tides in the coastal region is to vary the capsize based on the ocean bathymetry of the grid nodes. This results in the selection of data as near the coastline as possible, allowing for the better capturing of spatial variability. The most obvious drawback to this approach is that in some regions, there could be insufficient SLA data to make reliable estimations, resulting in either erroneous estimations or gaps within the model. Additionally, bathymetry products contain varying accuracy levels and can suffer in regions of sparse data, which could impact the capsize determination. The use of a bathymetry-based capsize approach is tested in this thesis based on the GEBCO2019 product (`https://www.gebco.net/data_and_products/gridded_bathymetry_data/gebco_2019/gebco_2019_info.html`). When the depth is above 400 meters, a capsize of 330 km is used, but when the depth (in meters) of the grid node is below 400 meters, the cap (degrees) is calculated as:

$$cap = 0.575 * depth + 100. \tag{4.12}$$

Experiments were done to compare these approaches with a fixed capsize approach, which is determined based on the maximum separation of the TP/JA/S6 orbit. Figure 4.7 shows the total number of observations retrieved from eleven altimetry datasets in each node based on the different capsizes. The two different capsize approaches significantly reduce the amount of data used by the model with respect to the fixed approach. A reduction in observations can be seen for all capsizes along the coast, relating to the coastal flagging procedure described in the next section. Considering the reduced number of observations obtained when using the bathymetry-dependent approach in the shelf region of the North Sea, spatial characteristics of the estimated tides may be inaccurate.

When analysing the major tidal constituents from the model compared to in-situ tide gauge measurements, an overall increased error in the bathymetry-dependent approach was found compared to both other approaches. Overall, the latitude-dependent approach proved to be the best approach, not only in the North Sea but also in other regions, for maintaining the reliability of tidal estimations and improving the estimation of the tides in the coastal region. Therefore, for the remaining experiments and in the publications of this thesis (**P-1**, **P-2** and **P-3**), this capsize approach is used throughout.

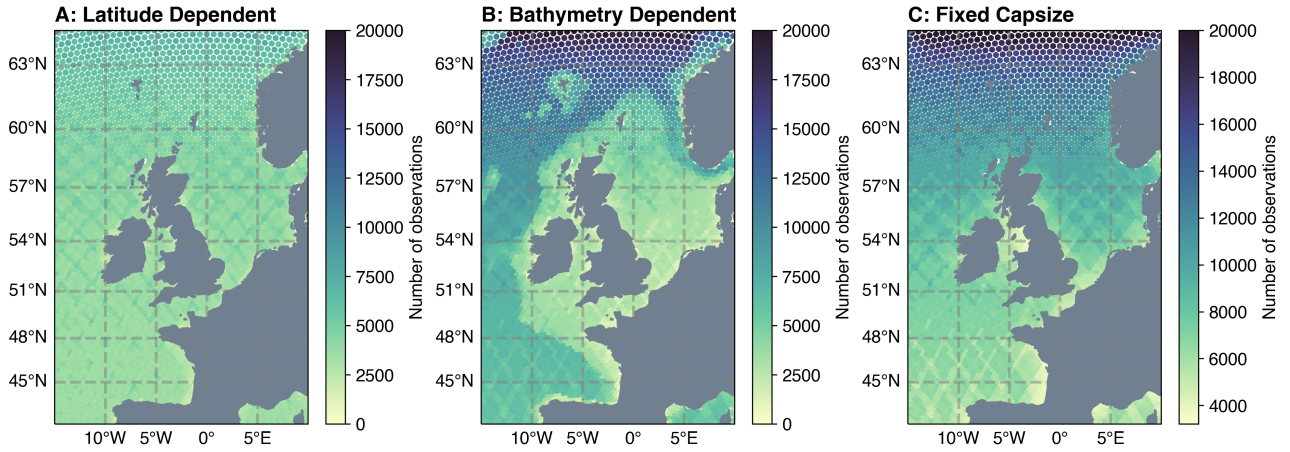

Figure 4.7 The number of altimetry observations obtained for each grid node based on the respective capsize approaches: (A) Latitude Dependent, (B) Bathymetry Dependent and (C) Fixed.

4.5 Land-sea mask

The defined land-sea mask is vital in the application of the model either for altimetry or model forcing purposes, as well as in the validation of the model. This is due to artefacts and errors being introduced into the model caused by interpolation when the land-sea mask is not appropriately defined. Several different options for land-sea masks were assessed and compared. Options which were explored include the land-sea mask provided by the Generic Mapping Tools (GMT), which is based on the GSHHG (A Global, self-consistent, hierarchical, high-resolution shoreline database, Wessel et al., 2019) as well as self-created masks based on GEBCO2019 and ETOPO (NOAA, 2022) topography data. Experiments showed that due to the spatial resolution of the tide model, 0.125°, differences between the land-sea masks derived by these products show no significance to the model results and, therefore, land-sea masks are produced using GMT moving forward, which is also used within OpenADB, which provides the altimetry data, to define the coastlines.

Examples are presented here of regional models of EOT with and without an appropriate land-sea mask for New Zealand and the Yellow Sea (Figure 4.8). There are clear artefacts when the mask is not included, for example, with the southern part of New Zealand demonstrating unrealistic variations in phase-lag, but when adding the mask, these artefacts are removed. These artefacts can be seen along the coastline, and if used to derive the tides at these coastal positions, particularly in complex regions such as estuaries and small coastal inlets, these results would be incorrect. In complex tidal regimes where the tidal amplitudes can change drastically, the land-sea mask is vital. Depending on the methodology used to validate models with in-situ measurements or to derive the tidal correction, these artefacts can creep in and produce unrealistic measurements.

For the New Zealand example presented in Figure 4.8A and B, the RMS compared to TICON for all eight major tides was improved when applying this mask, while the RSS of the model improved by 0.2 cm. In the even more complex coastal region of the Yellow Sea (Figure 4.8C and D), a complete improvement in RMS is found for all major constituents, with RSS of the model improving by 0.5 cm. These positive results, also seen in other regions, demonstrate the importance of appropriately defining the land-sea boundary of the model and, therefore, this boundary will be taken from GMT throughout this thesis.

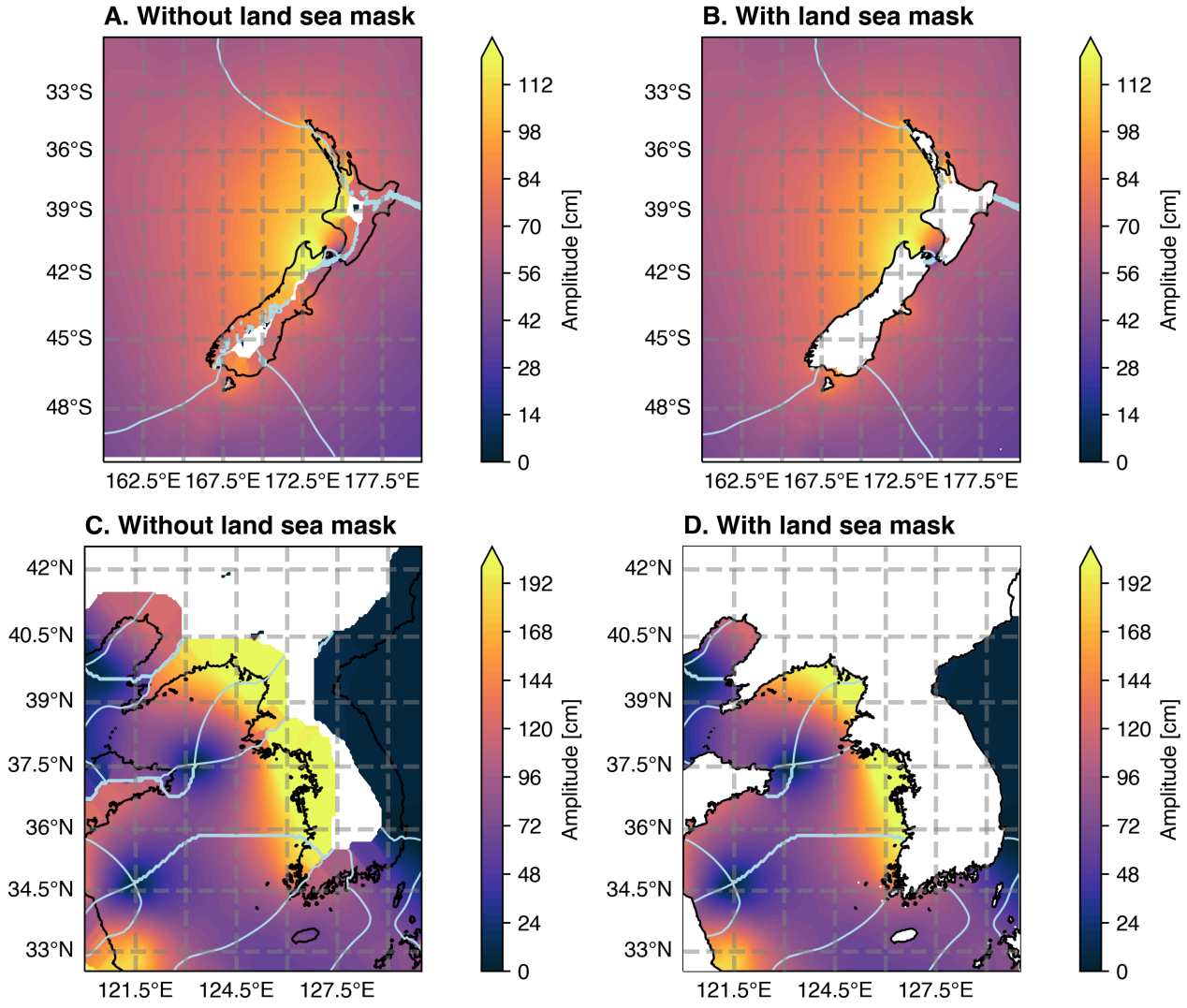

Figure 4.8 The EOT model (A and C) without an accurate land-sea mask and (B and D) with a land-sea mask derived from GMT Wessel and Smith (1996) in New Zealand and in the Yellow Sea, respectively. The map represents the amplitude of the M_2 tide, while the light blue lines represent each 60° phase contour.

4.6 Model coastal flagging

As you get closer to the coast, satellite altimetry becomes less reliable, primarily due to the land contamination of the radar returns. A concerted effort has been made in recent years to get more reliable radar returns closer to the coast by the use of different retracking algorithms. One such algorithm is the Adaptive Leading Edge Subwaveform retracker (ALES Passaro et al., 2014), which has been shown to provide reliable retrievals of sea-level data in near-coastal regions and has been successfully utilised in ocean tide applications (Piccioni et al., 2018, 2019b). The ALES retracker has been shown to reliably provide sea-level estimations, on average, up to 3 km from the coast (Birol et al., 2021). Not all of the altimetry missions are currently retracked using the ALES retracker and rely on the standard retrackers provided by the Sensor Geophysical Data Record (SGDR) of the mission, which only provides reliable estimations up to 10 km from the coast.

Therefore, to achieve the goal of optimising the EOT model for the coastal region, a coastal flag needed to be implemented to allow for the combination of altimetry using different retrackers. This was important not only for coastal accuracy but also in maintaining the long-time series of altimetry, which is crucial for optimising the estimation of tidal constituents. The implementation of this flag had significant impacts on the model results, as the increased retrieval of sea-level data showed significant improvements in the model accuracy. Table 4.3 demonstrates the results of a regional experiment on the implementation of the coastal flag around the complex tidal region of New Zealand. Compared to eleven tide gauges, when the flag is used (EOT-WF), every single constituent tested improved with respect to not using the coastal flag (EOT-NF), with the overall RSS reducing by 4.73 cm. An improvement was found when including the flag in several different regions.

A conclusion was made that the coastal flag was crucial in allowing for the usage of the ALES retracker and resulted in significant improvements of the model in the near-coastal regions. Therefore, the coastal flag was used for all of the remaining experiments within this thesis and in the publications **P-1**, **P-2** and **P-3**.

4.7 P-1: EOT20: a global ocean tide model from multi-mission satellite altimetry

Summary

The experiments presented previously provided strong motivation for the extension of these analyses throughout the global ocean to provide improved estimation of tides in the coastal region **O-1**. This manuscript, **P-1**, focuses on the development and production of a new global empirical ocean tide model, EOT20. Eleven altimetry datasets taken from OpenADB (Schwatke et al., 2014) were used, with the same geophysical corrections applied to derive the SLA. The selection of these corrections was aimed at optimising the performance of the model in the coastal regions.

The model is run to derive the residual ocean tides with the FES2014b tide model (Lyard et al., 2021) being used as the reference model. The amplitude, phase, real and imaginary components, as well as the respective standard deviation of these estimations as outputted by the harmonic analysis, are provided for every one of the seventeen constituents produced in EOT20. The results for the amplitude and the real and imaginary components of the M_2 and S_2 constituents are shown in Figure 4.9. As expected, residual amplitudes are around 0.5 cm and are in line with previously known residual amplitude estimates of other models (Savcenko and Bosch, 2012). Higher residuals are seen in regions of high non-tidal variability, such as western boundary currents. These regions are historically challenging for tidal estimates due to signal-to-noise related issues (Desai et al., 1997; Ray and Byrne, 2010).

Once the residual tides are obtained, the ocean and load tides are separated and combined with FES2014b to create the final EOT20 model. The model itself was restricted to be between 66°N and 66°S due to the reliance of the model on the TP/JA/S6 series of satellites which is restricted to these latitudes.

Table 4.3 The RMS (in cm) and RSS (in cm) compared to 11 tide gauges of EOT-NF and EOT-WF model versions.

Model	M_2	N_2	S_2	K_2	K_1	O_1	P_1	Q_1	**RSS**
EOT-NF	12.92	2.68	2.60	0.57	0.73	0.32	0.47	0.23	**13.49**
EOT-WF	8.27	1.79	2.03	0.41	0.67	0.32	0.45	0.23	**8.76**

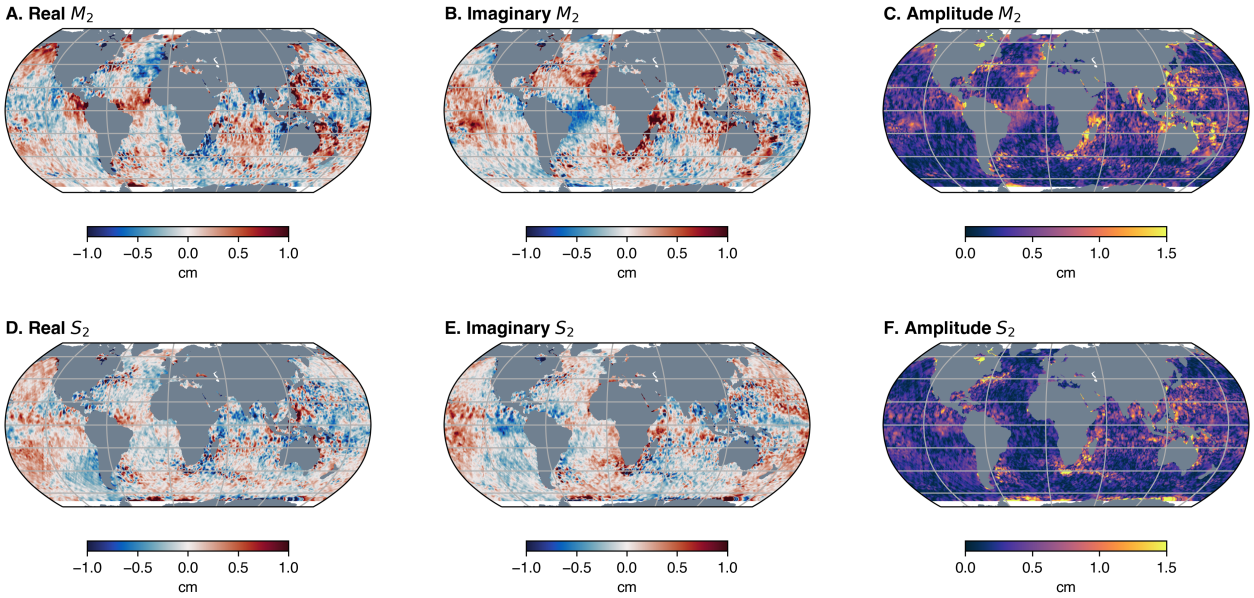

Figure 4.9 The real and imaginary components as well as the amplitude of the residual M_2 and S_2 constituents from the EOT20 model.

The other missions included in EOT extend to higher latitudes but are sun-synchronous and, therefore, cannot be used to estimate the important solar constituents, particularly S_1 and S_2. Above these latitudes, the FES2014 model is provided. Once created, the model is validated against in-situ tide gauges and ocean bottom pressure sensors and contrasted to frequently used global ocean tide models. The results of the tide gauge analysis demonstrated that EOT20 showed the lowest RMS in the coastal regions with respect to the in-situ measurements compared to all the models tested. In the shelf and open ocean, EOT20 improved on the previous iteration of the model, EOT11a, and remained in line with other models in terms of model errors. The next step was to evaluate the impact of the model on sea level variances of three satellite altimetry missions. To do so, the tidal constituents from EOT20, EOT11a and FES2014b were used to derive tidal corrections for all three missions' entire life span. This analysis showed that the tidal correction obtained when using EOT20 resulted in a reduction in variances compared to using the other two models, particularly in the coastal region.

The conclusion of this publication was that the newly developed EOT20 model achieved its aim of improving the understanding of ocean tides in the coastal region but also remained in line with other global models in the open ocean and shelf seas. The results demonstrate that the use of EOT20 as a tidal correction is beneficial for many studies of sea level from satellite altimetry, particularly in coastal regions.

The subsequent publication and dissemination of the EOT20 model data (**AD-5**) within the greater scientific community has resulted in the use of the model in a variety of studies. At the time of submission, EOT20 has been used in more than fifty published articles, which demonstrate the usability of the model in additional applications and scenarios than those presented within this thesis. These include studies marine gravity field recovery (Li et al., 2022), regional evaluation of tidal dynamics (Pan et al., 2022; Wang et al., 2022b), model development (Wang et al., 2022a), reviews of ocean circulation (Morrow et al., 2023), model accuracy assessments (Sun et al., 2022), ocean tide loading (You and Yuan, 2021), coastal sea level variability (Zemunik et al., 2022; Sharp, 2022), coastal vulnerability (Hamid et al., 2021), satellite laser ranging (Bloßfeld et al., 2021) and terrestrial reference frames computations (Glomsda et al., 2023).

Manuscript citation

Hart-Davis, M. G., Piccioni, G., Dettmering, D., Schwatke, C., Passaro, M., and Seitz, F. 2021. EOT20: a global ocean tide model from multi-mission satellite altimetry, Earth Syst. Sci. Data, 13, 3869–3884, https://doi.org/10.5194/essd-13-3869-2021.

Copyright

Declaration of Own Contribution

(MHD: M. Hart-Davis, GP: G. Piccioni, DD: D. Dettmering, CS: C. Schwatke, MP: M. Passaro, FS: F. Seitz)

The design of the study was done by MHD. MHD and GP developed the empirical ocean tide model, and MHD did the model refinements to optimise the coastal estimation of ocean tides and to produce the final global model version, EOT20. MHD did the model validation, including both the tide gauge validation and the variance analysis of the along-track ocean tidal correction for satellite altimetry. MHD wrote the manuscript, drafted interpretations of the results and produced all the figures and tables of the manuscript. DD aided in the design of the study and in the interpretation of the results. CS and DD are responsible for the appropriate satellite altimetry data used in the model creation. MP is the author of the retracking algorithm and sea state bias correction used in EOT20. FS supervised the research. All authors read, commented and reviewed the final manuscript.

Table 4.4 Criteria and estimated contribution share of Michael Hart-Davis for P-1

Criteria	Estimated own contribution
Computation and results	65%
Ideas and study design	75%
Analysis and interpretation	80%
Manuscript Writing	80%
Figure and Table Creation	100%
Total	**80**%

4.8 P-2: Regional Evaluation of Minor Tidal Constituents for Improved Estimation of Ocean Tides

Summary

Producing an ocean tidal correction for satellite altimetry requires accurate knowledge of hundreds of individual tidal constituents. From an empirical modelling perspective, deriving each of these hundreds of constituents is not possible due to several factors, including computational effort and difficulty in observing the small signals of all of these tidal constituents. The latter is particularly an issue for satellite altimetry, as signal-to-noise ratios often mean it is impossible to resolve several tidal frequencies. However, including these minor constituents is crucial for improving the accuracy of predictions as well as reducing the variances of the current estimations (Egbert and Ray, 2017). A common approach to solve this problem is to use linear admittances (Munk and Cartwright, 1966; Petit and Luzum, 2010). This approach allows for the inferences of minor tidal constituents from known major tidal constituents, which has successfully aided in improving tidal estimations (Egbert and Ray, 2017).

Although these used approaches have positive impacts on tidal corrections and predictions, they are sometimes imperfect in their techniques, and alternative approaches may be more suitable for deriving tidal constituents. Generally, tidal prediction software used to derive tidal heights infers a set number of constituents following conventions such as Petit and Luzum (2010). However, the increased availability of satellite altimetry data has meant that several of the constituents recommended to be inferred can now be directly estimated. Additionally, numerical modelling efforts have significantly advanced in model accuracy, and they are able to derive a much broader spectrum of tidal constituents (Sulzbach et al., 2022).

Investigating the suitability of current approaches and introducing alternative approaches for deriving these minor constituents, will benefit the estimation of tidal heights used in both satellite altimetry and gravimetry (**O-2**). Therefore, **P-2** investigates techniques of deriving several minor constituents based on linear admittance approaches or direct modelling estimations from both data-constrained models and purely numerical models and evaluates the impact they have on the tidal correction for along-track satellite altimetry. Three regional experiments were selected to test the different approaches to estimating eight minor tides and were compared with in-situ measurements and as corrections for satellite altimetry.

It was concluded that of the eight constituents, four of them should be directly estimated from the EOT model used, and four should be inferred from the major tides. Additionally, a proposition of building hybrid corrections from multiple ocean tide models was investigated, and it concluded that although the constituents tested did not show significant changes overall compared to using one model alone to derive the correction, in some regions, there is a benefit and further research should be done to investigate this influence with more constituents, particularly of the third-degree constituents (Sulzbach et al., 2022).

Copyright

Citation: Hart-Davis, M.G., Dettmering, D., Sulzbach, R., Thomas, M., Schwatke, C. and Seitz, F. 2021. Regional Evaluation of Minor Tidal Constituents for Improved Estimation of Ocean Tides. Remote Sens., 13, 3310. https://doi.org/10.3390/rs13163310.

Declaration of Own Contribution

(MHD: M. Hart-Davis, DD: D. Dettmering, RS: R. Sulzbach, MT: M. Thomas, CS: C. Schwatke, FS: F. Seitz)

The conceptualisation of this study was done by MHD, DD, RS and MT. MHD developed the various regional model versions, did the computation, the validation and the interpretation of the results. MHD produced all figures and tables of the manuscript and wrote the manuscript. DD, RS and MT aided in the interpretation of the results. RS provided model results to be included in the computation and in the results. CS and DD are responsible for the appropriate satellite altimetry data used in the model creation. DD, MT and FS supervised the research. All authors read, commented and reviewed the final manuscript.

The overall contribution of MHD for P-2 is estimated at 90%, which is the average value of the percentage values estimated for the five criteria listed in the table below (Table 4.5).

Table 4.5 Criteria and estimated contribution share of Michael Hart-Davis for P-2

Criteria	Estimated own contribution
Computation and results	100%
Ideas and study design	70%
Analysis and interpretation	90%
Manuscript Writing	90%
Figure and Table Creation	100%
Total	**90%**

4.9 Additional altimetry data for high-resolution regional tide modelling

More altimetry missions continue to be launched, which either continue on preexisting orbits or explore different orbits. Both have obvious benefits for sea-level studies. The continued sampling of the same orbit has implications for long-term sea level change studies. At the same time, in the context of tides, these more extended time series allow for the improved estimation of tides and their changes and more constituents to be estimated. The new orbits provide greater coverage of the sea surface, meaning that the spatial variation of ocean tides can be better captured, and estimations can be made at higher resolutions.

As the final objective of this thesis (**O-3**) involved attempting to improve the ocean tidal boundary forcing of an operational model of the Northwest European Continental Shelf, accurately capturing these spatial variations is crucial for improving model accuracy. To do so, a regional EOT model was developed in the region, termed EOT-NECS, which exploited for the first time several additional altimetry missions. These missions include Sentinel-6a and SARAL, which extend the preexisting orbits of TP/JA/S6 and ERS/EN/SA, respectively. Additionally, the drifting phase of SARAL, SARAL-DP, as well as Sentinel-3a and Sentinel-3b were included in this model. The impact these additions had on the spatial coverage of the model is shown in Figure 4.10.

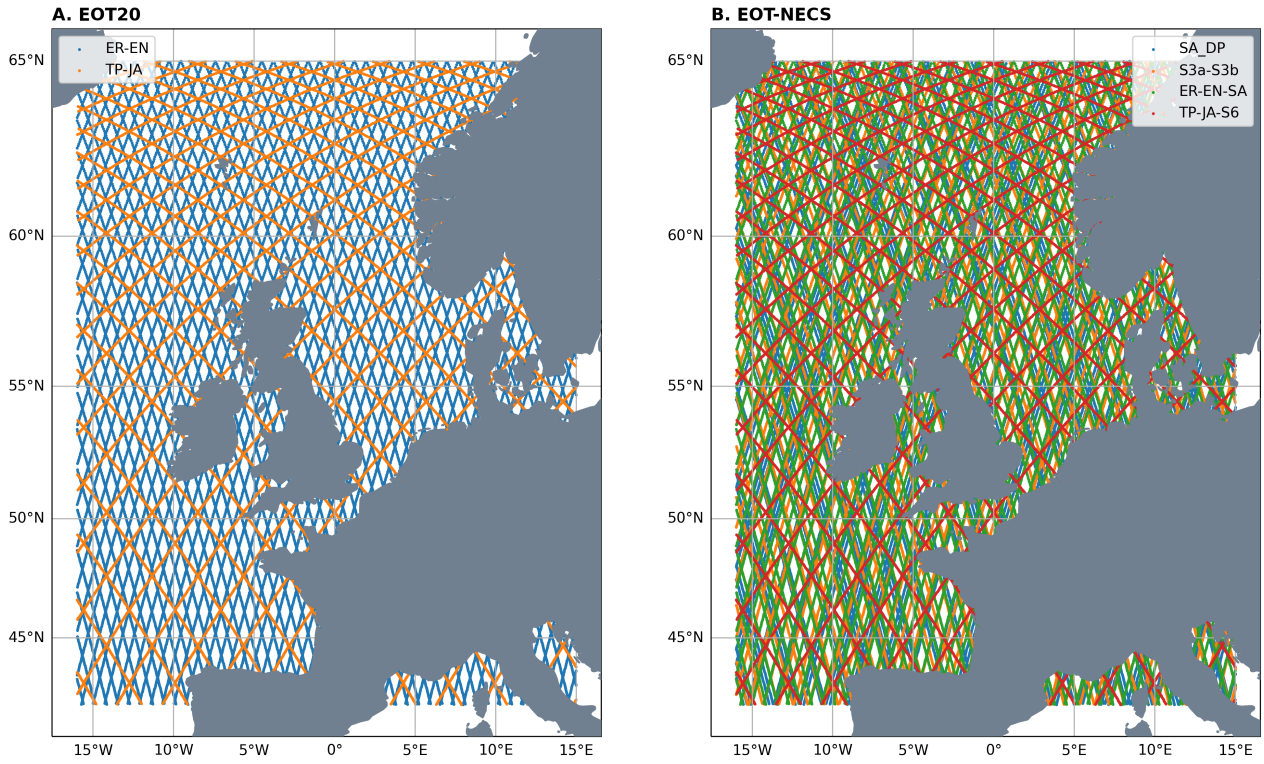

Figure 4.10 The along-track coverage of the altimetry missions used within EOT20 compared to EOT-NECS in the Northwest European Continental Shelf.

This increased spatial coverage resulted in an increased spatial resolution of EOT-NECS (0.0625°) with respect to EOT20 (0.125°). Furthermore, because of the increased total time-series length of the altimetry dataset used in the model creation, several more tidal constituents are estimated than what was previously provided within EOT. This included certain constituents which were not contained within FES2014 and, therefore, were estimated from purely empirical estimations. These constituents were identified as applicable to be estimated from the altimetry data used and were deemed necessary to help improve the boundary forcing of DCSM-FM.

The resultant EOT-NECS model is validated against the TICON-3 tide gauge dataset, presented in Chapter 3.1.2, and applied as the boundary forcing of the Dutch Continental Shelf Model in Flexible Mesh (DCSM-FM) model in Chapter 5.3 and within **P-3**.

CHAPTER 5

APPLICATION OF TIDAL DEVELOPMENTS

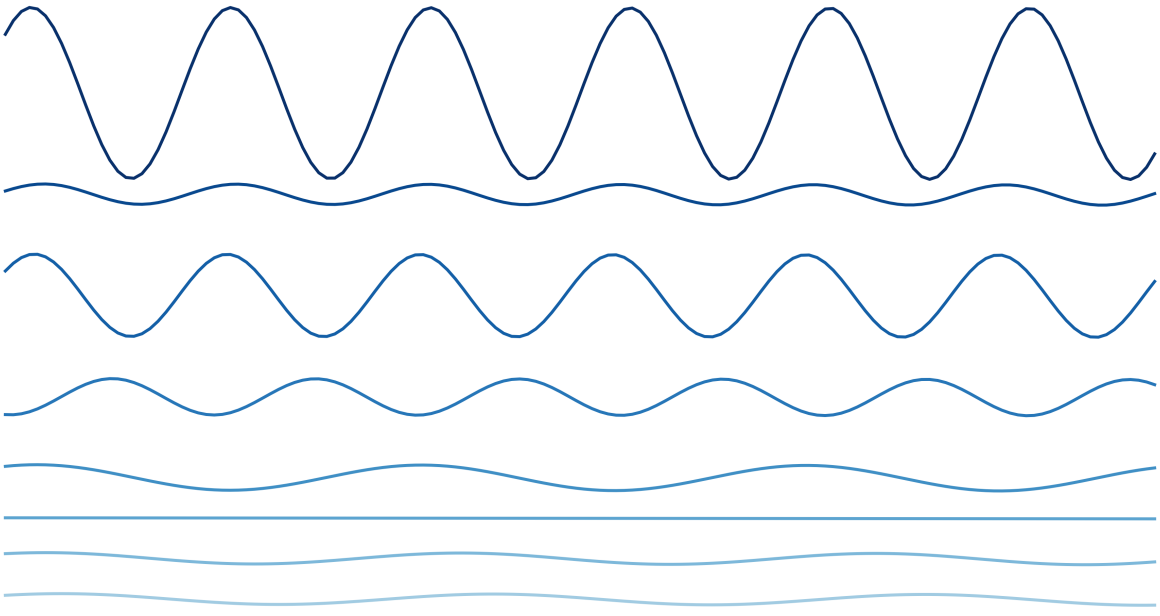

Nowhere is more powerful and unforgiving, yet more beautiful and endlessly fascinating than the ocean.

- Sir David Attenborough

5 Application of tidal developments

The ocean tide developments based on models and in-situ datasets produced within this thesis are applicable to a wide variety of oceanographic and geodetic applications. This is a consequence of the vast importance of ocean tides on sea level processes, general ocean circulation, and mass distribution. For example, the global EOT20 model is utilised in several applications as mentioned in Chapter 4.7, particularly as a tidal correction for satellite altimetry of data provided by OpenADB (`https://openadb.dgfi.tum.de/`).

To contextualise the importance of the developments produced within this thesis, three applications are presented. The first two applications exploit the unique in-situ tidal constituent databases to validate modelled third-degree tides and tides in the Arctic Ocean. The final application assesses the use of ocean tide estimates from a regional EOT model to force an operational forecasting model at the open boundaries and to assess the impact on water level predictions across the Northwest European Continental Shelf. All three of these applications were published in scientific journals.

5.1 Third degree tides

The full tidal signal is described mainly by a small number of tidal constituents, with Egbert and Ray (2017) describing that 99% of the total tidal variance can be captured by fourteen harmonic constituents and 99.99% by eighty constituents. Tide models traditionally estimate a relatively small number of constituents, with the most constituents provided by a data-constrained model being thirty-four (Lyard et al., 2021). However, some of these constituents, which are not traditionally estimated, can have amplitudes that exceed one centimetre and, therefore, in the context of providing the most accurate tidal height estimations, they must be addressed. Modelling efforts usually focus on second-degree tides, which include diurnal, semi-diurnal and long-period tides. However, the tidal bulge is not perfectly symmetrical due to the side opposite the Moon being slightly weaker than that of the side closest, giving rise to higher spherical harmonics in the tidal potential, notably third-degree tides (Ray, 2020b).

Estimating these third-degree constituents is not easy from altimetry-derived models, as their signals are often exceeded by the noise of the altimetry data used. Woodworth (2019) produced a global assessment of the $^3M_1$ tide that found amplitudes reach nearly 1 cm in several regions, particularly in the Northwest European Seas, based on in-situ gauges and a numerical model. A recent publication by Ray (2020b) provided the first assessment of several third-degree tides based on nearly three decades of satellite altimetry. The results described amplitudes approaching 1 cm, but the altimetry-based maps still contained large amounts of noise (Ray, 2020b). Numerical tide models, although usually less accurate than data-constrained models for the large tidal constituents, are not limited by these data-related problems. Therefore, they are crucial tools for studying the dynamical features of these third-degree tidal constituents.

With that in mind, a data-unconstrained numerical model, TiME22 (Sulzbach et al., 2021), was used to produce global estimations of four third-degree tides to complement the work of Ray (2020b). To validate and tune the atlases provided by the model, superconducting gravimetry and tide gauge data were used. The latter was the TICON-td dataset (**AD-4**), described in Chapter 3.1.1, which specially processed tide gauge data to produce the four required third-degree tidal constituents at 134 stations across the global ocean. The third-degree tides evaluated were the ${}^3M_1$, ${}^3N_2$, ${}^3L_2$ and ${}^3M_3$ constituents.

TiME22 after model tuning and TICON-td are compared in Figure 5.1, with agreement being found between the two, with TiME22 having an RMS deviation of 1 mm for each tidal constituent. For the ${}^3M_1$ tide specifically, the TICON-td dataset could be contrasted with an ocean bottom pressure dataset containing this constituent from Ray (2013). Analysis of the TiME22 model compared to these two datasets showed similar results with respect to the RMS of TiME22, with differences being less than one millimetre. This provides confidence in the processing steps done to produce TICON-td and, subsequently, the use of these data in the evaluation and tuning experiments of the TiME22 model. The results of this application of TICON-td were published in **AP-1** (Sulzbach et al., 2022).

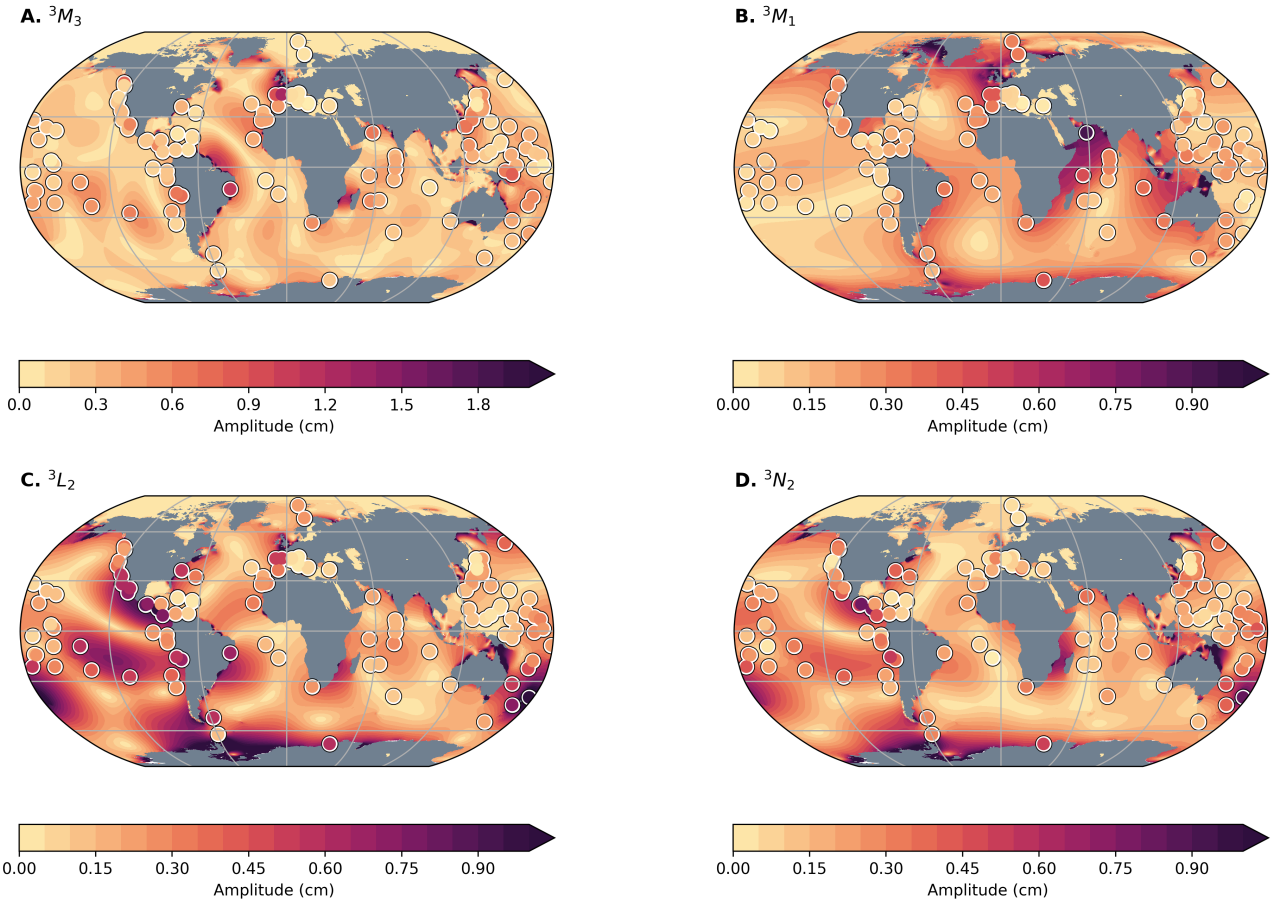

Figure 5.1 The global distribution of TICON-td compared to the global TiME model for the ${}^3M_1$, ${}^3N_2$, ${}^3L_2$ and ${}^3M_3$ constituents.

5.2 Polar ocean tides

In the polar ocean, estimating ocean tides is extremely challenging, largely due to the not well-understood relationship with sea ice. Models in this region show some of the highest RMS values with respect to in-situ measurements (Stammer et al., 2014) and models show a large deviation from one another (Figure 4.1 and Hauk et al., 2023). Numerical models suffer due to poorly resolved bathymetry products that are available in the polar oceans, as a result of the geo-political sensitivity of data in these regions. Altimetry-derived models are negatively influenced by the limited availability of SLA data resulting from sea ice as well as the lack of non-sun-synchronous altimeters orbiting the higher latitudes.

The ERS/EN/SA orbit missions do reach a latitude of 82°N/S, but their orbit is sun-synchronous, meaning the determination of all tidal constituents, particularly the major S_1 and S_2 tides, is not possible. In recent years, the Cryosat-2 mission has provided unprecedented coverage over higher latitudes, which has proven crucial for sea-level research. A study by Zaron (2018) evaluated the usability of Cryosat-2 in the higher latitudes for ocean tides estimations, with the results suggesting that data-constrained models would strongly benefit from the incorporation of the Cryosat-2 data. Based on these results, it is clear that significant progress will be made in tide modelling based on Cryosat-2 in both the Arctic and Antarctic seas in the future years.

With that in mind, the ArcTiCA in-situ dataset was created and presented in Chapter 3.1.3 with an eye on future model developments which require data for both validation and assimilation. The ArcTiCA dataset provides a well-distributed dataset of tidal constituents in the Arctic, with 399 sites located above 70°N, which allows for evaluating the regional accuracy of model developments. ArcTiCA serves as a complement to the already existing Antarctica Tide Gauge database (AntTG) produced by Howard et al. (2020).

For the altimetry-derived DTU22 tide model, the Cryosat-2 data were incorporated, and an assessment of the modelled accuracy of tidal estimations was done in the polar regions. This model is similar to EOT as it is a residual tide model, using FES2014b (Lyard et al., 2021) as the reference model, but instead of using the harmonic methods, it uses the response method. The response method, described in Munk and Cartwright (1966), has been shown to perform as accurately as the harmonic method (Cheng and Andersen, 2011) and in the analysis of highly aliased tides in short time-series datasets, should even be preferred (Ray, 1998).

Using ArcTiCA and AntTG, the DTU22 model was evaluated in the polar oceans. The results of the validation in the Arctic suggest that the DTU22 model outperforms FES2014b for the eight major tidal constituents, with an RMS reduction for the M_2 and S_2 tides being 1.8 cm and 4.0 cm, respectively. For the amplitude of the M_2 tide, shown in Figure 5.2, the DTU22 model estimates differences with respect to FES2014b exceeding 2 cm in the areas of large tidal amplitudes Baffin Bay, Barents Sea and the Northwest Passages which is more in line with the in-situ measurements of these regions. These results highlight the importance of the Cryosat-2 data, which are not assimilated in FES2014b, in improving model accuracy in the polar oceans. Furthermore, the ArcTiCA dataset allows for a proper model comparison in the Arctic, which was previously not possible based on the available in-situ constituent databases.

This study was replicated in Antarctica, where similar positive results were seen in the DTU22 model with respect to AntTG. A further discussion on the modelling of ocean tides in the polar regions, particularly using Cryosat-2 as well as the validation by using the ArcTiCA and AntTG databases, is presented in **AP-3** (Andersen et al., 2023). The ArcTiCA dataset is described and compared to other global tide models in the Arctic region in **AP-2**.

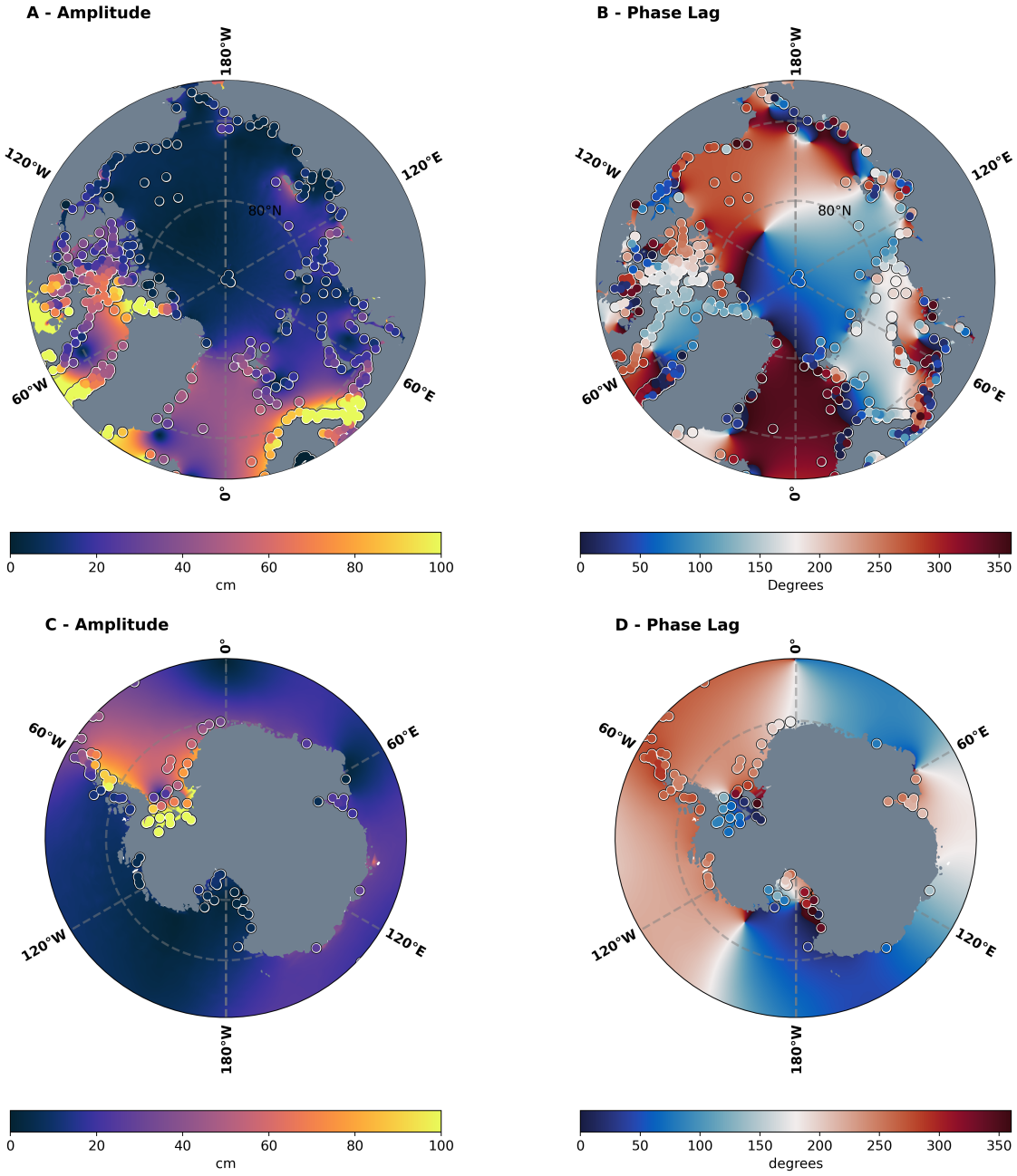

Figure 5.2 (A) Amplitude and (B) phase lag of the M_2 tidal constituent from the ArcTiCA dataset overlaid onto tidal estimations provided by the DTU22 tide model. (C) and (D) are the same but for the Antarctic region with the AntTG database.

5.3 P-3: Altimetry-derived tide model for improved tide and water level forecasting along the European Continental Shelf

Summary

In a changing climate, short-term forecasting of water levels has become increasingly important. In low-lying regions, such as the Netherlands, which are susceptible to storm surges and flooding events, these predictions are critical for deploying flood mitigation measures. Accurately determining when to deploy these measures is not only critical for the safety of the population along the coast but also to reduce costs of any damages caused or costs related to deploying these safety measures.

The final objective of this thesis (**O-3**) involved attempting to improve the ocean tidal boundary forcing of an operational model of the Northwest European Continental Shelf, which is relied upon by the Rijkswaterstaat, part of the Dutch Ministry of Infrastructure and Water Management, for the protection of the Dutch coastline.

The Dutch Continental Shelf Model in Flexible Mesh (DCSM-FM) is developed by Deltares and operated by Rijkswaterstaat to provide such predictions of the total water levels (see an example of a snapshot from the model in Figure 5.3) (Zijl and Groenenboom, 2019). The model has been developed in the Delft3D Flexible Mesh Suite (Kernkamp et al., 2011), which allows for an unstructured grid approach.

This model is forced at the boundary by a variety of oceanographic and atmospheric forcings, including ocean tides. Ocean tides are one of the main drivers of variability in total water levels, particularly along the Dutch coastline, which has a relatively large tidal range. This means that accurately forcing the model along the boundaries of the DCSM-FM model can have significant implications on the water level predictions. Publication **P-3** of this thesis presents the development of a new high-resolution version of the EOT model with several additional tidal constituents, EOT-NECS, to be used in a series of experiments to force DCSM-FM. The model itself is available in **AD-1**

The spatial extent of EOT-NECS was designed to match the boundary regions of the DCSM-FM model to allow for further experimentation as a boundary forcing. This was done by extracting the amplitudes and phases of individual tidal constituents along the boundary and using them to force the model over a one-year period, 2017. The selection of which constituents to use in the experiments was determined by preliminary experiments on DCSM-FM based on identifying constituents with relatively high RMS values with respect to tide gauges as well as incorporating constituents at the boundaries that had previously never been used to force the model. Previously, the model was forced at the boundaries by a total of 39 constituents taken from either FES2014b or GTSM (Wang et al., 2022a).

The first initial experiments of the EOT-NECS model focused on the estimation of 42 tidal constituents and comparison with the FES2014b and GTSM models. An additional three constituents were estimated that previously were not used to force DCSM-FM at the boundaries, which were the MA_2, $\rho 1$ and MB_2 constituents. At the time of writing, these constituents are not available from any public global empirical tide models. A tide gauge analysis was then done using TICON-3 on the tidal constituents to determine which should be used to force DCSM-FM. For the major eight tidal constituents, EOT-NECS showed a significant advancement with respect to both EOT20 and FES2014b, having an average RSS reduction of 0.42 cm. However, initial experiments forcing the DCSM-FM model concluded that the use of GTSM for the Dutch coastline was preferable over using EOT-NECS or FES2014b. This is due to these tidal constituents taken from GTSM being calibrated to the tide gauges along the Dutch coast, which was the main focus of the operational use of the model by Rijkswaterstaat.

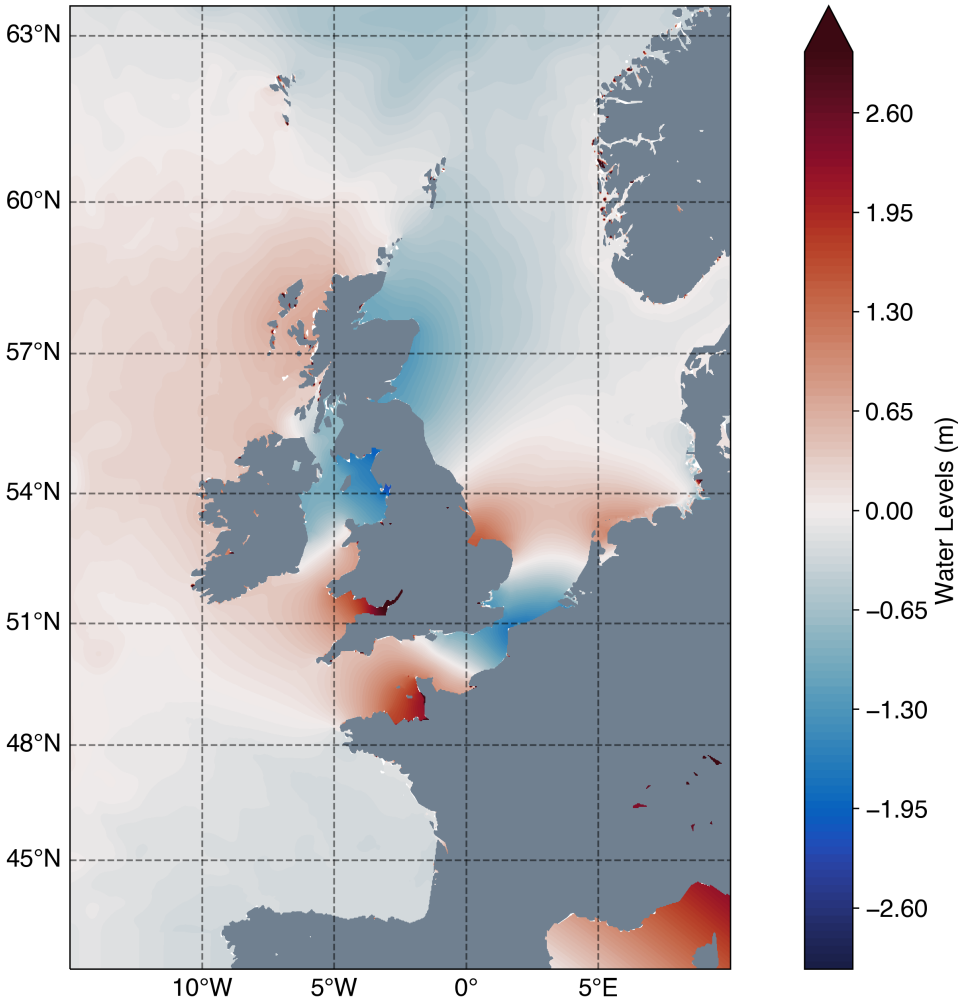

Figure 5.3 A snapshot of water level predictions from the DCSM-FM, demonstrating the rise and fall of water levels in the order of meters caused by the tidal variability of the region.

After analysing the constituents for errors with respect to tide gauges and based on their performance relative to GTSM and FES2014b, a total of fourteen constituents were chosen for experiments within DCSM-FM. Finally, based on the selected tidal constituents, the total water levels were improved across the Northeast European continental shelf and particularly along the Dutch coastline. The outcome of this manuscript is that the EOT-NECS model is now used to provide several tidal constituents for the operational forecasting model run by the Rijkswaterstaat to help in the mitigation of hazardous events along the Dutch coastline.

Copyright

Citation: Hart-Davis, M., Laan, S., Schwatke, C., Backeberg, B., Dettmering, D., Zijl, F., Verlaan, M., Passaro M., Seitz, F. 2023. Altimetry-derived tide model for improved tide and water level forecasting along the European Continental Shelf. Ocean Dynamics.

Declaration of Own Contribution

(MHD: M. Hart-Davis, SL: S. Laan, CS: C. Schwatke, BB: B. Backeberg, DD: D. Dettmering, FZ: F. Zijl, MV: M. Verlaan, MP: M. Passaro, FS: F. Seitz)

This manuscript involved two models, one being an empirical model developed by MHD and one being a numerical model developed by SL, FZ and MV with insights in the context of this manuscript being provided by MHD. The conceptualisation of this study was done by MHD and SL. The empirical model development, computation, validation, production of all figures and tables, interpretation of the results and the writing of the manuscript was done by MHD. SL produced the numerical model simulations of the DCSM-FM model with the help of FZ. CS and DD produced the appropriate satellite altimetry data which was used in the empirical models. BB aided in the interpretation of both model versions' results. MV and FZ supervised the developments in the numerical model simulations. MP conducted additional altimetry retracking used in the empirical model. FS supervised the research. All authors read, commented and reviewed the final manuscript.

The overall contribution of MHD for P-3 is estimated as 78%, which is the average value of the percentage values estimated for the five criteria listed in Table 5.1 below.

Table 5.1 Criteria and estimated contribution share of Michael Hart-Davis for P-3

Criteria	Estimated own contribution
Computation and results	60%
Ideas and study design	70%
Analysis and interpretation	85%
Manuscript Writing	85%
Figure and Table Creation	92%
Total	**78**%

CHAPTER 6

CONCLUSION AND OUTLOOK

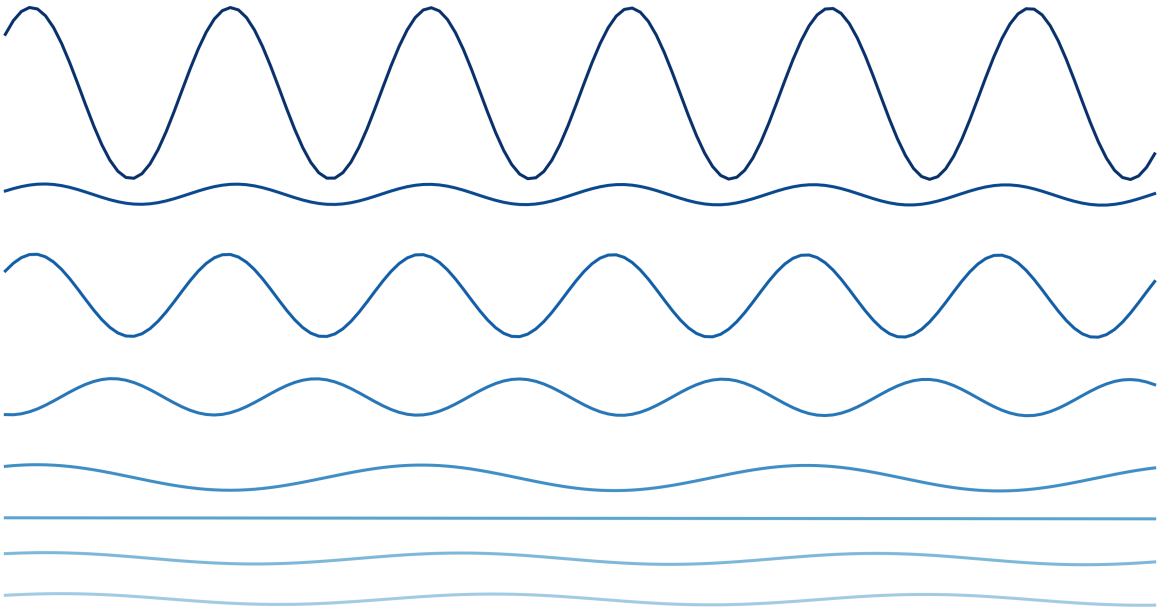

The difficult is what takes a little time; the impossible is what takes a little longer

- Fridtjof Nansen

6 Conclusion and Outlook

This thesis discusses the development of a satellite altimetry-derived ocean tide model for applications in various geophysical applications. Special attention was placed on improving the estimation of ocean tides in the coastal regions in a new global tide model, EOT20, by exploiting the latest advances in coastal altimetry and refining the model for the optimised use of these data. To achieve the aim of this thesis, three objectives were identified and are discussed below.

6.1 Conclusions on objectives

O-3:

O-1: Reduce the error with respect to tide gauges of an updated global ocean tide model while remaining in line with global models in the open ocean and shelf regions.

The production of EOT20 within **P-1** showed positive improvements in the accuracy of ocean tide estimates in the coastal region relative to the previous EOT11a model but also with respect to other major global tide models. In the tide gauge analysis compared to two different tidal constituent databases, EOT20 demonstrated the lowest RSS values in the coastal regions of all the models tested. A particular advancement was seen in the M_2 constituent in the coastal region, with the mean RMS values being 0.3 cm lower than any other model. When applying EOT20 as a tidal correction for satellite altimetry and evaluating the resultant sea level variances using the SLAVA tool for each of the three satellites tested, EOT20 outperformed EOT11a in reducing the variances. With respect to the commonly used FES2014b model, EOT20 also showed lower variances, particularly in the coastal regions, with the two models converging towards the open ocean.

EOT20, therefore, achieved the objective of producing improved tidal estimations in the coastal region with respect to EOT11a and other major ocean tide models. The developments made to the model, as well as the utilised coastal altimetry, helped produce a coastally improved tide model. The full description of the results to achieve **O-1** is presented in **P-1**.

O-2: Increasing the accuracy of the tidal correction for satellite altimetry by optimising the methods of accounting for minor tidal constituents.

Although minor tides tend to have less of a contribution to the overall tidal heights, they remain crucial in reducing the error of tidal predictions (Egbert and Ray, 2017). **P-2** focused on assessing different methods of deriving some of the largest minor tides in several regional experiments. The methods used were the frequently used linear admittances approach, direct estimations from empirical models and direct estimations from purely numerical models. These methods were evaluated against in-situ tide gauges from TICON as well as by applying each method to altimetry corrections.

Three regional experiments were chosen: the Australian coastline, New Zealand coastline as well as the combined Japan Sea and East China Sea. The direct estimations were taken from different regional EOT models, which extended the EOT20 model configuration to include the additional required tidal constituents. Additionally, estimates from FES2014b and TiME22 were used as alternative ways of estimating these tides.

It was concluded that instead of being inferred, four tidal constituents should be directly estimated: J_1, L_2, μ_1 and ν_1, and four tidal constituents should be inferred: ${}^2N_2$, ϵ_2, M_{SF} and T_2. Finally, a first look into merging individual constituents across different models to form a hybrid tidal correction was evaluated. This hybrid correction is aimed at utilising the individual model strengths and capabilities to optimise the correction overall. On average, the hybrid correction shows very little difference compared to taking all the constituents from the EOT model alone, but there are certain regions where improvements can be seen. It could be expected that further expansion on the constituent list might result in a future hybrid correction being favoured.

The different experiments and further explanations of the regional differences are described in **P-2**.

O-3: Improve the prediction of ocean tides within an operational ocean model of the Northwest European Continental Shelf by improving the ocean tide forcing at the open boundaries.

Tides are an essential contribution to the total water levels, and therefore, accurate prediction of tides is crucial for floods and storm surges across the globe, particularly in regions susceptible to these hazards, e.g., the Dutch coastline. Local authorities and agencies develop ocean and weather models to better predict these hazards. One such model, developed by Deltares and the Rijkswaterstaat, is the Dutch Continental Shelf Model in Flexible Mesh (DCSM-FM), which aims to produce, among other things, forecasts of total water levels to aid in the deployment of flood protection methods. This model is forced at its boundaries by ocean tides, and the results described at **P-1** and **P-2** provided motivation that improvements could be made to their model by incorporating EOT at its boundaries.

To test this, a regional EOT model was designed, which incorporated newly available data from five additional altimeters. This allowed for an extension of the time series used in deriving tidal constituents and increased coverage from the new altimeter orbits. The resultant model for the North European Continental Shelf (EOT-NECS) was evaluated against an updated tide gauge dataset, TICON-3, and showed significant improvements for all tidal constituents compared to the global EOT20 model and FES2014b. Several experiments were done within DCSM-FM utilising different numbers of tidal constituents from EOT-NECS and evaluating the impact this has on the total water height prediction from the model. It was concluded that eleven constituents should be taken from the EOT-NECS model and used to operationally force DCSM-FM to improve the accuracy of water level predictions across the North European coast, particularly along the Dutch coastline.

In **P-3**, the developed EOT-NECS model is validated and described, and the different DCSM-FM model experiments are presented and evaluated.

6.2 Recommendations and future work

This thesis demonstrates an advance in tidal estimation in the coastal regions, seeing significant improvements in estimations of individual constituents with respect to other global models. Additionally, the experiments and developments of this thesis provided a great deal of insight into altimetry-derived ocean tide models, validation techniques, and the importance of tides in geophysical applications. The subsequent discussion and evaluation of the results presented within this thesis have raised several additional questions which could provide further improvements in tidal estimations. Below are several recommendations for future work:

Optimisation of geophysical corrections for tide modelling

EOT20 achieved its objective of providing vast improvements in the coastal and shelf regions while remaining aligned with expectations in the open ocean. Despite these improvements, the impacts of the geophysical corrections on the resultant tidal accuracy were concluded as being an avenue where the model can still be improved. A recent publication by Ray (2020a) presented a comparison of the differences between ionospheric corrections and demonstrated significant differences, shown in Figure 2.8 in this thesis, which impact the accuracy of the ocean tide estimations. These differences are also seen in other geophysical corrections. Additionally, Ray et al. (2023) demonstrated significant tidal signals in the Dynamic Atmospheric Correction (DAC), which would influence the resultant ocean tide estimations. The continued evaluation should be done on the geophysical corrections to assess whether any aliasing issues can be found within these corrections and to provide optimised estimations of ocean tides in the regions of interest, such as the coastal regions. The same can be said based on the applications of interest.

In recent years, new geophysical corrections have been developed to remove the contributions of specific processes. This includes the internal tide correction as well as a so-called mesoscale correction. The internal tide correction is aimed at removing the surface expression of internal tides (Ray and Zaron, 2011), which is particularly important for the SWOT mission (Zaron, 2017). The most used internal tide model for altimetry applications, HRET, is itself altimetry-derived data and has already been corrected for the ocean tide contribution (Zaron, 2015, 2017). Studies on the impact of applying this correction on the SLA before doing residual tidal analysis would provide interesting insight into the relationship between ocean tides and internal tides. The results of such investigations could result in improvements in tide models.

The mesoscale correction aims to reduce the mesoscale noise found within SLA data before conducting a tidal analysis (Zaron and Ray, 2018). Doing so helps improve the signal-to-noise ratio, making it easier to better estimate tidal constituents. Mesoscale variability was also identified within error maps of EOT20 for certain tidal constituents as well as in the variance estimations, where mesoscale features appeared to influence tidal estimations. The application of the mesoscale correction has significant impacts on tidal estimations (see, e.g. Ray and Byrne, 2010), with a preliminary EOT version, EOT-MESO, showing improved accuracy in a region of high mesoscale variability for all major constituents and a clear influence on resultant tidal amplitudes (Figure 6.1). This first experiment provides strong motivation for including this correction in future iterations of the global model. Further experimentation should be done in other regions, particularly in regions of low mesoscale variability. Additionally, the approach of Zaron and Ray (2018) using the DUACS products (Pujol et al., 2016) can be compared to other techniques of estimating the mesoscale correction, such as that of Bonaduce et al. (2021).

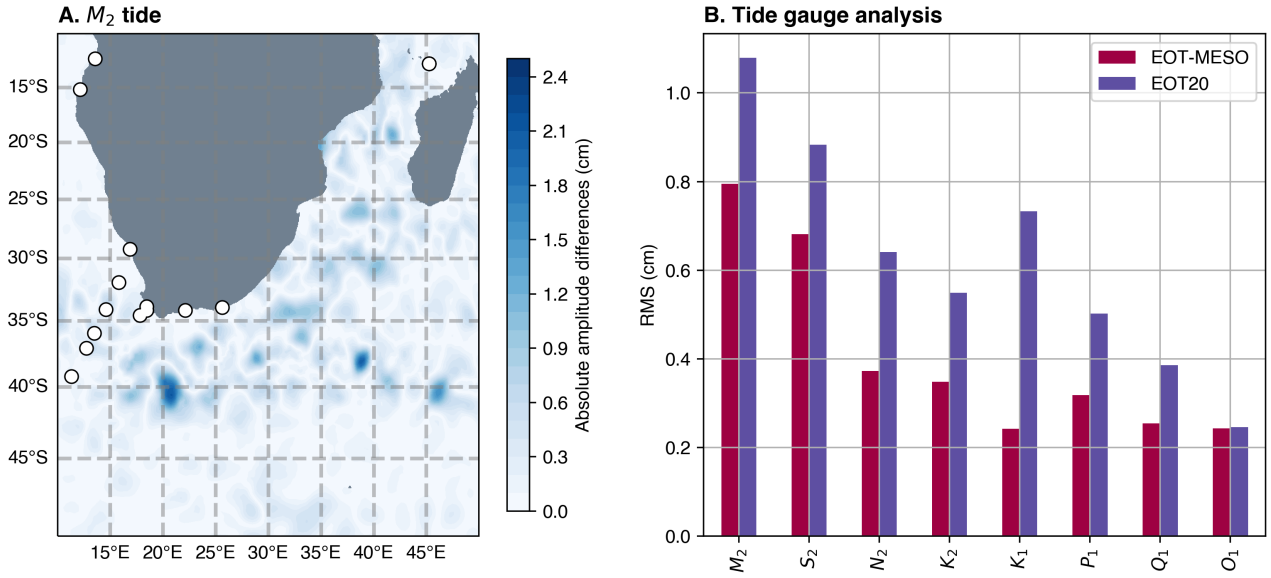

Figure 6.1 (A) The absolute amplitude difference for the M_2 tide between correcting the SLA for mesoscale variability against not doing so. (B) The results of tide gauge analysis against TICON-3 and the RR dataset for the major eight tidal constituents.

Empirical modelling in the polar oceans

The EOT20 model provides near-global estimations of ocean tides; however, these estimations were restricted to be between 66°N and 66°S. This was mainly related to the available altimetry data, particularly altimeters that were non-sun-synchronous, which is limited in the higher latitudes. Furthermore, the influence of sea ice on the altimetry retrievals and limited in-situ observations for validation purposes resulted in these latitudinal restrictions being chosen for EOT20.

The limitations of in-situ measurements in the polar regions have been a common difficulty for most oceanographic applications, particularly for tidal research. The reasons behind this are the geopolitical sensitivity of the regions, harsh weather conditions for regular maintenance and deployments of measurement devices, and the sheer cost related to these measurements. The work done in **AP-2** to collect and harmonise all the available in-situ measurements in the Arctic Ocean has provided a great framework for continued modelling efforts to be done. This will allow for the validation and evaluation of models in the Arctic and provide guidance on where the models need to be improved.

Advances have taken place in the processing of satellite altimetry in the polar regions thanks to improved retracking (Passaro et al., 2018b) and sea-ice classification approaches (Passaro et al., 2018a; Müller et al., 2023). This has resulted in more reliable retrievals of radar returns and, therefore, more reliable SLA estimates in previously challenging regions, e.g. in sea ice leads. These advancements would be crucial for allowing EOT to make its first empirical estimations in the polar regions.

In recent years, several studies have investigated the use of Cryosat-2 for tidal estimations in the higher latitudes, largely thanks to its 28-day sub-cycle (Zaron, 2018). This has resulted in a significantly greater SLA coverage in both the Arctic and Antarctic, which is critical for ocean tide estimations. In **AP-3** of this thesis, updates to the DTU ocean tide model, DTU22 (Andersen et al., 2023), were done based on utilising Cryosat-2 in the polar regions, which showed significant improvements with respect to FES2014b in both regions.

These results, coupled with the advanced processing techniques and available in-situ networks, mean that making tidal estimates in the polar regions is now possible from satellite altimetry. There is also a need to experiment on the merging of Cryosat-2 data with pre-existing altimetry data from ERS/EN/SA missions as well as the Sentinel-3a and -3b missions to see if this provides further improvements to tide models in the region. Currently, no model exists that combines all these data, and therefore, it is recommended to evaluate the combination of these altimeters for tidal predictions.

Merged empirical and numerical models for improved tidal predictions

Minor ocean tides are commonly inferred via linear admittance approaches as they are not capable of being directly estimated from empirical ocean tide models due to aliasing errors (Egbert and Ray, 2017). In **P-2**, an alternative approach of merging different tide models was presented, aiming to exploit the strengths of the respective models. In most cases, altimetry-derived tide models are more accurate than data-unconstrained models (Stammer et al., 2014). However, they are not capable, either relating to aliasing issues or computational demand, of providing estimations for the large number of tidal constituents that influence the overall tidal variability. Although hundreds of constituents exist (see the list maintained by the International Hydrological Office `https://iho.int/mtg_docs/com_wg/IHOTC/IHOTC_Misc/TWCWG_Constituent_list.pdf`), not all of them are required for tidal predictions as the majority of the tidal variability, 99.99%, is captured by about eighty constituents (Egbert and Ray, 2017).

As shown in paper **P-2**, the linear admittance approaches, which are used to infer many constituents not provided by models, are not always perfect. It is, therefore, possible that the combination of a series of constituents from a data-constrained model with those from a data-unconstrained model will be more beneficial than the currently used linear admittance approaches in improving tidal predictions. For that reason, investigating the combination of models, such as EOT20 and TiME22, in several geodetic applications could result in improved tidal predictions and, therefore, subsequent downstream estimations such as sea level and gravity field.

Improved reliability and coverage of in-situ datasets

In-situ measurements remain critical for understanding ocean processes and for model validation. The GESLA database provides hourly time series of tide gauges from around the world that have been utilised to derive global tidal constituent datasets (Piccioni et al., 2019a; Hart-Davis et al., 2022). Ocean bottom pressure sensors have also been shown to be useful for tidal analysis and model validations (Ray, 2013) and, more recently, efforts have been made to derive tidal constituents from GNSS-R, particularly by Tabibi et al. (2020) and Larson et al. (2013). However, both suffer from limited spatial coverage and short time series compared to tide gauges. Despite this, these three data sources together are an excellent resource for tidal research, such as demonstrated in **AP-2**.

The estimation of tides is extremely sensitive to the input data provided, not only the sea level time series but also the time data itself. An example is presented in Figure 6.2, where the same tide gauge is provided from three different sources, which all cause differences in the phase estimates of the M_2 constituent. These phase differences are caused by the different sources containing different time references. In this example, the NHS (Norwegian Mapping Authority) provider changed its time reference in 1980, which had drastic impacts on tide estimations. In practice, this is easy to solve following the conversion techniques presented in Schureman (1958). However, identifying the time reference used in each case is sometimes very difficult and time-consuming. In

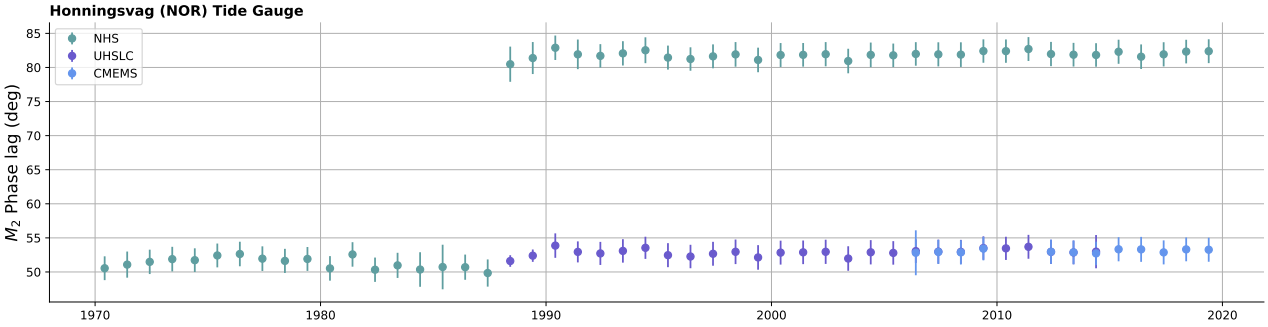

Figure 6.2 The yearly phase estimations of the M_2 constituent from the Honningsvag tide gauge in Norway which were taken from three different data sources within the GESLA-3 database.

TICON-3, for example, over 3,500 individual time series are analysed, and it is impractical to sieve through each time series to identify either changes in the time references or the original time references.

Furthermore, in cases when the time reference changes within the time series, such as that in this example, the conversion of the tidal constituents is not possible, and the time series itself needs to be converted directly.

It is, therefore, recommended for continued development of datasets such as TICON to improve the reliability of constituent estimations and to identify issues relating to time references and relating to discontinuities in the time series. Approaches such as the yearly tidal estimation presented in Figure 6.2 and in **AP-2** as well as software that are designed to find dataset discontinuities can be used, for example, that presented in Oelsmann et al. (2022). Furthermore, a harmonisation globally of all available tide gauges with data from both ocean bottom pressure and GNSS-R will allow for a consistent, one-stop-shop of measurements for both data validation and assimilation.

Changes in tides in the altimetry era

In several applications, ocean tides are considered stationary based on the predictability of the astronomical forcing (i.e. the relative position between the Earth, Sun and Moon). However, scientists as far back as the research of Doodson (1924) have discussed and studied the changes in tidal 'constants'. In Haigh et al. (2020), a comprehensive review of the non-astronomical changes in ocean tides is presented, demonstrating the changes in tidal constants from both tide gauge observations and numerical model simulations. Schindelegger et al. (2018) presented a global evaluation in different numerical scenarios of pseudo increases in the sea level and demonstrated changes in the amplitude of the M2 tide due to the increased sea level. These changes to the M2 amplitude, however, were not consistent throughout the global ocean, with some regions showing increases while other regions showed decreases in the amplitude.

Satellite altimetry has heavily bolstered our understanding of ocean tides, resulting in a vast improvement to tidal estimations (Provost et al., 1995; Ray, 1999; Savcenko and Bosch, 2012). As of 2023, over 30 years worth of altimetry data is available. This time series is helpful for full tidal estimations but also in providing temporal evaluations of the variability of the major tides. This has been comprehensively done from numerical studies, and recent studies have begun to assess tidal changes from altimetry, e.g. Bij de Vaate et al. (2022); Ray et al. (2023). Further investigation on changes in altimetry-derived tides as caused by non-astronomical changes is required, as well as an evaluation of the impact these changes have on other sea-level applications.

Using SWOT to study tides

The Surface Water and Ocean Topography (SWOT) satellite was launched in late 2022 and promised to provide an entirely new perspective of the ocean surface. SWOT provides both NADIR and KaRIn (Ka-band Radar Interferometer) data, the latter being unique as it provides an approximately 120 km wide swath of the ocean surface. These data give rise to the opportunity to better resolve the spatial characteristics of ocean tides both in the open ocean and in the coastal regions (Arbic et al., 2015). This has the potential to significantly advance the EOT model both in terms of spatial resolution and also in deriving tides in complex coastal regions, including in fjords and coastal inlets where modern-day altimetry struggles to provide reliable estimates. As fjords or complex inlets are usually too small to be captured appropriately by tide model resolutions, this improved coverage will allow models to provide suitable corrections instead of the previously relied upon interpolation techniques. Therefore, it is recommended that experiments be conducted to investigate whether these data from SWOT can be incorporated with the other satellite altimeters within the EOT model.

Bibliography

Andersen, O. B. (1995). Global ocean tides from ERS 1 and TOPEX/POSEIDON altimetry. *Journal of Geophysical Research*, 100(C12):25249.

Andersen, O. B., Rose, S. K., and Hart-Davis, M. G. (2023). Polar ocean tides- revisited using cryosat-2. *Remote Sensing*, 15(18).

Andersen, O. B. and Scharroo, R. (2011). Range and geophysical corrections in coastal regions: and implications for mean sea surface determination. In *Coastal altimetry*, pages 103–145. Springer.

Andersen, O. B., Stenseng, L., Piccioni, G., and Knudsen, P. (2016). The DTU15 MSS (mean sea surface) and DTU15LAT (lowest astronomical tide) reference surface. In *ESA Living Planet Symposium 2016*.

Andersson, A. (2020). *Observing ocean tidal loading with GNSS*. PhD thesis, Chalmers University of Technology.

Apel, J. R. (1987). *Principles of ocean physics*. International Geophysics. Academic Press, San Diego, CA.

Arbic, B. K., Lyard, F., Ponte, A., Ray, R. D., Richman, J. G., Shriver, J. F., Zaron, E., and Zhao, Z. (2015). Tides and the SWOT mission: Transition from science definition team to science team. *Civil and Environmental Engineering Faculty Publications and Presentations*, 336.

Benveniste, J. (2011). *Radar Altimetry: Past, Present and Future*, pages 1–17. Springer Berlin Heidelberg, Berlin, Heidelberg.

Bij de Vaate, I., Slobbe, D. C., and Verlaan, M. (2022). Secular trends in global tides derived from satellite radar altimetry. *Journal of Geophysical Research: Oceans*, 127(10):e2022JC018845. e2022JC018845 2022JC018845.

Bij de Vaate, I., Vasulkar, A. N., Slobbe, D. C., and Verlaan, M. (2021). The influence of Arctic landfast ice on seasonal modulation of the M_2 tide. *Journal of Geophysical Research: Oceans*, 126(5).

Birol, F., Léger, F., Passaro, M., Cazenave, A., Niño, F., Calafat, F. M., Shaw, A., Legeais, J.-F., Gouzenes, Y., Schwatke, C., and others, . (2021). The X-TRACK/ALES multi-mission processing system: New advances in altimetry towards the coast. *Advances in Space Research*, 67(8):2398–2415.

Bloßfeld, M., Hart-Davis, M., Glomsda, M., and Dettmering, D. (2021). The impact of the EOT20 global ocean tide model on space geodetic measurements, satellite orbits and derived geodetic parameters. In *International Association of Geodesy (IAG) Scientific Assembly 2021*.

Bonaduce, A., Cipollone, A., Johannessen, J. A., Staneva, J., Raj, R. P., and Aydogdu, A. (2021). Ocean Mesoscale Variability: A Case Study on the Mediterranean Sea From a Re-Analysis Perspective. *Frontiers in Earth Science*, 9.

Bosch, W., Dettmering, D., and Schwatke, C. (2014). Multi-mission cross-calibration of satellite altimeters: Constructing a long-term data record for global and regional sea level change studies. *Remote Sensing*, 6(3):2255–2281.

Brockley, D. J., Baker, S., Féménias, P., Martinez, B., Massmann, F.-H., Otten, M., Paul, F., Picard, B., Prandi, P., Roca, M., et al. (2017). REAPER: Reprocessing 12 years of ERS-1 and ERS-2 altimeters and microwave radiometer data. *IEEE Transactions on Geoscience and Remote Sensing*, 55(10):5506–5514.

Cancet, M., Griffin, D., Cahill, M., Chapron, B., Johannessen, J., and Donlon, C. (2019). Evaluation of GlobCurrent surface ocean current products: A case study in Australia. *Remote sensing of environment*, 220:71–93.

Carrere, L., Arbic, B. K., Dushaw, B., Egbert, G., Erofeeva, S., Lyard, F., Ray, R. D., Ubelmann, C., Zaron, E., Zhao, Z., et al. (2021). Accuracy assessment of global internal-tide models using satellite altimetry. *Ocean Science*, 17(1):147–180.

Carrere, L., Faugère, Y., and Ablain, M. (2016). Major improvement of altimetry sea level estimations using pressure-derived corrections based on ERA-Interim atmospheric reanalysis. *Ocean Science*, 12(3):825–842.

Carrère, L., Faugère, Y., Bronner, E., and Benveniste, J. (2011). Improving the dynamic atmospheric correction for mean sea level and operational applications of atimetry. In *Proceedings of the Ocean Surface Topography Science Team (OSTST) Meeting, San Diego, CA, USA*, page 19–21.

Cartwright, D. (2001). On the origins of knowledge of the sea tides from antiquity to the thirteenth century. *Earth Sciences History*, 20(2):105–126.

Cartwright, D. E. (1999). *Tides : a scientific history / David Edgar Cartwright.* Cambridge University Press, Cambridge, UK ;.

Cartwright, D. E. and Ray, R. D. (1991). Energetics of global ocean tides from Geosat altimetry. *Journal of Geophysical Research: Oceans*, 96(C9):16897–16912.

Chambers, D., Hayes, S., Ries, J., and Urban, T. (2003). New TOPEX sea state bias models and their effect on global mean sea level. *Journal of Geophysical Research: Oceans*, 108(C10).

Chelton, D. B., Ries, J. C., Haines, B. J., Fu, L.-L., and Callahan, P. S. (2001). Chapter 1 Satellite Altimetry. In Fu, L.-L. and Cazenave, A., editors, *Satellite Altimetry and Earth Sciences*, volume 69 of *International Geophysics*, pages 1–ii. Academic Press.

Cheng, Y. and Andersen, O. B. (2011). Multimission empirical ocean tide modeling for shallow waters and polar seas. *Journal of Geophysical Research: Oceans*, 116(C11).

Cheng, Y. and Andersen, O. B. (2017). Towards further improving DTU global ocean tide model in shallow waters and Polar Seas. In *OSTST, Poster in: Proceedings of the Ocean Surface Topography Science Team (OSTST) Meeting, Miami, FL, USA*, pages 23–27.

Codiga, D. L. (2011). Unified tidal analysis and prediction using the UTide Matlab functions. Technical report.

Darwin, G. H. (1891). XI. On the harmonic analysis of tidal observations of high and low water. *Proceedings of the Royal Society of London*, 48(292-295):278–340.

Desai, S. D., Wahr, J. M., and Chao, Y. (1997). Error analysis of empirical ocean tide models estimated from TOPEX/POSEIDON altimetry. *Journal of Geophysical Research: Oceans*, 102(C11):25157–25172.

Dettmering, D., Schmidt, M., Heinkelmann, R., and Seitz, M. (2011). Combination of different space-geodetic observations for regional ionosphere modeling. *Journal of Geodesy*, 85(12):989–998.

Doodson, A. T. (1921). The harmonic development of the tide-generating potential. *Proceedings of the Royal Society of London. Series A, Containing Papers of a Mathematical and Physical Character*, 100(704):305–329.

Doodson, A. T. (1924). Perturbations of harmonic tidal constants. *Proceedings of the Royal Society of London. Series A, Containing Papers of a Mathematical and Physical Character*, 106(739):513–526.

Doodson, A. T. and Warburg, H. D. (1941). Admiralty manual of tides. *Great Britain. Hydrographic Department*.

Egbert, G. D. and Erofeeva, S. Y. (2002). Efficient inverse modeling of barotropic ocean tides. *Journal of Atmospheric and Oceanic technology*, 19(2):183–204.

Egbert, G. D., Erofeeva, S. Y., and Ray, R. D. (2010). Assimilation of altimetry data for nonlinear shallow-water tides: Quarter-diurnal tides of the northwest european shelf. *Continental Shelf Research*, 30(6):668–679. Tides in Marginal Seas - A special issue in memory of Prof Alexei Nekrasov.

Egbert, G. D. and Ray, R. D. (2017). Tidal prediction. *Journal of Marine Research*, 75(3):189–237.

Eicker, A. (2008). *Gravity field refinement by radial basis functions from in-situ satellite data*. Univ. Bonn, Inst. für Geodäsie und Geoinformation.

Erdogan, E., Schmidt, M., Goss, A., Görres, B., and Seitz, F. (2020). Adaptive modeling of the global ionosphere vertical total electron content. *Remote Sensing*, 12(11).

Farrell, W. E. (1972). Deformation of the earth by surface loads. *Reviews of Geophysics*, 10(3):761.

Fernandes, M. J. and Lázaro, C. (2016). GPD+ wet tropospheric corrections for CryoSat-2 and GFO altimetry missions. *Remote Sensing*, 8(10):851.

Fok, H. S. (2012). *Ocean tides modeling using satellite altimetry*. PhD thesis, The Ohio State University.

Fuchs, D. (2016). Geodesics on regular polyhedra with endpoints at the vertices. *Arnold Mathematical Journal*, 2(2):201–211.

Glomsda, M., Seitz, M., Bloßfeld, M., and Seitz, F. (2023). Effects of non-tidal loading applied in VLBI-only terrestrial reference frames. *Journal of Geodesy*, 97(8).

Gommenginger, C., Thibaut, P., Fenoglio-Marc, L., Quartly, G., Deng, X., Gómez-Enri, J., Challenor, P., and Gao, Y. (2011). *Retracking Altimeter Waveforms Near the Coasts*, pages 61–101. Springer Berlin Heidelberg, Berlin, Heidelberg.

Hagen, R., Plüß, A., Jänicke, L., Freund, J., Jensen, J., and Kösters, F. (2021). A combined modeling and measurement approach to assess the nodal tide modulation in the north sea. *Journal of Geophysical Research: Oceans*, 126(3):e2020JC016364. e2020JC016364 2020JC016364.

Haigh, I. D., Marcos, M., Talke, S. A., Woodworth, P. L., Hunter, J. R., Hague, B. S., Arns, A., Bradshaw, E., and Thompson, P. (2022). GESLA Version 3: A major update to the global higher-frequency sea-level dataset. *Geoscience Data Journal*.

Haigh, I. D., Pickering, M. D., Green, J. A. M., Arbic, B. K., Arns, A., Dangendorf, S., Hill, D. F., Horsburgh, K., Howard, T., Idier, D., Jay, D. A., Jänicke, L., Lee, S. B., Müller, M., Schindelegger, M., Talke, S. A., Wilmes, S.-B., and Woodworth, P. L. (2020). The tides they are a-changin': A comprehensive review of past and future nonastronomical changes in tides, their driving mechanisms, and future implications. *Reviews of Geophysics*, 58(1).

Hamid, A., Din, A., Abdullah, N., Yusof, N., Hamid, M., and Shah, A. (2021). Exploring space geodetic technology for physical coastal vulnerability index and management strategies: A review. *Ocean and Coastal Management*, 214:105916.

Hart-Davis, M. G., Dettmering, D., and Seitz, F. (2022). TICON: Tidal Constants. *PANGAEA*.

Hauk, M., Wilms, J., Sulzbach, R., Panafidina, N., Hart-Davis, M., Dahle, C., Müller, V., Murböck, M., and Flechtner, F. (2023). Satellite Gravity Field Recovery Using Variance-Covariance Information From Ocean Tide Models. *Earth and Space Science*, 10(10).

Holgate, S. J., Matthews, A., Woodworth, P. L., Rickards, L. J., Tamisiea, M. E., Bradshaw, E., Foden, P. R., Gordon, K. M., Jevrejeva, S., and Pugh, J. (2013). New Data Systems and Products at the Permanent Service for Mean Sea Level. *Journal of Coastal Research*, 29(3):493 – 504.

Howard, S. L., King, M., and Padman, L. (2020). Antarctic Tide Gauge Database, version 1. *U.S. Antarctic Program (USAP) Data Center*.

Kernkamp, H., van Dam, A., Stelling, G., and de Goede, E. (2011). Efficient scheme for the shallow water equations on unstructured grids with application to the continental shelf. *Ocean Dynamics: theoretical, computational oceanography and monitoring*, 61(8):1175–1188.

Kowalik, Z. and Proshutinsky, A. Y. (1994). *The Arctic Ocean Tides*, pages 137–158. American Geophysical Union (AGU).

Landskron, D. and Böhm, J. (2018). VMF3/GPT3: refined discrete and empirical troposphere mapping functions. *Journal of Geodesy*, 92(4):349–360.

Larson, K. M., Ray, R. D., Nievinski, F. G., and Freymueller, J. T. (2013). The Accidental Tide Gauge: A GPS Reflection Case Study From Kachemak Bay, Alaska. *IEEE Geoscience and Remote Sensing Letters*, 10(5):1200–1204.

Li, Z., Guo, J., Ji, B., Wan, X., and Zhang, S. (2022). A review of marine gravity field recovery from satellite altimetry. *Remote Sensing*, 14(19).

Lyard, F. H., Allain, D. J., Cancet, M., Carrère, L., and Picot, N. (2021). FES2014 global ocean tide atlas: design and performance. *Ocean Science*, 17(3):615–649.

Morrow, R., Fu, L.-L., Rio, M.-H., Ray, R., Prandi, P., Traon, P.-Y. L., and Benveniste, J. (2023). Ocean circulation from space. *Surveys in Geophysics*, 44(5):1243–1286.

Müller, F. L., Paul, S., Hendricks, S., and Dettmering, D. (2023). Monitoring Arctic thin ice: a comparison between CryoSat-2 SAR altimetry data and MODIS thermal-infrared imagery. *The Cryosphere*, 17(2):809–825.

Munk, W. H. and Cartwright, D. E. (1966). Tidal spectroscopy and prediction. *Philosophical Transactions of the Royal Society of London. Series A, Mathematical and Physical Sciences*, 259(1105):533–581.

Männel, B., Dobslaw, H., Dill, R., Glaser, S., Balidakis, K., Thomas, M., and Schuh, H. (2019). Correcting surface loading at the observation level: impact on global GNSS and VLBI station networks. *Journal of Geodesy*, 93(10):2003–2017.

Newton, I. (1833). *Philosophiae naturalis principia mathematica*, volume 1. G. Brookman.

NOAA (2022). ETOPO 2022 15 Arc-Second Global Relief Model. *NOAA National Centers for Environmental Information*.

Oelsmann, J., Passaro, M., Sánchez, L., Dettmering, D., Schwatke, C., and Seitz, F. (2022). Bayesian modelling of piecewise trends and discontinuities to improve the estimation of coastal vertical land motion. *Journal of Geodesy*, 96(9).

Pan, H., Devlin, A. T., Xu, T., Lv, X., and Wei, Z. (2022). Anomalous 18.61-Year Nodal Cycles in the Gulf of Tonkin Revealed by Tide Gauges and Satellite Altimeter Records. *Remote Sensing*, 14(15).

Panikkar, N. and Srinivasan, T. (1971). The concept of tides in Ancient India. *Indian Journal of History of Science*, 6(1):36–50.

Parke, M. E., Stewart, R. H., Farless, D. L., and Cartwright, D. E. (1987). On the choice of orbits for an altimetric satellite to study ocean circulation and tides. *Journal of Geophysical Research: Oceans*, 92(C11):11693–11707.

Parker, B. (2018). *Tides*. Springer International Publishing, Cham, Germany.

Passaro, M., Cipollini, P., Vignudelli, S., Quartly, G. D., and Snaith, H. M. (2014). ALES: A multi-mission adaptive subwaveform retracker for coastal and open ocean altimetry. *Remote Sensing of Environment*, 145:173–189.

Passaro, M., Müller, F. L., and Dettmering, D. (2018a). Lead detection using Cryosat-2 delay-doppler processing and Sentinel-1 SAR images. *Advances in Space Research*, 62(6):1610–1625. The CryoSat Satellite Altimetry Mission: Eight Years of Scientific Exploitation.

Passaro, M., Rautiainen, L., Dettmering, D., Restano, M., Hart-Davis, M. G., Schlembach, F., Särkkä, J., Müller, F. L., Schwatke, C., and Benveniste, J. (2022). Validation of an Empirical Subwaveform Retracking Strategy for SAR Altimetry. *Remote Sensing*, 14(16).

Passaro, M., Rose, S. K., Andersen, O. B., Boergens, E., Calafat, F. M., Dettmering, D., and Benveniste, J. (2018b). ALES+: Adapting a homogenous ocean retracker for satellite altimetry to sea ice leads, coastal and inland waters. *Remote Sensing of Environment*, 211:456–471.

Pawlowicz, R., Beardsley, B., and Lentz, S. (2002). Classical tidal harmonic analysis including error estimates in MATLAB using T_TIDE. *Computers & Geosciences*, 28(8):929–937.

Peng, D., Hill, E. M., Meltzner, A. J., and Switzer, A. D. (2019). Tide gauge records show that the 18.61-year nodal tidal cycle can change high water levels by up to 30 cm. *Journal of Geophysical Research: Oceans*, 124(1):736–749.

Petit, G. and Luzum, B. (2010). IERS conventions (2010). Technical report, Verlag des Bundesamts für Kartographie und Geodäsie.

Piccioni, G. (2021). *Exploit satellite altimetry to improve coastal tide estimation*. PhD thesis, Technische Universität München.

Piccioni, G., Dettmering, D., Bosch, W., and Seitz, F. (2019a). TICON: TIdal CONstants based on GESLA sea-level records from globally located tide gauges. *Geoscience Data Journal*, 6(2):97–104.

Piccioni, G., Dettmering, D., Passaro, M., Schwatke, C., Bosch, W., and Seitz, F. (2018). Coastal improvements for tide models: the impact of ALES retracker. *Remote Sensing*, 10(5):700.

Piccioni, G., Dettmering, D., Schwatke, C., Passaro, M., and Seitz, F. (2019b). Design and regional assessment of an empirical tidal model based on fes2014 and coastal altimetry. *Advances in Space Research*.

Provost, C. L., Bennett, A. F., and Cartwright, D. E. (1995). Ocean tides for and from TOPEX/POSEIDON. *Science*, 267(5198):639–642.

Pugh, D. and Woodworth, P. (2014). *Sea-Level Science: Understanding Tides, Surges, Tsunamis and Mean Sea-Level Changes*. Cambridge University Press.

Pugh, D. T. (1987). *Tides, surges and mean sea level*.

Pujol, M.-I., Dupuy, S., Vergara, O., Sánchez-Román, A., Faugère, Y., Prandi, P., Dabat, M.-L., Dagneaux, Q., Lievin, M., Cadier, E., Dibarboure, G., and Picot, N. (2022). Refining the resolution of DUACS along track (level 3) altimeter Sea Level products. *Earth System Science Data Discussions*, 2022:1–40.

Pujol, M.-I., Faugère, Y., Taburet, G., Dupuy, S., Pelloquin, C., Ablain, M., and Picot, N. (2016). DUACS DT2014: the new multi-mission altimeter data set reprocessed over 20 years. *Ocean Science*, 12(5):1067–1090.

Ray, R. D. (1998). Spectral analysis of highly aliased sea-level signals. *Journal of Geophysical Research: Oceans*, 103(C11):24991–25003.

Ray, R. D. (1999). *A global ocean tide model from TOPEX/POSEIDON altimetry: GOT99. 2*. National Aeronautics and Space Administration, Goddard Space Flight Center.

Ray, R. D. (2007). Tidal analysis experiments with sun-synchronous satellite altimeter data. *Journal of Geodesy*, 81:247–257.

Ray, R. D. (2013). Precise comparisons of bottom-pressure and altimetric ocean tides. *Journal of Geophysical Research: Oceans*, 118(9):4570–4584.

Ray, R. D. (2017). On tidal inference in the diurnal band. *Journal of Atmospheric and Oceanic Technology*, 34(2):437–446.

Ray, R. D. (2020a). Daily harmonics of ionospheric total electron content from satellite altimetry. *Journal of Atmospheric and Solar-Terrestrial Physics*, 209:105423.

Ray, R. D. (2020b). First global observations of third-degree ocean tides. *Science Advances*, 6(48).

Ray, R. D. (2022). Technical note: On seasonal variability of the M_2 tide. *Ocean Science*, 18(4):1073–1079.

Ray, R. D. and Byrne, D. A. (2010). Bottom pressure tides along a line in the southeast Atlantic Ocean and comparisons with satellite altimetry. *Ocean dynamics*, 60(5):1167–1176.

Ray, R. D. and Ponte, R. M. (2003). Barometric tides from ECMWF operational analyses. *Annales Geophysicae*, 21(8):1897–1910.

Ray, R. D., Schindelegger, M., and Opel, L. (2023). A tentative picture of changes in the open-ocean M2 tide since 1992.

Ray, R. D. and Zaron, E. D. (2011). Non-stationary internal tides observed with satellite altimetry. *Geophysical Research Letters*, 38(17).

Rieser, D., Mayer-Gürr, T., Savcenko, R., Bosch, W., Wünsch, J., Dahle, C., and Flechtner, F. (2012). The ocean tide model EOT11a in spherical harmonics representation. *Technical Note, Institute of Theoretical Geodesy and Satellite Geodesy (ITSG), TU Graz, Austria*.

Savcenko, R. and Bosch, W. (2007). Residual Tide Analysis in Shallow Water-Contributions of ENVISAT and ERS Altimetry. In *Envisat Symposium*.

Savcenko, R. and Bosch, W. (2012). Eot11a-empirical ocean tide model from multi-mission satellite altimetry. *DGFI Report No. 89*.

Scharroo, R. and Smith, W. H. (2010). A global positioning system–based climatology for the total electron content in the ionosphere. *Journal of Geophysical Research: Space Physics*, 115(A10).

Schindelegger, M., Green, J. A. M., Wilmes, S.-B., and Haigh, I. D. (2018). Can we model the effect of observed sea level rise on tides? *Journal of Geophysical Research: Oceans*, 123(7):4593–4609.

Schureman, P. (1958). Manual of harmonic analysis and prediction of tides. [revised 1940 edition reprinted 1958 with corrections, reprinted 2001].

Schwatke, C., Dettmering, D., Bosch, W., Göttl, F., and Boergens, E. (2014). OpenADB: An Open Altimeter Database providing high-quality altimeter data and products. In *Ocean Surface Topography Science Team Meeting, Lake Constance, Germany*.

Schwiderski, E. W. (1980). On charting global ocean tides. *Reviews of Geophysics*, 18(1):243.

Sharp, Y.-T. (2022). *Towards better exploitation of coastal altimetry: combined contributions of hydrodynamic modeling à high-resolution and new sea level mapping techniques using GNSS*. Theses, Université de La Rochelle.

Shum, C. K., Woodworth, P. L., Andersen, O. B., Egbert, G. D., Francis, O., King, C., Klosko, S. M., Le Provost, C., Li, X., Molines, J.-M., Parke, M. E., Ray, R. D., Schlax, M. G., Stammer, D., Tierney, C. C., Vincent, P., and Wunsch, C. I. (1997). Accuracy assessment of recent ocean tide models. *Journal of Geophysical Research: Oceans*, 102(C11):25173–25194.

Smith, A. J. E., Ambrosius, B. A. C., Wakker, K. F., Woodworth, P. L., and Vassie, J. M. (1997). Comparison between the harmonic and response methods of tidal analysis using TOPEX/POSEIDON altimetry. *Journal of Geodesy*, 71(11):695–703.

Stammer, D., Ray, R. D., Andersen, O. B., Arbic, B. K., Bosch, W., Carrère, L., Cheng, Y., Chinn, D. S., Dushaw, B. D., Egbert, G. D., Erofeeva, S. Y., Fok, H. S., Green, J. A. M., Griffiths, S., King, M. A., Lapin, V., Lemoine, F. G., Luthcke, S. B., Lyard, F., Morison, J., Müller, M., Padman, L., Richman, J. G., Shriver, J. F., Shum, C. K., Taguchi, E., and Yi, Y. (2014). Accuracy assessment of global barotropic ocean tide models. *Reviews of Geophysics*, 52(3):243–282.

Sulzbach, R., Dobslaw, H., and Thomas, M. (2021). High-resolution numerical modeling of barotropic global ocean tides for satellite gravimetry. *Journal of Geophysical Research: Oceans*, 126(5).

Sulzbach, R., Hart-Davis, M., Dettmering, D., and Thomas, M. (2023). Regularized Empirical Variance-Covariance-Matrices for stochastic gravity modeling of 8 major ocean tides.

Sulzbach, R., Wziontek, H., Hart-Davis, M., Dobslaw, H., Scherneck, H.-G., Van Camp, M., Omang, O. C. D., Antokoletz, E. D., Voigt, C., Dettmering, D., et al. (2022). Modeling gravimetric signatures of third-degree ocean tides and their detection in superconducting gravimeter records. *Journal of Geodesy*, 96(5):35.

Sun, W., Zhou, X., Zhou, D., and Sun, Y. (2022). Advances and accuracy assessment of ocean tide models in the antarctic ocean. *Frontiers in Earth Science*, 10.

Tabibi, S., Geremia-Nievinski, F., Francis, O., and van Dam, T. (2020). Tidal analysis of GNSS reflectometry applied for coastal sea level sensing in Antarctica and Greenland. *Remote Sensing of Environment*, 248:111959.

Teunissen, P. J. G. and Amiri-Simkooei, A. R. (2007). Least-squares variance component estimation. *Journal of Geodesy*, 82(2):65–82.

Tierney, C. C., Parke, M. E., and Born, G. H. (1998). An investigation of ocean tides derived from along-track altimetry. *Journal of Geophysical Research: Oceans*, 103(C5):10273–10287.

Wang, X., Verlaan, M., Veenstra, J., and Lin, H. X. (2022a). Data-assimilation-based parameter estimation of bathymetry and bottom friction coefficient to improve coastal accuracy in a global tide model. *Ocean Science*, 18(3):881–904.

Wang, Y. (2004). Ocean tide modeling in the Southern Ocean. Technical report, Ohio State University. Division of Geodetic Science.

Wang, Y., Zhang, Y., Xu, M., Wang, Y., and Lv, X. (2022b). Ocean tides near hawaii from satellite altimeter data. part II. *Journal of Atmospheric and Oceanic Technology*, 39(7):1015–1029.

Wessel, P., Luis, J. F., Uieda, L., Scharroo, R., Wobbe, F., Smith, W. H. F., and Tian, D. (2019). The Generic Mapping Tools Version 6. *Geochemistry, Geophysics, Geosystems*, 20(11):5556–5564.

Wessel, P. and Smith, W. H. F. (1996). A global, self-consistent, hierarchical, high-resolution shoreline database. *Journal of Geophysical Research: Solid Earth*, 101(B4):8741–8743.

Williams, J., Irazoqui Apecechea, M., Saulter, A., and Horsburgh, K. J. (2018). Radiational tides: their double-counting in storm surge forecasts and contribution to the highest astronomical tide. *Ocean Science*, 14(5):1057–1068.

Woodworth, P. L. (2019). The global distribution of the M1 ocean tide. *Ocean Science*, 15(2):431–442.

Woodworth, P. L., Hunter, J. R., Marcos, M., Caldwell, P., Menéndez, M., and Haigh, I. (2016). Towards a global higher-frequency sea level dataset. *Geoscience Data Journal*, 3(2):50–59.

You, X. and Yuan, L. (2021). The sensitivity of ocean tide loading displacements to the structure of the upper mantle and crust of taiwan island. *Earth, Planets and Space*, 73(1).

Zaron, E. D. (2015). Nonstationary internal tides observed using dual-satellite altimetry. *Journal of Physical Oceanography*, 45(9):2239 – 2246.

Zaron, E. D. (2017). Mapping the nonstationary internal tide with satellite altimetry. *Journal of Geophysical Research: Oceans*, 122(1):539–554.

Zaron, E. D. (2018). Ocean and ice shelf tides from cryosat-2 altimetry. *Journal of Physical Oceanography*, 48(4):975 – 993.

Zaron, E. D. and de Carvalho, R. (2016). Identification and reduction of retracker-related noise in altimeter-derived sea surface height measurements. *Journal of Atmospheric and Oceanic Technology*, 33(1):201–210.

Zaron, E. D. and Ray, R. D. (2018). Aliased tidal variability in mesoscale sea level anomaly maps. *Journal of Atmospheric and Oceanic Technology*, 35(12):2421–2435.

Zemunik, P., Denamiel, C., Šepić, J., and Vilibić, I. (2022). High-frequency sea-level analysis: Global distributions. *Global and Planetary Change*, 210:103775.

Zijl, F. and Groenenboom, J. (2019). Development of a sixth generation model for the NW European Shelf (DCSM-FM 0.5nm). Technical report, Deltares, Deltares.

List of Figures

1.1 Spectral analysis of two different tide gauge time-series taken from GESLA-3 (Haigh et al., 2022), showing the power spectral density at respective frequencies in cycles per day (cpd). The tide gauges presented here are from Wellington, New Zealand and Brest, France. 3

2.1 A schematic demonstrating the tide generating forces of the Earth-Moon system. Schematic inspired by Pugh and Woodworth (2014). 8
2.2 An example of the latitudinal differences of the Equilibrium Tide amplitudes as derived from Equation 2.2 for the long-period, diurnal and semi-diurnal tidal species'. 9
2.3 Schematic describing the dynamic nature of the ocean tides. 10
2.4 The yearly estimated (A) amplitude and (B) phase of the M_2 tide with and without applying the nodal modulation terms estimated from the Newlyn tide gauge in Cornwall, Great Britain, obtained from GESLA-3 (Haigh et al., 2022). 12
2.5 Global atlas of the amplitude (solid lines) and phase (dashed lines) of the M_2 tide, as derived by the Schwiderski model and taken from Schwiderski (1980). 14
2.6 The available past and currently orbiting satellite altimetry datasets taken from the OpenADB website of DGFI-TUM (Schwatke et al., 2014). 15
2.7 (A) Sea level estimation from a Jason-3 cycle which is not corrected for ocean tides. (B) The tidal height estimated from FES2014b (Lyard et al., 2021). (C) The sea level estimation corrected for the tides from B. (D) is a time series of a single along-track position either corrected or uncorrected for ocean tides. 16
2.8 The S_1 [A and B] and K_1 [D and E] amplitudes determined from two different ionospheric corrections and their respective differences [C and F]. Inspired by Ray (2020a). 18
2.9 Schematic of three tidal constituents sampled at exactly one day, with the black line representing the tidal amplitude over time while the blue line represents the sampled tidal amplitude every one day. 19
2.10 [A] The aliasing period in days of the ERS/EN/SA and TP/JA/S6 satellites as well as the Rayleigh criteria calculated for these satellites, respectively [B and C]. 20

3.1 Global distribution of the TICON-3 database, showing the estimated amplitude of the M2 tidal constituent. 25
3.2 The distribution of the sources of data used to create the ArcTiCA dataset. 26
3.3 Demonstration of the capabilities of the TIPTOE software to predict the tidal height over time in multiple scenarios. 27
3.4 The tidal height estimated from EOT20 constituents for cycle 10 of Jason-3 (A) and across the entire Atlantic Ocean for 24 hours (B to E). 28

3.5 The gridded SLAVA estimated for the Sentinel-3A mission using EOT20 (A) and GTSM (B) ocean tide corrections. (C) presents the variance differences between using GTSM and EOT20, with negative differences (blue) indicating a higher variance when using GTSM and positive differences (red) when EOT20 has a higher variance. 29

4.1 Standard deviation of the M_2 tidal amplitude from the five major global ocean tide models. Deviations below 0.5 cm are masked out with white to emphasise regions of high deviations. . 32
4.2 Distribution of in-situ measurements from the TICON-1 database (o) (Piccioni et al., 2019a) and the RR dataset (◃) (Ray, 2013). 33
4.3 The distribution of the regional experiments done within this thesis. 34
4.4 SLA within a grid point obtained from seventeen altimetry datasets before the radial error is applied (blue colours) and after the radial error correction is applied (red). 35
4.5 An example of the spatial variability of the weighting (in ‰) of four of the eleven altimetry datasets used, obtained for each grid node of the model after the VCE estimation has been done. 37
4.6 The amplitude of the (A) elastic tide, (B) ocean tide and (C) load tide of the M_2 tidal constituent from EOT11a. 39
4.7 The number of altimetry observations obtained for each grid node based on the respective capsize approaches: (A) Latitude Dependent, (B) Bathymetry Dependent and (C) Fixed. . . . 41
4.8 The EOT model (A and C) without an accurate land-sea mask and (B and D) with a land-sea mask derived from GMT Wessel and Smith (1996) in New Zealand and in the Yellow Sea, respectively. The map represents the amplitude of the M_2 tide, while the light blue lines represent each 60° phase contour. 42
4.9 The real and imaginary components as well as the amplitude of the residual M_2 and S_2 constituents from the EOT20 model. 44
4.10 The along-track coverage of the altimetry missions used within EOT20 compared to EOT-NECS in the Northwest European Continental Shelf. 48

5.1 The global distribution of TICON-td compared to the global TiME model for the ${}^3M_1$, ${}^3N_2$, ${}^3L_2$ and ${}^3M_3$ constituents. 51
5.2 (A) Amplitude and (B) phase lag of the M_2 tidal constituent from the ArcTiCA dataset overlaid onto tidal estimations provided by the DTU22 tide model. (C) and (D) are the same but for the Antarctic region with the AntTG database. 53
5.3 A snapshot of water level predictions from the DCSM-FM, demonstrating the rise and fall of water levels in the order of meters caused by the tidal variability of the region. 55

6.1 (A) The absolute amplitude difference for the M_2 tide between correcting the SLA for mesoscale variability against not doing so. (B) The results of tide gauge analysis against TICON-3 and the RR dataset for the major eight tidal constituents. 61
6.2 The yearly phase estimations of the M_2 constituent from the Honningsvag tide gauge in Norway which were taken from three different data sources within the GESLA-3 database. 63

List of Tables

2.1 Astronomical arguments taken from Egbert and Ray (2017) 11
2.2 The characteristics of the major tidal constituents within each tidal species, with the Equilibrium Tide amplitudes taken from Apel (1987). 11
2.3 The orbit details of several altimetry missions used within this thesis. 19

4.1 List of corrections and parameters used to compute SLA. 34
4.2 The RMS with respect to TICON-3 of the eight major tidal constituents of the modelled elastic and ocean tides in the North West European continental shelf. To contextualise these errors, the mean tidal signal is also derived. 39
4.3 The RMS (in cm) and RSS (in cm) compared to 11 tide gauges of EOT-NF and EOT-WF model versions. 43
4.4 Criteria and estimated contribution share of Michael Hart-Davis for P-1 45
4.5 Criteria and estimated contribution share of Michael Hart-Davis for P-2 47

5.1 Criteria and estimated contribution share of Michael Hart-Davis for P-3 56

A Appendix

A.1 Publications

A.1.1 P-1 EOT20: a global ocean tide model from multi-mission satellite altimetry

Earth Syst. Sci. Data, 13, 3869–3884, 2021
https://doi.org/10.5194/essd-13-3869-2021

Open Access Earth System Science Data

EOT20: a global ocean tide model from multi-mission satellite altimetry

Michael G. Hart-Davis[1], Gaia Piccioni[1,a], Denise Dettmering[1], Christian Schwatke[1], Marcello Passaro[1], and Florian Seitz[1]

[1]Deutsches Geodätisches Forschungsinstitut der Technischen Universität München (DGFI-TUM), Arcisstraße 21, 80333 Munich, Germany
[a]now at: Enel Global Trading S.p.A., Viale Regina Margherita 125, 00198 Rome, Italy

Correspondence: Michael G. Hart-Davis (michael.hart-davis@tum.de)

Received: 22 March 2021 – Discussion started: 26 March 2021
Revised: 30 June 2021 – Accepted: 1 July 2021 – Published: 10 August 2021

Abstract. EOT20 is the latest in a series of empirical ocean tide (EOT) models derived using residual tidal analysis of multi-mission satellite altimetry at DGFI-TUM. The amplitudes and phases of 17 tidal constituents are provided on a global 0.125° grid based on empirical analysis of seven satellite altimetry missions and four extended missions. The EOT20 model shows significant improvements compared to the previous iteration of the global model (EOT11a) throughout the ocean, particularly in the coastal and shelf regions, due to the inclusion of more recent satellite altimetry data as well as more missions, the use of the updated FES2014 tidal model as a reference to estimated residual signals, the inclusion of the ALES retracker and improved coastal representation. In the validation of EOT20 using tide gauges and ocean bottom pressure data, these improvements in the model compared to EOT11a are highlighted with the root sum square (RSS) of the eight major tidal constituents improving by ~ 1.4 cm for the entire global ocean with the major improvement in RSS (~ 2.2 cm) occurring in the coastal region. Concerning the other global ocean tidal models, EOT20 shows an improvement of ~ 0.2 cm in RSS compared to the closest model (FES2014) in the global ocean. Variance reduction analysis was conducted comparing the results of EOT20 with FES2014 and EOT11a using the Jason-2, Jason-3 and SARAL satellite altimetry missions. From this analysis, EOT20 showed a variance reduction for all three satellite altimetry missions with the biggest improvement in variance occurring in the coastal region. These significant improvements, particularly in the coastal region, provide encouragement for the use of the EOT20 model as a tidal correction for satellite altimetry in sea-level research. All ocean and load tide data from the model can be freely accessed at https://doi.org/10.17882/79489 (Hart-Davis et al., 2021). The tide gauges from the TICON dataset used in the validation of the tide model, are available at https://doi.org/10.1594/PANGAEA.896587 (Piccioni et al., 2018a).

1 Introduction

The regular fluctuations of the sea surface caused by ocean tides have intrigued and fascinated scientists for centuries based on their influence on oceanic processes. Understanding ocean tides is vital for a variety of geophysical fields, with it being of particular importance in studies of the coastal environment and ocean mixing. Precise knowledge of ocean tides is also important for satellite altimetry and in determining high-resolution temporal gravity fields from, for example, the GRACE missions (Tapley et al., 2004).

In certain studies of non-tidal signals using satellite altimetry data, such as in sea-level and ocean circulation research, ocean tides need to be removed from the data signal to properly study these processes. These so-called tidal corrections are usually provided by ocean tide models that have been specially developed to predict the tidal signals throughout the global ocean. The ever-evolving and improving field of ocean tide modelling has resulted in significant leaps in the accuracy of estimations of ocean tides (Shum et al., 1997; Stammer et al., 2014). There are several ocean tide models that

have been developed using different techniques and for different applications, with a comprehensive summary of these models being presented in Stammer et al. (2014). In general, ocean tides are known in the open ocean region to an accuracy of approximately 2 cm (Savcenko and Bosch, 2012); however, models show large discrepancies between one another and compared to in situ observations in the coastal region (Ray et al., 2011). Improvements continue to be made, with estimations significantly improving in the coastal and polar regions (Ray et al., 2019). Poorer results are seen in the coastal region due to poorly resolved bathymetry, the complexity of ocean tides and due to land contamination of satellite altimetry radar signals (Fok, 2012).

One type of ocean tide model, known as semi-empirical models, is derived from empirical harmonic analysis of satellite altimetry data relative to a reference model. These semi-empirical tide models rely heavily upon satellite altimetry data. Recently, significant advancements have been made to coastal altimetry in several fields including key improvements in correction fields, more detailed and coastal-specific data editing, and new schemes for radar echo analysis (retracking) (Cipollini et al., 2017). Piccioni et al. (2018b) demonstrated an improvement greater than 2 cm for single tidal constituents when using the ALES (Adaptive Leading Edge Subwaveform: Passaro et al., 2014) retracker that enhances the performances of sea level retrieval in the coastal region and the corresponding sea state bias correction (Passaro et al., 2018). The continued developments of altimetry in the coastal region coupled with the increased number of altimetry missions have had a positive impact on the ability of models to more accurately estimate ocean tides.

EOT11a (Savcenko and Bosch, 2012), the latest in a series of global ocean tide models developed at DGFI-TUM, is an example of a semi-empirical tide model developed using residual tidal analysis of multi-mission satellite altimetry. EOT11a exploits altimetry observations of the sea level anomaly (SLA) corrected using a reference ocean tide model (FES2004) to estimate the tidal harmonic constants. EOT11a showed significant improvements compared to the previous iterations of the model, EOT08a and EOT10a, with noticeable improvements being seen in the shallow water regions (Savcenko and Bosch, 2012). The model has continued to be developed, with regional studies being conducted by Piccioni et al. (2021) based on improvements being made in the coastal region. These improvements are largely driven by the progresses in accuracy and precision of altimetry measurements in the coastal zone and the use of the updated FES2014 (Lyard et al., 2020) tide model as the reference model for the residual tidal analysis.

In this paper, the latest global version of the EOT model, EOT20, is presented based on recent developments made in the field of tide modelling, coastal altimetry and the availability of an increased number of altimetry missions. The objective of the EOT20 model is to improve the accuracy of tidal estimations in the coastal region while remaining consistent in the open ocean. In Sect. 2, a description of the altimetry data used and how EOT20 is produced through residual tidal analysis is given. Following this, a comparison of the results of the EOT20 model with in situ observations and other global tide models is presented in Sect. 3, with a conclusion and summary given in Sect. 5.

2 Residual tidal analysis of satellite altimetry

The development of EOT20 focused on improving tidal estimations in the coastal region which has been a historically difficult region to accurately estimate tides. EOT20 follows a similar scheme as the former model, EOT11a, consisting of three major steps: the creation of an SLA product including the correction of a reference ocean tide model; the estimation of the residual tides based on this SLA product; and the combination of the reference model with the residual tides to form a new global ocean tide model. These three steps provide a summary of the creation of EOT20 which is expanded in the following sections.

2.1 The altimetry SLA product

The tidal analysis is based on the analysis of SLA derived from satellite altimetry missions (Table 1) obtained from the Open Altimeter Database (OpenADB, https://openadb.dgfi.tum.de, last access: 5 August 2021, Schwatke et al., 2014). These missions are selected as they provide extended time series along similar altimetry tracks, with the Jason missions being a follow-on from TOPEX/Poseidon and Envisat a follow-on of the ERS missions, thus providing appropriate data for the estimation of tidal signals. The SLA from these altimetry missions is calculated according to that described in Andersen and Scharroo (2011):

$$\mathrm{SLA} = H - R - \mathrm{MSS} - h_{\mathrm{geo}}, \quad (1)$$

where H is the orbital height of the satellite, R the range, MSS the mean sea surface and h_{geo} is the sum of the geophysical corrections (as listed in Table 2). For all of the missions, satellite orbits in ITRF2008 are used. For the ERS and TOPEX these are taken from GFZ VER11 (Rudenko et al., 2018), while for the Jason missions and Envisat CNES GDR-E solutions are used. The corrections used are chosen to optimise the estimations of the SLA in the coastal region, without harming the estimations in the open ocean regions.

The same corrections are used for each satellite altimetry mission to allow for consistency, with the only differences occurring in the sea state bias correction. The ALES retracker (Passaro et al., 2014) is applied to the Jason missions and the Envisat mission based on data availability at the time of running the model, with the other altimetry missions using the REAPER (Brockley et al., 2017) and TOPEX sea state bias corrections (Chambers et al., 2003). This discrepancy in the chosen retracker is designed to benefit from the ability

Table 1. The satellite altimeter data used in this study obtained from OpenADB at DGFI-TUM (Schwatke et al., 2014). The corrections listed in Table 2 are applied to all these missions. Most missions are retracked using the ALES retracker (Passaro et al., 2018), marked by *, with TOPEX and ERS using ocean ranges as provided in SGDR datasets.

Mission	Cycles	Period
TOPEX	001–365	25 Sep 1992–15 Aug 2002
TOPEX Extended Mission	368–481	16 Sep 2002–8 Oct 2005
Jason-1*	001–259	15 Jan 2002–26 Jan 2009
Jason-1 Extended Mission*	262–374	10 Feb 2009–3 Mar 2012
Jason-2*	000–296	4 Jul 2008–25 Jul 2016
Jason-2 Extended Mission*	305–327	13 Oct 2016–17 May 2017
Jason-3*	001–071	12 Feb 2016–21 Jan 2018
ERS-1c	082–101	25 Mar 1992–24 Dec 1993
ERS-1g	144–156	24 Mar 1995–2 Jun 1996
ERS-2	000–085	14 May 1995–2 Jul 2003
Envisat*	006–094	14 May 2002–26 Nov 2010

Table 2. List of corrections and parameters used to compute SLA for tidal residuals estimation.

Parameter	Model	Reference
ALES sea state bias	ALES	Passaro et al. (2018)
ERS sea state bias	REAPER	Brockley et al. (2017)
TOPEX sea state bias	TOPEX	Chambers et al. (2003)
Atmospheric loading before 2017	DAC-ERA	Carrere et al. (2016)
Atmospheric loading from 2017	DAC	Carrère et al. (2011)
Wet troposphere	GPD+	Fernandes and Lázaro (2016)
Dry troposphere	VMF3	Landskron and Böhm (2018)
Ionosphere	NIC09	Scharroo and Smith (2010)
Ocean and load tide	FES2014	Lyard et al. (2020)
Solid earth and pole tide	IERS 2010	Petit and Luzum (2010)
Mean sea surface (MSS)	DTU18MSS	Andersen et al. (2016)
Radial error	MMXO17	Bosch et al. (2014)

of the ALES retracker in obtaining data closer to the coast which Piccioni et al. (2021) showed had positive improvements on the accuracy of the EOT tide model for the major tidal constituents compared to using the other retracked data. Therefore, depending on the retracker that is used, a coastal flag is implemented into the model that limits the distance to the coast. For missions using the REAPER and TOPEX retrackers, a coastal flag is implemented that restricts the use of SLA data up to 7 km from the coastline. For missions using the ALES retracker, however, this distance to the coast is decreased to 3 km (Passaro et al., 2021). An additional flag is also added limiting the absolute value of sea level anomalies to ± 2.5 m (Savcenko and Bosch, 2012). The altimetry data are further adjusted to account for radial errors estimated in the cross-calibration of the SLA data using the multi-mission crossover analysis approach presented in Bosch et al. (2014).

As shown in Table 2, the ocean and load tide correction for all missions is the FES2014 oceanic tide model. This is one of the major changes from the previous version of the global EOT model, EOT11a, which used one of the previous versions of the FES model, FES2004. The results of Lyard et al. (2020) showed considerable improvements in FES2014, particularly in the coastal and shelf regions. These improvements are largely driven by the improved efficiency of data assimilation and the accuracy of hydrodynamic solutions. It is, therefore, anticipated that large parts of the improvements made between the versions of EOT will be due to the improvement in the reference model.

Once all these corrections are applied, the SLA can be estimated for all 11 altimetry datasets which are then gridded onto a triangular grid based on the techniques presented in Piccioni et al. (2021). The triangular grids are chosen based on the efficiency of the model and allow for consistency of grid sizes throughout the ocean, thus not over-utilising data in regions of dense data availability. For each grid point, SLA values are collected within a variable capsize, with the radius, ψ (in km), of the capsize being a function of latitude (φ in degrees) where $\psi = 165 - 1.5\,(\varphi)$. Other capsize techniques are available based on a fixed or depth-based capsize, but they do not make significant changes to the results of the estimated tidal residuals and depreciate the efficiency of the

model. The choice of the variable capsize is also to compensate for the greater data density available in higher latitudes.

Once collected, the data are then weighted using a Gaussian function based on the distance to the grid point. The use of data from multiple satellite tracks for each node provides a long SLA time series, which is important in reducing the aliasing effect and in decorrelating tidal signals with alias periods close to each other (Savcenko and Bosch, 2012). These issues occur due to the low temporal resolution obtained from satellite altimetry (e.g. the Jason missions only sample the same position once every 9915 d) resulting in tides not being properly estimated. The alias periods for the major tidal constituents for the Jason and the ERS orbits are presented in Le Provost (2001). The use of nodes with data from multiple altimetry missions, therefore, creates a long enough time series to improve the temporal resolution and reduce possible aliasing effects in the tidal estimations.

2.2 Residual tidal analysis

From the weighted SLA, residual tidal analysis is performed using weighted least-squares and the variance component estimation (VCE) for each grid point of the model. The least-squares approach is applied to the harmonic formula to derive the amplitudes and phases of single tidal constituents from the SLA observations. In EOT20, the 17 tidal constituents considered and computed are 2N2, J1, K1, K2, M2, M4, MF, MM, N2, O1, P1, Q1, S1, S2, SA, SSA and T2. The weighted least square analysis follows a standard procedure solving the following equation for each grid point (Piccioni et al., 2021):

$$\boldsymbol{x} = (\mathbf{A}^T\mathbf{W}\mathbf{A})^{-1}\mathbf{A}^{\tau}\mathbf{W}\boldsymbol{l}, \tag{2}$$

with $\boldsymbol{l}$ being the vector of SLA values, $\mathbf{A}$ the design matrix, $\mathbf{W}$ the diagonal matrix of weights, and $\boldsymbol{x}$ the vector of unknowns. The unknowns of vector $\boldsymbol{x}$ are the in-phase and quadrature coefficients of the tidal constituents being considered, the sea level trend, and the constant values defined as the mean sea level from each specific mission at each node (Piccioni et al., 2021).

The VCE is implemented to allow for the combination of datasets from multiple satellite missions and allows for the appropriate weighting of different missions m, $m = 1, \ldots, k$, (Savcenko and Bosch, 2012) based on their variances, to provide a more accurate estimation. The VCE method has been utilised in a variety of applications, and it was introduced into the previous global model, EOT11a (Savcenko and Bosch, 2012), which followed the formulation detailed in Teunissen and Amiri-Simkooei (2008) and Eicker (2008). The VCE is calculated using iterations as the unknowns, and the variances, σ, are initially unknown. The formulation is as follows:

$$N_x\boldsymbol{x} = N_y, \tag{3}$$

with N_x and N_y equal to the weighted sum:

$$N_x = \sum_{m=1}^{k} \frac{1}{\sigma_m^2} N_{x,m} \qquad N_y = \sum_{m=1}^{k} \frac{1}{\sigma_m^2} N_{y,m}. \tag{4}$$

The variances are iteratively calculated by

$$\sigma_m^2 = \frac{\Omega_{\mathrm{m}}}{r_{\mathrm{m}}}, \tag{5}$$

where r_{m} is the partial redundancy with $\Omega_{\mathrm{m}} = \hat{\boldsymbol{v}}\mathbf{P}_{\mathrm{bb}}\hat{\boldsymbol{v}}$, $\hat{\boldsymbol{v}}$ being the vector of residuals, and $\mathbf{P}_{\mathrm{bb}}$ is the dispersions matrix of measurements (Savcenko and Bosch, 2012). Following the residual analysis, significant residual signals were obtained for all of the tidal constituents. For the M2 and N2 tides (Fig. 1), for example, the residual amplitudes can exceed 2 cm with the largest residual tides being seen in the coastal region. Relatively high residual tides are also seen in the western boundary currents, such as the Agulhas Current and the Gulf Stream.

The tides observed are the residual elastic tides that consist of both the ocean and the load tides. Therefore, additional analysis has been done to separate these two components for further analysis. There are several techniques that are described that make this possible (e.g. Francis and Mazzega, 1990) with EOT using the method presented in Cartwright and Ray (1991). This method involves using the complex elastic ocean tide admittance decomposed in complex spherical harmonics as described by Savcenko and Bosch (2012):

$$Z(\phi, \lambda) = \sum_{n,m} a_{n,m} Y_{n,m}(\phi, \lambda). \tag{6}$$

The ocean spherical harmonic admittances of the load tides are described as

$$Z_{\mathrm{l}}(\phi, \lambda) = \sum_{n,m} \beta_n a^o_{n,m} Y_{n,m}(\phi, \lambda), \tag{7}$$

where $\beta_n = \frac{\alpha_n}{1+\alpha_n}$ with $\alpha_n = \frac{3}{2n+1}\frac{\rho_{\mathrm{w}}}{\rho_{\mathrm{e}}}h'_n$. The love numbers, h'_n, were taken from Farrell (1972) with ρ_{w} and ρ_{e} being the density of the ocean and earth. After synthesis of the load tides, the residual ocean tides were computed as the difference between the load and the elastic tide, $Z_{\mathrm{o}}(\phi, \lambda) = Z(\phi, \lambda) - Z_{\mathrm{l}}(\phi, \lambda)$.

2.3 Model formation

Once the ocean and load tide residuals are produced, the full tidal signal is restored by adding the residuals to the FES2014 tidal atlas. The residuals are interpreted onto a 0.125° resolution grid with the FES2014 model interpreted onto the same grid resolution. The outputting of the data onto a regular grid is simply done to allow for an easy combination with the FES2014 model as well as to be more user friendly. The north–south extent of the model extends 66° N and 66° S,

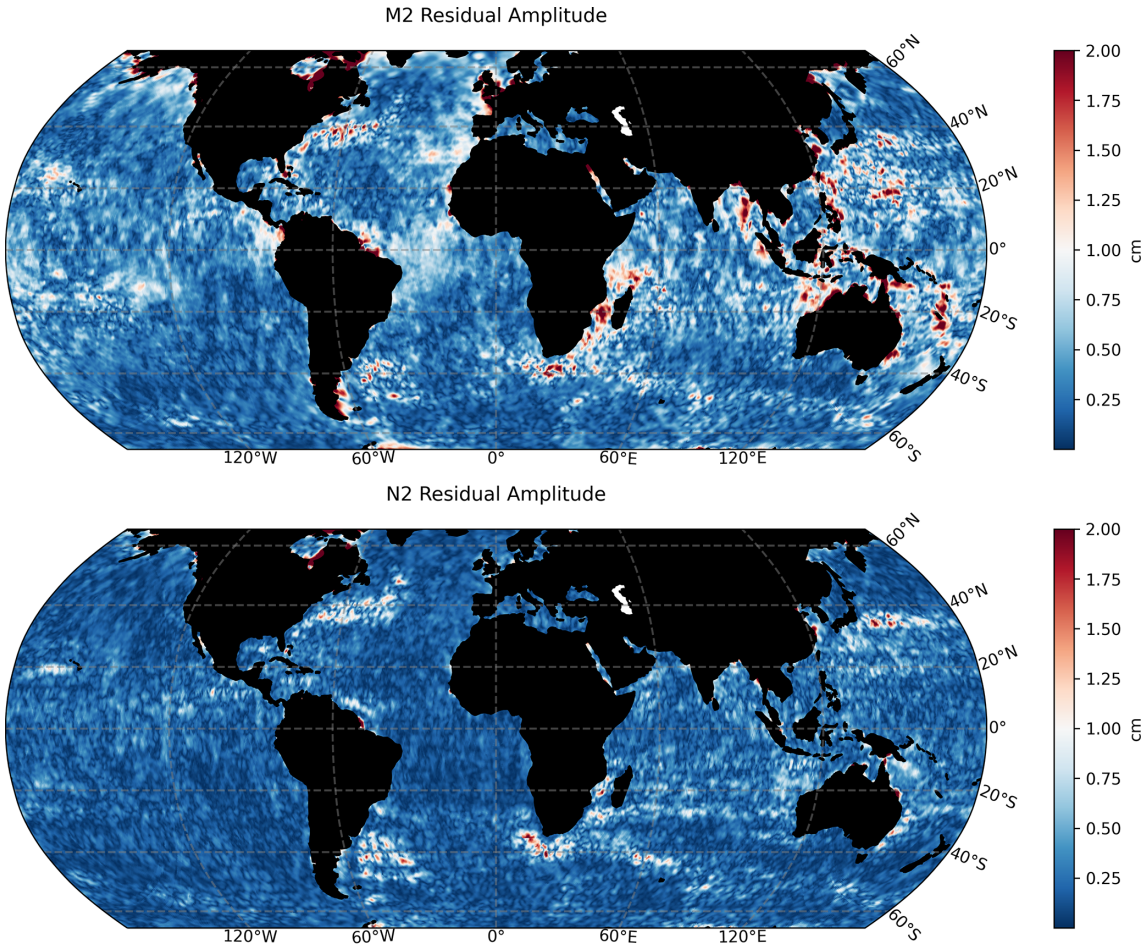

Figure 1. Maps of the residual amplitudes of the M2 and N2 tidal constituents as estimated by residual tidal analysis.

with the model defaulting to the FES2014 tides in the higher latitudes. This extent is chosen due to the limited altimetry data further beyond this latitudinal band and the difficulty in modelling the tides in the polar regions. Dedicated studies to the Arctic region such as that of Cancet et al. (2019) demonstrate the complexity of modelling ocean tides in the polar regions and emphasise their importance for satellite altimetry.

Future iterations of the EOT model will tackle the estimation of tides in the higher latitudes. A land–sea mask was added to the model based on the GMT that uses the GSHHG coastline database (Wessel and Smith, 1996), which is a high-resolution database that contains information about coastlines as well as lake and river boundaries. These data have a mean point separation of 178 m which has been interpolated to a 0.125° resolution for use in the EOT20 model. In complex coastal regions, such as regions with islands or in semi-enclosed bays, properly defining the coastlines becomes extremely valuable when validating the model against in situ tide gauges. This is largely a result of artifacts forming when estimating tides in regions where the coastline has not been properly defined. For example, the Cook Strait between the two islands of New Zealand provides a unique coastal structure which shows a sharp change in the amplitude of major tides (e.g. M2, N2, S2 and K2 as shown in Walters et al., 2001) and, therefore, requires a more accurate coastline definition. Preliminary studies of EOT20 (not shown) demonstrated that for tide gauges within the Cook Strait the root sum square (RSS) difference between the model and tide gauges was reduced by 0.2 cm for the eight major tidal constituents when applying a more accurate land–sea mask. An overall reduction in RSS is seen throughout the ocean when using an accurate land–sea mask.

3 Tide model assessment and validation

3.1 The global EOT20 model

EOT20 presents global estimations of 17 tidal constituents with these tidal atlases being available from https://doi.org/10.17882/79489 (Hart-Davis et al., 2021). Global atlases of both ocean and load tides are provided, containing information about the amplitudes and phases as well

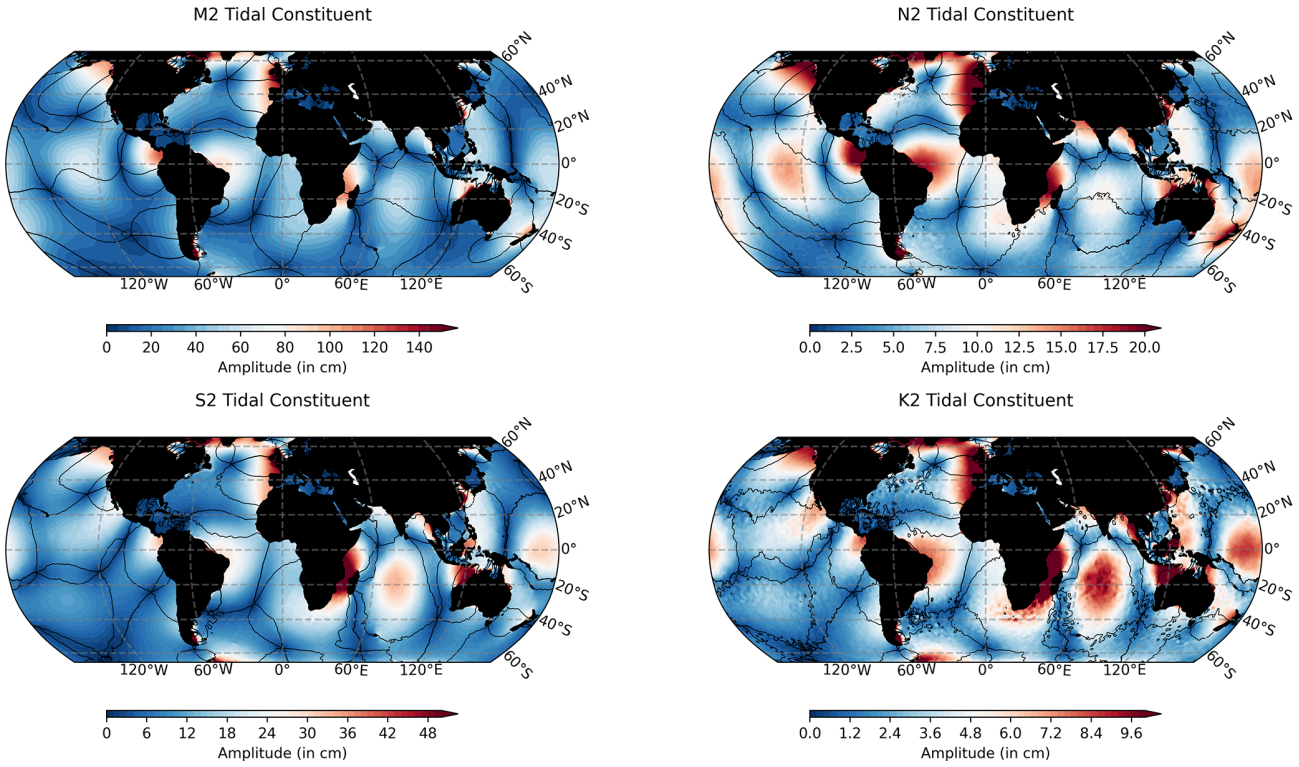

Figure 2. The amplitude (in cm) and the phase (in 60° increments) of four ocean tidal constituents produced by the EOT20 model.

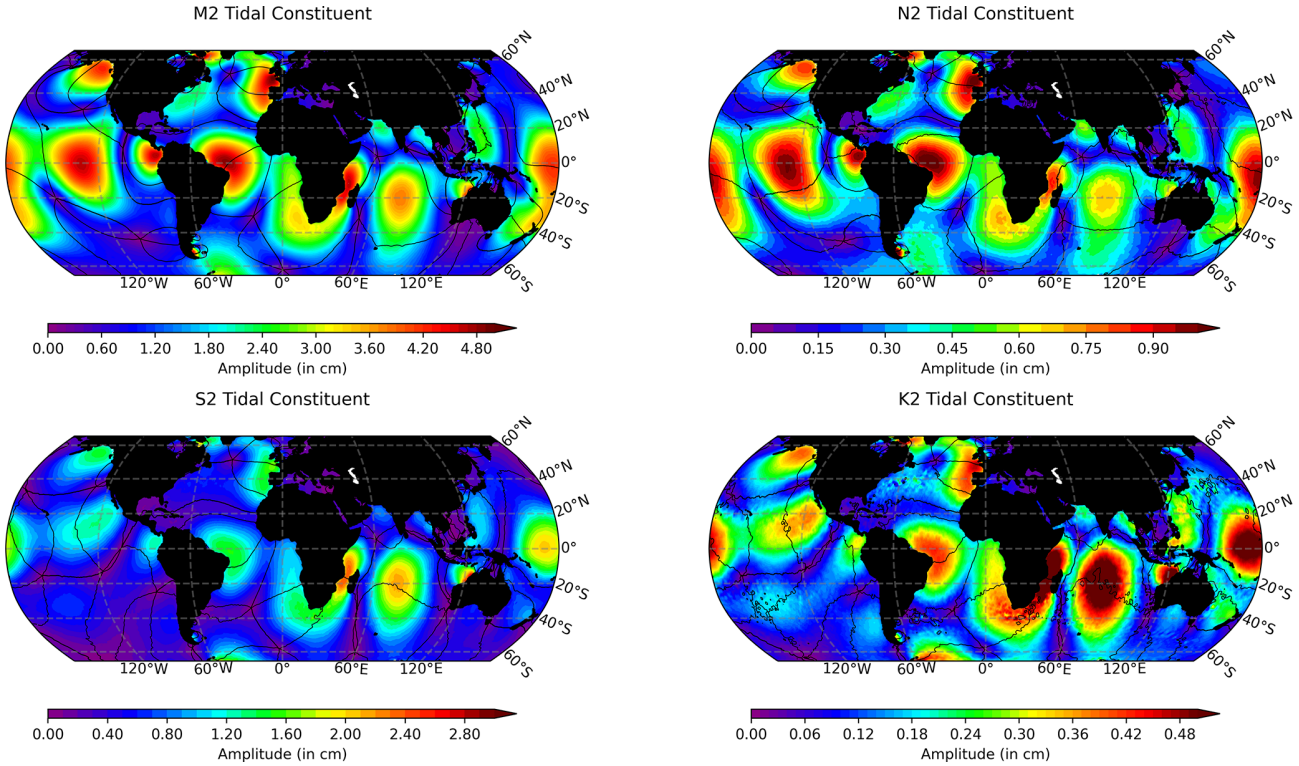

Figure 3. The amplitude (in cm) and phase (in 60° increments) of the four load tide constituents produced by the EOT20 model. It should be noted that EOT20 does not make an estimation for the load tides on land.

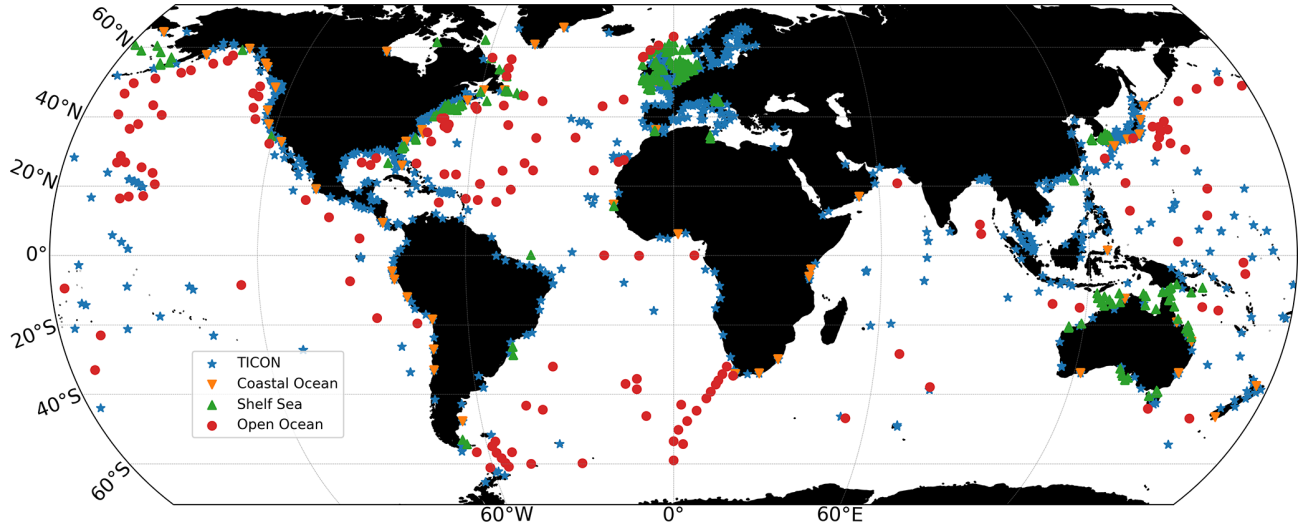

Figure 4. The global array of tide gauges and ocean bottom pressure sensors that were used in the validation of the EOT20 model from the TICON dataset and from Stammer et al. (2014): the coastal ocean, shelf sea and open ocean datasets.

as the real and imaginary components for all of the tidal constituents. Here, the ocean (Figs. 2 and A1) and load (Figs. 3 and A2) tides from EOT20 are presented. Building on from EOT11a an additional four tidal constituents have been estimated in the EOT20 product. which are the T2, J1, SA and SSA tidal constituents. The SSA and SA tides are included in the EOT20 model data, but users should be aware that these tides include the full signal at these periods, i.e. gravitational as well as meteorological tides. Thus, caution should be taken when interpreting the results of the tidal correction when these two tides are included as they will likely remove the seasonal signals seen in the altimeter data.

The EOT20 model follows the framework of the EOT11a model when estimating the tide via residual analysis. However, significant changes and additions have been done to EOT20 with the objective of improving coastal estimations. These changes are in the reference tide model used in the residual analysis, the use of more recent developments in coastal altimetry (e.g. the development of the ALES retracker Passaro et al., 2014), the increased coverage of satellite altimetry based on the launching of further missions (e.g. Jason-3), the use of an accurate land–sea mask onto the model output data, and using a triangular grid for the residual analysis. These additions all combine to optimise the estimation of ocean tides in the EOT20 model.

3.2 Tide gauge comparison

Since the 1800s, tide gauges have been used to study the ocean tides and the variation in sea level. Over the years, more and more tide gauges have been installed around the world, resulting in a vast array. This comprehensive record of tide gauges can be used to evaluate the changes in sea level over time as well as to better understand the ocean tides. Tide gauges, therefore, provide a suitable source of data in the validation of ocean tide models, particularly in the coastal region. There are limitations particularly in the distribution of tide gauges, with certain regions containing a vast number of tide gauges (e.g. in northern Europe) and some regions containing little to no data (e.g. the Mozambique Channel). Furthermore, tide gauges are mostly restricted to the coastal region and, therefore, do not provide sufficient observations of the open ocean region. With that in mind, Ray (2013) estimated tidal constants from bottom pressure stations in the open ocean regions which have been used to compare and assess the accuracy of global ocean tide models (Stammer et al., 2014). These data are combined with coastal and shelf data from Stammer et al. (2014), henceforth referred to as the R. Ray dataset, as well as the TICON dataset (Piccioni et al., 2019) to create a comprehensive dataset of tidal constants (shown in Fig. 4) to evaluate the accuracy of the EOT20 model throughout the global ocean. As the tide gauge and bottom pressure sensor distributions are already split into coastal, shelf and open ocean tide gauges from Stammer et al. (2014), the TICON dataset is also divided into three regions with the coast being defined as any tide gauges found shallower than 10 m, the shelf defined as being from 10 to 100 m depth and open ocean being anything deeper than 100 m. This is done to assess how the model performs in the coastal region, a historically difficult region to model accurately.

Several major ocean tide models are also compared to the same tide gauges in order to act as reference to the ability of the EOT20 model. The models used are EOT11a (Savcenko and Bosch, 2012), FES2014 (Lyard et al., 2020), GOT4.8 (Ray, 2013) and DTU16 (Cheng and Andersen, 2017). To provide suitable comparisons, duplicate tide gauges were removed and restrictions were implemented based on the model characteristics (i.e. only tide gauges between 66° S

Table 3. The rms, in cm, of the tide gauge analysis of 1226 tide gauges for the EOT20 model as well as several other global ocean tide models. The values marked in bold indicate the model with the smallest rms for each row.

Constituent	GOT4.8	DTU16	EOT11a	FES2014	EOT20
M2	5.623108	5.004819	5.280010	4.772177	**4.464017**
N2	2.300585	1.671615	2.468593	1.576893	**1.529496**
S2	3.447332	2.509648	3.249990	2.551011	**2.472494**
K2	2.022579	1.591654	1.940183	**1.506642**	1.539770
K1	1.904853	1.612598	1.940803	**1.429822**	1.473370
O1	1.709011	1.544578	1.306820	1.110750	**1.066416**
P1	1.722085	1.691374	1.694566	1.621030	**1.602048**
Q1	0.878571	0.827265	0.853390	**0.769279**	0.806851
RSS	7.948183	6.723504	7.574531	6.366756	**6.105453**

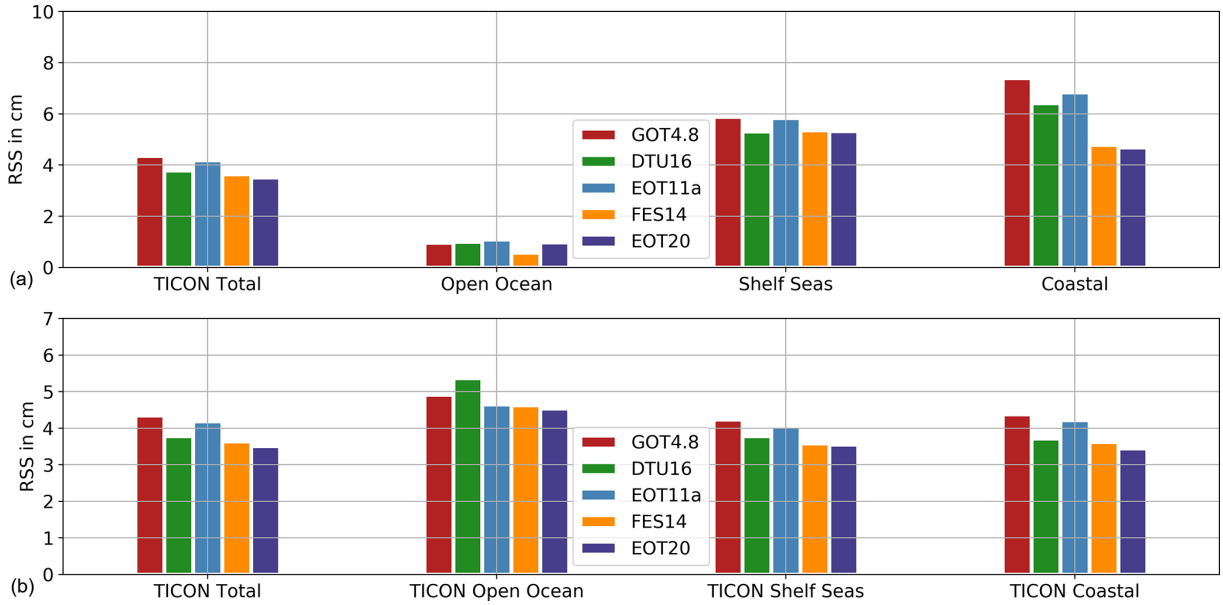

Figure 5. **(a)** RSS (cm) between the tide gauge databases and the global tidal models, for the eight major tidal constituents. **(b)** The RSS of subset regions of the TICON database as well as the full database.

and 66° N were used). This results in 1226 tide gauges and bottom pressure sensors being available for validation of the models. The TICON dataset provides standard deviations for individual constituents, with the average standard deviation for the tide gauges used in this study being 0.09 mm. No uncertainty estimates are provided in the R. Ray dataset. It should also be noted that 230 of the tide gauges used in this study are assimilated into the FES2014 model. The root mean square (rms) and root sum square (RSS) are then estimated for the eight major tidal constituents (M2, N2, S2, K2, K1, O1, P1 and Q1) which are commonly available from the tide models studied, following the techniques presented in Stammer et al. (2014).

The comparison between EOT11a and EOT20 shows a significant improvement in the EOT20 model for the full dataset (Table 3). This is consistent for all of the tidal constituents, with a major improvement seen in the M2 tide (0.8 cm) and the S2 tide (0.8 cm). For all of the regions (Fig. 5), EOT20 continues to show improvements compared to EOT11a particularly in the coastal region with a mean RSS reduction of 2.2 cm. In the coastal region, EOT20 shows a reduced rms for all the tidal constants with large reductions occurring again for the M2 (1.3 cm) and S2 tide (1.1 cm) with significant reductions in the K2 (0.5 cm) and N2 (1.3 cm) tidal constituents. Reductions in RSS are also seen in the other regions; however, the magnitude is not as large as in the coastal region, which results in smaller differences seen in the overall dataset (Table 3). This suggests that the adjustments and additions made to the EOT model, such as the incorporation of the ALES retracker in the estimation of the SLA, produce substantial differences to the performance of the model in the coastal region without harming the performances in other regions.

EOT20 also shows a reduced RSS when compared to the other global models, particularly compared to the reference model, FES2014. The largest improvement comes in the M2 tidal constituent while the results for the remaining tidal constituents are quite consistent between FES2014 and EOT20. In the coastal region, EOT20 shows significant improvements compared to the other models, being approximately 0.2 cm better than the closest model in this region (Fig. 5). The better performance of EOT20 seen in Table 3, therefore, can mostly be put down to the results seen in the coastal region. This is further highlighted in the TICON dataset, which contains significantly more coastal tide gauges compared to the other two regions (Fig. 5). In this dataset, EOT20 shows a reduction in rms for the M2 tidal constituent of 0.3 cm compared to the next best model (FES2014). For the remaining tidal constituents, EOT20 and FES2014 never vary by more than 1 mm in terms of rms values. This improvement compared to FES2014 is mainly seen in the coastal region (Fig. 5), which is in line with previous regional studies of EOT done using FES2014 as the reference tide model and the ALES retracker (Piccioni et al., 2018b).

In the shelf region, the reduction of rms in the M2 tide from EOT20 is still seen compared to FES2014 but reduces to less than 1 mm. The RSS of EOT20 and FES2014 match one another, only differing by less than 0.005 mm, while DTU16 is within 1 mm of both of these models in this region. This suggests that these three tide models are on par with one another in the shelf regions. In the open ocean, the similar results continue with the RSS spread between all of the models not exceeding 2 mm, with the only exception being the strong performance of the FES2014 model in this region. FES2014 outperforms the next best tide model, EOT20, by showing a reduction in RSS of 4 mm. For all of the tidal constituents, FES2014 shows a lower rms compared to EOT20 in the open ocean region.

The constituents not included in the previous analysis are compared to the FES2014 model and the TICON tide gauge dataset (presented in Fig. A3). Only the TICON tide gauge dataset is used based on the availability of appropriate tidal constituents for the analysis. For six of the seven tidal constituents presented here, the two tide models show similar results to one another. For the J1 and M4 constituents, a slight improvement can be seen from EOT20 when compared to FES2014 while for the remaining tidal constituents, EOT20 shows a higher rms. Despite showing similar results for these constituents, it is clear that the solutions of EOT20 for these tides are still imperfect with the higher rms values caused by the difficultly to estimate the small signals of these tides from an altimetry perspective as well as due to the effects of temporal aliasing. Through the increased number of altimetry missions as well as improved processing techniques, these minor tidal constituents will be better estimated in future iterations of the EOT model. It should also be noted that the assessment of the models using in situ tide gauges themselves would benefit from additional high-quality extended time series in order to more accurately estimate the long-period constituents presented here (MM and MF).

The S1 tidal constituent is the relatively worst performing tidal constituent from the EOT20 model with an increased rms of 0.2 cm compared to FES2014. This problematic result is likely influenced by errors from the ionospheric correction, NIC09, that is used in the creation of the SLA product, which may leak into the estimation of the ocean tides (Ray, 2020). The ionospheric correction used in EOT20 is aimed at optimising the performance of the tide model in the coastal region; however, this may be negatively impacting the estimation of certain tidal constituents, like the S1 tide. Furthermore, Ray and Egbert (2004) discuss the impact that geophysical corrections (mainly inverse barometer and dry troposphere) have on the estimations of the S1 tide from altimetry data. A future study of the EOT model will investigate the use of different geophysical corrections to optimise the estimation of ocean tides with particular focus on the S1 tidal constituent.

The results of the tide gauge and ocean bottom pressure analysis suggest rather encouraging results from the EOT20 model. The estimated tidal constituents of EOT20 are notably improved compared to the previous EOT11a model. The performance of the model in the coastal region is noteworthy particularly in the representation of the M2 tidal constituent. Furthermore, the model remains on par with the other global tide models in the open ocean and shelf regions.

3.3 Sea level variance reduction analysis

In order to further assess the models ability, sea level variance reductions of three satellite altimetry missions were assessed and are presented. As seen in Fig. 4, tide gauges and ocean bottom pressure do not provide full coverage of the open ocean, so comparing the sea level variances of ocean tide models provides a suitable assessment of the performances of the models. The missions chosen are Jason-2 and Jason-3, which are used in the residual tide analysis as well as SARAL, which is not used in the analysis. A few steps are required in order to estimate sea level variance reduction. First, the along-track SLA is estimated using the corrections listed in Table 2 with the only differences being in the ocean and load tide correction. For this correction, two tide models (EOT11a and FES2014) were used to be compared to EOT20. The SLA for each cycle of all three missions was then estimated and then gridded onto a 4° grid. Once done, the variance of each of the SLA products was estimated (Savcenko and Bosch, 2012).

Figure 6 presents the results of the scaled SLA variance differences between the three tide models. For the Jason-2 mission, which is the mission with the most cycles, the SLA variance differences between all tide models are very similar to one another with EOT20 showing an overall mean-variance reduction of 0.054 and 0.026 cm^2 when compared to EOT11a and FES2014 respectively. The largest discrepancy

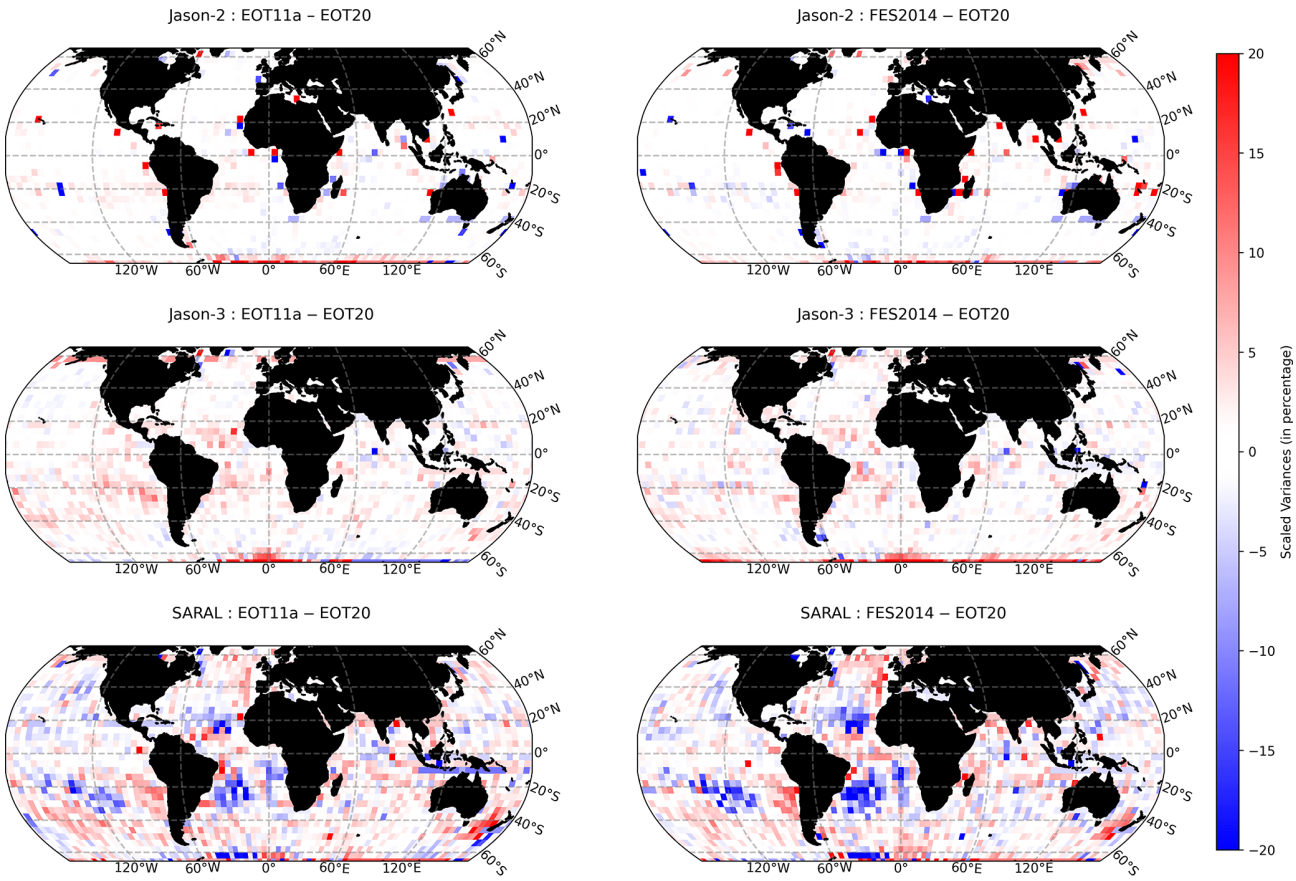

Figure 6. The global scaled SLA variances differences for Jason-2, Jason-3 and SARAL in percentages. The colour bar is chosen for ease of understanding with the variance differences scaled to highlight the differences between the results. The colours are chosen so that when there are regions of red colours EOT20 shows a lower variance, while when regions are blue the other tide model (EOT11a or FES2014) has a lower variance.

is around 60 to 66° south, where EOT20 shows a lower SLA variance compared to EOT11a and FES2014. When looking at how the SLA variance differences change based on the distance to coast for Jason-2 (Fig. 7, top), it can be seen that EOT20 shows the largest reduction of variance in the coastal region. This is particularly the case when looking at the differences between EOT11a, with EOT20 reducing the variance by approximately 0.4 cm^2 in the first 100 km from the coast. As they move further from the coast, the difference between the two models begins to reduce and converge towards zero. The variance difference between FES2014 and EOT20 shows similar results. Closer to the coast, EOT20 shows a reduced variance compared to that of FES2014 with differences exceeding 0.1 cm^2, but as they move further from the coast the difference between the two models converges towards zero. Like with the EOT11a model, FES2014 begins to show a reduced variance compared to EOT20 800 km from the coast.

For the Jason-3 mission, a reduction in SLA variance can be seen from the EOT20 model, with the discrepancies between the models again being very small (Fig. 6). The mean-variance reduction of EOT20 is 0.092 and 0.089 cm^2 when compared to EOT11a and FES2014 respectively. The variance reduction can be seen throughout the ocean, with larger reductions in the coastal region (Fig. 7, middle). Like in the Jason-2 mission, the variance differences decrease further away from the coast. Although the variance reduction diminishes further from the coast, unlike in the other two missions EOT20 shows continued variance reduction throughout the ocean.

The SARAL mission presents differing results from those seen in the Jason missions. It should be noted that SARAL has considerably fewer cycles and has a different orbit compared to the Jason missions. However, the results still provide valuable insights into the performances of the models. When looking at the scaled variance differences, the results become a bit more variable between the models with EOT20 showing reductions in variance in regions such as the Indian Ocean and the North Atlantic Ocean but showing increased variance in regions such as the South Atlantic Ocean and the South Pacific Ocean. Overall, EOT20 shows a mean reduction of variance compared to EOT11a of 0.129 cm^2 despite

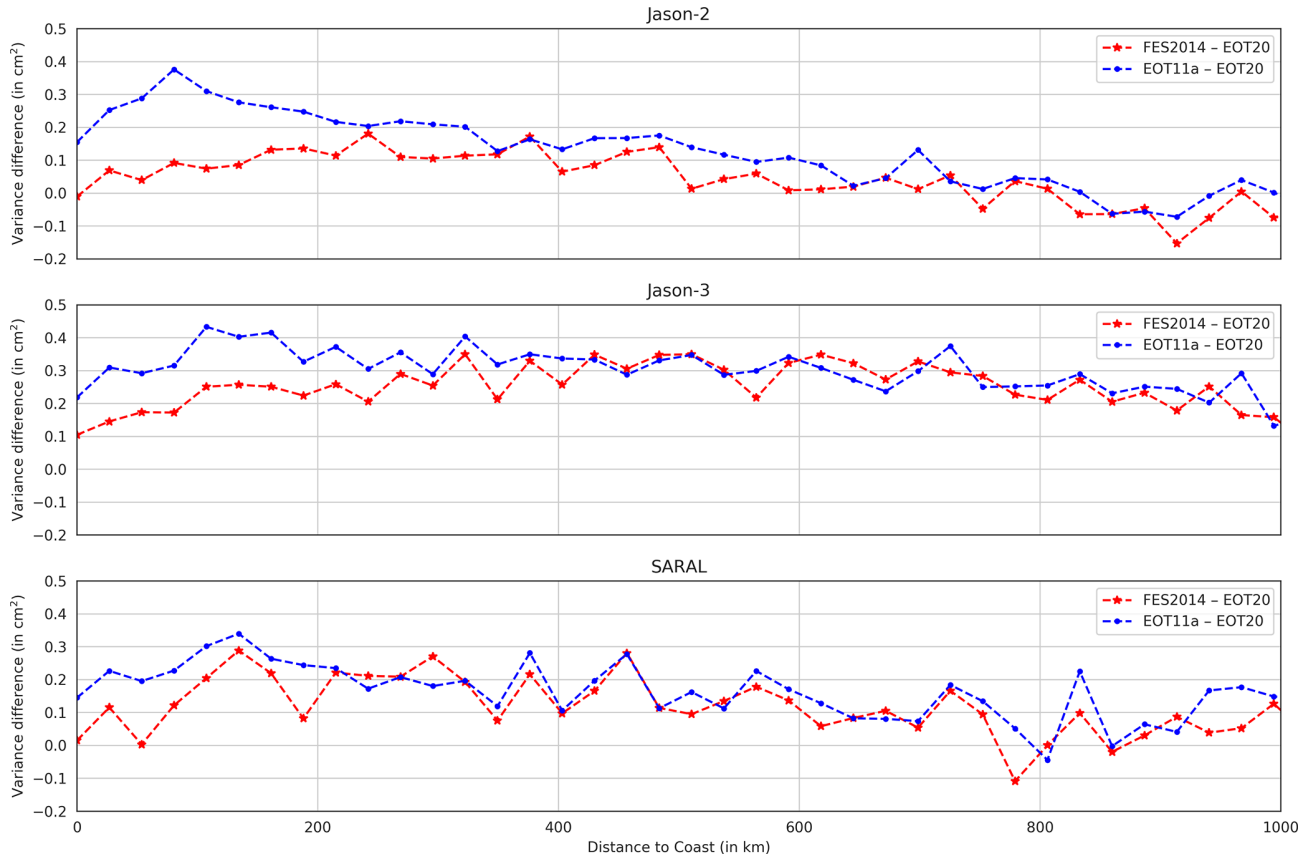

Figure 7. A line graph showing the mean SLA variance differences between the tide models as a function of distance to coast (in km) for all three satellite altimetry missions. The red line represents FES2014 − EOT20, while the blue line represents EOT11a − EOT20.

EOT11a outperforming the model in certain regions. The mean-variance reduction of EOT20 compared to FES2014 is 0.035 cm^2; however, there are regions where FES2014 shows better performance, particularly in the South Atlantic. Again, the overall reduction in variance is largely driven by the models' performance closer to the coast (Fig. 7, bottom) with reductions compared to EOT11a and FES2014 exceeding 0.3 and 0.2 cm^2 respectively closer to the coast, while these differences reduce towards zero further away from the coast.

4 Data availability

The ocean and load tides from EOT20 are available at https://doi.org/10.17882/79489 (Hart-Davis et al., 2021). The GMT data used to create the land–sea mask can be found at http://gmt.soest.hawaii.edu (last access: 5 August 2021). The satellite altimetry data used in the model creation can be found at https://openadb.dgfi.tum.de/ (last access: 5 August 2021). The tide gauges from the TICON dataset used in the validation of the tide model are available at https://doi.org/10.1594/PANGAEA.896587 (Piccioni et al., 2018a).

5 Conclusions

In this study, an updated version of a global ocean tide model, EOT20, is presented. Model developments were aimed at updating the previous model, EOT11a, with a focus on improving the coastal estimations of ocean tides by utilising recent developments in coastal altimetry, particularly the use of the ALES retracker and sea state bias correction. In the residual analysis, SLA data are gridded into a triangular grid aimed at increasing the efficiency of the model and thus better-describing tides in the coastal and higher latitudinal regions. A further update was in the use of a newer version of the reference model (FES2014) for the residual analysis performed to create the EOT20 model, which showed significant improvements to the previous reference model used, FES2004 (Lyard et al., 2020).

To evaluate the performance of the EOT20 model, validation against in situ observations and through sea level variance analysis was done. First, the models performance was compared with tide gauges and ocean bottom pressure sensors for the eight major tidal constituents. The results suggested that EOT20 showed significant improvements compared to EOT11a throughout the global ocean, with ma-

jor improvements being seen in the coastal region. Furthermore, when compared to other global ocean tide models, EOT20 had the lowest overall RSS for the major eight tidal constituents, In particular, improvements are seen in the coastal region, where EOT20 shows a reduced RSS of 0.2 cm compared to the closest model (FES2014). The rms differences between individual constituents show that EOT20 and FES2014 show clear improvements for all the tides compared to the other global models. EOT20 and FES2014 each had the lowest rms for half of the major tidal constituents presented, with the largest reduction in rms being seen in the M2 tide from EOT20. This positive performance was largely driven by the improved accuracy of the model compared to observations in the coastal region. In the shelf and open ocean regions, EOT20 was on par with the best tide models in these regions, DTU16 and FES2014, but there is still room for improvement compared to the FES2014 model in the open ocean.

The additional tidal constituents provide valuable data for the creation of the tidal correction used for satellite altimetry. The results of these additions show positive results compared to the FES2014 model, but improvements can still be made in determining some of these tides, particularly the S1 tidal constituent. Further investigations will be done at DGFI-TUM into the estimation of additional minor tidal constituents as well as the optimisation of the current estimations.

The sea level variance analysis continued to show positive results for EOT20. EOT20 reduced the mean variance compared to both FES2014 and EOT11a for all three satellite altimetry missions studied. Again, the largest reason for the improvement was seen in the coastal region with EOT20 showing similar results compared to the other models in the open ocean regions. These results of the new EOT20 model suggest that it will serve as a useful tidal correction for satellite altimetry.

Errors resulting from tide models are considered to be one of the main limiting factors for temporal gravity field determination and the derivation of mass transport processes (Koop and Rummel, 2007; Pail et al., 2016). In the creation of EOT20, a first look into the uncertainties of residual tide estimations was done, but due to the unavailability of uncertainty estimations from the FES2014 model used as the reference model these uncertainties are incomplete and, therefore, are not presented. This is a topic of discussion and future development that will be assessed in future studies.

As the fields of coastal altimetry and ocean tides develop, the ideas and methods of improving the EOT model continue to grow. A clear next step for the EOT model is to assess its ability to estimate tides in higher latitudes by including more satellite missions (e.g. CryoSat-2) and to introduce further data such as synthetic aperture radar altimetry from Sentinel-3. Furthermore, more recent developments in the estimation of internal tide models (Carrere et al., 2021) suggest that improvements may be made to the estimation of ocean tides from residual analysis when the internal tidal correction is applied to the SLA data. These potential avenues of improvement will be addressed in future iterations of the EOT model.

Appendix A

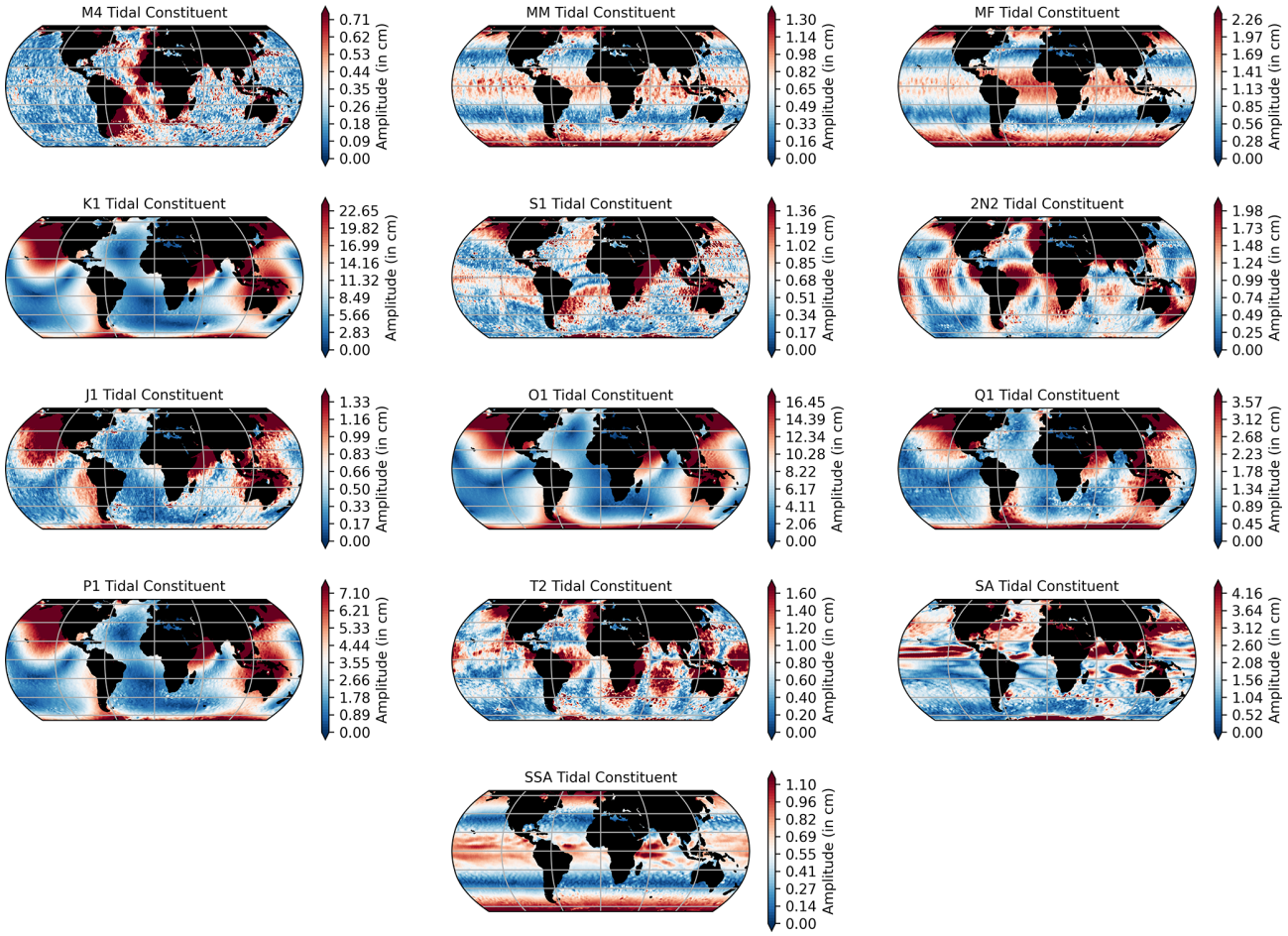

Figure A1. The amplitude of the remaining ocean tide constituents provided by EOT20.

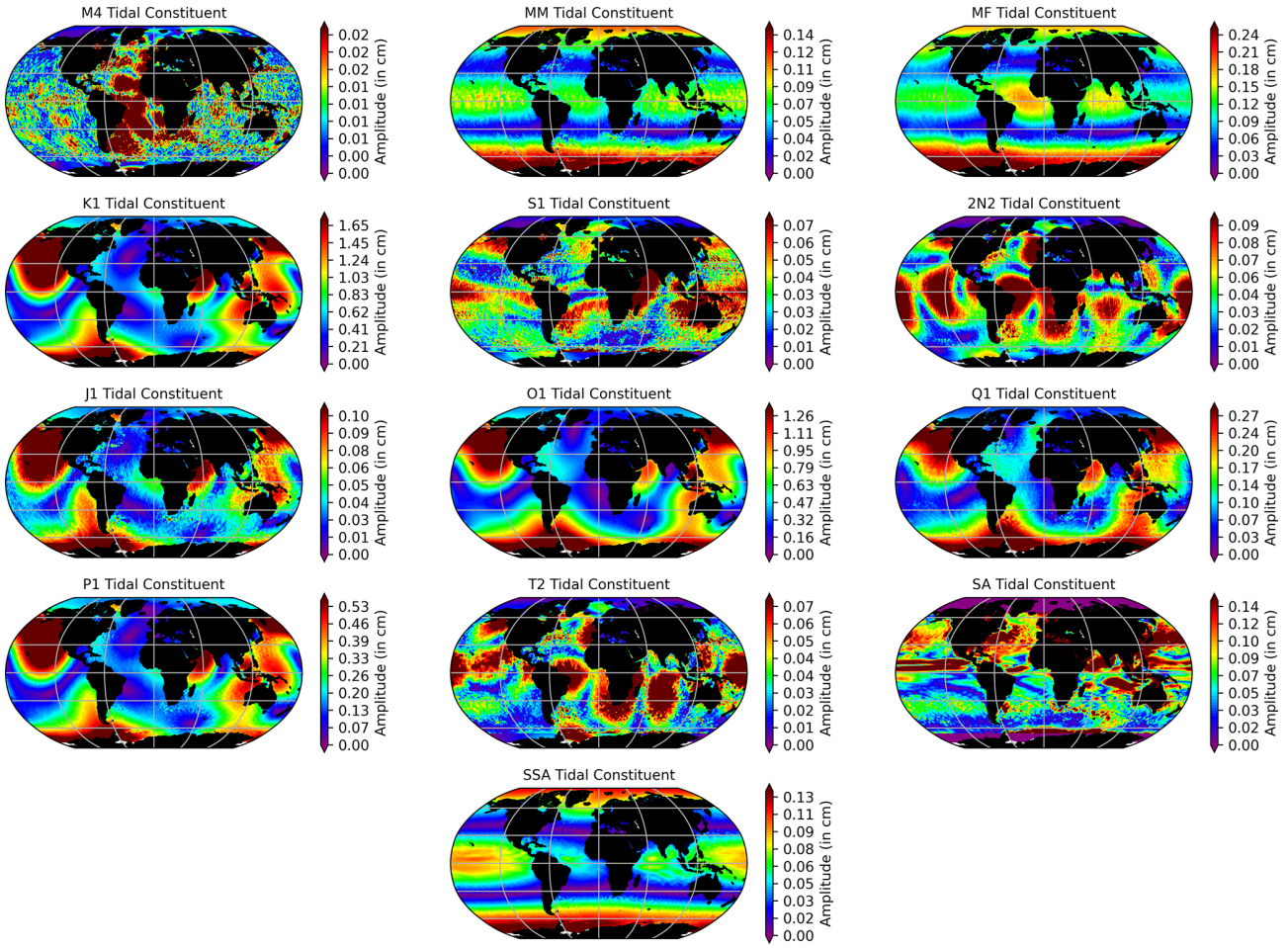

Figure A2. The amplitude of the remaining load tide constituents provided by EOT20. It should be noted that EOT20 does not make an estimation for the load tides on land.

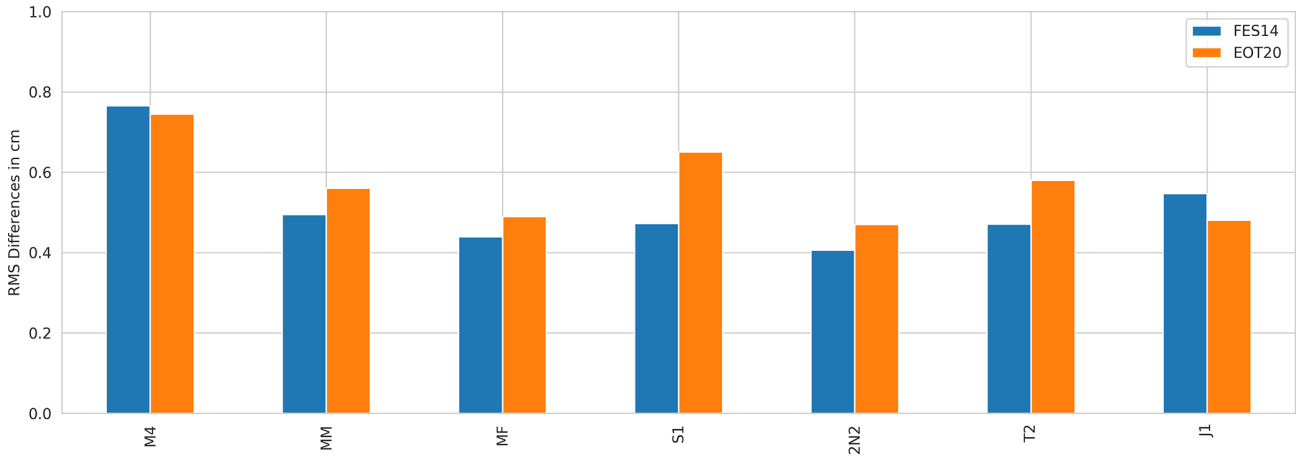

Figure A3. The rms and RSS of the remaining tidal constituents compared to the tide gauge datasets for both FES2014 and EOT20. A total of 1059 of tide gauges were used for this analysis only from the TICON dataset due to the availability of appropriate tidal constituents.

Author contributions. MGHD wrote the manuscript and performed the validation of the model. MGHD and DD were involved with designing the study and in interpreting the results. MGHD and GP were responsible for the development of the EOT20 model. CS and DD were responsible for the appropriate satellite altimetry data and assisted in the variance reduction validation. MP is the author of the retracking algorithm and of the sea state bias correction used in the model. FS provided the resources making the study possible and coordinates the activities of the research group at DGFI-TUM. All authors read, commented and reviewed the final manuscript.

Competing interests. The authors declare that they have no conflict of interest.

Disclaimer. Publisher's note: Copernicus Publications remains neutral with regard to jurisdictional claims in published maps and institutional affiliations.

Acknowledgements. The authors thank NOVELTIS, LEGOS, CLS Space Oceanography Division, CNES and AVISO for providing the FES2014 model. The authors would like to thank the anonymous reviewers for their input on the manuscript. We would also like to thank colleagues within the community for their comments on the model and results presented, particularly Sergiy Rudenko, Mathilde Cancet and Richard Ray.

Review statement. This paper was edited by Giuseppe M. R. Manzella and reviewed by two anonymous referees.

References

Andersen, O. B. and Scharroo, R.: Range and geophysical corrections in coastal regions: and implications for mean sea surface determination, in: Coastal altimetry, edited by: Vignudelli, S., Kostianoy, A., Cipollini, P., and Benveniste, J., Springer, Berlin, Heidelberg, pp. 103–145, 2011.

Andersen, O. B., Stenseng, L., Piccioni, G., and Knudsen, P.: The DTU15 MSS (mean sea surface) and DTU15LAT (lowest astronomical tide) reference surface, in: ESA Living Planet Symposium 2016, Prague, Czech Republic, 9–13 May, 2016.

Bosch, W., Dettmering, D., and Schwatke, C.: Multi-mission cross-calibration of satellite altimeters: Constructing a long-term data record for global and regional sea level change studies, Remote Sens.-Basel, 6, 2255–2281, 2014.

Brockley, D. J., Baker, S., Féménias, P., Martinez, B., Massmann, F.-H., Otten, M., Paul, F., Picard, B., Prandi, P., Roca, M., Rudenko, S., Scharroo, R., and Visser, P.: REAPER: Reprocessing 12 years of ERS-1 and ERS-2 altimeters and microwave radiometer data, IEEE T. Geosci. Remote, 55, 5506–5514, 2017.

Cancet, M., Andersen, O., Abulaitijiang, A., Cotton, D., and Benveniste, J.: Improvement of the Arctic Ocean Bathymetry and Regional Tide Atlas: First Result on Evaluating Existing Arctic Ocean Bathymetric Models, in: Fiducial Reference Measurements for Altimetry, edited by: Mertikas, S. and Pail, R., Springer, Cham, Switzerland, pp. 55–63, 2019.

Carrère, L., Faugère, Y., Bronner, E., and Benveniste, J.: Improving the dynamic atmospheric correction for mean sea level and operational applications of atimetry, in: Proceedings of the Ocean Surface Topography Science Team (OSTST) Meeting, San Diego, CA, USA, 16–21 October 2011, 19–21, 2011.

Carrere, L., Faugère, Y., and Ablain, M.: Major improvement of altimetry sea level estimations using pressure-derived corrections based on ERA-Interim atmospheric reanalysis, Ocean Sci., 12, 825–842, https://doi.org/10.5194/os-12-825-2016, 2016.

Carrere, L., Arbic, B. K., Dushaw, B., Egbert, G., Erofeeva, S., Lyard, F., Ray, R. D., Ubelmann, C., Zaron, E., Zhao, Z., Shriver, J. F., Buijsman, M. C., and Picot, N.: Accuracy assessment of global internal-tide models using satellite altimetry, Ocean Sci., 17, 147–180, https://doi.org/10.5194/os-17-147-2021, 2021.

Cartwright, D. E. and Ray, R. D.: Energetics of global ocean tides from Geosat altimetry, J. Geophys. Res.-Oceans, 96, 16897–16912, 1991.

Chambers, D., Hayes, S., Ries, J., and Urban, T.: New TOPEX sea state bias models and their effect on global mean sea level, J. Geophys. Res.-Oceans, 108, 3305, https://doi.org/10.1029/2003JC001839, 2003.

Cheng, Y. and Andersen, O. B.: Towards further improving DTU global ocean tide model in shallow waters and Polar Seas, OSTST, in: Proceedings of the Ocean Surface Topography Science Team (OSTST) Meeting, Miami, FL, USA, 23–27 October 2017.

Cipollini, P., Benveniste, J., Birol, F., Fernandes, M. J., Obligis, E., Passaro, M., Strub, P. T., Valladeau, G., Vignudelli, S., and Wilkin, J.: Satellite altimetry in coastal regions, in: Satellite altimetry over oceans and land surfaces, edited by: Stammer, D. and Cazenave, A., CRC Press, Florida, USA, pp. 343–380, 2017.

Eicker, A.: Gravity field refinement by radial basis functions from in-situ satellite data, Inst. für Geodäsie und Geoinformation, Univ. Bonn, 2008.

Farrell, W.: Deformation of the Earth by surface loads, Rev. Geophys., 10, 761–797, 1972.

Fernandes, M. J. and Lázaro, C.: GPD+ wet tropospheric corrections for CryoSat-2 and GFO altimetry missions, Remote Sens.-Basel, 8, 851, https://doi.org/10.3390/rs8100851, , 2016.

Fok, H. S.: Ocean tides modeling using satellite altimetry, PhD thesis, The Ohio State University, Ohio, USA, 2012.

Francis, O. and Mazzega, P.: Global charts of ocean tide loading effects, J. Geophys. Res.-Oceans, 95, 11411–11424, 1990.

Hart-Davis, M., Piccioni, G., Dettmering, D., Schwatke, C., Passaro, M., and Seitz, F.: EOT20 – A global Empirical Ocean Tide model from multi-mission satellite altimetry, SEANOE [data set], https://doi.org/10.17882/79489, 2021.

Koop, R. and Rummel, R.: The Future of Satellite Gravimetry: Report from the Workshop on The Future of Satellite Gravimetry, ESTEC, Noordwijk, the Netherlands, 2007.

Landskron, D. and Böhm, J.: VMF3/GPT3: refined discrete and empirical troposphere mapping functions, J. Geodesy, 92, 349–360, 2018.

Le Provost, C.: Chapter 6 Ocean Tides, in: Satellite Altimetry and Earth Sciences, edited by: Fu, L.-L. and Cazenave, A., vol. 69 of International Geophysics, Academic Press, San Diego,

https://doi.org/10.1016/S0074-6142(01)80151-0, pp. 267–303, 2001.

Lyard, F. H., Allain, D. J., Cancet, M., Carrère, L., and Picot, N.: FES2014 global ocean tide atlas: design and performance, Ocean Sci., 17, 615–649, https://doi.org/10.5194/os-17-615-2021, 2021.

Pail, R., Hauk, M., Daras, I., Murböck, M., and Purkhauser, A.: Reduction of ocean tide aliasing in the context of a next generation gravity field mission, EGU General Assembly 2016, Vienna, Austria, 17–22 April 2016, EPSC2016-5491, 2016.

Passaro, M., Cipollini, P., Vignudelli, S., Quartly, G. D., and Snaith, H. M.: ALES: A multi-mission adaptive subwaveform retracker for coastal and open ocean altimetry, Remote Sens. Environ., 145, 173–189, 2014.

Passaro, M., Nadzir, Z. A., and Quartly, G. D.: Improving the precision of sea level data from satellite altimetry with high-frequency and regional sea state bias corrections, Remote Sens. Environ., 218, 245–254, 2018.

Passaro, M., Müller, F. L., Oelsmann, J., Rautiainen, L., Dettmering, D., Hart-Davis, M. G., Abulaitijiang, A., Andersen, O. B., Høyer, J. L., Madsen, K. S., Ringgaard, I. M., Särkkä, J., Scarrott, R., Schwatke, C., Seitz, F., Tuomi, L., Restano, M., and Benveniste, J. Absolute Baltic Sea Level Trends in the Satellite Altimetry Era: A Revisit, Front. Mar. Sci., 8, 647607, https://doi.org/10.3389/fmars.2021.647607, 2021.

Petit, G. and Luzum, B.: IERS conventions (2010), Tech. rep., Bureau International des Poids et mesures sevres (France), 2010.

Piccioni, G., Dettmering, D., Bosch, W., and Seitz, F.: TICON: Tidal Constants based on GESLA sea-level records from globally distributed tide gauges [data set], PANGAEA, https://doi.org/10.1594/PANGAEA.896587, 2018a.

Piccioni, G., Dettmering, D., Passaro, M., Schwatke, C., Bosch, W., and Seitz, F.: Coastal improvements for tide models: the impact of ALES retracker, Remote Sens.-Basel, 10, 700, https://doi.org/10.3390/rs10050700, 2018b.

Piccioni, G., Dettmering, D., Bosch, W., and Seitz, F.: TICON: TIdal CONstants based on GESLA sea-level records from globally located tide gauges, Geosci. Data J., 6, 97–104, 2019.

Piccioni, G., Dettmering, D., Schwatke, C., Passaro, M., and Seitz, F.: Design and regional assessment of an empirical tidal model based on FES2014 and coastal altimetry, Adv. Space Res., 68, 1013–1022, 2021.

Ray, R., Egbert, G., and Erofeeva, S.: Tide predictions in shelf and coastal waters: Status and prospects, in: Coastal altimetry, edited by: Vignudelli, S., Kostianoy, A., Cipollini, P., and Benveniste, J., Springer, Berlin, Heidelberg, 191–216, 2011.

Ray, R., Loomis, B., Luthcke, S. B., and Rachlin, K. E.: Tests of ocean-tide models by analysis of satellite-to-satellite range measurements: an update, Geophys. J. Int., 217, 1174–1178, 2019.

Ray, R. D.: Precise comparisons of bottom-pressure and altimetric ocean tides, J. Geophys. Res.-Oceans, 118, 4570–4584, 2013.

Ray, R. D.: Daily harmonics of ionospheric total electron content from satellite altimetry, J. Atmos. Sol.-Terr. Phy., 209, 105423, https://doi.org/10.1016/j.jastp.2020.105423, 2020.

Ray, R. D. and Egbert, G. D.: The global S1 tide, J. Phys. Oceanogr., 34, 1922–1935, 2004.

Rudenko, S., Schöne, T., Neumayer, K., Esselborn, S., Raimondo, J.-C., and Dettmering, D.: GFZ VER11 SLCCI precise orbits of altimetry satellites ERS-1, ERS-2, Envisat, TOPEX/Poseidon, Jason-1 and Jason-2 in the ITRF2008, in: Proceedings of the Ocean Surface Topography Science Team (OSTST) Meeting, Reston, Virginia, USA, 20–23, 20–23 October 2015, 2018.

Savcenko, R. and Bosch, W.: EOT11a-empirical ocean tide model from multi-mission satellite altimetry, DGFI Report No. 89, Deutsches Geodätisches Forschungsinstitut, Munich, Germany, 49 pp., 2012.

Scharroo, R. and Smith, W. H.: A global positioning system–based climatology for the total electron content in the ionosphere, J. Geophys. Res.-Space, 115, A10318, https://doi.org/10.1029/2009JA014719, 2010.

Schwatke, C., Dettmering, D., Bosch, W., Göttl, F., and Boergens, E.: OpenADB: An Open Altimeter Database providing high-quality altimeter data and products, in: Ocean Surface Topography Science Team Meeting, Lake Constance, Germany, 7–31 October 2014.

Shum, C., Woodworth, P., Andersen, O., Egbert, G. D., Francis, O., King, C., Klosko, S., Le Provost, C., Li, X., Molines, J.-M., Parke, M. E., Ray, R. D., Schlax, M. G., Stammer, D., Tierney, C. C., Vincent, P., and Wunsch, C. I.: Accuracy assessment of recent ocean tide models, J. Geophys. Res.-Oceans, 102, 25173–25194, 1997.

Stammer, D., Ray, R., Andersen, O. B., Arbic, B., Bosch, W., Carrère, L., Cheng, Y., Chinn, D., Dushaw, B., Egbert, G., Erofeeva, S. Y., Fok, H. S., Green, J. A. M., Griffiths, S., King, M. A., Lapin, V., Lemoine, F. G., Luthcke, S. B., Lyard, F., Morison, J., Müller, M., Padman, L., Richman, J. G., Shriver, J. F., Shum, C. K., Taguchi, E., and Yi, Y.: Accuracy assessment of global barotropic ocean tide models, Rev. Geophys., 52, 243–282, 2014.

Tapley, B. D., Bettadpur, S., Ries, J. C., Thompson, P. F., and Watkins, M. M.: GRACE measurements of mass variability in the Earth system, Science, 305, 503–505, 2004.

Teunissen, P. J. and Amiri-Simkooei, A.: Least-squares variance component estimation, J. Geodesy, 82, 65–82, 2008.

Walters, R. A., Goring, D. G., and Bell, R. G.: Ocean tides around New Zealand, New Zeal. J. Mar. Fresh., 35, 567–579, 2001.

Wessel, P. and Smith, W. H.: A global, self-consistent, hierarchical, high-resolution shoreline database, J. Geophys. Res.-Sol. Ea., 101, 8741–8743, 1996.

A.1.2 P-2 Regional Evaluation of Minor Tidal Constituents for Improved Estimation of Ocean Tides

remote sensing

MDPI

Article

Regional Evaluation of Minor Tidal Constituents for Improved Estimation of Ocean Tides

Michael G. Hart-Davis [1,*], Denise Dettmering [1], Roman Sulzbach [2,3], Maik Thomas [2,3], Christian Schwatke [1] and Florian Seitz [1]

[1] Deutsches Geodätisches Forschungsinstitut der Technischen Universität München (DGFI-TUM), Arcisstrasse 21, 80333 München, Germany; denise.dettmering@tum.de (D.D.); christian.schwatke@tum.de (C.S.); florian.seitz@tum.de (F.S.)
[2] Deutsches Geoforschungszentrum (GFZ), Telegrafenberg, 14473 Potsdam, Germany; sulzbach@gfz-potsdam.de (R.S.); mthomas@gfz-potsdam.de (M.T.)
[3] Institut für Meteorologie, Freie Universität Berlin (FUB), Carl-Heinrich-Becker-Weg 6-10, 12165 Berlin, Germany
* Correspondence: michael.hart-davis@tum.de

Abstract: Satellite altimetry observations have provided a significant contribution to the understanding of global sea surface processes, particularly allowing for advances in the accuracy of ocean tide estimations. Currently, almost three decades of satellite altimetry are available which can be used to improve the understanding of ocean tides by allowing for the estimation of an increased number of minor tidal constituents. As ocean tide models continue to improve, especially in the coastal region, these minor tides become increasingly important. Generally, admittance theory is used by most global ocean tide models to infer several minor tides from the major tides when creating the tidal correction for satellite altimetry. In this paper, regional studies are conducted to compare the use of admittance theory to direct estimations of minor tides from the EOT20 model to identify which minor tides should be directly estimated and which should be inferred. The results of these two approaches are compared to two global tide models (TiME and FES2014) and in situ tide gauge observations. The analysis showed that of the eight tidal constituents studied, half should be inferred (2N2, ϵ_2, MSF and T2), while the remaining four tides (J1, L2, μ_2 and ν_2) should be directly estimated to optimise the ocean tidal correction. Furthermore, for certain minor tides, the other two tide models produced better results than the EOT model, suggesting that improvements can be made to the tidal correction made by EOT when incorporating tides from the two other tide models. Following on from this, a new approach of merging tidal constituents from different tide models to produce the ocean tidal correction for satellite altimetry that benefits from the strengths of the respective models is presented. This analysis showed that the tidal correction created based on the recommendations of the tide gauge analysis provided the highest reduction of sea-level variance. Additionally, the combination of the EOT20 model with the minor tides of the TiME and FES2014 model did not significantly increase the sea-level variance. As several additional minor tidal constituents are available from the TiME model, this opens the door for further investigations into including these minor tides and optimising the tidal correction for improved studies of the sea surface from satellite altimetry and in other applications, such as gravity field modelling.

Keywords: ocean tides; minor tides; satellite altimetry; tide models

Citation: Hart-Davis, M.G.; Dettmering, D.; Sulzbach, R.; Thomas, M.; Schwatke, C.; Seitz, F. Regional Evaluation of Minor Tidal Constituents for Improved Estimation of Ocean Tides. *Remote Sens.* **2021**, *13*, 3310. https://doi.org/10.3390/rs13163310

Academic Editor: Kaoru Ichikawa

Received: 22 June 2021
Accepted: 19 August 2021
Published: 21 August 2021

1. Introduction

Investigations of global sea level from satellite altimetry have been done for almost three decades following the launch of the ERS-1 and TOPEX/Poseidon altimeters in the early 1990s. Since then, several additional altimeter missions have followed, allowing for the continued assessment of sea level trends both in the open ocean and in the coastal

regions (e.g., [1–3]). However, errors resulting from ocean tide signals continue to affect the studying of sea surface processes using along-track altimetry.

The launch of the TOPEX/Poseidon mission provided unprecedented global data that was used to significantly advance the field of global ocean tide modelling (see [4–6]). In the years that have followed, several empirical ocean tide models have been developed based on the increased availability of altimeter observations, which has resulted in the increased accuracy of tidal estimations in the open ocean and coastal regions [5,7]. However, difficulties remain in the coastal region due to the land-contamination of signals, inaccurate bathymetry information, and the complex nature of ocean tides closer to the coast. Recent advances in coastal altimetry, such as the ALES retracker for improved retrieval of coastal signals [8], has been influential in advancing the accuracy of tidal estimations in the coastal region [9,10].

One such model that has recently shown significant improvements in the coastal region resulting from these advances is the EOT20 model. EOT20 is the latest in a series of global empirical ocean tide (EOT) models produced by residual tidal analysis of multi-mission along-track satellite altimetry [10]. EOT20 produced an increased consistency with tide gauges compared to other state-of-the-art ocean tide models, particularly in the coastal region. EOT20 uses the FES2014 tide model [11] as the reference model for the residual analysis and can, therefore, provide the full tidal signals of the 34 constituents provided by FES. In fact, further tidal constituents can be inferred from EOT when assuming that the reference tidal signals are close to zero. However, difficulties remain, such as the computational load required to globally estimate tides based on the decades of altimetry, tidal aliasing, as well as difficulties in accurately estimating very small tidal constituents. These difficulties mean that providing additional global estimations of tidal constituents is not as easy as it sounds. A total of seventeen tidal constituents are provided globally by the EOT20 model [12], with additional minor constituents being inferred via admittance theory in the creation of the tidal correction.

Minor tides have long been included in the estimation of tidal corrections [13] and play an important role in the prediction of sea level from satellite altimetry. Their inference from major tides allows additional constituents to be provided and, therefore, aids in reducing errors in the tidal correction [14,15]. Furthermore, admittance theory is used in satellite altimetry analysis to infer tides that cannot be estimated due to noise or tidal aliasing problems [16]. In the International Earth Rotation and Reference Systems Service (IERS) conventions [17], a list of tidal constituents are suggested for which linear admittance of tides in the diurnal and semi-diurnal bands can be done. The concept of admittance, the relation of the tidal height with respect to the amplitude of the corresponding tide generating potential for a specific tidal wave [18], is assumed to be a smooth function of frequency [19]. Based on these assumptions, minor tides can be linearly interpolated for long-period, diurnal, and semi-diurnal tides [18] according to the formulations presented in [17].

As stated in Foreman and Henry [14], knowing when to directly estimate minor tides through least-squares analysis and when to infer them is not easily answered. Since then, there have been several studies on minor tides comparing direct and inferred estimations (e.g., [16,20]). However, questions still arise on whether the accuracy of these inferred tides is sufficient in reducing errors in the altimetry correction. The Reference Ray [16] showed how, for certain models, the inferred P1 tidal constituent produced better results compared to the direct estimation, with the opposite being the case for the J1 tide. The Reference Karbon et al. [20] compared different techniques of inferring minor tides with the direct estimations of FES2012, and found an RMS difference of less than 0.75 cm, with higher differences seen in the coastal regions. As we continue to improve the coastal estimations of tides, these discrepancies between inferred and direct estimations become increasingly valuable in understanding the errors in ocean tide estimations.

With this in mind, this paper aims to identify the tidal constituents that are required to be directly estimated during the least-squares harmonic analysis performed on satellite

altimetry by the EOT model. An evaluation of a new approach of producing the ocean tidal correction for satellite altimetry by combining the major and minor tidal constituents of two different tide models is also presented. To do so, the aliasing periods and Rayleigh criteria for the satellite altimetry missions used are evaluated in Section 2 for all the tidal constituents available from the FES2014 model.

In Section 3, three regional studies are done comparing the direct and inferred minor tide estimations, as well as a purely hydrodynamic model and a data-constrained hydrodynamic model with in situ tide gauge data. Following on from this, the use of these minor tidal estimations are evaluated in the context of providing the tidal correction for satellite altimetry. Finally, a summary and outlook are given in Section 4.

2. Data and Methodology

The global EOT20 model showed significant improvements in the estimation of ocean tides in the coastal and open ocean region compared to other state-of-the-art global ocean tide models [10]. The EOT20 model is a semi-empirical tide model that is derived from residual tidal analysis of multi-mission satellite altimetry [21]. EOT20 relies on the FES2014 model [11] as a reference model for which residual analysis is performed to determine the residual tidal signals. A regional version of the EOT model is compared to both the FES2014 and the TiME global ocean tide models. The FES2014 model is the latest in a series of finite element solution (FES) global ocean tide atlases that have been produced to serve as a tidal correction for along-track satellite altimetry [11]. FES2014 is considered to be one of the leading ocean tide models and, therefore, the provided minor tides can serve as a good reference point to compare the results of minor tide estimations made by other models and techniques. The recently updated TiME model presented in Sulzbach et al. [22] is a numerical tide model that provides a vast number of minor tidal constituents that, when compared to inferred tides from data-constrained models, has been shown to improve the accuracy of several minor tides. TiME solves the shallow water equations on a truly global 1/12° grid under consideration of dynamic effects, that are known to exert a critical influence on tidal oscillation systems. Further profiting from an upgraded bathymetric map, the obtained open ocean accuracy for the main semi-diurnal lunar M2-tide was found to be below 3.4 cm with respect to the FES2014 model [22]. Being independent of data constraints, the model accuracy with respect to the tidal signal only drops moderately for minor tides, rendering TiME useful for the continued evaluation of smaller tidal signals to improve the understanding of the full tidal spectrum needed to produce the tidal correction for satellite altimetry.

2.1. Estimation of Minor Tides Using the EOT Approach

EOT applies the least-squares approach to the harmonic formula to derive the residual amplitude and phase of single tidal constituents from the observations of the sea-level anomaly obtained from multi-mission satellite altimetry [10]. Due to the approach being a data-intensive approach which relies on the input of several decades of satellite altimetry data in order to make estimations, only 17 tidal constituents are estimated in the global EOT20 configuration, while FES2014 provides global maps of 34 tidal constituents. The estimation of additional tidal constituents may be important in improving the accuracy of the model particularly in the creation of the tidal correction. Therefore, based on the same residual harmonic analysis performed by the global EOT20 model, the model has been run to include the same 34 tidal constituents as presented in FES2014 in three different regions; henceforth, this (R)egional version of the model will be referred to as EOT-R. Regional studies are preferred over a global study due to the high computational load required from running a global configuration. The three regions chosen are: the Yellow Sea and the surrounding ocean, which includes the Japan Sea and East China Sea (henceforth, this region is referred to as the Yellow Sea); Australia; and New Zealand, which were all chosen based on their complex coastlines, relatively high minor tide signals, and high variability between tide models for the major tides [7].

2.2. Inference of Minor Tides Using Admittance Theory

The concept of admittance, the relation of the tidal height with respect to the amplitude of the corresponding tide generating potential for a specific tidal wave [18], is assumed to be a smooth function of frequency [19]. Therefore, several unknown minor tides can be inferred from the major tides given in global tide models [18].

This inference is valuable, particularly when providing predictions that require the full tidal spectrum [16,23]. This has resulted in the continued development of techniques and softwares (examples given in [18] and https://github.com/tsutterley/pyTMD (accessed on 22 June 2021)) that have been designed to optimise the estimation of these minor tides. The IERS conventions provide a list of 71 minor tides that can be inferred from the linear admittance theory [17]. To provide an example of a tide that can be inferred using admittance theory, the L2 tidal constituent is presented in Figure 1 which is inferred from the K2 and M2 tidal constituents.

Differences can be noted between the estimations with the modelled amplitudes matching the amplitudes of the observations for most of the tide gauges, particularly in the Cook Strait between the two islands. For the relatively complex coastline of the northern island of New Zealand, however, the amplitude of the inferred L2 tide shows a clear underestimation compared to the observed L2 tide, while the modelled tides provide a better estimation. The in-phase (A) and quadrature (B) component of the L2 tide is inferred as the following:

$$A_{L2} = \frac{(f_{M2} - f_{L2})}{(f_{M2} - f_{K2})} \frac{H_{L2}}{H_{K2}} A_{K2} + \frac{(f_{L2} - f_{K2})}{(f_{M2} - f_{K2})} \frac{H_{L2}}{H_{M2}} A_{M2} \quad (1)$$

$$B_{L2} = \frac{(f_{M2} - f_{L2})}{(f_{M2} - f_{K2})} \frac{H_{L2}}{H_{K2}} B_{K2} + \frac{(f_{L2} - f_{K2})}{(f_{M2} - f_{K2})} \frac{H_{L2}}{H_{M2}} B_{M2}, \quad (2)$$

with f being the frequency of the tide expressed in cycles per day, while H is the known tide-generating potential of the constituent.

Using this approach, eight additional tidal constituents were inferred from the EOT20 model based on the ability to be inferred via admittance, as well as the availability of these tide maps from the respective ocean tide models and the availability of in situ tide gauges needed to validate the tidal solutions. These constituents are: T2, ϵ_2, J1, L2, μ_2, MSF, ν_2 and 2N2. For more information about these tidal constituents, please refer to Chapter 6 of Petit and Luzum [17]. In practice, admittance theory is used to improve the estimation of the full tidal height [16] and in this application, we apply the admittance theory to validate the accuracy of this inference compared to in situ tide gauge observations and with direct estimations from the ocean tide models presented above.

2.3. Aliasing Periods

As the EOT methodology relies on satellite altimetry which only samples the same locations at varying times based on their orbits (i.e., Jason altimeters sampling the same position every 9.9156 days and Envisat altimeters every 35 days), the aliasing period of the tidal constituents should be taken into account to determine whether the empirical model can provide an appropriate estimation of tidal constituents. The aliasing periods have been estimated for the Jason-series and the Envisat-series based on the research conducted by Wang [24], and are presented in Figure 2. When considering the length of data available from the Jason-series (more than 9000 days) and the Envisat-series (more than 6500 days), for 32 of the 34 tidal constituents considered the aliasing period does not have an influence on the determination of these tidal constituents. However, a known problem in the Envisat-series can be seen for the S1 and S2 tidal constituents in Figure 2. The altimetry missions that follow the orbit of the Envisat mission are all sun-synchronous, which means the aliasing period of these two solar tides becomes infinite and cannot be resolved by these missions alone. However, by incorporating the Jason-series of data that follow a different orbit, EOT can still provide an estimation of these two tidal constituents.

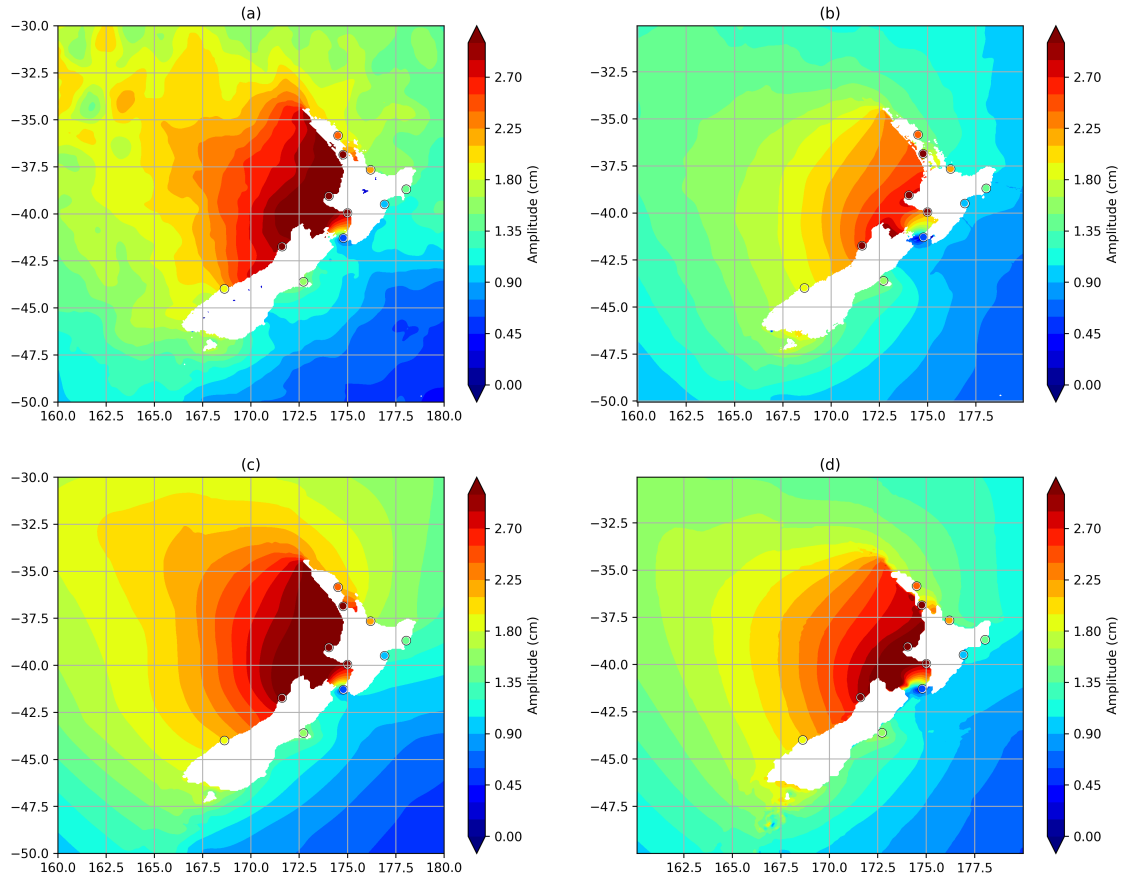

Figure 1. The L2 tidal amplitude for (**a**) EOT-R, (**b**) Inferred from EOT20, (**c**) TiME and (**d**) FES2014 compared to the L2 amplitudes from the tide gauge observations (circles).

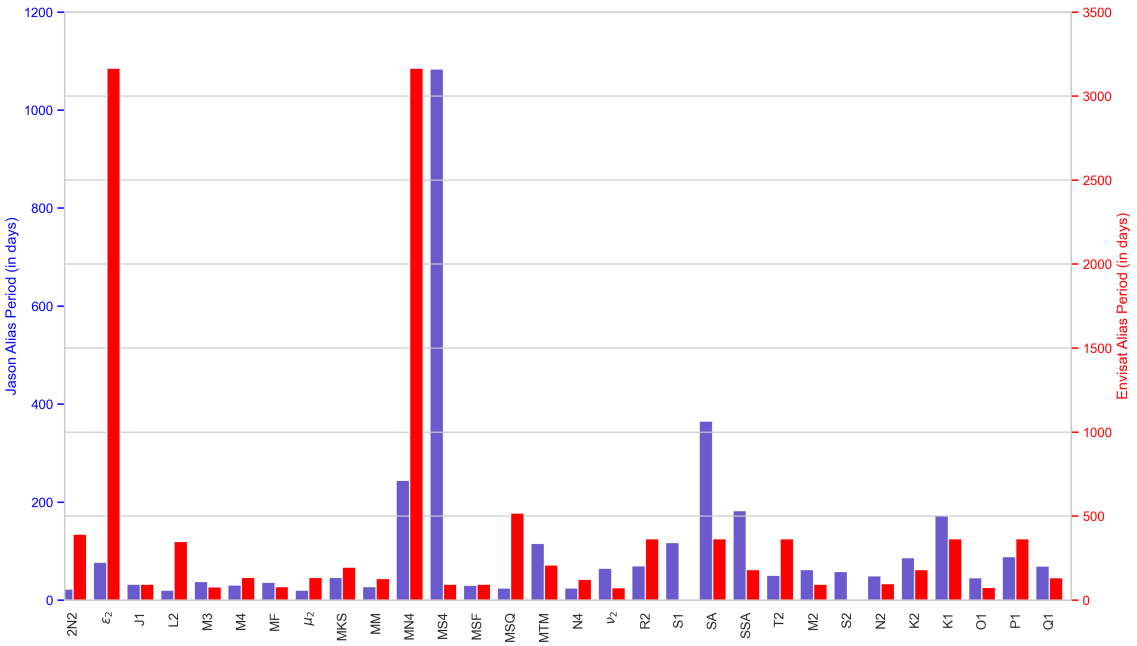

Figure 2. The alias period (in days) for all the tidal constituents available from FES2014, with the blue bars indicating the Jason orbit missions and the red bars representing Envisat orbit missions. The S1 and S2 tidal constituents of the Envisat orbit have an aliasing period of infinity due to their sun-synchronous orbit.

Also important in the estimation of ocean tides from satellite altimetry, is the Rayleigh criteria which provides information on the length of time-series required to separate tidal constituents of similar angular frequencies [25]. Again, this varies based on the orbits and repeat cycles of the altimetry missions used, and with that in mind, the Rayleigh criteria are presented in Figure 3.

In this figure, the lower-left triangle represents the Rayleigh criteria (in days) of the Jason-series, while the upper-right triangle is that of the Envisat-series. For the Jason-series of data, the Rayleigh criteria is satisfied for all of the tidal constituents but this is not the case for the Envisat-series. Focusing on the minor tides that will be investigated later in this study, the Rayleigh criteria indicates difficulties in estimating the semi-diurnal solar T2 tidal constituents, as well as the ϵ_2 and MSF tidal constituents. It can, therefore, be suggested that these tidal constituents may benefit from their inferences from their major tidal constituents, but inaccuracies in these tides may be compensated by the Jason-series, for which this is not an issue.

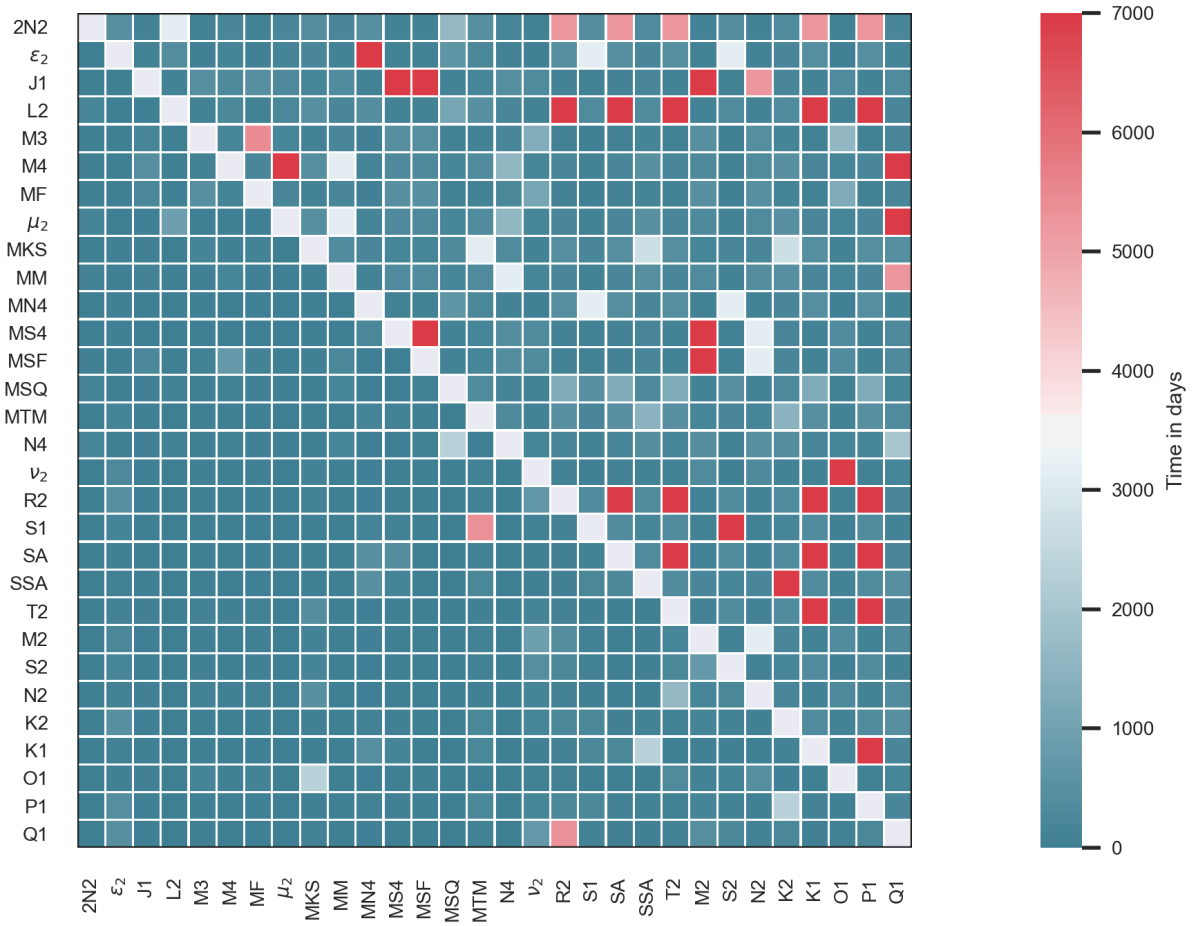

Figure 3. Rayleigh coefficient in days of the Jason orbit (lower-left corner) and the Envisat orbit (upper-right corner) missions. The maximum time in days seen in the colourbar is chosen to be the temporal extent of the Envisat orbit used in the EOT model.

3. Results and Discussion

3.1. Tide Gauge Analysis

Three regional studies were conducted to assess the accuracy and importance of minor tidal constituents. For each of these regions, the EOT-R, FES2014, and TiME tide models, as well as tides inferred from the EOT20 model (EOT-I), were compared to tide gauges obtained from the TICON dataset [26]. TICON is a global tide gauge dataset derived from the Global Extreme Sea Level Analysis (GESLA) project which provides tidal constants for individual tide gauges that have been estimated through least-squares-based harmonic analysis.

The TICON data have been extensively quality controlled and provide all the tidal constituents available from the FES2014 tide model [26]. Therefore, this tide gauge dataset is used due to the availability of the appropriate minor tides for which comparisons should take place between the four tide models. The models are compared to the tide gauges using root-mean-square differences (RMS) and the root-sum-square (RSS) as presented in Hart-Davis et al. [10] with the tidal signal estimated following Stammer et al. [7], with the RMS, RSS, and tidal signal being presented in Figure 4.

For all of the tide gauges presented, EOT-R shows a lower root-square-sum (RSS) compared to all of the tide models, but there are several constituents where the RMS is higher than that of the other models (Figure 4d). For the Australia and New Zealand regions, EOT-R shows a lower RSS compared to all of the tide models and shows relatively low RMS results for all of the constituents. In the Yellow Sea (Figure 4b), however, EOT-R shows a relatively poor RMS for the MSF tide, which results in the RSS in this region being slightly higher than the FES2014 model. Additionally, this is also the only region where EOT-R shows a higher RMS for the T2 tide compared to both EOT-I and FES2014.

The MSF and T2 tides, as shown in Figure 3, were constituents where the Rayleigh coefficient for the Envisat missions was not satisfied. In fact, as seen in Figure 4, MSF is one of two tides where an overall improvement was not seen compared to the reference tide model, FES2014, indicating that this tidal constituent cannot be accurately determined via the least-squares analysis done by EOT. This is further confirmed by the RMS results of the EOT-I for the MSF and T2 tides, where the mean results are lower than that of the EOT-R model.

The tidal signal of MSF is the lowest of all the tides, indicating known difficulties in direct estimation of smaller tides from satellite altimetry. The tides used to infer the MSF tide are the MM and MF tides, while T2 is inferred from the M2 and K2 constituents [17], which are already processed in the creation of the global EOT20 model and it is, therefore, recommended that these tides be inferred in order to reduce the influence of any errors forming from the failure to meet the Rayleigh criteria for Envisat-orbit missions.

The estimation of the 2N2 constituent is the only other tide where EOT-R shows a higher RMS compared to both EOT-I and FES2014. This tide is provided in the global EOT20 tide model and used in the inference of the ϵ_2 constituent [17] and, therefore, requires special consideration regarding whether it should or should not be directly estimated via harmonic analysis. Overall, the RMS of the 2N2 tide from EOT-R is very similar to the results of both FES2014 and EOT-I, while for the ϵ_2 tide, EOT-R shows slightly improved results. Based on the relatively high tidal signal of the 2N2 tide, all models do well in estimating this tide compared to the tide gauges, while for ϵ_2, the models show a relatively high RMS compared to the signal itself. When inferring ϵ_2 from the inferred 2N2 tide (not shown), the RMS of the ϵ_2 tide compared to tide gauges is reduced by 0.1 mm and becomes in line with the RMS of EOT-R and FES2014. This means that the 2N2 and the ϵ_2 tide can be inferred by the EOT model and do not need to be directly estimated through harmonic analysis.

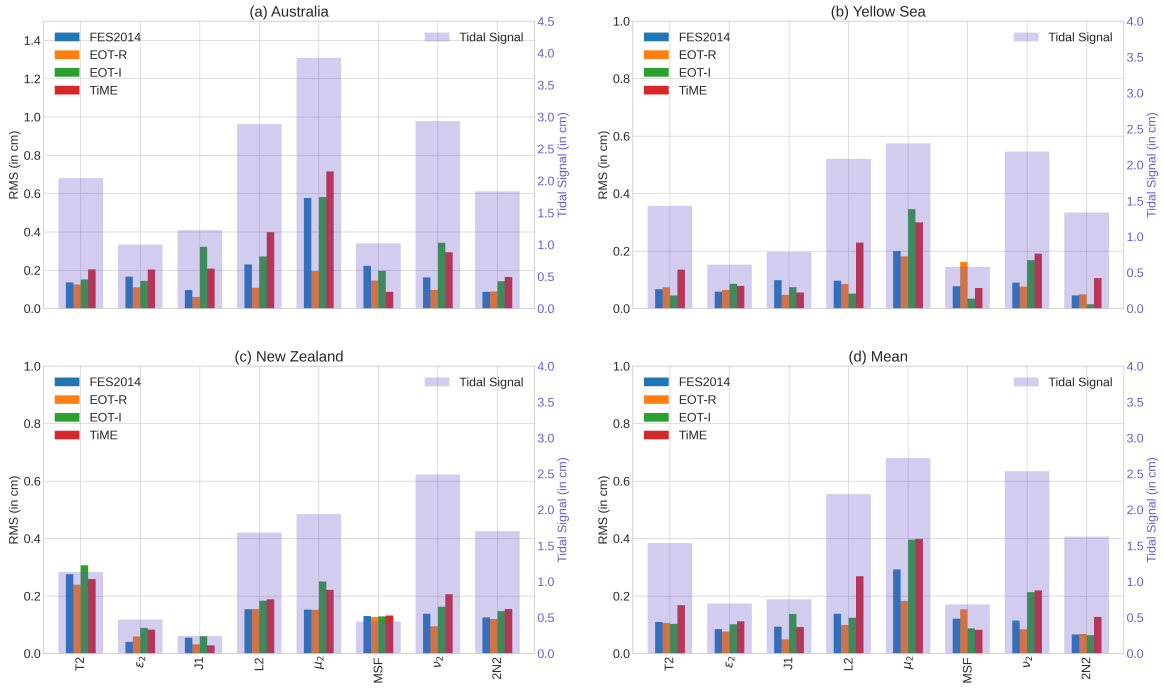

Figure 4. The RMS, in cm, of the minor tides from all three regions for the EOT-R, EOT-I, FES2014, and TiME tide models. The RMS is overlaid above the tidal signals (blue axis) of each individual constituent in each of the regions. The number of tide gauges for each region is 27 for Australia, 65 for the Yellow Sea, and 12 for New Zealand, with the mean being of all 104 tide gauges.

For the remaining constituents, EOT-I shows significantly larger RMS values compared to EOT-R. The results for μ_2, ν_2 and J1 tides are consistent for all of the regions, implying the inference does not provide an accurate estimation of these tides. These results are in line with what has previously been shown for the J1 tide in Ray [16]. For the L2 tide, however, the picture is not as clear. In the Yellow Sea, EOT-I outperforms EOT-R, while in New Zealand and Australia, the results are vice versa. However, the inferred L2 tide shows an RMS that is more than double that of the EOT-R in Australia. With this high RMS, coupled with the overall larger RMS for EOT-I, it is recommended that the L2, as well as the remaining three tides, be directly estimated by the EOT model. When considering that EOT-R and FES2014 are optimised for the estimation of tides in the coastal region, the performance of TiME compared to the tide gauge observations exceeds expectations. TiME shows the lowest overall RMS for the MSF tidal constituent and is within 2 mm of the overall RSS estimations of the EOT-I and FES2014 models.

Furthermore, the higher RSS of the TiME model is strongly influenced by poorer estimations of the L2 and μ_2 tidal constituents, while for the remaining constituents, the RMS of TiME is closer to those of the other models. The high RMS in the μ_2 is driven by larger errors seen in the Australian region, with relatively high errors also seen in the FES2014 and EOT-I results. For L2, TiME shows consistency in having the highest RMS value, with this influencing the RSS differences between EOT-I and TiME. With this tide removed from the analysis, the overall RSS of TiME reduces to be within 0.1 mm of EOT-I. This suggests that TiME provides valuable minor tide estimations that can potentially be used to improve the understanding of minor tides, as well as improve tidal corrections.

The results of the tide gauge analysis provide important insight for the estimation of tides from the current availability of satellite altimetry and, therefore, the EOT ocean tide model. Coupled with Figure 3, it can be recommended that of the constituents presented, 2N2, ϵ_2, MSF, and T2 tides do not need to be directly estimated during the harmonic analysis of satellite altimetry. For the remaining J1, L2, μ_2 and ν_2 tides, it is recommended to directly estimate these tides when using the approach combining both Envisat- and

Jason-orbit altimetry missions. For the most part, the results of TiME and FES2014 are outperformed by the EOT-R model, however, when compared to the inferred constituents, both models show encouraging results. Therefore, instead of using linear admittance to infer minor tidal constituents for use in the tidal correction, models such as FES2014 and TiME could be coupled with the EOT major tides to provide an accurate tidal correction.

3.2. Regional Sea Level Variance Analysis

In this section, the above-mentioned tide models are used to create tidal corrections for satellite altimetry observations. To evaluate the accuracy of the tidal corrections, regional sea-level variance analysis is presented within the three regions described above. For this, the sea level anomaly (SLA) is estimated for the Jason-2 altimeter following the same technique used in Andersen and Scharroo [27] and Hart-Davis et al. [10]: $SLA = H - R - h_{geo} - MSS$, where H is the orbital height, R the range, MSS the mean sea surface, and h_{geo} is the geophysical corrections, with the same parameters and corrections being used as in Table 2 of Hart-Davis et al. [10].

Here, the only variable that is changed is the ocean tidal correction for which four different tidal corrections were computed. For all of these corrections, the eight minor tides as presented in Figure 4 are used from the tide models and are combined with the major tides of the EOT-R model. The use of the major tides from the EOT-R model is kept consistent so that the SLA variance is only influenced by the minor tides. These major tides are M2, K2, K1, S2, N2, O1, P1, and Q1, as well as the long-period tides MM, MF, SA, and SSA. Several additional constituents are available from each model, but these are chosen based on consistency between models and the ability to infer via linear admittance. It should also be made clear that there will potentially be small errors resulting from inconsistencies between model-defined coastlines, as well as variable spatial resolutions.

For each cycle of Jason-2, the SLA was gridded onto a 3-degree grid and, finally, this was then used to calculate the SLA variance for each of the scenarios created. The SLA variance differences are then presented for Australia (Figure 5), New Zealand (Figure 6), and the Yellow Sea (Figure 7) with the mean differences being presented in Table 1.

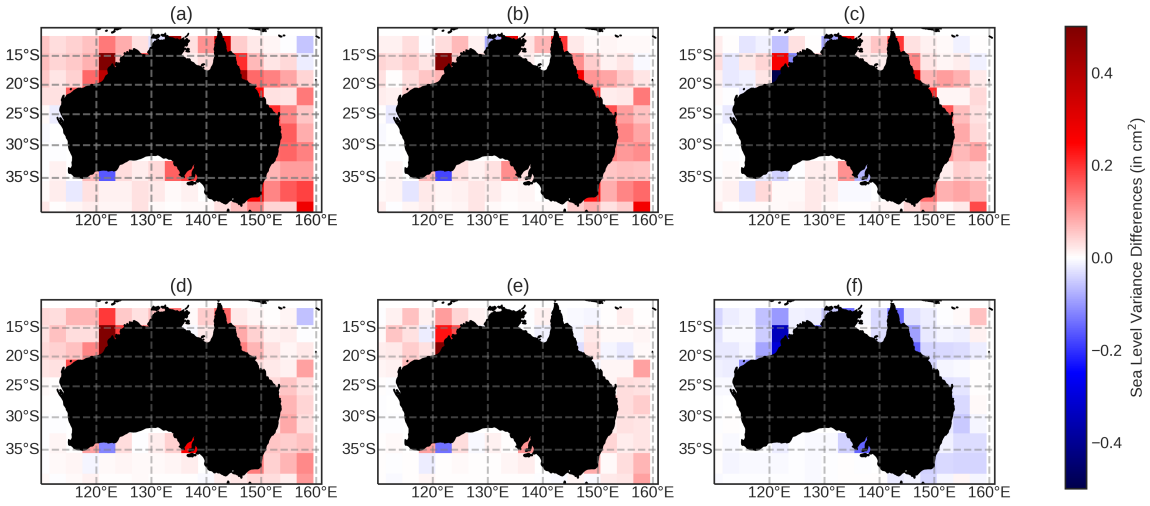

Figure 5. The sea-level variance differences between the scenarios presented for the Jason-2 altimeter in the Australia region. The subplots of sea-level variance differences are as follows: (**a**) modTiME–EOT-R; (**b**) modTiME–EOT-I; (**c**) modTiME–modFES; (**d**) modFES–EOT-R; (**e**) modFES–EOT-I; and (**f**) EOT-R–EOT-I. The figures are designed so that when the colours are blue, the first model has a lower variance, while when the regions are red, the first model has a higher variance compared to the second model.

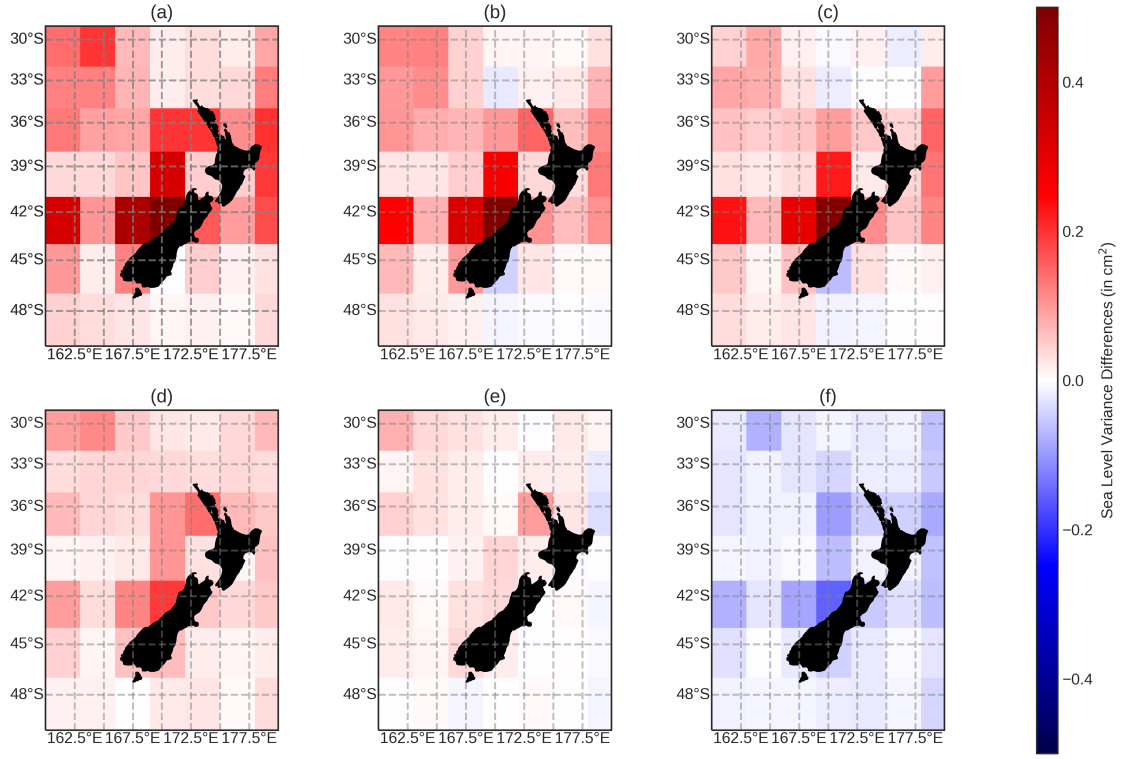

Figure 6. The same as in Figure 5, but for the New Zealand region.

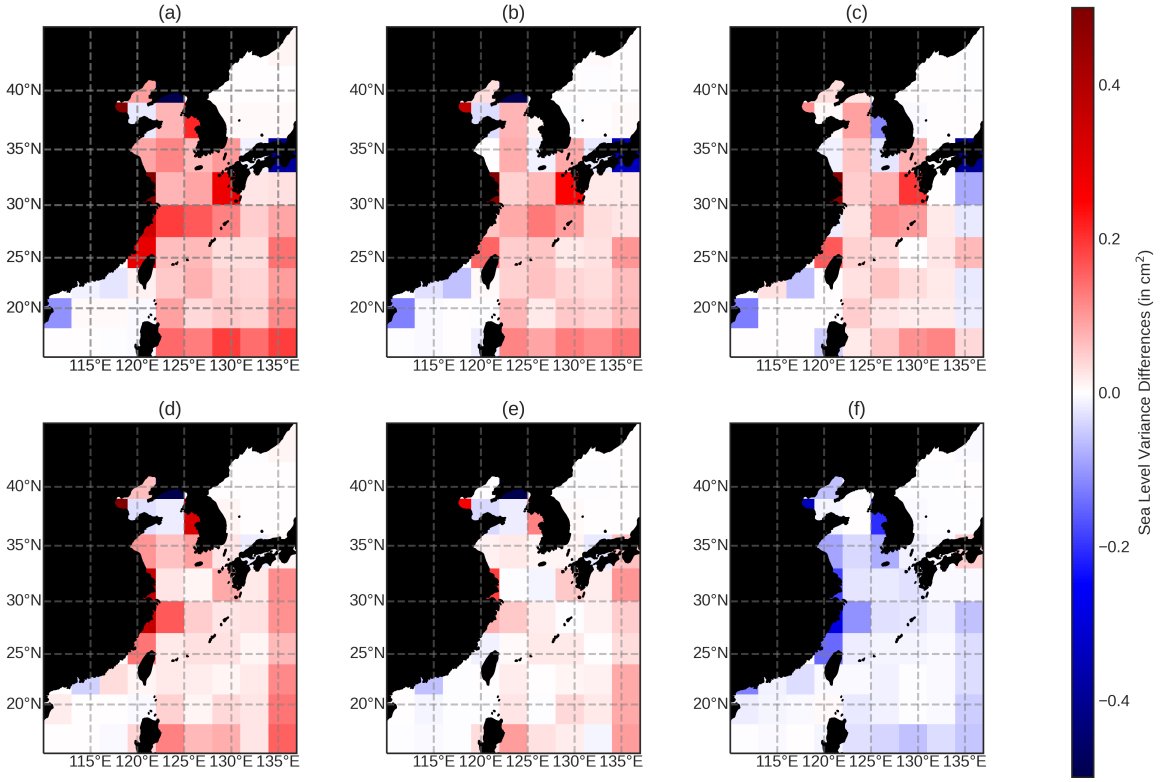

Figure 7. The same as in Figure 5, but for the Yellow Sea region.

Table 1. The mean sea-level variance difference (in cm^2) estimated for each of the listed scenarios.

Scenario	Australia	New Zealand	Yellow Sea	Mean Difference
modTiME–EOT-R	0.081089	0.110182	0.058563	0.083278
modTiME–EOT-I	0.046603	0.075467	0.022314	0.048128
modTiME–modFES	0.010556	0.062240	0.026581	0.033126
modFES–EOT-R	0.076972	0.047942	0.031982	0.052299
modFES–EOT-I	0.036719	0.013227	−0.004267	0.015226
EOT-R–EOT-I	−0.040252	−0.034715	−0.037577	−0.037515
EOT-H–EOT-R	0.000348	−0.001323	−0.005408	−0.002128

The results of the regions of New Zealand and Australia show that the inferred minor tides reduce the variance compared to both TiME and FES2014 'hybrid' tidal corrections (henceforth referred to as modTiME and modFES, respectively), with modFES showing a reduction compared to modTiME. For the most part, the variance differences are small, rarely exceeding 0.1 cm^2; however, in the coastal region, the modTiME model shows relatively high variances compared to the other model estimations. This is somewhat expected, due to the FES and EOT models being optimised for the coastal regions. The differences between modFES and EOT-I are also largely in the coastal regions, with variances being very similar further away from the coast.

In Hart-Davis et al. [10], improvements were seen in the estimation of tides in EOT20 compared to FES2014 in the coastal region based on the incorporation of the ALES retracker and the improved coastal representation, while in the open ocean regions, the models showed similar results for the estimation of tides. Although those results were for major tides, similar results can be seen here for the minor tides.

For the Yellow Sea region (Figure 7), the mean SLA variance differences between the models generally decreases, with modFES slightly outperforming EOT-I. Like in the other two regions, the general strong point for EOT-I is in the coastal region, with the model differences decreasing further away from the coast. However, in the Yellow Sea, there are, in fact, certain coastal points where EOT-I, as well as EOT-R, perform relatively poorly. For example, the grid points at 40°N and 125°E, as well as 35°N and 135°E show high sea-level variance for EOT-R and EOT-I and relatively low variances for modTiME and modFES. This region was where EOT-R was outperformed by FES2014 in the tide gauge analysis and where EOT-R had the highest RMS for the MSF tide. This suggests that EOT-R is not providing a good estimation of the minor tides in the sub-regions identified in Figure 7, which could be caused by either the complexity of these two regions (being areas of several islands) or the size of the grids used in this analysis. With these two sub-regions removed, the mean differences between the models of the Yellow Sea show similar results to what was seen in the Australia and New Zealand regions.

Despite the tide gauge analysis suggesting problematic tides, such as the MSF tide, it was somewhat anticipated that the minor tides of the EOT-R model would provide an improved tidal correction, and this has proved to be the case. Compared to the other configurations in every region (Table 1), EOT-R shows a mean reduction in sea-level variance, although the mean differences only exceed 0.1 cm^2 for the modTiME model in the New Zealand region. There are sub-regions where EOT-R shows a large reduction exceeding 0.2 cm^2 compared to both modTiME and modFES; however, overall, the differences remain small. Furthermore, EOT-R shows a reduction for all of the regions except two grid cells compared to EOT-I but, again, the differences are minimal. Although EOT-R shows better results compared to the other models overall, the mean differences between the models are small, which is driven by smaller variance differences between the models away from the coasts.

In the coastal regions, EOT-R shows a large reduction in variances compared to the other models, as well as the inferred tides. These differences could potentially decrease when larger errors in individual tides, for example in the L2 tide (Figure 4), are addressed

in the other minor tide estimations. However, this further highlights the importance of either investigating different techniques to infer the minor tides, or directly estimating them to provide a better tidal correction in the coastal region for use in sea-level studies using satellite altimetry.

A final comparison between two tidal corrections is presented in Figure 8. In this comparison, a tidal correction is created based on the recommendations produced in the tide gauge analysis on which tides to infer and which tides to directly estimate in the EOT model, to produce a '(H)ybrid' ocean tidal correction called EOT-H. To reiterate, the tides recommended to infer were 2N2, ϵ_2, MSF, and T2 tides, and those recommended to directly estimate were J1, L2, μ_2, and ν_2 tides. The overall mean differences show a reduced variance for EOT-H compared to EOT-R in both Australia and the Yellow Sea, while EOT-R showed a reduced variance in the New Zealand region. The variance differences remain very low and never exceed 0.01 cm^2, with the average difference being 0.002 cm^2 in favour of EOT-H (Table 1).

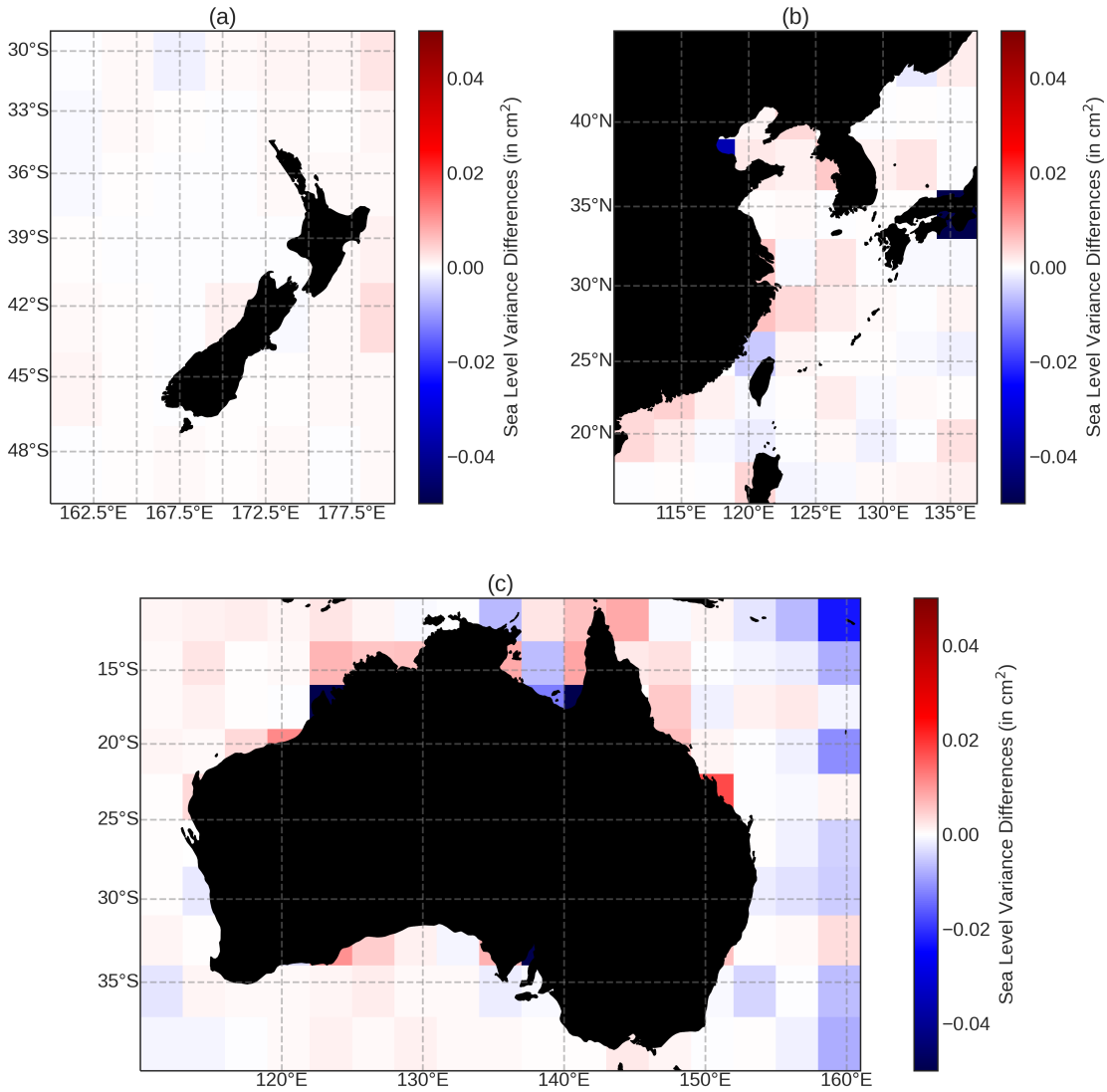

Figure 8. The sea-level variance differences between EOT-R and EOT-H for (**a**) New Zealand, (**b**) the Yellow Sea and (**c**) Australia. Please note the adjusted color bar compared to Figures 5–7. Here, when the regions are colored red, EOT-R shows a reduction in SLA variance, while the opposite is the case in blue regions.

Generally, the differences in the coastal region favour EOT-R; however, there are certain regions where the EOT-H shows a reduction in variance, particularly around 140°E

and 15°S in Australia. The region where there is the highest improvement from EOT-H is in the eastern coast of Australia, near a western boundary current known as the East Australian Current. Generally, a higher SLA variance is seen in western boundary currents [28] resulting from difficulties, among other things, to accurately estimate the ocean tides in regions of high non-tidal variability [29].

By determining which tides can accurately be inferred and directly estimated, EOT-H allows for maintenance of the higher accuracy tidal estimations, but also utilises admittance theory to infer tides where satellite altimetry struggles to do so. The recommendation of tides to infer and directly estimate, therefore, produces results that are suitable for use in an ocean tidal correction of satellite altimetry.

4. Summary and Outlook

This paper presented an evaluation of the accuracy of the estimation of minor tidal constituents and the implications this has on the estimation of the sea level from along-track satellite altimetry. Furthermore, a new technique of merging constituents calculated from different models to utilise strengths of individual models was presented. The use of minor tides is valuable for the estimation of the sea level from along-track satellite altimetry [13]. For the EOT tide model, estimating minor tides is made difficult due to tidal aliasing and due to the small signals of these tides which are challenging to detect from satellite altimetry. Four different tide models were compared to one another: EOT-R which is a regional model created following the exact configuration of EOT20 [10] simply with additional constituents; EOT-I which is the minor tides that are inferred from the EOT20 model using linear admittance theory; and FES2014 [11] and TiME [22].

The tide gauge analysis provides valuable insight for the EOT model on which tidal constituents need to be directly estimated during the harmonic analysis and which tides can be inferred via admittance theory. Based on these results, it is recommended that the J1, L2, μ_2 and ν_2 tides be directly estimated and that the 2N2, ϵ_2, MSF and T2 be inferred. This will reduce the computational load while still providing an accurate tidal correction for satellite altimetry. On average, EOT-R outperforms all of the other models, but there are regions and constituents for which the other models show better results. The results of the SLA variance analysis showed that the minor tide correction created based on the recommendations of the tide gauge analysis provided the best results in terms of the tidal correction. However, the differences between the four different minor tide estimations are relatively low. Although TiME produced relatively large errors for certain tides, the results are rather encouraging compared to the FES2014, EOT-R and EOT-I minor tide estimations, despite being a purely hydrodynamic model and not being optimised for the estimation of tides in the coastal region. As stated by Sulzbach et al. [22], the accuracy of the TiME model is lower than that of data-constrained models for major tidal constituents, but improvements can be seen in certain minor tides, with this being confirmed by the tide gauge analysis in Figure 4, particularly for the MSF constituent.

Additional factors limit the ability of the estimation of minor tides in the EOT model, such as errors resulting from the failure to satisfy the Rayleigh criteria for certain tidal constituents based on the altimetry used. This is somewhat accounted for by combining multiple satellite altimetry missions, however, certain tides are still challenging to estimate, as seen in Figures 3 and 4. Furthermore, as EOT is a purely empirical model that relies on decades of altimetry observations, computational limitations restrict the ability of the model to globally estimate a large number of constituents. This means that the inference of tides from major constituents is still used to help reduce these errors. However, the inference of certain tides is still imperfect compared to direct estimations.

Therefore, EOT may still benefit from the use of the minor tides obtained from the purely hydrodynamic TiME model, which could increase the number of constituents available to provide a more complete estimation of ocean tides. However, care should be taken in developing a technique to merge these two models to optimise the estimation of the ocean tides and to take into account things such as the different spatial resolutions

and gridding techniques of the models. Additionally, the numerical models may have constraints for certain tidal constituents based on their relationships to other tides and, therefore, the combination of these tides with EOT may result in inconsistencies creeping into the tidal corrections. Furthermore, the development and implementation of improved techniques to infer the minor tides from the major tides may also provide better estimations for minor tides in the coastal regions. These avenues for the improvement of minor tide estimations will be the subject of future studies alongside the continued development of the EOT and TiME ocean tide models.

This work additionally serves as a framework to expand into additional regions and to study more complex tidal constituents. As more satellite altimetry missions are launched and the current orbits are being continued, for example, via missions such as Sentinel-6, the number of constituents able to be directly estimated continues to rise. The Reference Ray [30] demonstrated the ability of satellite altimetry to directly estimate third-degree ocean tides and showed the importance of these signals for the prediction of ocean tides. As the coastal altimetry field continues to grow, these smaller tidal constituents become vital in helping to accurately monitor the changes in the global sea level.

Author Contributions: M.G.H.-D., D.D., R.S. and M.T. conceptualised the idea of the research as part of the TIDUS research group within the DFG research unit, NEROGRAV. M.G.H.-D. developed the methodology, performed the analysis and validation, and wrote the paper. D.D. contributed to the interpretation of the results and the formulation of the paper. R.S. and M.T. provided the TiME tide model data and assisted in the interpretation of the results. C.S. provides and maintains the satellite altimetry database and the OpenADB tools that was used in the creation of the EOT20 model and in the sea-level variance analysis. F.S. provided the resources making the study possible and coordinates the activities of the research group at DGFI-TUM. All authors have read and agreed to the published version of the manuscript.

Funding: The authors acknowledge funding by the DFG project TIDUS (grant DE2174/12-1 and grant TH864/15-1) within the DFG research unit NEROGRAV (RU 2736/1). This work used resources of the Deutsches Klimarechenzentrum (DKRZ) granted by its Scientific Steering Committee (WLA) under project ID 499.

Institutional Review Board Statement: Not applicable.

Informed Consent Statement: Not applicable.

Data Availability Statement: The ocean tides from EOT20 are available at: https://doi.org/10.17882/79489 (accessed on 1 July 2021). The satellite altimetry data used in the sea-level variance study can be found at: https://openadb.dgfi.tum.de/ (accessed on 1 July 2021). The tide gauges from the TICON dataset used in the tide gauge analysis, are available at: https://doi.pangaea.de/10.1594/PANGAEA.896587 (accessed on 1 July 2021). The Python code based on estimating the aliasing period, can be found at: https://github.com/hart-davis/alias_periods.git (accessed on 1 July 2021).

Conflicts of Interest: The authors declare no conflict of interest.

References

1. Ablain, M.; Legeais, J.; Prandi, P.; Marcos, M.; Fenoglio-Marc, L.; Dieng, H.; Benveniste, J.; Cazenave, A. Satellite altimetry-based sea level at global and regional scales. *Surv. Geophys.* **2017**, *38*, 7–31. [CrossRef]
2. The Climate Change Initiative Coastal Sea Level Team. Coastal sea level anomalies and associated trends from Jason satellite altimetry over 2002–2018. *Sci. Data* **2020**, *7*, 357. [CrossRef]
3. Passaro, M.; Müller, F.L.; Oelsmann, J.; Rautiainen, L.; Dettmering, D.; Hart-Davis, M.G.; Abulaitijiang, A.; Andersen, O.B.; Høyer, J.L.; Madsen, K.S.; et al. Absolute Baltic Sea Level Trends in the Satellite Altimetry Era: A Revisit. *Front. Mar. Sci.* **2021**, *8*, 546. [CrossRef]
4. Andersen, O.B. Global ocean tides from ERS 1 and TOPEX/POSEIDON altimetry. *J. Geophys. Res. Oceans* **1995**, *100*, 25249–25259. [CrossRef]
5. Shum, C.; Woodworth, P.; Andersen, O.; Egbert, G.D.; Francis, O.; King, C.; Klosko, S.; Le Provost, C.; Li, X.; Molines, J.M.; et al. Accuracy assessment of recent ocean tide models. *J. Geophys. Res. Oceans* **1997**, *102*, 25173–25194. [CrossRef]
6. Savcenko, R.; Bosch, W. *EOT11a-Empirical Ocean Tide Model from Multi-Mission Satellite Altimetry*; DGFI Report No. 89; Deutsches Geodätisches Forschungsinstitut (DGFI): München, Germany, 2012. [CrossRef]

7. Stammer, D.; Ray, R.; Andersen, O.B.; Arbic, B.; Bosch, W.; Carrère, L.; Cheng, Y.; Chinn, D.; Dushaw, B.; Egbert, G.; et al. Accuracy assessment of global barotropic ocean tide models. *Rev. Geophys.* **2014**, *52*, 243–282. [CrossRef]
8. Birol, F.; Léger, F.; Passaro, M.; Cazenave, A.; Niño, F.; Calafat, F.M.; Shaw, A.; Legeais, J.F.; Gouzenes, Y.; Schwatke, C.; et al. The X-TRACK/ALES multi-mission processing system: New advances in altimetry towards the coast. *Adv. Space Res.* **2021**, *67*, 2398–2415. [CrossRef]
9. Piccioni, G.; Dettmering, D.; Passaro, M.; Schwatke, C.; Bosch, W.; Seitz, F. Coastal improvements for tide models: The impact of ALES retracker. *Remote Sens.* **2018**, *10*, 700. [CrossRef]
10. Hart-Davis, M.G.; Piccioni, G.; Dettmering, D.; Schwatke, C.; Passaro, M.; Seitz, F. EOT20: A global ocean tide model from multi-mission satellite altimetry. *Earth Syst. Sci. Data* **2021**, *13*, 3869–3884. [CrossRef]
11. Lyard, F.H.; Allain, D.J.; Cancet, M.; Carrère, L.; Picot, N. FES2014 global ocean tide atlas: Design and performance. *Ocean Sci.* **2021**, *17*, 615–649. [CrossRef]
12. Hart-Davis, M.; Piccioni, G.; Dettmering, D.; Schwatke, C.; Passaro, M.; Seitz, F. EOT20—A Global Empirical Ocean Tide Model from Multi-Mission Satellite Altimetry. SEANOE [Dataset]. 2021. Available online: https://doi.org/10.17882/79489 (accessed on 1 July 2021). [CrossRef]
13. Schrama, E.; Ray, R. A preliminary tidal analysis of TOPEX/POSEIDON altimetry. *J. Geophys. Res. Oceans* **1994**, *99*, 24799–24808. [CrossRef]
14. Foreman, M.G.G.; Henry, R.F. The harmonic analysis of tidal model time series. *Adv. Water Resour.* **1989**, *12*, 109–120. [CrossRef]
15. Egbert, G.D.; Ray, R.D. Tidal prediction. *J. Mar. Res.* **2017**, *75*, 189–237. [CrossRef]
16. Ray, R. On tidal inference in the diurnal band. *J. Atmos. Ocean. Technol.* **2017**, *34*, 437–446. [CrossRef]
17. Petit, G.; Luzum, B. *IERS Conventions (2010)*; Technical Report; Verlag des Bundesamts für Kartographie und Geodäsie: Frankfurt am Main, France 2010.
18. Rieser, D.; Mayer-Gürr, T.; Savcenko, R.; Bosch, W.; Wünsch, J.; Dahle, C.; Flechtner, F. *The Ocean Tide Model EOT11a in Spherical Harmonics Representation*; Technical Note; Institute of Theoretical Geodesy and Satellite Geodesy (ITSG): Graz, Austria, 2012.
19. Munk, W.H.; Cartwright, D.E. Tidal spectroscopy and prediction. *Philos. Trans. R. Soc. Lond. Ser. A Math. Phys. Sci.* **1966**, *259*, 533–581.
20. Karbon, M.; Balidakis, K.; Belda, S.; Nilsson, T.; Hagedoorn, J.; Schuh, H. Long-term evaluation of ocean tidal variation models of polar motion and UT1. In *Geodynamics and Earth Tides Observations from Global to Micro Scale*; Springer: Cham, Switzerland, 2019; pp. 17–35.
21. Piccioni, G.; Dettmering, D.; Schwatke, C.; Passaro, M.; Seitz, F. Design and regional assessment of an empirical tidal model based on FES2014 and coastal altimetry. *Adv. Space Res.* **2021**, *68*, 1013–1022. [CrossRef]
22. Sulzbach, R.; Dobslaw, H.; Thomas, M. High-Resolution Numerical Modeling of Barotropic Global Ocean Tides for Satellite Gravimetry. *J. Geophys. Res. Oceans* **2021**, *126*. [CrossRef]
23. Le Provost, C.; Lyard, F.; Molines, J.M. Improving ocean tide predictions by using additional semidiurnal constituents from spline interpolation in the frequency domain. *Geophys. Res. Lett.* **1991**, *18*, 845–848. [CrossRef]
24. Wang, Y. *Ocean Tide Modeling in the Southern Ocean*; Technical Report; Division of Geodetic Science, Ohio State University: Columbus, OH, USA, 2004.
25. Savcenko, R.; Bosch, W. Residual Tide Analysis in Shallow Water-Contributions of ENVISAT and ERS Altimetry. In Proceedings of the Envisat Symposium, Montreux, Switzerland, 23–27 April 2007.
26. Piccioni, G.; Dettmering, D.; Bosch, W.; Seitz, F. TICON: TIdal CONstants based on GESLA sea-level records from globally located tide gauges. *Geosci. Data J.* **2019**, *6*, 97–104. [CrossRef]
27. Andersen, O.B.; Scharroo, R. Range and geophysical corrections in coastal regions: And implications for mean sea surface determination. In *Coastal Altimetry*; Springer: Berlin/Heidelberg, Germany, 2011; pp. 103–145.
28. Zaron, E.D. Mapping the nonstationary internal tide with satellite altimetry. *J. Geophys. Res. Oceans* **2017**, *122*, 539–554. [CrossRef]
29. Ray, R.D.; Byrne, D.A. Bottom pressure tides along a line in the southeast Atlantic Ocean and comparisons with satellite altimetry. *Ocean Dyn.* **2010**, *60*, 1167–1176. [CrossRef]
30. Ray, R.D. First global observations of third-degree ocean tides. *Sci. Adv.* **2020**, *6*, eabd4744. [CrossRef] [PubMed]

nts along the Dutch coastline.

A.1.3 P-3 Altimetry-derived tide model for improved tide and water level forecasting along the European Continental Shelf

Ocean Dynamics
https://doi.org/10.1007/s10236-023-01560-0

Altimetry-derived tide model for improved tide and water level forecasting along the European continental shelf

Michael G. Hart-Davis[1] · Stendert Laan[2] · Christian Schwatke[1] · Björn Backeberg[2,3] · Denise Dettmering[1] · Firmijn Zijl[2] · Martin Verlaan[2,4] · Marcello Passaro[1] · Florian Seitz[1]

Received: 9 February 2023 / Accepted: 30 May 2023

Abstract
With the continued rise in global mean sea level, operational predictions of tidal height and total water levels have become crucial for accurate estimations and understanding of sea level processes. The Dutch Continental Shelf Model in Delft3D Flexible Mesh (DCSM-FM) is developed at Deltares to operationally estimate the total water levels to help trigger early warning systems to mitigate against these extreme events. In this study, a regional version of the Empirical Ocean Tide model for the Northwest European Continental Sea (EOT-NECS) is developed with the aim to apply better tidal forcing along the boundary of the regional DCSM-FM. EOT-NECS is developed at DGFI-TUM by using 30 years of multi-mission along-track satellite altimetry to derive tidal constituents which are estimated both empirically and semi-empirically. Compared to the global model, EOT20, EOT-NECS showed a reduction in the root-square-sum error for the eight major tidal constituents of 0.68 cm compared to in situ tide gauges. When applying constituents from EOT-NECS at the boundaries of DCSM-FM, an overall improvement of 0.29 cm was seen in the root-mean-square error of tidal height estimations made by DCSM-FM, with some regions exceeding a 1 cm improvement. Furthermore, of the fourteen constituents tested, eleven showed a reduction of RMS when included at the boundary of DCSM-FM from EOT-NECS. The results demonstrate the importance of using the appropriate tide model(s) as boundary forcings, and in this study, the use of EOT-NECS has a positive impact on the total water level estimations made in the northwest European continental seas.

Keywords Ocean tides · Numerical modelling · Sea level · Satellite altimetry · EOT

1 Introduction

The ocean is influenced by a variety of physical processes which create complex circulation structures and variable sea surface patterns. One of these processes is the motion caused by the gravitational interaction between the Earth, Sun and Moon called ocean tides. Ocean tides are a significant contributor to the circulation and water levels of the global ocean. In the coastal regions, events that cause episodic rises in the sea level, such as storm surges, can be further exacerbated when coinciding with high oceanic tides and can therefore increase the likelihood of coastal flooding (Muis et al. 2016). For this reason, alongside having high importance for geodetic and altimetric applications, tides should be carefully considered to improve our understanding of the ocean surface and the implications of short- and long-term sea level rise events (Arns et al. 2017; Intergovernmental Panel on Climate Change 2022).

The theory of ocean tides is well-known due to the relative simplicity and predictability of its forcing (Egbert and Ray 2017). The development of the harmonic method (Darwin 1891) allowed for the decomposition of ocean tides into a finite number of harmonic constants or constituents which can be estimated and combined to provide predictions of the full tidal signal (Pugh 1987; Cartwright 1999). In practice, models of ocean tides do not provide full estimations of the hundreds of tidal constants due to the computational effort as

Responsible Editor: Alejandro Orfila

Michael G. Hart-Davis
michael.hart-davis@tum.de

[1] Deutsches Geodätisches Forschungsinstitut, Technische Universität München (DGFI-TUM), Munich, Germany

[2] Deltares, Delft, Netherlands

[3] Nansen Environmental and Remote Sensing Center, Bergen, Norway

[4] Delft Institute of Applied Mathematics, TU Delft, Delft, Netherlands

Published online: 22 July 2023

well as the complexity of modelling these constituents. However, the majority of the ocean tide signal can be derived, in most regions, from a small number of these constants termed the major tidal constituents. A study by Egbert and Ray (2017) demonstrates that 99% of the total tidal variance can be captured by fourteen harmonic constants and 99.99% of the variance by eighty constants. This demonstrates the importance of accurately estimating these major tidal constituents to reduce the overall error in ocean tide prediction. However, accounting for the additional smaller constituents, either through direct estimations or inferences using linear admittance, remains crucial for the full tidal estimations (Hart-Davis et al. 2021b).

Although tides have been studied and observed for hundreds of years, advances in our understanding are continuing to take place (Woodworth et al. 2021). This is largely due to the availability of satellite altimetry which allows for a larger spatial observation of the global sea surface than what can be provided by in situ measurements obtained, for example, from tide gauges. The TOPEX/Poseidon (TP) and Jason (JA) series of satellite altimeters have provided a consistent sampling on a tide-favourable orbit for 30 years, which has allowed for ocean tides in the open ocean to be well studied during this period (for example, Provost et al. 1995; Andersen 1995; Egbert and Ray 2003; Savcenko and Bosch 2012; Hart-Davis et al. 2021a). Additionally, data from the Envisat-ERS-Saral altimeters have provided a large temporal dataset on a constant orbit that is different to that of the TP-JA orbit. When these data are combined and used in empirical models, there has been an overall improvement in the tidal estimations (Hart-Davis et al. 2021a).

Recent developments in tidal modelling have continued to improve our understanding of global ocean tides (Lyard et al. 2021). Although the estimation of open ocean tides is relatively reliable, largely thanks to the previously mentioned availability of satellite altimetry, weaknesses continue to remain in the coastal and shelf regions (Stammer et al. 2014). Land contamination of satellite altimetry data nearer to the coast and poorly resolved bathymetry products are key culprits to these weaknesses, not to mention the complexity of tides in the coastal regions. Satellite altimetry-derived empirical ocean tide models benefit from developments made in the field of coastal altimetry, with clear evidence being shown in two recent publications (Cheng and Andersen 2017; Hart-Davis et al. 2021a), with the latter demonstrating the importance of the retrieval of data closer to the coast, made possible by the use of the ALES retracker (Passaro et al. 2014). As these tide models continue to improve, they become more valuable as corrections within coastal altimetry applications, but these improvements serve several different applications. One such application is the use of these tide models as boundary forcings for operational ocean models, which rely on tide models to account for the tidal influence which is crucial in terms of improving the model accuracy.

One such operational model is a series of hydrodynamic models for the Northwest European Shelf developed for the Dutch Directorate-General for Public Works and Water Management (Rijkswaterstaat) (Goede 2020). The latest model, the Dutch Continental Shelf Model in Delft3D Flexible Mesh (DCSM-FM), has been developed using the state-of-the-art unstructured hydrodynamic modelling software Delft3D Flexible Mesh Suite (Zijl and Groenenboom 2019; Kernkamp et al. 2011). Previous generation models were specifically aimed at operational forecasting of water levels under daily storm surge conditions and were schematized as depth-averaged 2D tide-surge models (Zijl et al. 2013, 2015). This latest generation model has been proven to be suitable for a wider range of applications such as water quality and ecology studies, oil spill modelling, search and rescue and providing three-dimensional boundary conditions of salinity and temperature for detailed models. The high value of water level forecasting within DCSM-FM underlines the importance of providing appropriate tidal boundary forcings, which play a significant role in determining the accuracy of the model.

The aims of this manuscript are two-fold: the first is to develop a regional high-resolution version of an empirical ocean tide model that improves on the global configuration with respect to in situ measurements and provides additional tidal constituents previously not included. The second aim is to apply this improved regional tide model to the hydrodynamic model DCSM-FM at the boundaries to improve the model's estimation of the tidal height and total water levels with respect to in situ measurements along the northwest European continental shelf. The manuscript is structured as follows: a detailed description of the developed regional Empirical Ocean Tide for the North European Continental Shelf (EOT-NECS) model, as well as the presentation of an updated tide gauge dataset (TICON-3), is presented in Section 2. The EOT-NECS model is then validated against these tide gauges and, where appropriate, is contrasted to both EOT20 and the FES2014 tide models in Section 3. In Section 4, DCSM-FM is described before several experiments are presented and evaluated that aim at improving the models' tidal height and total water level estimations. Finally, a conclusion is made based on both of the aims mentioned above, and potential further developments which would benefit DCSM-FM are discussed.

2 Data and methodology

2.1 EOT-NECS

The EOT20 model provided a valuable global ocean tide product that has proved to be useful for the field of satellite

altimetry, particularly in its use in the tidal correction (Hart-Davis et al. 2021a). Through the continued use of the model as well as user feedback, several avenues were identified that would benefit the accuracy of the model. The most obvious initial addition to the Empirical Ocean Tide (EOT) model configuration is the inclusion of several additional satellite altimetry missions. These altimeter datasets are the Sentinel-3A (S3A), Sentinel-3B (S3B), Saral (SA), Saral drifting phase (SDP) and Sentinel-6A (S6A) missions, the latter being the latest extension of the long-standing TP-JA orbit (an overview of the missions used and their respective time-period is provided in Fig. 1). There is additional value in the inclusion of the SA altimeter which continues the orbit of the ERS-Envisat (ER-EN) missions also previously included in EOT20; however, due to the sun-synchronous orbit of these missions, also for S3A and S3B, these orbits cannot be used alone to derive a full estimation of the ocean tides.

The additional altimetry missions provide new orbits into the model (Fig. 2), which are appropriate for optimising the weighted sea-level anomaly (SLA) estimations for each node of the EOT configuration. Using these data, two EOT models are created: (1) a purely empirical model made out of only satellite altimetry data and uses no reference tide model to correct the SLA data and (2) a residual tide model based on using the FES2014 as a tidal correction for the SLA data. These two models follow the same methodology described in Hart-Davis et al. (2021a). The SLA data were obtained from along-track altimetry by applying the altimetry corrections listed in Table 2 of Hart-Davis et al. (2021a). Additionally, the model configuration was refined to more accurately deal with the instrument error from the altimetry observations and improve the outlier detection to allow for more reliable input data used in the tidal analysis. These two refinements are important points to account for the difficulties of sea level retrieval from satellite altimetry (Cipollini et al. 2017). These were identified as points of improvement in EOT20 since it is clear that when not appropriately accounted for, outliers and errors in SLA data will negatively influence the amplitude and phase determinations of tidal constituents. As described in Savcenko and Bosch (2012) and Hart-Davis et al. (2021a), a variance component estimation (VCE) is also conducted within EOT to allow for the combination of different missions by weighting each mission based on their variances calculated for each node using an iterative process. In addition, all the missions used were cross-calibrated and adjusted to each other by applying radial corrections (Bosch et al. 2014).

Once completed, the tidal analysis is conducted on the resultant SLA observations to estimate the harmonic constants of individual constituents of interest. Due to the resultant tidal estimation being the sum of the ocean and load tide contributions, known as the elastic tide, a final step to separate the ocean and load tide contributions is done following the technique presented in Cartwright and Ray (1991); Savcenko and Bosch (2012); Hart-Davis et al. (2021a), with only the ocean tide component being of interest for the rest of this study.

The models are gridded onto a 1/16 degree spatial resolution, which is an increased spatial resolution relative to the global EOT20 model (1/8 degree). A total of 42 constituents for both model versions are estimated. These constituents were chosen based on the requirements of the work presented later in this publication; however, these tides were also within the capabilities of the altimetry data used to make the tidal estimations. The two model versions allowed all constituents available in the reference tide model, FES2014, to be taken and additional constituents not contained within the FES2014 atlas to be estimated as purely empirical estimations. This combined residual and empirical set of constituents resulted in the Empirical Ocean Tide model for the Northwest European Continental Sea (EOT-NECS). The list of constituents used is the same as those presented in Section 4.

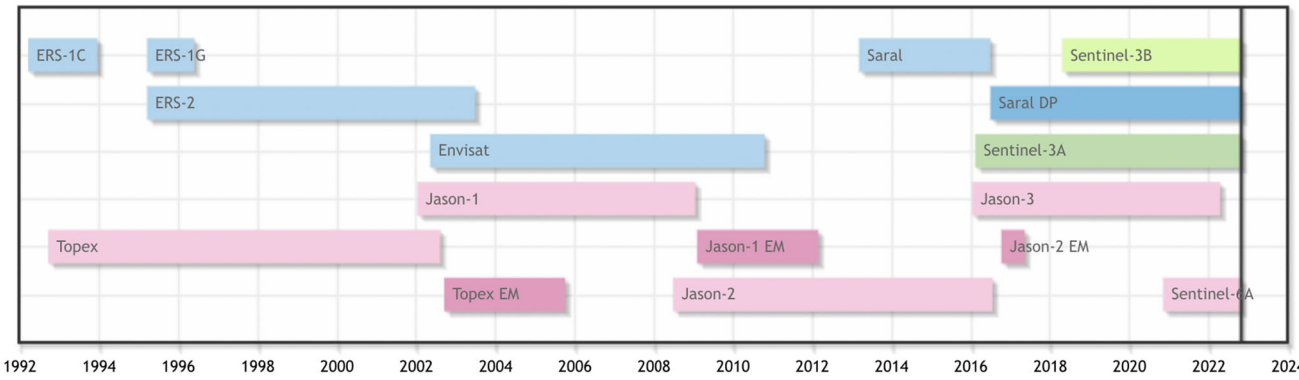

Fig. 1 The satellite altimetry data used in EOT-NECS, taken from OpenADB (https://openadb.dgfi.tum.de/en/). The missions presented with the same colours are those that follow the same orbit. Note for the final version of EOT-NECS data up until 2022-10-31 is used, indicated by the black vertical black line within the plot

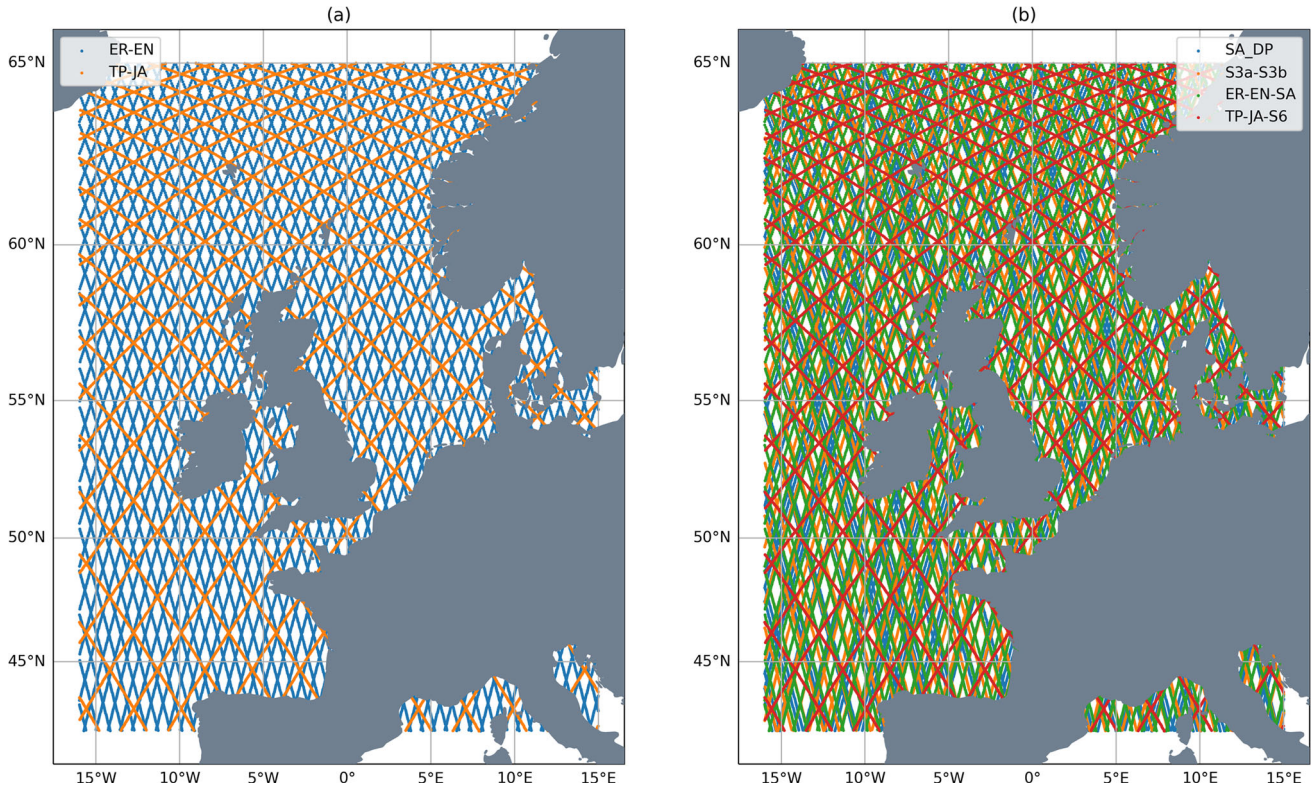

Fig. 2 The spatial coverage of the altimetry data used in the (**a**) EOT20 and (**b**) EOT-NECS tide models

Limitations can be placed on the estimation of certain tides if the orbit of the satellites are not able to properly resolve certain tidal constituents. The ER-EN-SA and the S3A/S3B orbit missions, for example, are not able to make estimations of the solar tides (S1, S2, etc) based on their sun-synchronous orbits. The aliasing period, the length of data required to estimate individual constituents based on the respective orbits of the missions, is also important to consider when including altimetry missions which have been providing data for a relatively short period. All 42 constituents can be safely estimated following the Rayleigh criteria following the technique presented in Smith (1999) with the resultant calculations shown in Fig. 11 in the Appendix.

2.2 Tide gauge validation dataset

Tide gauges provide valuable data for the validation of ocean tide models. Using the GESLA-2 tide gauge dataset, a dataset of TIdal CONstants (TICON) was produced in Piccioni et al. (2019). In late 2021, an update to the GESLA dataset called GESLA-3 was produced which quadrupled the number of globally available tide gauges (Haigh et al. 2022). Based on this, an update to TICON, termed TICON-3, was done, which increased the number of tide gauges and maintained the same 40 constituents included in the previous version of the dataset (Hart-Davis et al. 2022a). A total of 3471 tide gauges are now available within the TICON-3 dataset, with additional information being included from the provided GESLA-3 files about whether the tide gauge is a coastal, lake or river tide gauge. Figure 3 demonstrates the global distribution of TICON-3 and the subset in the north European shelf used to validate the developments of EOT-NECS model.

Although the GESLA-3 updated dataset includes 5119 tide gauges, several of these have a relatively short time series (less than 1 year) which does not meet the requirements of data required in the TICON processing to have at least 1 year of continuous data. Furthermore, there are several duplicated tide gauges which is a result of obtaining data from multiple data sources. In TICON-3, these gauges remain within the dataset to allow users themselves to distinguish which data sources they would like to use. In this study, duplicated tide gauges are removed from the analysis to reduce impacts on the estimated mean statistics. Additionally, for some of the minor tides estimated, not all tide gauges may be appropriate based on the length of available time series. Again, these data remain within the TICON-3 dataset; however, care should be taken when interpreting the resultant estimations for these minor tides. In this study, when validating the minor tidal constituents, only gauges with at least 5 years' worth of data are used to account for potential errors that may occur in shorter time series.

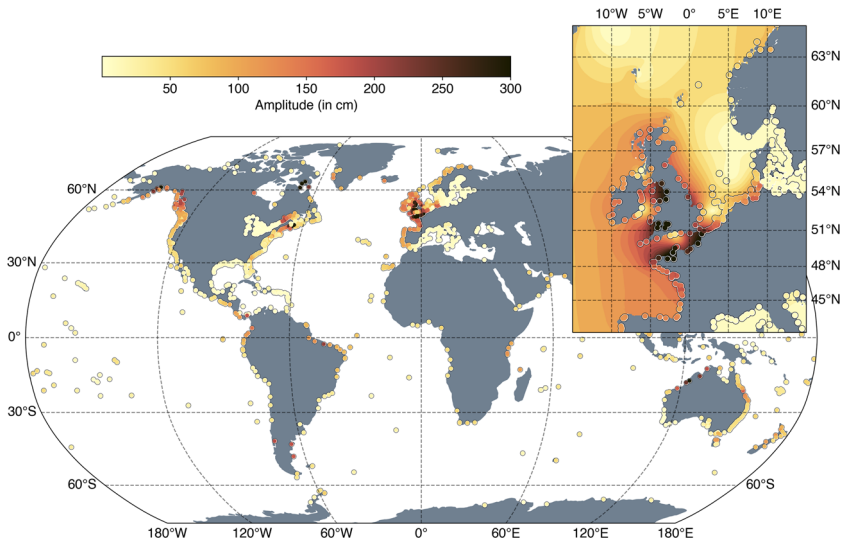

Fig. 3 The global distribution of tide gauges within the TICON-3 dataset, with a subplot shown to demonstrate the tide gauges used to validate EOT-NECS. The coloured dots represent the M2 amplitudes estimated at the individual tide gauges, while the background plot shows the M2 amplitude from EOT-NECS

3 Validation of EOT-NECS

The TICON-3 dataset, which contains 389 tide gauges in the domain of interest (Fig. 3), is used to validate the results of the developed EOT-NECS compared to both FES2014 and EOT20 (Fig. 4). Here, the root-mean-square error (RMS) for constituents and the root-square-sum error (RSS) for the eight major tides are compared, following the techniques presented in Stammer et al. (2014) which uses the modelled amplitude (A_m) and phase (p_m) and the observed amplitude (A_o) and phase (p_o) for each constituent to determine the RMS as follows:

$$RMS = \sqrt{(A_o.\cos(p_o) - A_m.\cos(p_m))^2 + (A_o.\sin(p_o) - A_m.\sin(p_m))^2}, \quad (1)$$

and then the RSS is estimated for each tide gauge based on the RMS of the eight major tides.

$$RSS = \sqrt{\sum RMS_{[M_2,S_2,K_1,K_2,N_2,P_1,O_1,Q_1]}}. \quad (2)$$

For each tide gauge, the RSS and RMS were estimated and are presented in both Figs. 4 and 5. For each of the major tides, there is an overall mean improvement in EOT-NECS compared to EOT20 with an average RSS improvement being 0.678 cm, with this being seen in the majority of tide gauges in the domain. This is somewhat expected based on the extension of the TP-JA orbit with the incorporation of additional data from Jason-3 as well as the inclusion of the recent Sentinel-6A. This extension means that the TP-JA orbit is sampled for 30 years allowing for a reliable estimation of the major tidal constituents and the additional estimation of some of the minor tidal constituents. Based on these results, the extension of the previously used altimetry datasets, the incorporation of new altimetry data and the improved spatial resolution of the model benefit the resultant tidal estimations.

In Fig. 5, the RMS of additional constituents is presented. Tides available in EOT20 continue to improve in the EOT-NECS model except for the SA tide, which showed a slightly degraded RMS. EOT-NECS improves the estimates for all constituents compared to FES2014 besides the NU2 tide, which shows a higher mean RMS. For the constituents where FES2014 does not contain data, these constituents in EOT-NECS were derived from purely empirical estimates and do not benefit from the use of the FES2014 reference model in the coastal region. Several of these constituents, which are minor tidal constituents having small tidal signals compared to the major tides and a small contribution to the overall tidal signal, have relatively high RMS values compared to tide gauges. These tides are difficult to estimate directly from satellite altimetry data based on their small signals compared to the noise of altimetry data retrieval, particularly in the coastal regions. However, these tides are not available in empirical estimations and were sources of errors in DCSM-FM, making them prime candidates for experimental testing later on in this study.

Of particular interest is the inclusion of the MA2 and MB2 constituents which can reach relatively large amplitudes in certain regions both globally and within the region of interest (Ray 2022). To the best of our knowledge, these tides are not available in any global empirical ocean tidal atlases that could be used in this region, at least none that are publicly available, which motivated their incorporation into the EOT-NECS developments and, eventually, within DCSM-FM. The tide gauges in this region indicate a mean tidal amplitude of 1.61 cm and 1.15 cm for the MA2 and MB2 constituents, respectively, reaching up to 10.30 cm and 8.69 cm, respectively. Considering the relatively small amplitudes, the RMS

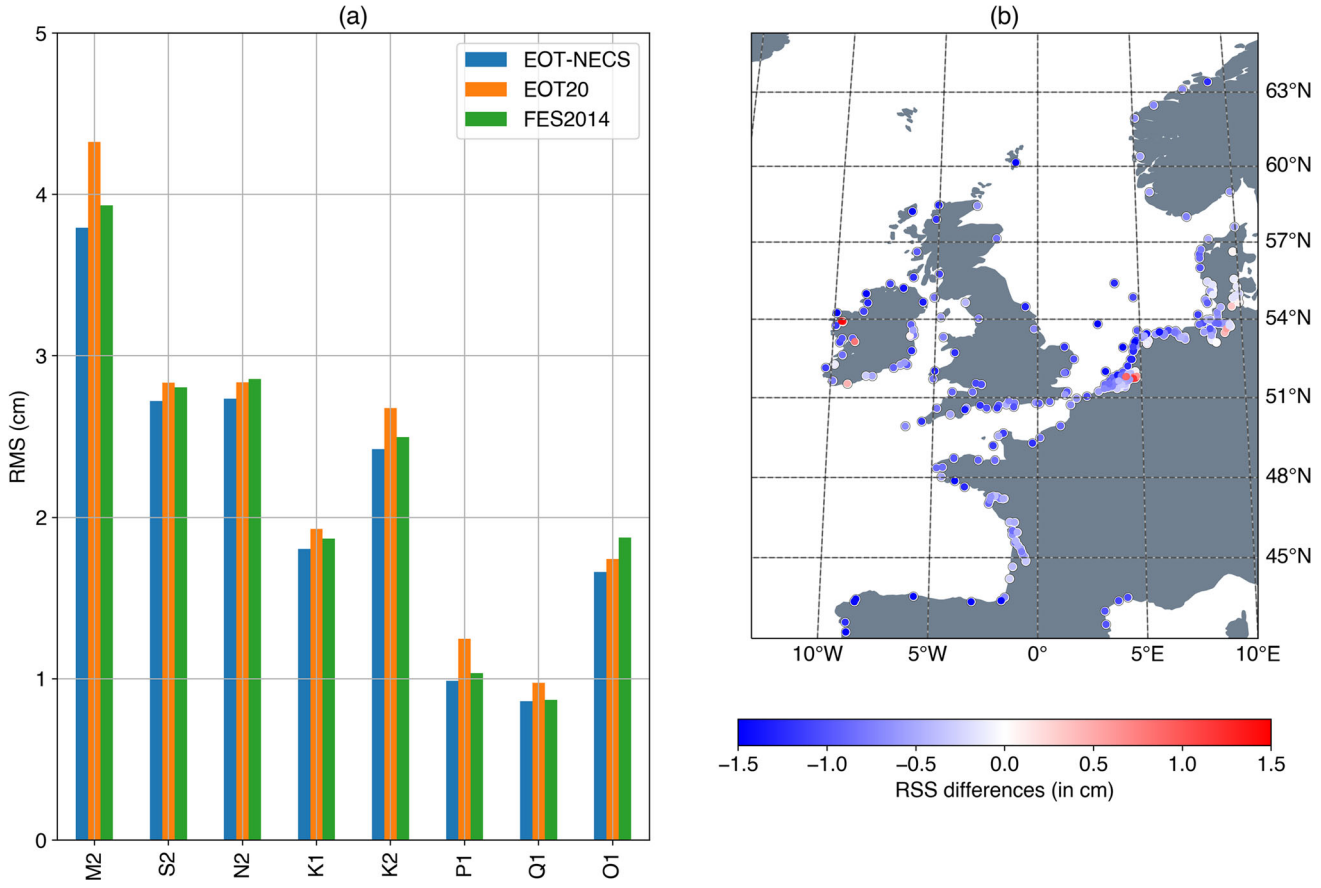

Fig. 4 (**a**) RMS against 389 tide gauges in the North-West European Coastline of the eight major tidal constituents. (**b**) RSS difference between EOT20 compared to EOT-NECS. Blue indicates a lower RSS for EOT-NECS, and red indicates a higher RSS

differences of EOT-NECS are relatively high for these two constituents, exceeding 1 cm on average. However, despite this, we expect the open ocean estimation of these tides to be better relative to the coastal region, and therefore, these two tides are still appropriate for testing as a tidal boundary forcing.

In the production of EOT20, a first look at uncertainties was conducted by estimating the variance factor of the model. This so-called variance of unit weight (see Bähr et al. 2007, for example) is determined during the VCE by evaluating the weighted sum of squares of the residuals for each node of the model based on the input altimetry datasets. Based on the results of the VCE, a variance factor can be determined for each node of the model and can be complemented with the tide gauge analysis to evaluate whether the tidal estimations are improving. Although this quantity does not represent the full model uncertainties, due to the absence of uncertainty metrics in FES2014, it provides valuable insights especially to assess performance differences between different model versions when combined with the full in situ tide gauge validation.

It is expected that if the variance factor of EOT-NECS decreases with respect to EOT20, the estimations of EOT-NECS are improved. To test this, the percentage variance factor difference is estimated following $var_{DIFF} = ((var_{EOT20} - var_{EOT-NECS})/var_{EOT20}).100$, with the results presented in Fig. 6. Throughout the model domain, there is a reduction in uncertainties in the updated model configuration. Larger variance reductions are seen in regions of large tidal ranges, particularly in the Bay of Biscay, the English Channel and the Irish Sea. The variance differences further cement the idea that the changes made to the EOT model have an overall positive impact on the estimation of tides.

4 Using EOT-NECS as boundary forcing of DCSM-FM

4.1 Description of DCSM-FM

The Dutch Continental Shelf Model in Delft3D Flexible Mesh (DCSM-FM) covers the Northwest European Continental Shelf from 15°W to 13°E and 43°N to 64°N. The model has been developed in the Delft3D Flexible Mesh Suite (Kernkamp et al. 2011), which allows for an unstructured grid

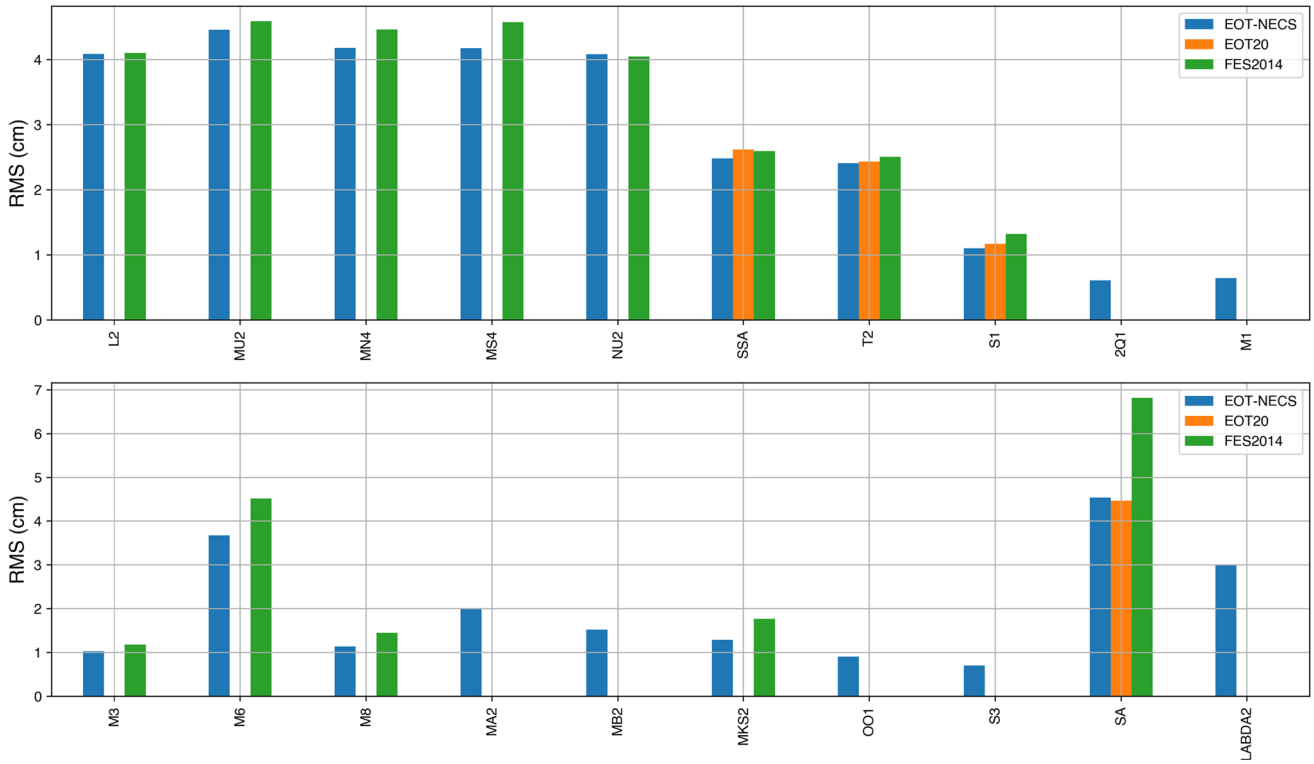

Fig. 5 RMS validation against TICON-3 for additional tidal constituents available from EOT-NECS. The RMS differences, where applicable, are compared to available constituents from EOT20 and FES2014

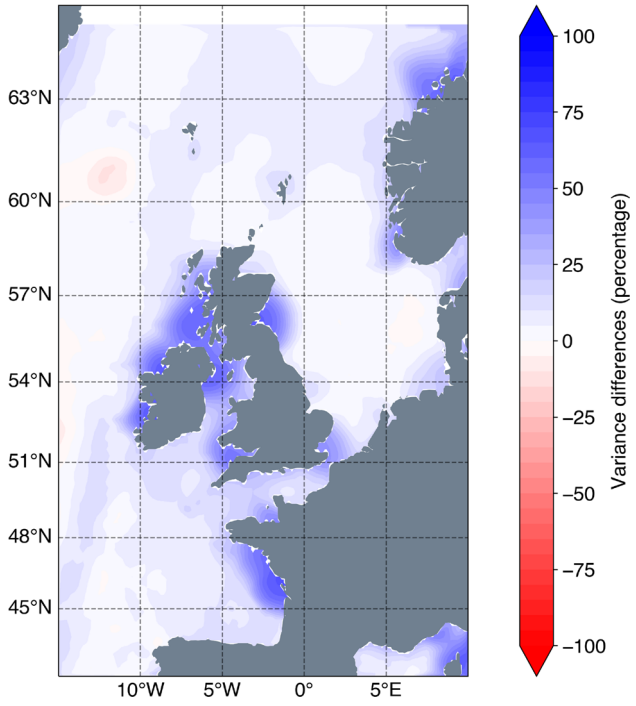

Fig. 6 The percentage variance factor change of EOT-NECS with respect to EOT20 as determined from the VCE described in (Savcenko and Bosch, 2012; Hart-Davis et al., 2021a). A reduction in variance is shown as blue, and an increase is red

approach. The grid of the horizontal schematization has an increasing resolution from 4 nm (nautical miles)/7.408 km in deep oceanic waters to 0.5 nm/0.926 km in shallow coastal waters and the southern North Sea. Refinements with a factor of 2 by 2 are placed at roughly the 800 m, 200 m and 50 m isobaths which ensures the grid cell size scales with the square root of the depth to limit variations in the wave Courant number.

The model bathymetry is derived from the bathymetric data of EMODnet Bathymetry Consortium (https://www.emodnet-bathymetry.eu/EMODnet Bathymetry Consortium 2020) and the Dutch Directorate-General for Public Works and Water Management (Rijkswaterstaat). Depths are written to the grid nodes based on the average value of the data within a surrounding area of the size of the corresponding grid cells. Other geometric information, such as dry areas, thin dams and weirs, are based on the World Vector Shoreline (https://shoreline.noaa.gov/) and data by Rijkswaterstaat. For the bottom roughness, a spatially varying Manning roughness coefficient is used. The Manning roughness coefficient varies from 0.012 to 0.050 $s/m^{1/3}$. This value is calibrated for multiple areas within the model domain to obtain an optimal water level representation. The method used is explained in Zijl et al. (2013). For this calibration, simulations with the 2D depth-averaged model were conducted for 2017 to converge

the model results to water level observations at more than 200 tide gauges within the model domain (Zijl et al. 2013).

The spatial forcing of the air-sea momentum flux in the model is taken from the ERA5 reanalysis dataset by ECMWF (Hersbach et al. 2017). For consistency with the atmospheric boundary layer in ERA5, the same temporally and spatially varying Charnock coefficient is used for the air-sea momentum exchange. In the 3D model, additional spatial forcing for the heat flux is included from ERA5. To account for the radiative heat fluxes, the surface net solar (short-wave) radiation and the surface downward long-wave radiation have been imposed, while the surface upward long-wave radiation is computed based on the modelled sea surface temperature. In addition, freshwater discharges at 847 locations are included as monthly mean discharges based on climatology from E-HYPE (Hackett et al. 2013). At the open boundaries, water levels are forced as a combination of different components, with the amplitude and phases of tidal constituents being included (see Fig. 7 for an illustration of the S1 tide). Currently, these tides have been taken from a combination of the DCSMv6, GTSMv4.1 and FES2014 models (Table 1). Based on the information provide by the models, a tidal water level signal is constructed within Delft3D Flexible Mesh as a combination of simple harmonic constituent motions. To determine this signal, the nodal amplitude factor and astronomical argument are automatically re-calculated every 6 h. In addition, tide-generating forces within the model domain are included. These forces are based on the gravitational forces of the terrestrial system on the water mass. Furthermore, an estimation of offshore surge levels is included by the addition of an inverse barometer correction (IBC) based on the local atmospheric pressure. Lastly, a daily mean sea surface height is forced to include the density-driven effects or the mean dynamic topography (MDT) at the boundaries taken

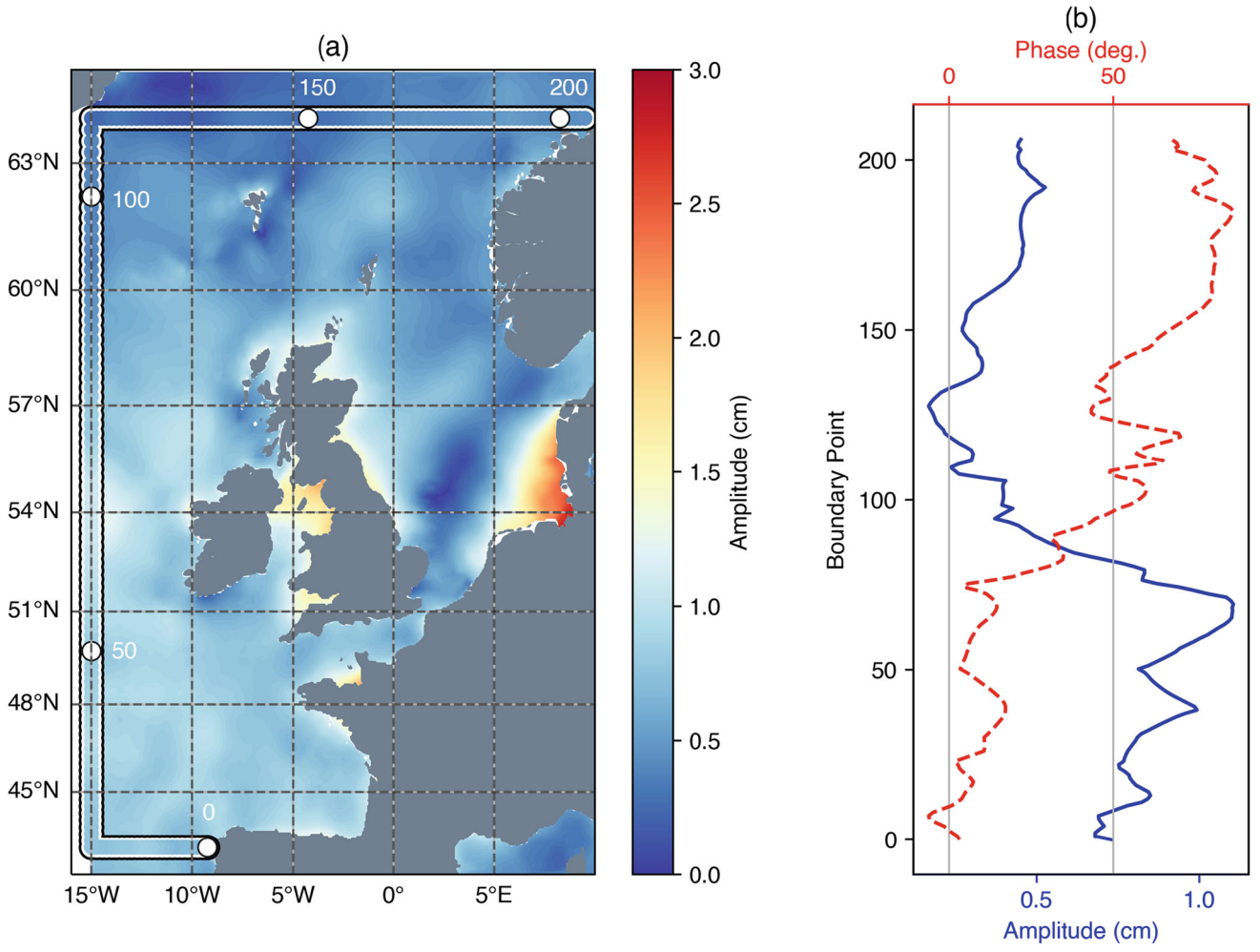

Fig. 7 The position of the lateral boundaries of the DCSM-FM model where the model is tidally forced. In this figure, the background is the EOT-NECS S1 tidal amplitude with the markers indicating the position of the boundary and the associated amplitude. (**b**) demonstrates the amplitude (cm) and phase (degrees) along the boundary of EOT-NECS. The white dotes in (**a**) correspond to the the respective boundary points which are to be used as reference for (**b**)

Table 1 The list of constituents and their associated angular frequency [°/h] used on the boundaries to force DCSM-FM, with original sources taken either from DCSMv6, GTSMv4.1 or FES2014. The column 'Experiment' describes the respective experiment where these tides are replaced with those from EOT-NECS. The $^{+}$ is used for the SA tide, which for the 2D model version uses DCSMv6 while the 3D model uses FES2014

Tide	Angular frequency	Source	Experiment
SA	0.041069	DCSMv6 $^{+}$	*3D-DCSM*
SSA	0.082137	FES2014	DCSM-D
MM	0.544375	FES2014	
MSF	1.015896	FES2014	
MF	1.098033	FES2014	
MFM	1.642408	FES2014	
MSQM	2.113929	FES2014	
2Q1	12.85429	GTSMv4.1	DCSM-D
SIGMA1	12.92714	GTSMv4.1	
Q1	13.39866	FES2014	
RHO1	13.471515	N/A	DCSM-C
O1	13.94304	FES2014	
NO1	14.49669	GTSMv4.1	
PI1	14.91786	GTSMv4.1	
P1	14.95893	FES2014	
S1	15	FES2014	DCSM-B
K1	15.04107	GTSMv4.1	
LABDA2	15.51259	FES2014	DCSM-D
J1	15.58544	FES2014	
EPSILON2	27.42383	FES2014	
2N2	27.89535	FES2014	
MU2	27.96821	FES2014	DCSM-D
N2	28.43973	GTSMv4.1	
NU2	28.51258	FES2014	DCSM-D
MA2	28.943036	N/A	DCSM-C
M2	28.9841	GTSMv4.1	
MB2	29.025173	N/A	DCSM-C
MKS2	29.06624	FES2014	DCSM-D
L2	29.52848	FES2014	DCSM-D
T2	29.95893	FES2014	DCSM-D
S2	30	FES2014	
R2	30.04107	FES2014	
K2	30.08214	GTSMv4.1	
ETA2	30.62651	GTSMv4.1	
M3	43.47616	GTSMv4.1	
N4	56.87946	FES2014	
MN4	57.42383	GTSMv4.1	
M4	57.96821	FES2014	
MS4	58.9841	GTSMv4.1	
S4	60	FES2014	
M6	86.95231	FES2014	DCSM-D
M8	115.9364	FES2014	DCSM-D

from the reanalysis dataset with the GLORYS model (https://doi.org/10.48670/moi-00021) as provided by the Copernicus Marine Environment Monitoring Service (CMEMS). Also, three-dimensional daily mean salinity, temperature and advection velocity data from the same source are forced at the open boundaries. In the 2D depth-averaged model, these last three forcings are not directly forced but indirectly included by spatially forcing the difference between the multiyear mean water level field computed by a 2D and 3D version of this model.

4.2 The impact of EOT-NECS on the 2D DCSM-FM

To evaluate the importance of including certain individual tidal constituents at the boundary forcings of DCSM-FM, several versions of the 2D configuration were run. These experiments assess the impacts of adding individual or groups of constituents on the overall accuracy of the model. Each of the 2D model simulations was run for a total of 5 years from 1st January 2013 to 1st January 2018, with the resultant estimated individual constituents and the total tidal heights and total water levels being the subject of evaluation within this study. The selection of which constituents to include in the experiments was based on the previous DCSM-FM versions which identified these constituents as being highly erroneous or constituents that were not previously available from other model estimations. Three model simulations are compared to a reference simulation of DCSM-FM (DCSM-A), which contains the constituents listed in Table 1, except for the MA2, MB2 and RHO1 constituents which were previously not forced at the boundary. The original 'Source' of constituents is described within Table 1.

The experiments are as follows: (A) being the reference run; (B) the S1 constituent from EOT-NECS is used; (C) the previously not included MA2, MB2 and RHO1 constituents are added from the EOT-NECS model; and (D) constituents that were previously available from other tide models are replaced by the EOT-NECS model constituents based on their relative accuracy compared to in situ tide gauge valuations (a breakdown of the constituents is given in the 'Experiment' column of Table 1). The experiments are designed to build on the previous experiment, as constituents continue to be used in the following experiments, i.e. DCSM-C also uses the S1 tide from EOT-NECS used in DCSM-B, and DCSM-D uses those from the DCSM-C experiment.

The first experiment was to test the impact of the S1 tidal constituent from the EOT-NECS model compared to using the FES2014 S1 tide on the accuracy of the model relative to tide gauges (Fig. 8A). This model version is termed DCSM-B. At the boundaries, the S1 tidal constituent showed relatively large differences between EOT20 and FES2014 and, within the reference simulation of DCSM-A, showed

high RMS values for both amplitude and phase compared to in situ tide gauges. Along the boundary of DCSM-FM, the mean difference between the amplitude and phase of EOT20 and FES2014 is 0.25 cm and 5.31° respectively. When including the S1 tide from EOT-NECS, the predicted S1 improves with respect to tide gauges (Fig. 8I). This improvement is particularly strong along the Dutch coastline, with the RMS reducing by 3.16 mm relative to the tide gauges in this region, with the rest of the domain having a reduction of 1.52 mm. Considering that the S1 tidal signals at these tide gauges (estimated following Stammer et al. 2014) are 7.19 mm, this is a median improvement of 28.10% and 43.95% overall and along the Dutch coastline, respectively.

The replacement of the S1 tide within DCSM-B does not have a major influence on other tides, no constituent changes by more than 1%. The RSS was estimated from all the tidal constituents that were forced at the boundary as seen in Table 1, except for the MA2, MB2 and RHO1 constituents which were previously not used to force DCSM-A. The mean RSS reduction relative to DCSM-A of the MA2, MB2 and RHO1 constituents (Fig. 8E) was 1.91 mm. More importantly, when assessing the influence that the S1 tide has on the tidal and water height levels estimated by DCSM-B, a mean RMS reduction of 2.21 mm and 1.73 mm was seen, respectively. This reduction in RMS in the DCSM-B tidal and water level estimations is consistent throughout the entire domain of DCSM-FM.

Based on being identified as highly erroneous constituents within the DCSM-A simulation results, the second experiment (DCSM-C) involved three additional tides from EOT-NECS which were previously not included in the boundary forcing of DCSM-FM: MA2, MB2 and RHO1. It is important to emphasise that these constituents have been added to the constituents used in the DCSM-B experiment, i.e. S1

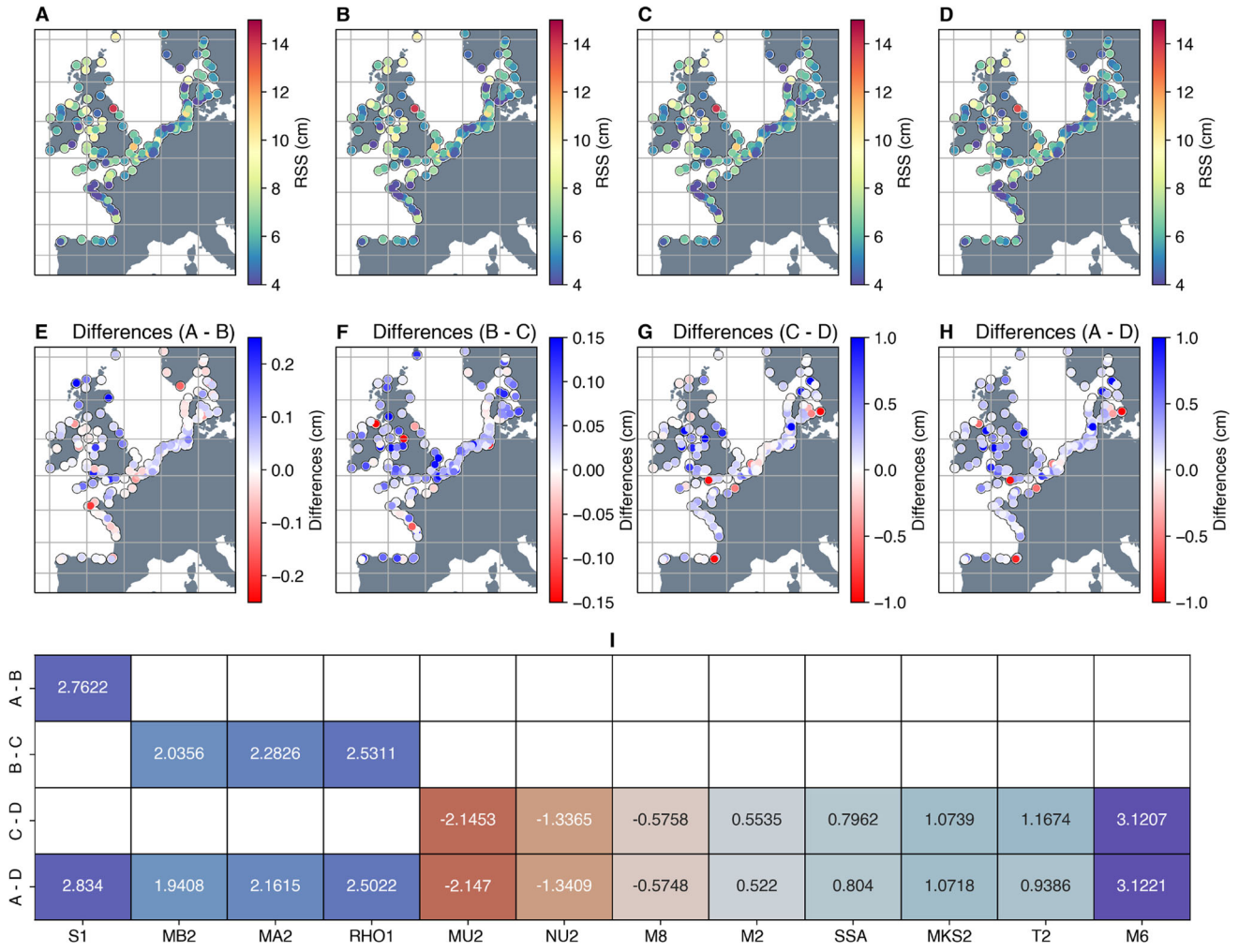

Fig. 8 The RSS of all the constituents tested in each version of DCSM-FM. **A** to **D** represent the different DCSM-FM experiments, while **E** to **H** describe the differences between the versions. **I** presents a table of the RMS differences (in mm) between the different experiments of individual constituents, with only constituents with an absolute RMS difference of more than 0.5 mm shown

from EOT-NECS is also used, and therefore, results will be contrasted to the results of DCSM-B and not DCSM-A. In DCSM-A, these tides demonstrated high RMS errors for these constituents of 5.80 cm and 1.61 cm respectively while RHO1 has an RMS error of 0.31 cm.

In this region, the maximum tidal signal estimated by EOT-NECS for the MA2, MB2 and RHO1 tides is 1.52 cm, 1.85 cm and 0.86 cm, while the mean tidal signal is 0.23 cm, 0.24 cm and 0.10 cm. In DCSM-C, all three of these tides show an improvement in their estimation with respect to DCSM-B (Fig. 8I). This improvement is consistent throughout the entire domain, with the Irish Sea and the Dutch-German coastlines being the regions with the greatest improvement for all three tides. When considering the tidal signals of these tides, all exceed a 20% improvement, with RHO1 improving by 52%. These results highlight the benefit of incorporating these tides from EOT-NECS at the boundary of DCSM-FM.

When estimating the RSS from all the constituents, DCSM-C has a mean reduction of 0.41 mm relative to DCSM-B, with improvements seen throughout the domain. The estimated total tidal and water height had a reduced RMS in DCSM-C of 0.24 mm and 0.21 mm, respectively. The magnitude of the reductions varies between regions, with the Bay of Biscay and Irish Sea showing a 0.60 mm and 0.39 mm reduction in tidal height RMS and a 0.63 mm and 0.33 mm reduction in total water level RMS, respectively. For the Skagerrak Strait, a negligible increase of 0.03 mm in RMS for both tidal height and total water levels.

The final experiment, DCSM-D, was to switch out some constituents already within DCSM-A with some now available from EOT-NECS. This was decided based on their performance with respect to tide gauges in Fig. 5, their ability to be reliably estimated from satellite altimetry (Fig. 11) as well as being tides where DCSM-A contained a relatively large errors. The chosen ten constituents were, again, added to those from the DCSM-C experiment. Unlike the previous experiments, which all resulted in positive impacts for each of the tides tested, for some tidal constituents, DCSM-D demonstrated a degradation relative to DCSM-C. The biggest two negative impacts were the MU2 and NU2, whose mean RMS values increased (Fig. 8I) consistently throughout the domain. In Hart-Davis et al. (2021b), these two tides were highlighted as tides that were not suitable to be directly estimated from along-track satellite altimetry within the EOT configuration for certain regions. Instead, it is recommended to obtain these tides from linear admittance or from a numerical model. In this study, they were included to provide a different test to those presented in Hart-Davis et al. (2021b). However, from these results as well as those presented in previous studies, it is clear that the MU2 and NU2 tides should not be directly estimated, at least not currently, within the EOT configuration. Instead, either linear admittance (Egbert and Ray 2017; Ray 2017) or a numerical model should be used to estimate MU2 and NU2, such as in the DCSM-A case where FES2014 was used. The only other tide with significant negative impacts is M8. Relative to this tide's tidal signal, 5.91 mm, an increase in RMS of 9.71% was seen; however, the negative result of this tide is region-dependent. When removing the Skagerrak Strait from the analysis, which accounted for most of the mean RMS increase of 1.58 mm, the RMS differences became negligible.

Mean RMS improvements were seen throughout the domain for the SSA, MKS2, T2 and M6 constituents (Fig. 8I). For the L2 and 2Q1 tides, negligible differences ($<$0.05 mm) between DCSM-C and DCSM-D were seen. Interestingly, in this simulation, a constituent that was not changed improved, namely the M2 tide. However, these changes relative to the tidal signal in this region, which can exceed 300 cm, should be considered insignificant, despite the positive result. The mean RSS differences between DCSM-C and DCSM-D were also negligible, being below 0.27 mm on average. However, this is predominantly driven by errors in the NU2 and MU2 constituents. As shown in Fig. 8G, despite the influence from MU2 and NU2, there are still certain regions where the RSS is improved. When these two tides are removed from the RSS estimation, there is a mean reduction of 2.03 mm, with this consistent throughout the domain (see Appendix Fig. 12).

For the total tidal and water height, both estimations show an improvement of 0.49 mm and 0.52 mm relative to DCSM-C, respectively. There were larger reductions in RMS in the Dutch and German coastlines, with an average of 0.98 mm in the tidal height and 1.01 mm in total water height in DCSM-D with respect to DCSM-C. As expected, regions where the M8, MU2 and NU2 errors are larger have a negative impact on the tidal and water height estimations. In the Skagerrak Strait, negative differences of 0.50 mm for the tidal height and 0.37 mm for the total water height were seen.

The overall change from DCSM-A to DCSM-D (Fig. 8H) was a 0.85 mm reduction in RSS, with this increasing to 2.61 mm when the MU2 and NU2 tides are removed from consideration. The overall mean improvement made from DCSM-A to DCSM-D based on tidal height and the total water level was 0.29 cm and 0.25 cm, respectively (Fig. 9) based on these experiments, which is a significant improvement made to the tidal estimations particularly based on errors in model derived tidal constituents exceeding 4 cm in the coastal region (Lyard et al. 2021; Hart-Davis et al. 2021a), also shown in Fig. 4. When considering that the mean sea level rise estimated from satellite altimetry in the North Sea is 2.6 mm/year (Dettmering et al. 2021) and errors in tidal estimates are a large contributor to the uncertainty of water level estimates (van de Wal et al. 2019; Prandi et al. 2021), these reductions in the overall error of tidal height and water level estimations within the model are crucial, particularly when considering that these constituents are considered minor tides, having much smaller contributions to the overall tidal height. In

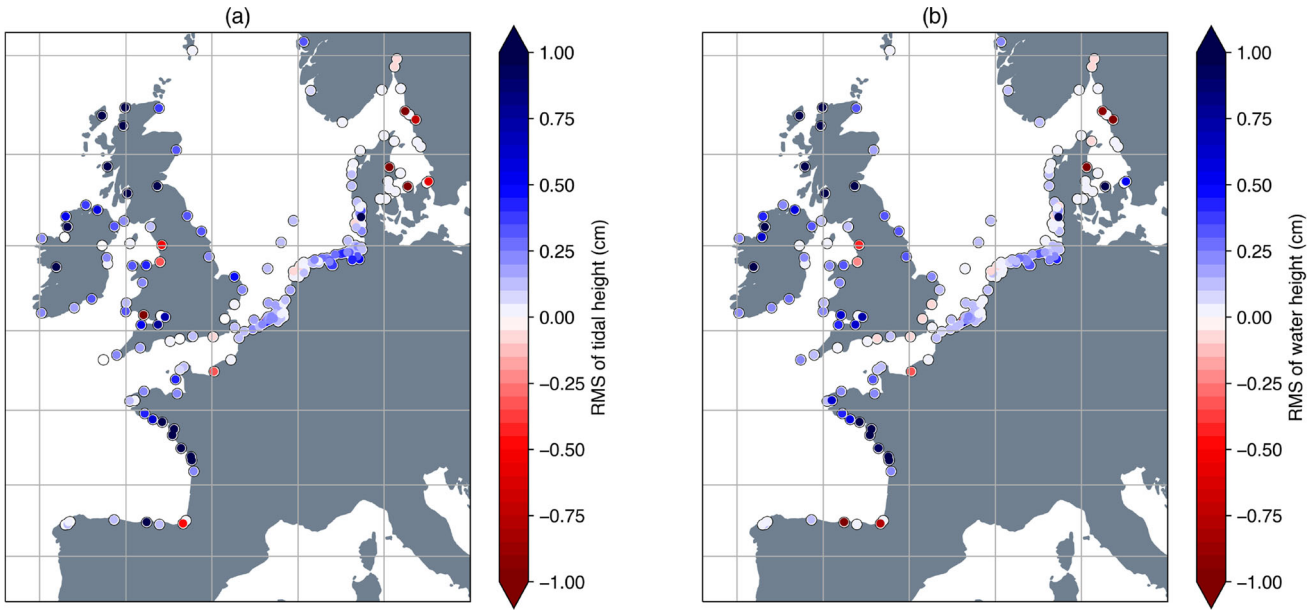

Fig. 9 The overall RMS changes with respect to tide gauge observations in both tidal height (**a**) and water levels (**b**) estimations from DCSM-A to DCSM-D. A blue value indicates a higher RMS in DCSM-A, while a red value indicates a higher RMS in DCSM-D

some regions, the overall improvements made to the model in the Bay of Biscay, the English Channel and the Irish Sea even surpass 1 cm (see Fig. 9). These improvements made to DCSM-FM, also along the Dutch coastline which is the main area of application of the 2D model, demonstrate the positive impact of the appropriate tidal forcing on the model's performance.

4.3 The impact of EOT-NECS on the 3D DCSM-FM

To evaluate the influence of these tidal constituents on the 3D version of DCSM-FM, two 3D model versions were run for a 1-year period, from 01 January 2017 to 01 January 2018. The first model version was a reference model (3D-DCSM-REF) that incorporated no tidal constituents from EOT-NECS, while the second model version included all the constituents from EOT-NECS that were used in DCSM-D of the 2D experiments (all the constituents listed mentioned in 'Experiment' in Table 1) as well as the inclusion of the SA tide (3D-DCSM-EOT). The inclusion of the SA tide was based on 3D-DCSM-REF previously using FES2014 to force this tide in the 3D model, recalling that the SA tide was taken from the DCSMv6 in the 2D experiments, and EOT-NECS showing an improvement in this tide with respect to FES2014.

Overall, the differences between the two models were very small, with both the total tidal height and total water level differences being less than 0.005 mm on average. Despite this negligible difference, there are differences in the RMS estimation of the individual constituents. A degradation of the SA tide of 7.08 mm was seen, while the S1, RHO1, MA2, MB2, M6 and MKS2 tides all showed improved RMSs of more than 0.5 mm when being included from EOT-NECS. The increased RMS of the SA tide causes an increase in the RSS estimation of the 3D-DCSM-EOT version (Fig. 10a). The SA tide from the EOT set of models, i.e. both EOT20 and EOT-NECS, is influenced by non-tidal variability, namely mesoscale and seasonal variability. This results in the tide from EOT not being appropriate for all applications, and based on the results seen in Fig. 10a, this is also the case for this application.

Furthermore, the SA tide is influenced by the dynamic atmospheric correction (DAC), which is used in the derivation of the SLA data used to make the tidal estimations in EOT-NECS. As the boundaries of DCSM-FM incorporates an inverse barometer correction which aims to incorporate signals similar to that estimated in the DAC, it is expected that this SA tide signal is being over-counted, which results in these reductions in accuracy with respect to tide gauges. Additionally, as mentioned previously, the density fields for the 3D model run are taken from the GLORYS ocean model, which will also have a contribution of the SA tide within. Accounting for these two contributions to the SA tide means that this constituent requires special treatment in future iterations of the model and cannot simply be taken as is from EOT-NECS to be used as a boundary forcing within DCSM-FM. Further experiments will take place in follow-up research to determine what the best solution for DCSM-FM is regarding this constituent.

Despite this, there is a clear benefit in including several tidal constituents from EOT-NECS. To demonstrate this, in

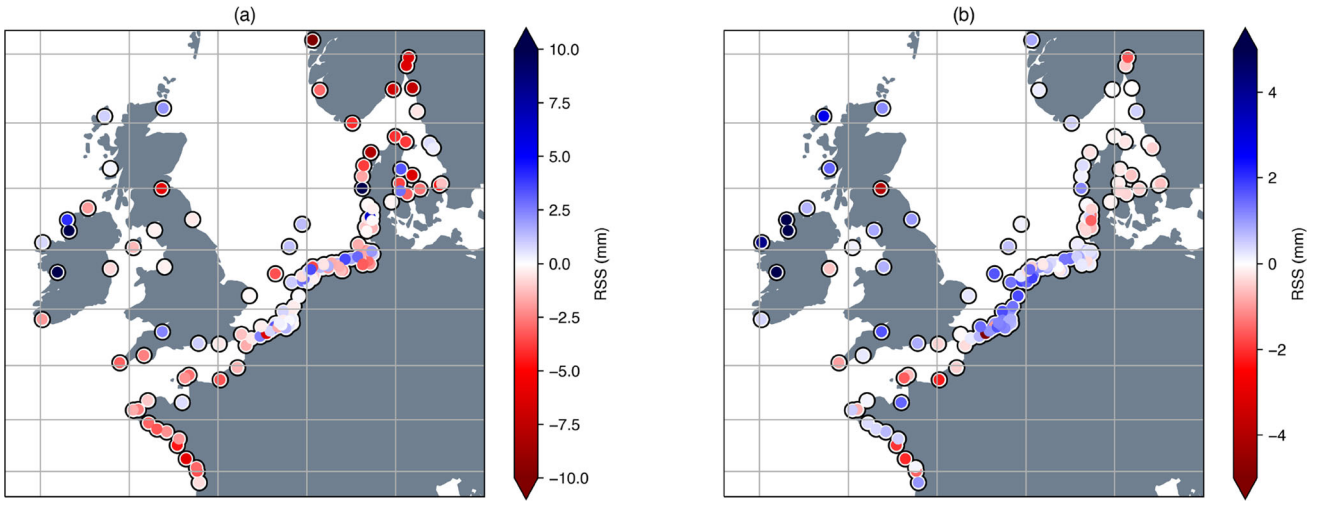

Fig. 10 The RSS difference of all the tidal constituents between the 3D-DCSM-REF and 3D-DCSM-EOT simulations. (**a**) is the RSS difference with all tides included in the results, and (**b**) is without the SA tide included

Fig. 10b, the SA has been removed from the RSS estimations to give a better illustration of the influence the other constituents have on the results of the model. Particularly, the S1, RHO1, M6, MA2, MKS2 and MB2 tidal constituents all showed improvements when incorporated from EOT-NECS. Table 2 shows the tides that had the biggest change in the 3D model, with a restriction being only tides that have exceed a 0.5 mm change in RMS values. Although the changes made to the overall tidal height and total water levels are considerably smaller compared to those seen in the 2D model, there remains a benefit in the model when forcing at the boundaries using the EOT-NECS model. Of particular value are the tides that were originally tested in DCSM-B and DCSM-C, which were originally identified as constituents which would benefit the most from as a boundary forcing from EOT-NECS, which all show to have the largest positive impact on the model. These findings and the negative impact seen by the SA tide demonstrate the significance of these studies to evaluate individual constituent influences in refining the overall tidal and total water height estimations.

4.4 The major tides

A clear omission from the above experiments is the major tidal constituents, which have been shown to be strongly improved in EOT-NECS with respect to EOT20 (Fig. 4). Initial experiments did test the incorporation of these major tides from both EOT20 and EOT-NECS at the boundaries of DCSM-FM. These constituents are originally provided by the FES2014 (O1, Q1, P1, S2) and the GTSMv4.1 (M2, N2, K1, K2) models respectively. In the simulation comparing these tides from EOT-NECS, these tides had negligible impacts on the overall results of the DCSM-FM configuration, with an overall mean RMS degradation of 0.02 mm when using these tides from EOT-NECS. This is expected as at the boundaries, the four tides taken from FES2014 and the tides taken from EOT-NECS show negligible differences.

Furthermore, the hydrodynamic model, GTSMv4.1, used for the other four major constituents, is calibrated using some of the tide gauges used in the validation of DCSM-FM along the Dutch coastline. Therefore, when coupling this calibration with the accuracy of GTSMv4.1 in this region as well as its high spatial resolution along the European shelf region ($1/90^o$) (Wang et al. 2022), it is expected that the major tides from GTSMv4.1 provide suitable boundary forcings for DCSM-FM. From the initial experiments comparing these major tides from either GTSMv4.1, FES2014 or EOT-NECS, this was the case (not shown). It is important to emphasise that the chosen tides for the above experiments were based on constituents that were highly erroneous within DCSM-FM and, therefore, would be of the greatest benefit in terms of improvements possible within DCSM-FM. However, avenues of merging the EOT-NECS and GTSMv4.1 based either on residual tidal analysis or a combination through machine learning or super-resolution (Barthélémy et al. 2022) begin to emerge to benefit from the performance of both of these models in this region. This is not the subject of this manuscript but will be investigated further in future studies.

5 Conclusion

This paper aimed to address two main points: (1) to develop an improved high-resolution EOT model and (2) to improve the representation of tides and water levels within DCSM-FM. Firstly, this involved the development and production of

a regional version of the empirical ocean tide model, EOT-NECS, which was designed to improve on the predecessor global configuration, EOT20, by making some model refinements as well as by including additional satellite altimetry missions to help improve the models' spatial resolution and allow for the estimation of additional tidal constituents. Analysis of the models' performance against in situ observations taken from the updated TICON-3 (Hart-Davis et al. 2022b) showed an improvement compared to the global EOT20 model of 0.678 cm for the eight major tidal constituents and showed a reduced RMS for all tidal constituents. These results allow for the conclusion that the new regional version of the model outperforms the global configuration in the North European Continental Sea region.

This has two positive implications, one being that this new EOT-NECS model should be preferred for applications within this region. Several applications such as the one in this paper but also regional altimetry-based applications (e.g. Birol et al. 2017; Rulent et al. 2020; Dettmering et al. 2021; Passaro et al. 2021) would also benefit from the regional improvements made to tidal estimations. These applications may also be supported by the incorporation of additional tidal constituents. Secondly, there is a potential that the model configuration will perform well in other regions, which opens the door for additional regional versions of the model. Evaluating the model in more regions is also essential in support of ongoing developments with future iterations of the global EOT model in mind.

Once developed, several experiments were designed to test the use of tidal constituents from EOT-NECS as boundary forcings for DCSM-FM. These experiments demonstrated positive implications on DCSM-FM based on the inclusion of most tidal constituents replaced or included from EOT-NECS. The experiments incorporating the S1, MA2, MB2 and RHO1 constituents resulted in mean reductions in the error of these individual constituents as well as the total tidal height and water levels within DCSM-FM. Thanks to the development of the regional configuration, MA2, MB2 and RHO1 constituents were estimated for the first time within EOT-NECS and forced at the boundary of DCSM-FM. For the S1 tide, previously taken from FES2014, an improvement was seen in including this tide from EOT-NECS. This is likely due to FES2014's S1 originating mostly from the atmospheric forcing (Lyard et al. 2021), which, due to DCSM-FM introducing the inverse barometer correction at the boundary, likely produces a double counting of diurnal variations in the air pressure, which is not the case when using the EOT-NECS S1 tide. The NU2, MU2, and M8 tidal constituents were the only added tides that showed a reduction in accuracy with DCSM-FM. In Hart-Davis et al. (2021b), in three different regions, it was concluded that the MU2 and NU2 tides should not be directly estimated from empirical models, and different techniques should be explored to include these tides in experiments. This study supports these findings and adds that despite making improvements to tidal estimations within the EOT-NECS model, these tides should still not be directly estimated, and in this case, taking these tides from FES2014 should be preferred.

The total changes made to the tidal boundary forcing of the DCSM-FM by incorporating the EOT-NECS tidal constituents had an overall positive impact on the model results. In total, the mean improvement was 0.29 cm in RMS for the tidal height and 0.25 cm for total water level when comparing the reference model with the final version, while in some regions, such as the French and the UK coastlines, there were reductions in RMS exceeding 1 cm. Considering that tides along the coastline are known to have errors relating to individual constituents exceeding 4 cm from global tide models (Stammer et al. 2014), this reduction is considerable in providing accurate water level estimations.

Furthermore, when putting into context that the constituents presented in this study are deemed 'minor' tides, having a considerably smaller influence on the overall tidal height estimation, these improvements are important. For the major tides, there are clear benefits in continuing to utilise the already calibrated GTSMv4.1 model in the DCSM-FM; however, potential future work based on the results seen in this study could involve developing techniques to merge the benefits of the EOT-NECS and GTSM models using either residual tidal analysis or machine learning techniques such as super-resolution (Barthélémy et al. 2022).

Although not the main focus of this study, the impacts on the 3D DCSM-FM estimated water levels and tides were also assessed. The total tidal height and total water level differences when including EOT-NECS constituents were negligible. The RSS estimation of the tidal constituents was negatively impacted by the inclusion of the SA tide, but when this tide was removed, the inclusion of EOT-NECS had positive impacts throughout the domain. This demonstrates a clear benefit based on individual constituent performances of including these tides within the 3D version of the model. The individually improved tides also correlate well with those tested in the 2D experiments, which further emphasises the importance of their inclusion, particularly due to the 3D model incorporating additional processes not included in the 2D model, such as baroclinic processes. It is clear that the SA tide requires special attention, and this will be done in future studies by attempting to remove the mesoscale variability from the SLA data used to derive the tidal constituents, so as not to double count for these effects within the 3D DCSM-FM, following techniques such as those presented in Zaron and Ray (2018) and Bonaduce et al. (2021).

This paper finally highlights the importance of testing different ocean tide models as boundary forcing for numerical models. It is expected that certain tide models perform better in different regions based on refinements made to processing techniques, spatial resolutions etc., so it is worth it to evaluate multiple when producing numerical model simulations that would benefit from tidal forcing along the boundary. Furthermore, a potential future study that could be conducted by the tide modelling community is to produce a comparison of ocean tide models from a spatial perspective to conclude on recommended tide models for applications in particular regions which would make it easier in applications like the above, as well as in the context of tidal correction for satellite altimetry, to decide on which tide model(s) are appropriate for particular applications.

Appendix A

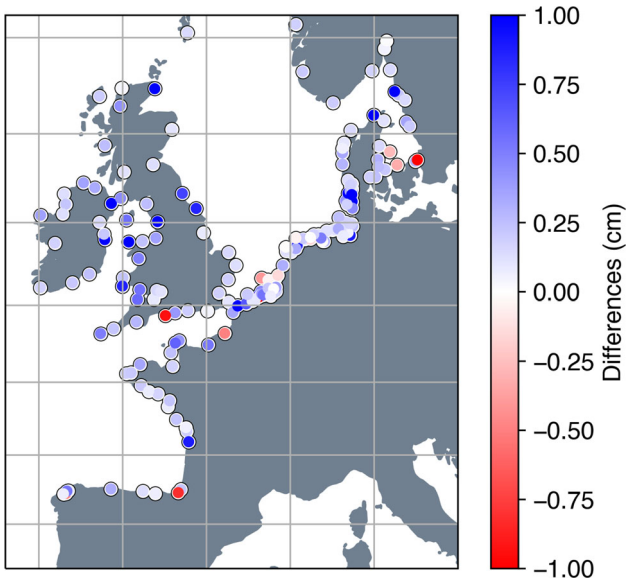

Fig. 12 The RSS differences between DCSM-D minus DCSM-C with the MU2 and NU2 tidal constituents being removed

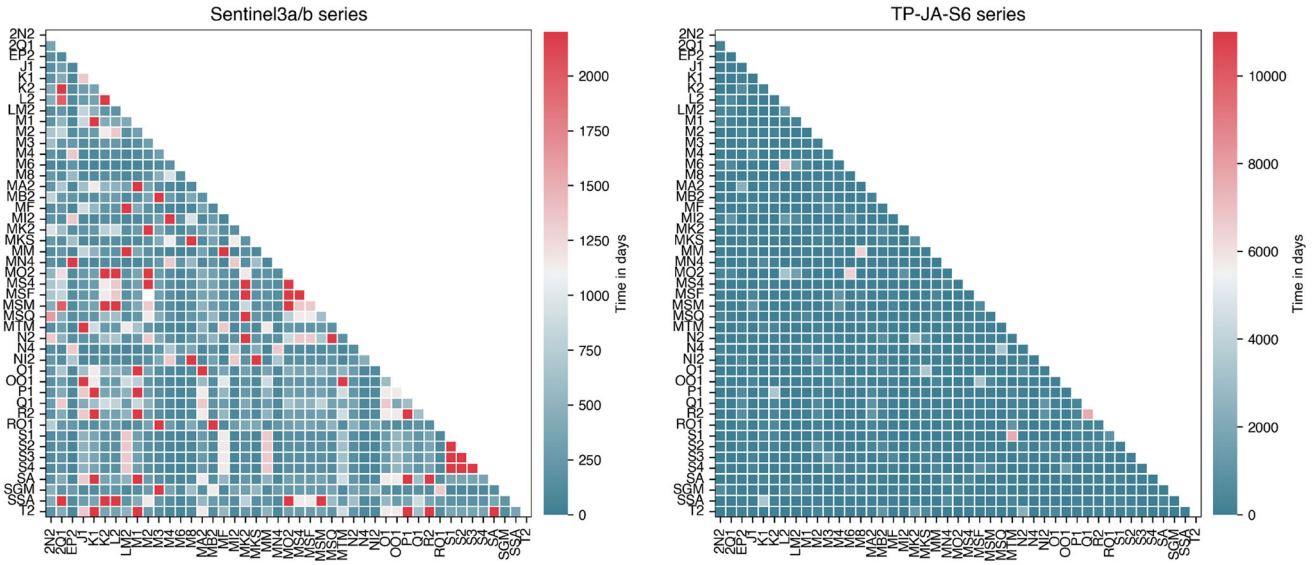

Fig. 11 Rayleigh coefficient of Sentinel3a/b and the TP-JA-S6 orbits

Table 2 RMS difference between the 3D model version of the tidal constituents that have an equal or exceed a difference of 0.5 mm

Constituent	RMS (mm)
SA	7.08
RHO1	−1.84
S1	−1.72
M6	−1.18
H2	−0.78
LABDA2	0.68
MKS2	−0.60
H1	−0.50

Positive values display an increased RMS when the particular EOT-NECS tide is included, and negative values mean a reduced RMS

Acknowledgements The authors acknowledge the DFG project TIDUS-2 (DE2174/12-2, Project Number 388296632) within the DFG research unit NEROGRAV (RU 2736), which partly funds this study.

Funding Open Access funding enabled and organized by Projekt DEAL.

Data Availibility The EOT-NECS data is available at SEANOE: https://doi.org/10.17882/94705/ (Hart-Davis et al. 2023). EOT20 can be downloaded here: https://doi.org/10.17882/79489. The satellite altimetry data used in this study is a modified version of that available from https://openadb.dgfi.tum.de/en/, and the GESLA-3 data used in the creation of TICON-3 is available at https://www.gesla.org/. The TICON-3 dataset is available at https://doi.pangaea.de/10.1594/PANGAEA.951610

Declarations

Conflict of interest The authors declare no competing interests.

References

Andersen OB (1995) Global ocean tides from ERS 1 and TOPEX/POSEIDON altimetry. J Geophys Res 100(C12):25–249. https://doi.org/10.1029/95jc01389

Arns A, Dangendorf S, Jensen J, et al (2017) Sea-level rise induced amplification of coastal protection design heights. Sci Reports 7(1). https://doi.org/10.1038/srep40171

Barthélémy S, Brajard J, Bertino L et al (2022) Super-resolution data assimilation. Ocean Dyn 72(8):661–678. https://doi.org/10.1007/s10236-022-01523-x

Birol F, Fuller N, Lyard F et al (2017) Coastal applications from nadir altimetry: example of the X-TRACK regional products. Adv Space Res 59(4):936–953. https://doi.org/10.1016/j.asr.2016.11.005 https://www.sciencedirect.com/science/article/pii/S0273117716306317

Bonaduce A, Cipollone A, Johannessen JA et al (2021) Ocean mesoscale variability: a case study on the Mediterranean Sea from a reanalysis perspective. Front Earth Sci 9. https://doi.org/10.3389/feart.2021.724879

Bosch W, Dettmering D, Schwatke C (2014) Multi-mission cross-calibration of satellite altimeters: constructing a long-term data record for global and regional sea level change studies. Remote Sens 6(3):2255–2281. https://doi.org/10.3390/rs6032255 https://www.mdpi.com/2072-4292/6/3/2255

Bähr H, Altamimi Z, Heck B (2007) Variance component estimation for combination of terrestrial reference frames. Tech. Rep. 6, Karlsruher Institut für Technologie (KIT), https://doi.org/10.5445/KSP/1000007363

Cartwright DE (1999) Tides : a scientific history / David Edgar Cartwright. Cambridge University Press, Cambridge, UK

Cartwright DE, Ray RD (1991) Energetics of global ocean tides from Geosat altimetry. J Geophys Res Oceans 96(C9):16897–16912. https://doi.org/10.1029/91JC01059 https://agupubs.onlinelibrary.wiley.com/doi/abs/10.1029/91JC01059 https://arxiv.org/abs/agupubs.onlinelibrary.wiley.com/doi/pdf/10.1029/91JC01059

Cheng Y, Andersen OB (2017) Towards further improving DTU global ocean tide model in shallow waters and Polar Seas. In OSTST, Poster in: Proceedings of the Ocean Surface Topography Science Team (OSTST) Meeting, Miami FL USA, pp 23–27. https://ftp.space.dtu.dk/pub/DTU16/OCEAN_TIDE/OSTST2017-tide.pdf

Cipollini P, Benveniste J, Birol F, et al (2017) Satellite altimetry in coastal regions. In Satellite Altimetry over Oceans and Land Surfaces. CRC Press, p 343–380. https://doi.org/10.1201/9781315151779-11

Darwin GH (1891) XI. on the harmonic analysis of tidal observations of high and low water. Proc R Soc Lond 48(292–295):278–340. https://doi.org/10.1098/rspl.1890.0041

Dettmering D, Müller FL, Oelsmann J et al (2021) North SEAL: a new dataset of sea level changes in the North Sea from satellite altimetry. Earth Syst Sci Data 13(8):3733–3753. https://doi.org/10.5194/essd-13-3733-2021 https://essd.copernicus.org/articles/13/3733/2021/

Egbert GD, Ray RD (2003) Semi-diurnal and diurnal tidal dissipation from TOPEX/Poseidon altimetry. Geophys Res Lett 30(17). https://doi.org/10.1029/2003GL017676 https://agupubs.onlinelibrary.wiley.com/doi/abs/10.1029/2003GL017676 https://arxiv.org/abs/https://agupubs.onlinelibrary.wiley.com/doi/pdf/10.1029/2003GL017676

Egbert GD, Ray RD (2017) Tidal prediction. J Mar Res 75(3):189–237. https://doi.org/10.1357/002224017821836761

EMODnet Bathymetry Consortium (2020) EMODnet digital bathymetry (DTM 2020). https://doi.org/10.12770/bb6a87dd-e579-4036-abe1-e649cea9881a

Goede EDD (2020) Historical overview of 2D and 3D hydrodynamic modelling of shallow water flows in the Netherlands. Ocean Dynamics 70(4):521–539. https://doi.org/10.1007/s10236-019-01336-5

Hackett B, Donnelly C, Sagarminaga Y (2013) Deliverable 4.1 report on validation of E-HYPE runoff data. https://www.researchgate.net/publication/259146801_Report_on_validation_of_E-HYPE_runoff_data

Haigh ID, Marcos M, Talke SA, et al (2022) GESLA Version 3: a major update to the global higher-frequency sea-level dataset.

Geoscience Data Journal n/a(n/a). https://doi.org/10.1002/gdj3.174 https://rmets.onlinelibrary.wiley.com/doi/abs/10.1002/gdj3.174 https://arxiv.org/abs/https://rmets.onlinelibrary.wiley.com/doi/pdf/10.1002/gdj3.174

Hart-Davis M, Dettmering D, Sulzbach R et al (2021) Regional evaluation of minor tidal constituents for improved estimation of ocean tides. Remote Sens 13(16):3310. https://doi.org/10.3390/rs13163310 https://www.mdpi.com/2072-4292/13/16/3310

Hart-Davis MG, Piccioni G, Dettmering D et al (2021) EOT20: a global ocean tide model from multi-mission satellite altimetry. Earth Syst Sci Data 13(8):3869–3884. https://doi.org/10.5194/essd-13-3869-2021 https://essd.copernicus.org/articles/13/3869/2021/

Hart-Davis MG, Dettmering D, Seitz F (2022a) TICON-3: tidal constants based on GESLA-3 sea-level records from globally distributed tide gauges including gauge type information (data). https://doi.pangaea.de/10.1594/PANGAEA.951610

Hart-Davis MG, Dettmering D, Seitz F (2022b) TICON: tidal constants. https://doi.org/10.1594/PANGAEA.946889

Hart-Davis MG, Schwatke C, Dettmering D, et al (2023) EOT-NECS Ocean Tide Model. https://doi.org/10.17882/94705

Hersbach H, Bell B, Berrisford P, et al (2017) Complete ERA5 from 1979: fifth generation of ECMWF atmospheric reanalyses of the global climate. Copernicus Climate Change Service (C3S) Data Store (CDS), ECMWF [data set]

Intergovernmental Panel on Climate Change (IPCC) (2022) Changing ocean, marine ecosystems, and dependent communities. https://doi.org/10.1017/9781009157964.007

Kernkamp H, van Dam A, Stelling G et al (2011) Efficient scheme for the shallow water equations on unstructured grids with application to the continental shelf. Ocean Dyn Theor Comput Oceanogr Monit 61(8):1175–1188. https://doi.org/10.1007/s10236-011-0423-6

Lyard FH, Allain DJ, Cancet M et al (2021) FES 2014 global ocean tide atlas: design and performance. Ocean Sci 17(3):615–649. https://doi.org/10.5194/os-17-615-2021

Muis S, Verlaan M, Winsemius HC, et al. (2016) A global reanalysis of storm surges and extreme sea levels. Nature Commun 7(1). https://doi.org/10.1038/ncomms11969

Passaro M, Cipollini P, Vignudelli S et al (2014) ALES: a multi-mission adaptive subwaveform retracker for coastal and open ocean altimetry. Remote Sens Environ 145:173–189. https://doi.org/10.1016/j.rse.2014.02.008 https://www.sciencedirect.com/science/article/pii/S0034425714000534

Passaro M, Müller FL, Oelsmann J et al (2021) Absolute Baltic Sea level trends in the satellite altimetry era: a revisit. Front Mar Sci 8:546. https://doi.org/10.3389/fmars.2021.647607

Piccioni G, Dettmering D, Bosch W et al (2019) TICON: tidal constants based on GESLA sea-level records from globally located tide gauges. Geosci Data J 6(2):97–104. https://doi.org/10.1002/gdj3.72

Prandi P, Meyssignac B, Ablain M, et al. (2021) Local sea level trends, accelerations and uncertainties over 1993–2019. Sci Data 8(1). https://doi.org/10.1038/s41597-020-00786-7

Provost CL, Bennett AF, Cartwright DE (1995) Ocean tides for and from TOPEX/POSEIDON. Science 267(5198):639–642. https://doi.org/10.1126/science.267.5198.639

Pugh DT (1987) Tides, surges and mean sea level. John Wiley and Sons https://www.osti.gov/biblio/5061261

Ray RD (2017) On tidal inference in the diurnal band. J Atmos Ocean Technol 34(2):437–446. https://doi.org/10.1175/JTECH-D-16-0142.1 https://journals.ametsoc.org/view/journals/atot/34/2/jtech-d-16-0142.1.xml

Ray RD (2022) Technical note: on seasonal variability of the m_2 tide. Ocean Sci 18(4):1073–1079. https://doi.org/10.5194/os-18-1073-2022 https://os.copernicus.org/articles/18/1073/2022/

Rulent J, Calafat FM, Banks CJ et al (2020) Comparing water level estimation in coastal and shelf seas from satellite altimetry and numerical models. Front Mar Sci 7. https://doi.org/10.3389/fmars.2020.549467 https://www.frontiersin.org/articles/10.3389/fmars.2020.549467

Savcenko R, Bosch W (2012) EOT11a-empirical ocean tide model from multi-mission satellite altimetry. DGFI Report No 89 https://doi.org/10.1594/PANGAEA.834232

Smith AJE (1999) Application of satellite altimetry for global ocean tide modeling. TU Delft. http://resolver.tudelft.nl/uuid:5e9c5527-220f-4658-b516-459528e62733

Stammer D, Ray RD, Andersen OB et al (2014) Accuracy assessment of global barotropic ocean tide models. Rev Geophys 52(3):243–282. https://doi.org/10.1002/2014RG000450 https://agupubs.onlinelibrary.wiley.com/doi/abs/10.1002/2014RG000450 https://arxiv.org/abs/agupubs.onlinelibrary.wiley.com/doi/pdf/10.1002/2014RG000450

van de Wal RSW, Zhang X, Minobe S et al (2019) Uncertainties in long-term twenty-first century process-based coastal sea-level projections. Surv Geophys 40(6):1655–1671. https://doi.org/10.1007/s10712-019-09575-3

Wang X, Verlaan M, Veenstra J et al (2022) Data-assimilation-based parameter estimation of bathymetry and bottom friction coefficient to improve coastal accuracy in a global tide model. Ocean Sci 18(3):881–904. https://doi.org/10.5194/os-18-881-2022 https://os.copernicus.org/articles/18/881/2022/

Woodworth PL, Green JAM, Ray RD et al (2021) Preface: Developments in the science and history of tides. Ocean Sci 17(3):809–818. https://doi.org/10.5194/os-17-809-2021 https://os.copernicus.org/articles/17/809/2021/

Zaron ED, Ray RD (2018) Aliased tidal variability in mesoscale sea level anomaly maps. J Atmos Ocean Technol 35(12):2421–2435. https://doi.org/10.1175/jtech-d-18-0089.1

Zijl F, Groenenboom J (2019) Development of a sixth generation model for the NW European Shelf (DCSM-FM 0.5nm). Tech rep, Deltares, Deltares

Zijl F, Verlaan M, Gerritsen H (2013) Improved water-level forecasting for the Northwest European Shelf and North Sea through direct modelling of tide, surge and non-linear interaction. Ocean Dyn 63(7):823–847. https://doi.org/10.1007/s10236-013-0624-2

Zijl F, Verlaan M, Sumihar J (2015) Application of data assimilation for improved operational water level forecasting on the Northwest European Shelf and North Sea. Ocean Dyn 65(12):1699–1716. https://doi.org/10.1007/s10236-015-0898-7

A.2 Additional publications

While working on this thesis, four different co-authored manuscripts and one additional first-author manuscript were produced, which used the algorithms and datasets presented in this thesis.

- **AP-1**: Sulzbach, R., Wziontek, H., Hart-Davis, M.G., Dobslaw, H., Scherneck, H.G., Van Camp, M., Omang, O.C.D., Antokoletz, E.D., Voigt, C., Dettmering, D. and Thomas, M., 2022. Modeling gravimetric signatures of third-degree ocean tides and their detection in superconducting gravimeter records. *Journal of Geodesy*, 96(5), pp.1-22, https://doi.org/10.1007/s00190-022-01609-w.
- **AP-2**: Hart-Davis M.G., Howard S., Ray R., Andersen O., Padman L., Nilsen F., Dettmering D. ArcTiCA: Arctic Tidal Constituents Atlas. *Nature Scientific Data* [in review]. Preprint: https://doi.org/10.21203/rs.3.rs-3277941/v1
- **AP-3**: Andersen, O.B., Rose, S.K. and Hart-Davis, M.G., 2023. Polar Ocean Tides—Revisited Using Cryosat-2. Remote Sensing, 15(18), p.4479. https://doi.org/10.3390/rs15184479
- **AP-4**: Passaro M., Rautiainen L., Dettmering D., Restano M., Hart-Davis M.G., Schlembach F., Särkkä J., Müller F. L., Schwatke C., Benveniste J., 2022. Validation of an Empirical Subwaveform Retracking Strategy for SAR Altimetry. *Remote Sensing*, 14(16), 4122, https://doi.org/10.3390/rs14164122
- **AP-5**: Hauk M., Wilms J., Sulzbach R., Panafidina N., Hart-Davis M., Dahle C., Müller V., Murböck M. and Flechtner F., 2023. Satellite gravity field recovery using variance covariance information from ocean tide models. AGU Earth and Space, https://doi.org/10.1029/2023EA003098

A.3 Associated Datasets

Within this thesis, several datasets were produced and are listed below:

- **AD-1:** Hart-Davis M., Schwatke C., Dettmering D., Passaro M., Seitz F.: EOT-NECS Ocean Tide Model. *SEANOE*, https://doi.org/10.17882/94705, 2023.
- **AD-2:** Sulzbach R., Hart-Davis M.G., Dettmering D., Thomas M.: Regularized Empirical Variance-Covariance-Matrices for stochastic gravity modeling of 8 major ocean tides. *GFZ Data Services*, https://doi.org/10.5880/nerograv.2023.003, 2023.
- **AD-3:** Hart-Davis M.G., Dettmering D., Seitz F.: TICON-3: Tidal Constants based on GESLA-3 sea-level records from globally distributed tide gauges including gauge type information. *Pangaea*, https://doi.org/10.1594/PANGAEA.951610, 2022.
- **AD-4:** Hart-Davis M.G., Sulzbach R., Dettmering D., Thomas M., Seitz F.: TICON-td: Third-degree tidal constants based on GESLA sea-level records from globally distributed tide gauges. *Pangaea*, https://doi.org/10.1594/PANGAEA.943444, 2022.
- **AD-5:** Hart-Davis M., Piccioni G., Dettmering D., Schwatke C., Passaro M., Seitz F. : EOT20-A global Empirical Ocean Tide model from multi-mission satellite altimetry. *SEANOE*, https://doi.org/10.17882/79489, 2021.

- **AD-6:** Hart-Davis M., Howard S., Ray R., Andersen O., Padman L., Nilsen F., Dettmering D.: ArcTiCA: Arctic Tidal Constituents Atlas. Arctic Data Center. https://doi.org/10.18739/A2D795C4N, 2023.

Acknowledgements

My PhD has been influenced by a variety of people from a variety of places, countries and continents. Properly acknowledging their contributions to my progress and my resultant thesis, would require another few hundred pages added to this thesis, but I would like to acknowledge a few in particular here.

Florian Seitz, thanks for taking the risk on a South African oceanographer and allowing me the freedom to discuss and experiment throughout my PhD. The thoughtful encouragement and advice throughout contributed significantly to my growth as a scientist. Denise Dettmering, thanks for the near-daily advice and discussions where you explained things to me, helped me understand more and helped me ask the right questions. I am not sure there would be someone better who would take someone with such limited knowledge at the beginning of my PhD and grow them into someone capable of writing a thesis on the topic. Here is to many years of sharing some nice South African wine (also, apologies for all the brackets in my emails). Marcello Passaro, I am so grateful that we shared an office. Your ideas and concepts, your questions and comments are so much appreciated. You were my introduction to the institute and the field, I will be forever grateful for the warm response you gave to my spontaneous mail that would eventually lead to me doing this research at DGFI.

My colleagues at DGFI-TUM, have had to put up with a lot when it comes to me. Constant questions, constant jokes and constant talking, but you all welcomed me in with open arms. Thanking you all individually would not justify your contributions to shaping my career and my thesis. Christian Schwatke always responded well to my ideas and always tried to make my work easier. The coffee breaks were nice for expanding ideas and developing new ones, so I look forward to many more of these. Julius Oelsmann (Stark), a greater friend and a greater young scientist, is surely not possible. Arguments, idea discussions and more arguments, all influenced my way of thinking and my interpretation of results. I am forever grateful that I met someone that was so keen to discuss topics, regardless of how ridiculous they were. It was a further pleasure to work with great, fun people: Marie-Christin Juhl, Maria Pisareva, Daniel Scherer and Alex Kehm.

This thesis is clearly benefited by the earlier work done by Gaia Piccioni which helped serve as a great framework for the work of this thesis to be built upon. Gaia, although we only interacted virtually, I am grateful for your contributions and guidance, particularly in the early stages of my thesis.

Björn Backeberg, to say that I would not be where I am today without your influence on my career is a severe understatement. Eight years before I submitted this thesis, you were the first person to take a chance on me, pushed me to become the scientist that I am today, and made it possible for me to expand my scientific career. I am glad that throughout my career and especially in my PhD, I could rely on you as a mentor both scientifically and personally. I am forever grateful to have and continue to work with you and to call you a friend. Johnny Johannessen, your contribution to my career is also not possible to properly acknowledge. I am grateful to have had you on my side since the start of my career, and your support, feedback and input has and will always be greatly received.

My colleagues within the NEROGRAV research group were a pleasure to work with and to discuss things with. In particular, was Roman Sulzbach, who raised me as a tide person and continues to teach me things to this day. Your vast knowledge of the fundamentals of tides and mathematics is something that regularly inspires me. I am thankful we have worked so nicely together and look forward to more of the same in the future. Maik Thomas, Michael Schindelegger and Henryk Dobslaw were also a pleasure to work with and discuss topics with. Michael Schindelegger received many an email, and we had many a video call, which I am forever grateful for.

Entering the field of tides, I was heavily inspired by some great scientists who both directly and indirectly contributed to my progress. Regular discussions and insights from Richard Ray and Ole Andersen, who are clearly some of the most knowledgeable tidal experts. Your positive welcome into the community, which led to a memorable 'tide people' dinner at IUGG with the other greats Gary Egbert, Phil Woodworth and Roman Sulzbach of tidal research, is very much appreciated. Your grace in responding to my (frequent) emails and silly ideas played a significant role in helping me grow as a scientist within this community.

To my colleagues at the Nansen Center in Bergen and the Nansen-Tut Center in Cape Town, your support and guidance have helped me a lot. For this I am grateful. Laurent Bertino, Antonio Bonaduce, Issufo Halo and Mathieu Rouault always left their doors open for me to chat and discuss topics with.

To Hermann Luyt, you were there from the beginning, and our near-daily catch-ups about work and the encouragement to make progress, helped during the good and tough times of this PhD. I am glad to have taken the journey, although far apart, together and with your support.

I was fortunate enough to attend several conferences, namely EGU and OSTST, and conduct several research visits to Deltares, TU Delft, NERSC, DTU Space and the Nansen Tutu Center, which allowed me to discuss topics and meet great scientists from a large variety of fields. The colleagues that I met through these visits have meant a great deal to me, both scientifically and personally, making this journey all the sweeter. Tadea Veng, Jelmer Veenstra and Stendert Laan in particular, were people that I got to spend time with during these conferences and these research visits. I am grateful for your friendships as well as your direct and indirect contributions to this thesis.

Lastly, I would like to acknowledge my friends and family. To my Mom, brother and sister, you are part of my journey and were all my inspiration for getting to this point. Thank you for the endless sacrifices you have made for me.

To Nadine Schulda. Goodness. The support, the sacrifices, the hope, the ambition, the passion, and the determination that you fed into me and my career is immeasurable. I am not sure I will ever be able to fully repay that, so thank you.